PB-241 189

ENTRAINMENT SEPARATORS FOR SCRUBBERS

INITIAL REPORT

A. P. T., Incorporated

October 1974

DISTRIBUTED BY:

NTIS

National Technical Information Service
U. S. DEPARTMENT OF COMMERCE

TECHNICAL REPORT DATA

(Please read Instructions on the reverse before completing)

PB 241 189

1. REPORT NO.
EPA-650/2-74-119-a

2.

5. REPORT DATE
October 1974

4. TITLE AND SUBTITLE
Entrainment Separators for Scrubbers--Initial Report

6. PERFORMING ORGANIZATION CODE

7. AUTHOR(S) Seymour Calvert, Indrakumar L. Jashnani, Shuichow Yung, and Samuel Stalberg

8. PERFORMING ORGANIZATION REPORT NO.

9. PERFORMING ORGANIZATION NAME AND ADDRESS
A. P. T., Inc.
P.O. Box 71
Riverside, CA 92502

10. PROGRAM ELEMENT NO.
1AB013; ROAP 21ACX-086

11. CONTRACT/GRANT NO.
68-02-0637

12. SPONSORING AGENCY NAME AND ADDRESS
EPA, Office of Research and Development
NERC-RTP, Control Systems Laboratory
Research Triangle Park, NC 27711

13. TYPE OF REPORT AND PERIOD COVERED
Initial; Through 6/74

14. SPONSORING AGENCY CODE

15. SUPPLEMENTARY NOTES

16. ABSTRACT
The report gives results of an evaluation of current technology relating to the separation of entrained drops of liquid from the gas leaving scrubbers. It includes results of experimental studies of entrainment separator characteristics, as well as theoretical analysis. Zigzag baffle, knitted mesh, tube bank, packed bed, and cyclone devices were tested. It reports collection efficiency and reentrainment as related to drop size. Pressure drop as a function of gas flow rate is also reported. Mathematical models for primary collection efficiency are satisfactory, but useful reentrainment models are not yet available. An auxiliary experiment was aimed at determining reentrainment from liquid sheets under the influence of an air stream. Work is still in progress on vertical gas flow systems, solids deposition, mathematical modeling, and the development of improved designs.

Reproduced by
NATIONAL TECHNICAL
INFORMATION SERVICE
US Department of Commerce
Springfield, VA. 22151

17. KEY WORDS AND DOCUMENT ANALYSIS

a. DESCRIPTORS	b. IDENTIFIERS/OPEN ENDED TERMS	c. COSATI Field/Group
Air Pollution	Air Pollution Control	13B
Scrubbers	Stationary Sources	07A
Entrainment	Entrainment Separators	07D
Efficiency	Collection Efficiency	14A
Mathematical Models		12A

PRICES SUBJECT TO CHANGE

18. DISTRIBUTION STATEMENT
Unlimited

19. SECURITY CLASS (This Report)
Unclassified

20. SECURITY CLASS (This page)
Unclassified

21. NO. OF PAGES
308

22. PRICE
#9.25-2.25

EPA Form 2220-1 (9-73)

EPA-650/2-74-119a

ENTRAINMENT SEPARATORS FOR SCRUBBERS - INITIAL REPORT

by

S. Calvert, I.L. Jashnani, S. Yung,
and S. Stalberg

A.P.T., Inc.
P.O. Box 71
Riverside, California 92502

Contract No. 68-02-0637
Program Element No. 1AB013
ROAP No. 21ACX-086

Project Officer: L.E. Sparks

Control Systems Laboratory
National Environmental Research Center
Research Triangle Park, North Carolina 27711

Prepared for

OFFICE OF RESEARCH AND DEVELOPMENT
ENVIRONMENTAL PROTECTION AGENCY
WASHINGTON, D.C. 20460

October 1974

ia

This report has been reviewed by the Environmental Protection Agency and approved for publication. Approval does not signify that the contents necessarily reflect the views and policies of the Agency, nor does mention of trade names or commercial products constitute endorsement or recommendation for use.

PREFACE

This report, "Entrainment Separators for Scrubbers", is the initial report submitted to the Control System Laboratory for E.P.A. Contract No. 68-02-0637.

The scope of work of this experimental and theoretical study was to

1. Evaluate present technology.
2. Conduct an experimental study of air water systems aimed at simulating the performance of various types of entrainment separators.
3. Develop improved engineering equations and methods for entrainment separator selection.
4. Develop and evaluate on a small pilot basis new entrainment separator designs.
5. Develop specific research and development recommendations.

Dr. Leslie E. Sparks, of the Control Systems Laboratory, National Environmental Research Center, Environmental Protection Agency, was the Project Officer for this program.

Dr. Seymour Calvert, of A.P.T., Inc., was the Project Director.

ACKNOWLEDGEMENT

A.P.T., Inc. wishes to express its appreciation for excellent technical coordination and for very helpful assistance in support of our technical effort to Dr. Leslie Sparks, E.P.A. Project Officer.

TABLE OF CONTENTS

Page

Acknowledgement iv
List of Figures ix
List of Tables .xvii
Nomenclature xix
Abstract xxv

Sections

Introduction 1-1
Summary and Conclusions 2-1
Literature Survey 3-1
    Collection Mechanisms 3-3
        Inertial Impaction 3-3
        Sedimentation 3-6
    Entrainment Drop Diameters 3-6
    Design Equations for Entrainment Separators . . 3-9
        Cyclone 3-10
            Primary Efficiency 3-10
            Pressure Drop 3-13
        Packed Bed 3-14
            Primary Efficiency 3-15
            Pressure Drop 3-16
        Zigzag Baffles 3-16
            Primary Efficiency 3-16
            Pressure Drop 3-21
        Tube Bank 3-21
            Primary Efficiency 3-21
            Pressure Drop 3-23
        Mesh 3-23
            Primary Efficiency 3-24
            Pressure Drop 3-25

Page

Sieve Plates 3-27
    Primary Efficiency 3-27
    Pressure Drop 3-27
Reentrainment 3-31
    Transition from Separated to Separator - Entrained Flow 3-32
        Horizontal Flow in Circular Tube . . . 3-33
        Vertically Upward Flow in a Circular Tube 3-36
        Vertically Downward Flow in a Circular Tube 3-38
        Effect of Impingement of Gas Jet . . . 3-38
        Interfacial Waves 3-38
        Entrained Fraction and Rate of Entrainment 3-47
        Drop Diameter of Reentrainment. 3-50
    Reentrainment Due to Rupture of Bubbles. . . 3-51
        Drop Diameter of Reentrainment. 3-52
        Formation of Jet After Bubble Burst . . 3-55
        Trajectory. 3-57
    Creeping of Fluids 3-60
    Shattering of Drops. 3-62
Manufacturers' Survey 3-62
Theory 4-1
    Zigzag Baffles. 4-1
        Primary Efficiency 4-1
        Pressure Drop 4-8
        Reentrainment 4-8
            Horizontal Baffles 4-11
            1. Derivation of Q_L 4-11
            2. Additional Equations. 4-15
            Vertical Baffles 4-16
            1. Liquid Flow Due to Pressure Gradient 4-18
            2. Liquid Flow Due to Gravity. 4-19
            3. Additional Equations. 4-20

Page

Cyclone 4-20
    Primary Efficiency 4-20
    Reentrainment 4-26
        Onset of Reentrainment 4-26
        Drop Diameter of Reentrainment 4-27
        Rate of Reentrainment 4-27
        Reentrainment Calculation 4-28
Auxiliary Experiment 5-1
    Sampling for Droplet Size Distribution 5-2
    Discussion 5-6
    Results 5-8
    Conclusions 5-17
Experimental Pilot Plant 6-1
    Description of the Pilot Plant 6-1
        Air Prefilter 6-2
        Blower 6-2
        Air Heater 6-2
        Spray Section 6-2
        Observation Sections 6-6
        Drainage of Liquid in the Test Section . . . 6-9
        Liquid Catch Tanks 6-10
        Liquid Supply Tanks 6-10
        Control Panel for Equipment 6-10
        Electrical Supply Panel 6-11
        Water Supply 6-11
    Test Section 6-11
        Mesh 6-12
        Packed Bed 6-13
        Zigzag Baffles 6-13
        Cyclone 6-13
        Tube Bank 6-17
    Calibration 6-17
    Experimental Procedure 6-20
    Sampling Procedure 6-21
    Problems and Possible Errors in the Experiments . 6-28

Page

Experimental Results and Discussion. 7-1
  Inlet Entrainment 7-1
  Experimental Results 7-9
    Packed Bed 7-10
      Overall Efficiency 7-10
      Pressure Drop 7-10
      Reentrainment 7-10
    Zigzag Baffles 7-16
      Overall Efficiency. 7-16
      Pressure Drop 7-21
      Reentrainment 7-21
      Liquid Flow on the Baffles. 7-29
    Mesh 7-33
      Overall Efficiency 7-33
      Pressure Drop 7-35
      Reentrainment 7-35
      Visual Observation of Reentrainment . . 7-42
    Tube Bank 7-44
      Overall Efficiency. 7-44
      Pressure Drop 7-49
      Reentrainment 7-53
  General Observations 7-53
    Pressure Drop. 7-53
    Reentrainment. 7-66
Future Research and Development Recommendation 8-1
Appendix
Glossary
References

LIST OF FIGURES

No. Page

3-1 Entrainment Separator 3-2

3-2 Theoretical Impaction Efficiency as a Function of Inertial Parameter for Different Targets 3-2

3-3 Terminal Settling Velocity and Reynolds Number for Water Drops in Air at 20°C and 760 mm Hg 3-8

3-4 Cyclone with Tangential Gas Inlet. 3-11

3-5 Generalized Flooding and Pressure Drop Correlation for Packed Beds 3-17

3-6 Theoretical and Experimental Collection Efficiencies of Rectangular Aerosol Jets . . . 3-22

3-7 Friction Factor, "f", Versus Reynolds Number, "N_{Re}", for Wire Mesh Entrainment Separator Without Entrainment Load 3-26

3-8 Pressure Drop Due to Presence of Liquid in the Knitted Mesh Wire with the Crimps in the Same Direction 3-28

3-9 Pressure Drop Due to Presence of Liquid in the Knitted Mesh with the Crimps in the Alternate Direction 3-29

3-10 Baker Chart. 3-34

3-11 Flow Pattern Diagram for Horizontal Flow . . . 3-35

3-12 Onset of Entrainment in Air-Water Flow 3-37

3-13 Comparison of Entrained Fraction in Upward and Downward Co-current Annular Flow in 1.25 cm I.D. Tube. 3-39

3-14 Extrapolation Method for Determination of Point of Onset of Entrainment for Vertical Downflow in 2.2 cm I.D. Tube 3-40

No. Page

3-15 Region of Wave Flow in Air-Water Flow in a 3.2 cm Bore Tube 3-42

3-16 Relationship Between Effective Roughness Height and Film Thickness. 3-45

3-17 Breakdown of Disturbance Wave by Undercutting. 3-46

3-18 Breakdown of Disturbance Wave by Rolling . . . 3-46

3-19 Correlation of Entrainment Data by Hughmark. . 3-49

3-20 Histogram Showing Size Distribution of Large and Small Drops Resulting from Bubble Burst 3-54

3-21 Sauter Mean Diameter D_s Against Bubble Diameter at 25°C 3-54

3-22 Time Against Velocity Curves for Drops of Varying Degree 3-59

3-23 Height Against Velocity Curves for Drops of Varying Diameter. 3-59

3-24 Calculated Collection Efficiency for Water Droplets in Air for ACS Mesh 3-64

3-25 Pressure Drop Versus Air Velocity for 10 cm Thick ACS Style 4CA Mesh 3-65

3-26 Pressure Drop Versus Steam Velocity at Various Pressures through 10 cm Thick ACS Mesh 3-66

3-27 Collection Efficiency Versus Particle Diameter for Air Purification Method Cyclone Separator with Inlet Velocity of 16-21 m/sec 3-68

3-28 Comparison of Pressure Drop Characteristics of Beco Engineering Type E/N-1 Pad and Conventional Pad 3-70

3-29 Efficiency Curves for Burgess Industries Centrifuge 3-72

No. Page

3-30 Pressure Drop Characteristics of 10 cm Thick Nu-Standard and 15 cm Thick Hi-Thruput Mist Eliminators 3-73

3-31 Safe Operating Limits for Nu-Standard and Hi-Thruput Mist Eliminators 3-74

3-32 Flooding Correlation for Fibrous Bed Structure by Porter and Lucas 3-77

3-33 Performance of Koch Fleximesh Separator. . . . 3-80

3-34 Collection Efficiency of Particulate Collectors 3-81

3-35 Efficiency Comparison of York Scrubber with Two Stage Wire Mesh Mist Eliminator . . . 3-83

4-1 Continuous Zigzag Baffles 4-2

4-2 Drag Coefficient Versus Reynolds Number After Foust et al. (1959), with Sphericity "Ψ" as the Parameter. 4-5

4-3 Penetration Versus Gas Velocity for Baffle Section 4-6

4-4 Comparison of Primary Efficiency Curves Based on Theoretical Model for Complete Mixing and For No Mixing Models. 4-7

4-5 Drag Coefficients for Flow Past Inclined Flat Plates. 4-9

4-6 Forces on An Element of Liquid Film on Baffle 4-12

4-7 Effects of Baffle Edges on Reentrainment . . . 4-12

4-8 Maximum Liquid Load, Q_L/Q_G, Versus Gas Velocity in Horizontal Baffle Section. . . 4-17

4-9 Predicted Effect of Liquid Loading in Inlet on Reentrainment from Vertical Baffles . 4-21

4-10 Predicted Effect of Liquid Loading in Inlet on Reentrainment from Vertical Baffles . 4-22

No. Page

4-11 Cross Section of a Cyclone 4-25

4-12 Predicted Effect of Inlet Gas Velocity on Reentrainment in Cyclone with $a = 9.2$ cm, $b - 28$ cm, $d_c = 127$ cm, $h_s = 132$ cm, and $d_e = 67$ cm 4-29

4-13 Predicted Effect of Liquid Loading in Inlet on Reentrainment in Cyclone with $a = 9.2$ cm, $b = 28$ cm, $d_c = 127$ cm, $h_s = 132$ cm and $d_e = 67$ cm 4-30

4-14 Predicted Effect of Inlet Gas Velocity on Efficiency of Cyclone with $a = 9.2$ cm, $b = 28$ cm, $d_c = 127$ cm, $h_s = 132$ cm and $d_e = 67$ cm 4-31

4-15 Predicted Collection Efficiency With and Without Reentrainment for Cyclone with $a = 9.2$ cm, $b = 28$ cm, $d_c = 127$ cm, $h_s = 381$ cm, and $d_e = 67$ cm 4-33

5-1 Apparatus to Study Onset of Entrainment Velocities 5-3

5-2 Predicted Effect of Drop Diameter on Capture Efficiency by 5 cm Diameter Filter Paper held Perpendicular to the Air Velocity 5-7

5-3 Distribution of Droplet Size in Air-Water Entrained-Separated Flow 5-9

5-4 Distribution of Droplet Size in Entrained-Separated Flow on Log-Probability Graph. . . . 5-10

5-5 Comparison of Drop Size by Different Investigators 5-11

5-6 Effect of Impingement Angle on Drop Size . . . 5-13

5-7 Effect of Liquid Flow Rate on Impingement Angle for Onset of Entrainment 5-14

5-8 Comparison of Entrainment Onset Velocity by Different Investigators 5-15

No. Page

6-1 Block Diagram of Experimental Apparatus. . . . 6-3

6-2 Top View of the Entrainment Separator Pilot Plant 6-4

6-3 Flow Diagram Showing Connection Between Various Tanks and Pumps. 6-5

6-4 Nozzle Position in the 30.5 cm x 61 cm Duct. . 6-8

6-5 Calculated Collection Efficiency for Water Droplets in Air 6-14

6-6 Pressure Drop Versus Air Velocity for 10 cm Thick ACS Style 4CA Mesh 6-15

6-7 Baffle Section 6-16

6-8 Cyclone Assembly 6-18

6-9 Test Section with Bank of Tubes 6-19

6-10 Form for Recording Test Data 6-22

6-11 Calibration of Whatman No. 1 Filter Paper. . . 6-25

6-12 Liquid Load Sampling 6-26

6-13 Sampling Device Consisting of Impactor, Heated Inlet Probe, Dry and Wet Bulb Thermometer and Accessories. 6-29

7-1 The Effect of Gas Velocity on the Mass Median Drop Diameter 7-3

7-2 Drop Diameter Versus Volume Percentage for Hollow Cone Nozzle Spraying Water at 10.2 atm Gauge Pressure. 7-6

7-3 Drop Diameter Versus Volume Percentage for Hollow Cone Nozzle Spraying Water at 6.8 atm Gauge Pressure 7-7

7-4 Drop Diameter Versus Volume Percentage for Fulljet Nozzles Spraying Water at 2.7 atm Gauge Pressure 7-8

7-5 Experimental Collection Efficiency of a Packed Bed as a Function of Gas Velocity with Horizontal Flow 7-11

No. Page

7-6 Dry Pressure Drop in Packed Bed Versus Gas Velocity 7-12

7-7 Wet Pressure Drop in Packed Bed Versus Gas Velocity 7-13

7-8 Maximum Drop Diameter in the Entrainment Versus Gas Velocity for 30 cm Packed Bed . . . 7-14

7-9 Mass Median Drop Diameter Versus Geometric Standard Deviation Downstream of 30.5 cm Packed Bed 7-15

7-10 Collection Efficiency Versus Gas Velocity in the Zigzag Baffle Device with n = 6 and $\theta = 30°$. 7-17

7-11 Collection Efficiency Versus Gas Velocity in the Zigzag Baffle Device with n = 6 and $\theta = 30°$, $d_{pg} = 380$ μm and $\sigma_g = 1.52$. . . . 7-18

7-12 Collection Efficiency Versus Gas Velocity in Zigzag Baffle Device with n = 6, $\theta = 30°$, $d_{pg} = 1,225$ μm and $\sigma_g = 1.75$. Theory Predicts 100% Efficiency. 7-19

7-13 Experimental Collection Efficiency as a Function of Gas Velocity in the Vertical Baffles. Solid Line Represents Theory 7-20

7-14 Dry Pressure Drop in Baffles Versus Gas Velocity 7-23

7-15 Wet Pressure Drop in Baffles Versus Gas Velocity 7-24

7-16 Outlet Drop Diameter Versus Gas Velocity for Zigzag Baffles with Inlet Mass Median Diameter of 380 μm 7-25

7-17 Outlet Drop Diameter Versus Gas Velocity for Zigzag Baffle with 1,225 μm Inlet Mass Median Drop Diameter. 7-26

7-18 Size Distribution of Drops Leaving Baffle Entrainment Separators 7-27

7-19 Maximum Outlet Drop Diameter in the Entrainment Versus Gas Velocity for Zigzag Baffles 7-28

No. Page

7-20 Drop Diameter Versus Geometric Standard Deviation at Zigzag Baffle Outlet 7-30

7-21 Effect of Gas Velocity and Liquid Load on Performance of Baffle Type Separator. . . . 7-31

7-22 Some Observed Phenomena in Entrainment Separator. 7-32

7-23 Experimental Collection Efficiency of Wire Mesh as a Function of Gas Velocity 7-34

7-24 Pressure Drop in Wire Mesh Versus Gas Velocity with Liquid Load as Parameter 7-36

7-25 Outlet Drop Diameter Versus Gas Velocity for Mesh with 82 μm Inlet Drop Diameter . . . 7-37

7-26 Outlet Drop Diameter Versus Gas Velocity for Mesh with 1,225 μm Inlet Drop Diameter . . 7-38

7-27 Maximum Outlet Drop Diameter in the Entrainment Versus Gas Velocity for Mesh . . . 7-39

7-28 Drop Diameter Versus Geometric Standard Deviation for Mesh 7-40

7-29 Effect of Gas Velocity and Liquid Load on Performance of Mesh 7-41

7-30 Onset of Reentrainment Velocity Curves for Mesh 7-43

7-31 Collection Efficiency Versus Gas Velocity in Tube Bank with n = 6, d_{pg} = 84 μm and σ_g = 1.32 7-45

7-32 Collection Efficiency Versus Gas Velocity in Tube Bank with d_{pg} = 380 μm and σ_g = 1.52 . 7-46

7-33 Collection Efficiency Versus Gas Velocity in Tube Bank 7-47

7-34 Dry Pressure Drop in Tube Bank Versus Gas Velocity 7-50

7-35 Wet Pressure Drop in Tube Bank Versus Gas Velocity 7-51

No. Page

7-36 Friction Factor Versus Gas Velocity in the Bank of Tubes 7-52

7-37 Outlet Drop Diameter Versus Gas Velocity for Tube Bank with 380 μm Inlet Drop Diameter 7-54

7-38 Outlet Drop Diameter Versus Gas Velocity for Tube Bank with 1,230 μm Inlet Drop Diameter 7-55

7-39 Size Distribution of Drops Leaving Tube Bank Entrainment Separators 7-56

7-40 Outlet Mass Median Drop Diameter Versus Geometric Standard Deviation for Tube Bank . . 7-57

7-41 Maximum Drop Diameter in the Entrainment Versus Gas Velocity for Tube Bank 7-58

7-42 Experimental Results Showing the Effect of Gas Velocity and Liquid Load on Performance of Tube Bank 7-59

7-43 Pressure Drop in the Empty Section Versus Gas Velocity 7-60

7-44 Dry Pressure Drop Versus Gas Velocity in Different Separators Used in Pilot Plant . . . 7-62

7-45 Pressure Drop Through Entrainment Separator As a Function of Superficial Gas Velocity . . 7-63

7-46 Comparison of Pressure Drop Data of Houghton and Radford with Present Data 7-64

7-47 Minimum Outlet Drop Diameter Versus Gas Velocity 7-70

LIST OF TABLES

No.		Page
3-1	Summary of Available Information on Entrainment Separators	3-4
3-2	Summary of Conventional Entrainment Separators	3-5
3-3	Packing Factors, "F", for Dumped Pieces	3-18
3-4	Packing Factors, "F", for Grids and Stacked Pieces	3-20
3-5	Knitted Mesh Specifications	3-30
3-6	Mesh Parameters	3-67
6-1	Nozzles Used in Spray Section	6-7
7-1	Nozzles Used in Spray Section	7-2
7-2	Drop Size Analysis	7-5
7-3	Comparison of Baffle Type Entrainment Separators	7-21
7-4	Comparison of Tube Banks	7-48
7-5	Comparison of Wire Mesh Demister	7-65
7-6	Effect of Liquid Load on Reentrainment in Different Entrainment Separators	7-67
7-7	Observed Minimum Drop Size in the Reentrainment	7-69
7-8	Reentrainment Observed by Kotov	7-71
A-1	Overall Performance of Entrainment Separator	A-1
A-2	Drop Diameters of the Entrainment Entering and Leaving the Test Section	A-8
A-3	Liquid Material Balance	A-16
A-4	Pressure Drop Data	A-23

NOMENCLATURE

Latin

A = fractional area of the entrained drops projected onto a plane

A = total flow area, cm^2

A' = measured value of the fractional area of a plane occupied by the drops

a = acceleration due to centrifugal force, cm/sec^2

a' = cross-sectional area of all the tubes in one row, cm^2

a_1 = height of entrance to cyclone, cm

a_2 = specific area of mesh; surface area of wires per unit volume of mesh pad, cm^2/cm^3

a_3 = constant of Equation (3-22)

a_4 = defined after Equation (3-52), constant

a_5 = defined in Equation (3-57), constant

a_6 = defined after Equation (3-59), constant

B = empirical constant for Equation (3-41)

b = spacing between two consecutive baffles in the same row, cm

b' = perpendicular distance between two consecutive baffles in the same row, cm

b_1 = width of entrance to cyclone, cm

b_e = diameter of bottom part of cone, cm

C = wave velocity

C = parameter reflecting the shape of the cyclone

C' = Cunningham correction factor

C_d = drag coefficient

c = number concentration, $\#/cm^3$

c_o = initial number concentration, $\#/cm^3$

c_1, c_2 = constants, defined by Equation (7-1)

Preceding page blank

d = bubble diameter, cm

d_o = duct diameter, cm

d_b = blot diameter, cm

d_b' = measured blot diameter, cm

d_c = cyclone diameter, cm

d_{c_1} = packing diameter, cm

d_e = diameter of exit pipe of cyclone, cm

d_{eq} = equivalent (hydraulic) diameter of liquid film, cm

d_h = sieve plate hole diameter, cm

d_{jet} = diameter of jet, cm

d_ℓ = size parameter, cm

d_m = knitted mesh wire diameter, cm

d_{mm} = mass median drop diameter, cm

dn_i = number of drops removed

d_p = drop diameter, cm

d_{pa} = aerodynamic drop diameter, cm $(g/cm^3)^{1/2}$

$(d_{pf}/dz)_L$ = frictional pressure gradient for liquid flowing alone in a tube, dyne/cm³

$(d_{pf}/dz)_G$ = frictional pressure gradient for gas flowing alone in a tube, dyne/cm³

d_{pg} = inlet mass median drop diameter, cm

d_s = Sauter mean diameter, cm

$d_{s,\ell}$ = diameter of large drops, cm

$d_{s,s}$ = diameter of small drops, cm

E = fractional collection efficiency of an entrainment separator

F = packing factor

F_1 = foam density, ratio of clear liquid height to total foam height

F_w = correction factor = 1.1

f = friction factor

f_D = drag coefficient

f_G = friction factor in the absence of liquid phase

f_h = fraction of the perforated open area in the plate

G = mass flow rate of gas, Kg/m^2sec

G_L = mass flow rate of liquid, Kg/m^2sec

G_G = mass flow rate of gas, Kg/m^2sec

g = acceleration of gravity, cm/sec^2

H_d = fractional liquid hold-up in the bed

h = overall cyclone height, cm

h_1 = height of a jet, cm

h_{dp} = dry-plate head loss

h_{ow} = head over the weir

h_r = residual pressure drop

h_s = height of vertical cylinder of cyclone, cm

h_w = weir height

j = ratio of channel width to packing diameter

K_p = inertial parameter

K = Kutateladze number

K_1 = constant

L = mass flow rate of liquid, Kg/m^2sec

ℓ = length of baffle, cm

ℓ_1 = natural height of vortex in cyclone, cm
ℓ_2 = length of mesh pad in the direction of flow, cm
ℓ_3 = unbroken length of jet, cm
ℓ_4 = broken length of jet, cm
N = number of blots in a given area if the blots do not overlap
N = number of stages in the tube bank
N' = number of blots in a given area
$N_{Re,D}$ = drop Reynolds number
$N_{Re,G}$ = gas Reynolds number
$N_{Re,L}$ = liquid Reynolds number
n = number of rows of baffles or tubes
n = vortex exponent
n_1 = number of semicircular bends in packed bed
n_j = collection efficiency for a given particle diameter in one stage of rectangular jet impingement
P = dimensionless parameter defined by Equation (5-15)
P = pressure, dyne/cm^2
P_o = pressure outside bubble, dyne/cm^2
P_1 = pressure due to gas velocity, dyne/cm^2
Pt = penetration
ΔP = pressure drop, cm W.C.
ΔP_{dry} = pressure drop in absence of liquid, cm W.C.
ΔP_L = pressure drop due to presence of liquid, cm W.C.
$\Delta P_{wet} = \Delta P_{dry} + \Delta P_L$

Q = volumetric flow rate, cm^3/sec

$Q_{L,g}$ = liquid flow rate due to gravity, cm^3/sec

R = entrainment parameter defined by Equation (3-41)

r = radius, cm

S = distance traveled by drop, cm

S_1 = height of exit pipe inside cyclone, cm

T = temperature, °K

t = time

t_1 = blot thickness, cm

u_1 = cyclone inlet velocity, cm/sec

u_G = superficial gas velocity, based on empty duct, cm/sec

u_G' = actual gas velocity, cm/sec

$\bar{u}_G$ = mean gas velocity, cm/sec

u_{GC} = reentrainment velocity, critical gas velocity for reentrainment, cm/sec

u_t = terminal deposition velocity, cm/sec

u_{tg} = tangential velocity, cm/sec

v_h = velocity of gas through hole in sieve plate, cm/sec

v_G' = actual gas velocity near the tubes

v_r = relative velocity, cm/sec

W = mass flow rate, g/sec

W_{LE} = mass flow rate of entrained liquid, g/sec

w = baffle width

w_1 = weir length, m

X = Martinelli parameter defined by Equation (3-40)

Y = distance from baffle to any point in the liquid film, cm

Z = bed length, cm

Greek

α = volumetric flow ratio

α_o = initial surface disturbance, cm

α_1 = amplitude of surface disturbance of a jet, cm

δ = liquid film thickness, cm

ε = bed porosity

η = target efficiency

θ = angle between baffle and gas flow

λ = defined in Equation (3-34)

μ = viscosity, poise

ν = kinematic viscosity, cm^2/sec

ρ = density, g/cm^3

σ = surface tension, dyne/cm

σ_G = geometric standard deviation of inlet entrainment

τ = shear stress, dyne/cm^2

ψ = size or operating characteristic of a cyclone

ψ_1 = defined in Equation (3-35)

Subscripts

a = air

i = interfacial

G = gas

L = liquid

p = drop

w = water

ABSTRACT

Entrained drops of liquid must be separated from the gas leaving scrubbers. This report gives results of an evaluation of present technology, experimental studies of entrainment separator characteristics, and theoretical analysis. A pilot plant with 85 m^3/min (3,000 CFM) maximum capacity was built and experiments performed on zigzag baffle, knitted mesh, tube bank, packed bed, and cyclone devices. Horizontal gas flow was used in all cases, and the cyclone axis was vertical.

Drop size distribution measurements on the inlet and outlet enable the determination of collection efficiency and reentrainment as related to drop size. Pressure drop as a function of gas flow rate is also reported. Mathematical models for primary collection efficiency are satisfactory but useful reentrainment models are not yet available.

An auxiliary experiment was made to determine reentrainment from liquid sheets under the influence of an air stream. Work is still in progress on vertical gas flow systems, solid deposition, mathematical modeling, and the development of improved designs.

INTRODUCTION

"Wet scrubber entrainment separators" are defined as devices which remove the liquid introduced in the scrubber for separation of particulate or gaseous contaminants from a gas. In general, entrainment separators are devices used to remove liquid or solid entrainment from the fluids. The most common entrainment separators are cyclones, zigzag baffles, mesh and packed beds.

In wet scrubbers the liquid introduced to remove gaseous, liquid or solid pollutants forms drops which are carried out by the gas. The function of the separator is to remove this liquid entrainment from the gas.

In the past relatively little attention was paid to entrainment separators because they did not create severe problems. Recent experience with sulfur dioxide scrubbers on utility boilers has shown that entrainment separator performance and operating problems are crucial to the operation of the entire scrubber system. Appreciable quantities of solids have been introduced in the effluent stream by entrained solution and/or slurry mist.

For the design of entrainment separators one needs relationships defining overall collection efficiency and pressure drop. The overall collection efficiency gives the combined effects of primary collection efficiency and reentrainment. The latter occurs at high gas velocity, reducing the overall collection efficiency, and thereby imposing a penalty for operation at high velocity.

One other cause for an upper limit on gas velocity is flooding. When the gas flow prevents liquid from draining, flooding takes place. Flooding is common in packed bed and wire mesh separators, where the specific surface area is high. Liquid drainage from the entrainment separator is a related problem. Poor drainage will contribute to increased effects of reentrainment and flooding.

Separators also suffer from plugging and caking due to particle deposition and solute precipitation. Plugging and caking increase pressure drop and corrosion rate. The return slurry may also plug the liquid draining pipe and flood the separator this way.

While some data have been collected to determine the overall performance of scrubber systems in the industry, it was usually assumed that the entrainment separator has 100% efficiency. Thus, data on industrial size entrainment separator efficiency have not previously been available.

SCOPE

This report was prepared by A.P.T., Inc. as required in E.P.A. Contract 68-02-0637. The Scope of Work was defined by E.P.A. as follows:

1. Evaluate Technology

   The Contractor shall evaluate the status of present technology relating to wet scrubber entrainment separators. The Contractor shall complete the following task:

   A. Review and assess the published literature and available unpublished information, including, where appropriate, information acquired through private communication with manufacturers, designers and users of entrainment separators.

   B. Determine the availability and adequacy of operational and design data for entrainment separators.

C. Determine and evaluate the adequacy of existing theoretical models and design methods for predicting the performance of entrainment separators.

D. Review and evaluate performance of all major types of entrainment separators currently available. Assess the advantages, disadvantages and limitations of each type of equipment.

E. Identify specific operating and maintenance problems associated with entrainment separators. Particular attention will be paid to the problems encountered in SO_2 scrubbing systems under development in E.P.A. programs.

2. Experimental Study

Conduct an experimental study of gas-water systems aimed at simulating the performance of various types of entrainment separators in the presence of soluble and insoluble particulate matter. The experimental study will investigate such variables as efficiency, pressure drop, reentrainment, velocity, plugging and related problems.

3. Selection and Design

Develop improved engineering equations and methods for entrainment separator selection and design.

4. Pilot Test

Develop and evaluate on a small pilot basis new entrainment separator designs which offer improved performance, e.g., efficiency, pressure drop, velocity, freedom from reentrainment, and freedom from plugging and related problems, when compared with available entrainment separator designs.

5. Recommendations

Develop specific research and development recommendations for improving wet scrubber entrainment separators.

SUMMARY AND CONCLUSIONS

This program of investigating wet scrubber entrainment separators has been partially completed at this time. The study indicates that presently available entrainment separators suffer from various shortcomings such as overdesigns which necessitate large equipment size, lower operating velocities due to flooding or reentrainment, lack of reliable operating data on industrial separators, and plugging.

The objectives of this study are to (1) Evaluate present technology, (2) Conduct an experimental study of air-water systems aimed at simulating the performance of various types of entrainment separators, (3) Develop improved engineering equations and methods for entrainment separator selection, (4) Develop and evaluate on a small pilot basis new entrainment separator design, and (5) Develop specific research and development recommendations.

EVALUATE PRESENT TECHNOLOGY

A literature search was carried out to evaluate the technology on wet scrubber entrainment separators. Visits were made to several libraries,and the literature available in the A.P.T. library and identified by an APTIC computer search was reviewed. Manufacturers of entrainment separators were contacted by mail and asked for information. Visits were made to E.P.A. and T.V.A. facilities to identify the specific operating and maintenance problems associated with entrainment separators.

The existing theoretical and empirical models to predict the performance of the entrainment separators were evaluated. The criteria for this evaluation were soundness of derivation and closeness of comparison with actual performance.

Experimental Study

A pilot plant to study wet scrubber entrainment separators was built. It has a gas flow capacity of 85 m^3/min (3,000 CFM) and it consists of prefilter, blower, heater, spray section, observation sections, test section, various supply and catch tanks, and auxiliary equipment. Five types of entrainment separators, namely, mesh, tube bank, packed bed, cyclone, and baffles were studied. Up to now, air-water systems with cross flow have been used in the experiments. Observations include collection efficiency, pressure drop, reentrainment, flooding, drainage, drop size distribution and other variables.

Selection and Design

Attempts are made to develop mathematical models where needed. Models for determining the following were developed in the present study:

1. Primary collection efficiency in zigzag baffle type entrainment separators.
2. Pressure drop in zigzag baffle type separators.
3. Primary collection based on either complete turbulent mixing or no mixing.
4. Reentrainment in vertical zigzag baffles.
5. Reentrainment in horizontal zigzag baffles.
6. Reentrainment in a cyclone.

Auxiliary Experiment

Equipment was constructed and experiments were conducted to determine (1) Onset of entrainment velocities in separated flow, (2) Drop size distribution of entrainment, (3) Effect of duct dimension, and (4) Effect of air jets impinging on liquid film at various angles.

CONCLUSIONS

1. The theoretical model developed to determine primary collection efficiency for zigzag baffle type separator agrees fairly well with experimental results. Thus, the flow through the zigzag baffles can be described as a series of alternating bends with inertial mechanism responsible for separation.
2. The pressure drop in zigzag baffles can be determined from drag coefficients for inclined plates held in the flow.
3. The overall collection efficiency in zigzag baffles can be increased by staggering the baffles. The pressure drop may be reduced by keeping 1-3 cm distance between rows.
4. Models based on turbulent mixing reach 100% efficiency as an asymtote with increasing gas velocity. On the other hand, models based on no mixing reach 100% efficiency as a straight line on efficiency-versus-gas-velocity curve. The assumption of turbulent mixing gives better agreement with actual performance of entrainment separators.
5. It is possible to predict the drop collection efficiency of entrainment separators at low gas velocities (under industrially used conditions), at least on pilot plant scale, from the available literature.
6. At high gas velocities, reentrainment is a definite problem. Reentrainment may take place by various mechanisms such as: a) Transition from separated flow to separated-entrained flow,

b) Rupture of bubbles, c) Creeping of liquid on the entrainment separator surface, and d) Shattering of liquid drops resulting from splashing.

7. Transition from separated flow to separated-entrained flow depends upon gas velocity, liquid Reynolds number and liquid properties. The transition does not depend upon the duct dimensions. The drop size distribution is independent of the duct dimensions. The average drop diameter resulting from this transition is about 250 μm. The reentrainment velocity is considerably reduced if jets of air stream strike the liquid film at an angle. Therefore, sharp angles should be reduced to avoid reentrainment.
8. The mechanism of reentrainment in zigzag baffles is tearing of the liquid sheets caused by high gas velocities and shattering of liquid drops. Reentrainment in cross flow baffles with horizontal gas flow should be less than in baffles with vertical gas flow. Zigzag baffles inclined at 30° from gas flow direction should have less reentrainment than baffles inclined at 45° from gas flow direction.
9. The reentrainment mechanisms in packed bed and mesh pad are shattering of drops and rupture of bubbles. Reentrainment resulting from small drops (less than 40 μm) due to rupture of bubbles is insignificant.
10. The mass median drop diameter due to reentrainment was determined to vary between 80 μm and 750 μm. Large drops (above 200 μm) are present due to shattering of drops.

11. Sampling of liquid drops and entrainment needs careful consideration. Due to large drop size in the reentrainment, a sedimentation effect is present.
12. Drainage arrangements should be designed with caution. An underdesign will lead to liquid creeping in the separator and an overdesign may result in reentrainment, from drainage, due to gas flow.
13. The capital cost and the operating cost of entrainment separators in wet scrubbers represent a significant factor and therefore entrainment separators should be given more design attention.
14. The experience with wet scrubbers in power plants indicates that performance of the entrainment separator is crucial to the whole operation of the scrubber.

LITERATURE SURVEY

The literature survey and background information discussed in this chapter are examples of the selected material on entrainment separators. For brevity, all the literature in the field of separators is not mentioned. The following material summarizes what can be distilled from a survey of the background information and is a concept of what was known at the onset of this study.

Figure 3-1 describes the entrainment separator. To determine the performance of the separator, one needs to know inlet loading (concentration and drop diameter), primary collection efficiency, reentrainment, secondary collection, liquid drainage and pressure drop. These factors may be considered from a design point of view. The inlet loading coupled with operating conditions will determine reentrainment and drainage. Also, different entrainment separators are limited to certain drop diameters, below which their efficiency falls off sharply. It is necessary to have engineering equations to determine primary collection efficiency and pressure drop.

If the reentrainment rate and the size distribution of the reentrained drops are known, secondary collection may be determined. At the time of this study, no work had been reported on the rate of reentrainment. All one can determine at this point is the range of gas velocities at which onset of reentrainment takes place. The size distribution of the reentrained drops may be guessed by assuming the most probable mechanism of reentrainment for a given separator.

Knowledge of the pressure drop through a system is important in calculating the energy loss incurred and in selecting the proper pumps and other auxiliary equipment to overcome that energy loss.

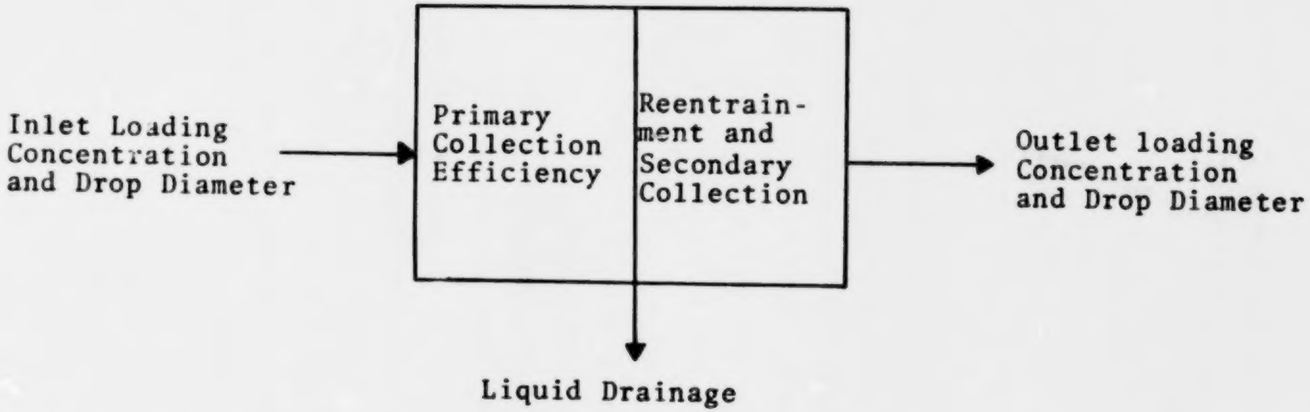
Inlet Loading
Concentration
and Drop Diameter
Primary
Collection
Efficiency
Reentrain-
ment and
Secondary
Collection
Outlet loading
Concentration
and Drop Diameter
Liquid Drainage

Figure 3-1. Entrainment separator

Information which has been obtained from the literature survey is presented in Tables 3-1 and 3-2. A summary of the literature search, dealing with primary collection efficiency, pressure drop, reentrainment, entrainment separator problems and details of separators now in use, follows.

COLLECTION MECHANISMS

Knowledge of the basic mechanisms of drop collection is fundamental to an understanding of entrainment separators. Some of these mechanisms are inertial impaction, interception, sedimentation, diffusion and electrostatic precipitation. Normal industrial operating conditions for wet scrubbers are such that exiting drop diameters are larger than 50 μm. The design and operating conditions of separators thus favor inertial impaction and sedimentation as the principal mechanisms of collection.

Inertial Impaction

This is the major drop collection mechanism in wet scrubber entrainment separators. When fluid approaches an obstacle the fluid streamlines spread around it. At the same time inertial forces carry drops across the streamlines so that the drops hit and stick to the obstacle. It is assumed that all drops colliding with the obstacle adhere to it.

Two factors determine impaction collection efficiency. The first is the velocity distribution of the gas flowing by the collector, which varies with the Reynolds number of the gas with respect to the collector. The second factor is the drop trajectory, which depends on the mass of the drop, its air resistance, the size and shape of the collector, and the rate of flow of the gas stream.

Table 3-1. SUMMARY OF AVAILABLE INFORMATION ON ENTRAINMENT SEPARATORS

	Typical Inlet Loading		Primary Collection Efficiency	Pressure Drop	Approx. Velocity for Reen-trainment	Reen-trainment Drop Diameter
	Concen-tration	Drop Diameter				
Cyclone	$< 2\ell/m^3$	>5μm	✓	✓	15-50m/sec	70-400μm
Mesh type Separator	$< 2.7\text{x}10^{-2}$ cm^3/sec cm^2 of liquid	> μ	✓	✓	5-15m/sec	100-500μm
Tube Bundle	--		✓	✓	< 20m/sec	
Packed Beds	$\frac{L}{G} < 3$	>3μm	✓	✓	1-1.5m/sec	100-500μm
Sieve Plates			✓	✓	≈3m/sec	small drops ≈50μm large drops ≈0.1cm
Baffles	--	>20μm	X	X	≈3.4m/sec	100-500μm
Mechani-cally Aided			X	X		
Impingement Type		>3μm	✓	✓	30-45m/sec	

✓ Design information available in literature
X Design information not avialable in literature

Table 3-2. SUMMARY OF CONVENTIONAL ENTRAINMENT SEPARATORS

Entrainment Separator (Construction Material)	Maximum Capacity m^3/sec	Minimum Drop Size	Gas Velocities m/sec	Separation Efficiency for Minimum Drop	Pressure Drop cm W.C.	Liquid Load Maximum	Comments
Cyclone (Steel,S.S.)	141	5μm (2μm for small cyclones	Maximum 15-20	95%	5-15		Surfaces may erode easily
Mesh (Any material that can be drawn into wire)		5μm (1-5μm for series combination)	0.3-5	95%	0.5-3	2.5×10^{-3} g/sec-cm^2	Basically 3 different mesh 1. Crimped in alternate direction. 2. Nested double layer. 3. Wound. (Can plug easily)
Fiber Bed (Needs fibers 1-10μm)		0.3μm	0.025-0.15	99%	10-15		Can plug easily
Packed Bed (Packing of any mat'l)	65	3μm	0.75-2.5	85%	5-10% of bed length	From generalized correlation	Better drainage in cross flow
Baffles (Any mat'l)		10μm	2-3.5	85-95%	2-2.5	5% of gas flow rate by weight	Vertical baffles give better drainage than horiz.

The equations of motion, the size and shape of the collector, the mass of the drop and operating conditions may be used to determine target collection efficiency. Figure 3-2, from Golovin and Putnam (1962), gives theoretical impaction efficiency as a function of the inertial parameter for different targets.

Sedimentation

The second collection mechanism important in entrainment separators is sedimentation. Figure 3-3, from Fuchs (1964), is a plot of drop terminal settling velocity versus drop radius. Drop diameters encountered in wet scrubber entrainment may vary from 50 to 500 μm, and the terminal settling velocity for these drops will therefore range from 0.1 to 2.0 m/sec. The gas velocities used in entrainment separators vary from 1.0 to 12.0 m/sec; however, except for cyclone-type separators, which operate at very high velocities, most operate below 4.0 to 5.0 m/sec. Therefore, sedimentation can be expected to affect the separation of drops.

ENTRAINMENT DROP DIAMETERS

To determine primary collection efficiency, it is necessary to know the inlet entrainment drop diameter, which depends on the entrainment source. The drop diameter may be obtained by direct measurement or by the following method if, as is often the case in wet scrubbers, entrainment is cuased by pneumatic atomization. A correlation presented by Nukiyama (1938, 1940) gives Sauter mean diameter as:

$$d_s = \frac{58,600}{v_r}\left(\frac{\sigma}{\rho_L}\right)^{0.5} + 597\,{\frac{\mu_L}{\sqrt{\rho_L \sigma}}}^{0.45}\left(1,000\,\frac{Q_L}{Q_G}\right)^{1.5} \qquad (3\text{-}1)$$

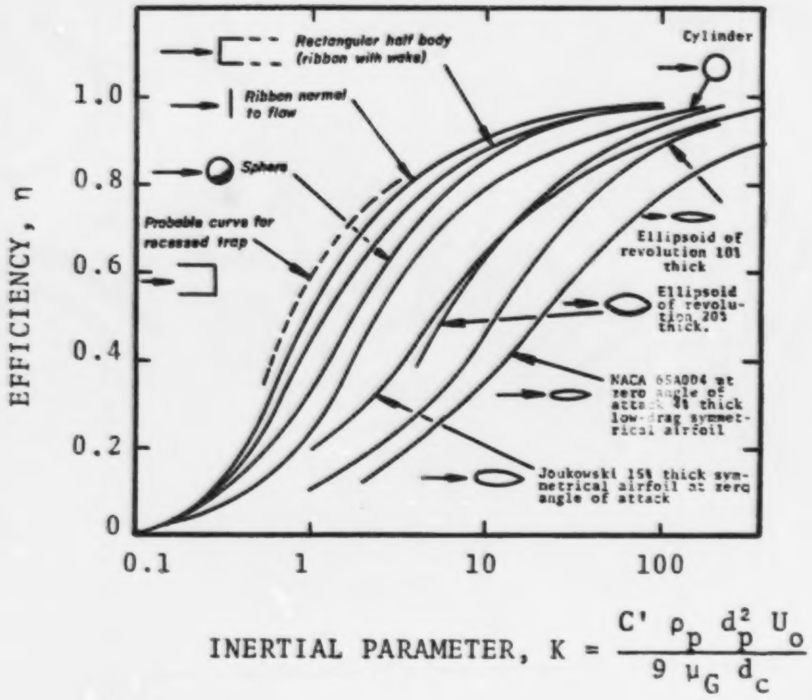

Figure 3-2 - Theoretical impaction efficiency as a function of inertial parameter for different targets.
Golovin & Putnam (1962)

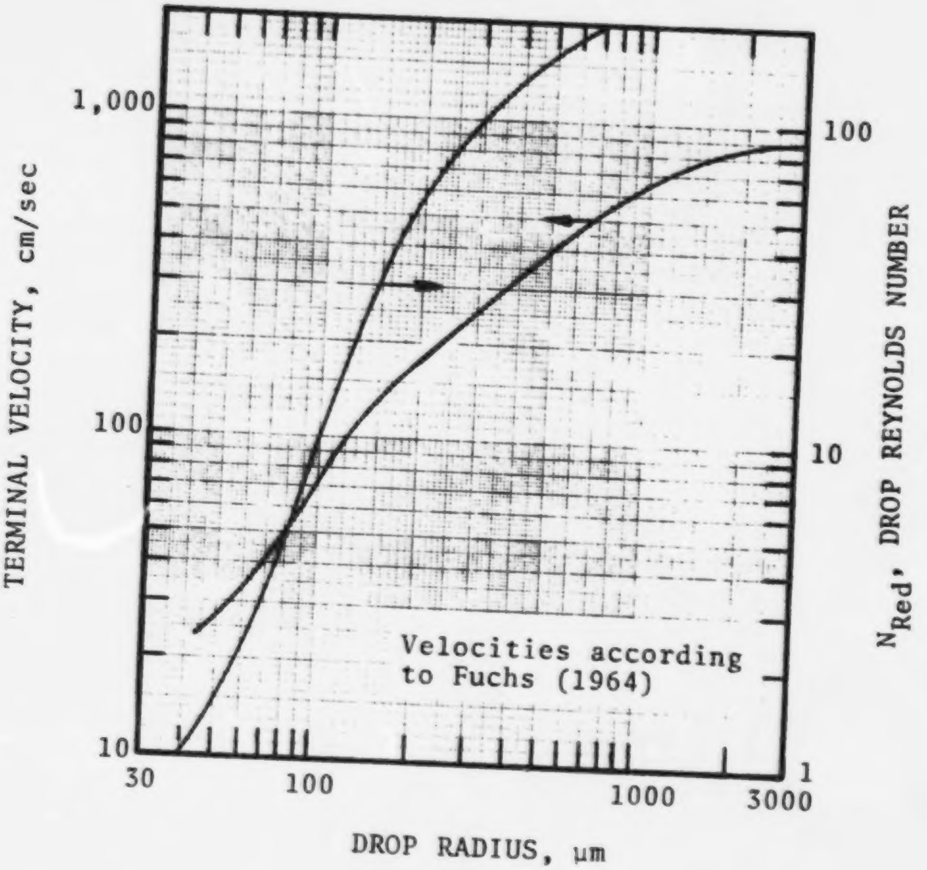

Figure 3-3 - Terminal settling velocity and Reynolds number for water drops in air at 20°C and 760 mm Hg. After Fuchs (1964)

where d_s = Sauter mean diameter, cm
v_r = relative velocity, cm/sec
σ = surface tension, dyne/cm
ρ_L = liquid density, g/cm^3
μ_L = liquid viscosity, poise
Q_L/Q_G = liquid to gas volumetric ratio

In wet scrubbers the liquid load, Q_L/Q_G, varies between 1.33×10^{-4} m^3/m^3 and 4×10^{-3} m^3/m^3 (1-30 gal/1,000 CFM). Gas velocities are on the order of 60-100 m/sec (200-300 ft/sec). The drop diameters obtained under these operating conditions are between 50 μm and 500 μm.

If the liquid entrainment is formed in any other manner, the entrainment drop diameter may be obtained as explained later in this chapter in the section for the appropriate reentrainment mechanism.

DESIGN EQUATIONS FOR ENTRAINMENT SEPARATORS

Our examination of collection mechanisms yielded the basis upon which equations for primary collection efficiency have been developed. Methods for determining entrainment drop diameter, a key variable in the calculation of primary efficiency, were also reviewed.

Another important factor in the design of entrainment separators is the pressure drop. A knowledge of the pressure drop through a separator is useful for the selection of auxiliary equipment such as blowers and for calculating the separator's operating costs.

Six different kinds of entrainment separators will be discussed in this section: cyclone, packed bed, zigzag baffles, tube bank, mesh and sieve plate. A brief description of each is given, after which, equations for primary efficiency and pressure drop are presented. These equations were selected as the best available expressions, based on agreement with experimental data and soundness of derivation. Calvert et al. (1972) have evaluated some of these equations.

The following assumptions are generally made in the derivation of the primary collection efficiency equations:

1. A drop is spherical in shape.
2. The motion of a drop is not influenced by the presence of neighboring drops.
3. All drops striking the collector surface adhere.

Cyclone

Commercially available cyclones in standard designs for entrainment separators have a maximum capacity of up to 141 m^3/sec (300,000 CFM) of gas. Efficiencies of about 95% are claimed for 5 μm diameter drops in a well-designed cyclone. Some manufacturers use a bundle of small cyclones (multicyclones), which can efficiently collect drops as small as 2 μm in diameter. However, this arrangement reduces the capacity of the device.

Primary Efficiency - Leith and Licht (1971) derived an equation to predict primary collection efficiency in conical bottom cyclones as pictured in Figure 3-4. With slight modification it can be applied to cylindrical cyclones. The following assumptions were made:

1. The drag force in the radial direction on the drop is given by Stokes law.
2. The tangential velocity component of the drop is related to the radial position by a modified form of the equation for a free vortex in an ideal fluid:

$$u_{tg} r^n = \text{constant} \qquad (3\text{-}2)$$

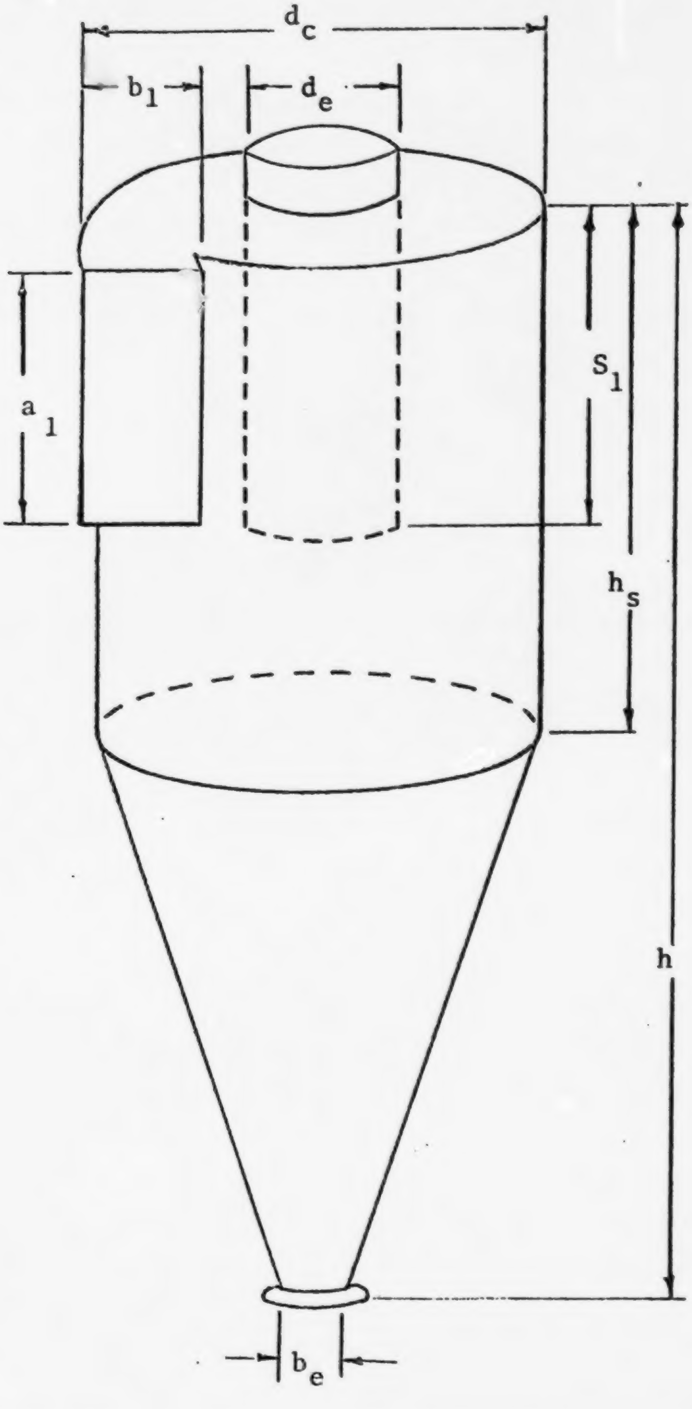
d_c
b_1
d_e
a_1
S_1
h_s
h
b_e

Figure 3-4. - Cyclone with tangential gas inlet.

where "r" is the distance from the vertical axis of the cyclone and "n" is defined below in equation (3-5).

3. Backmixing of the drops takes place in the gas phase.

The primary efficiency for a conical bottom cyclone is expressed as:

$$E = 1 - \exp\left[2\,(C\Psi)^{1/(2n+2)}\right] \qquad (3\text{-}3)$$

$$C = \frac{\pi\, d_c}{a_1 b_1}\left[2\left(1 - \frac{d_e}{d_c}\right)^2\left(S_1 - \frac{a_1}{2}\right) + \frac{1}{3}\left(\ell_1 + S_1 - h_s\right)\left(1 + \frac{d_e}{d_c} + \frac{d_e^2}{d_c^2}\right) + h_s - \frac{d_e^3}{d_c^2}\,\ell_1 - S_1\right] \qquad (3\text{-}4)$$

$$n = 1 - \left[\frac{T}{283}\right]^{0.3}\left[1 - \frac{(0.393\, d_c)^{.14}}{2.5}\right] \qquad (3\text{-}5)$$

$$d_\ell = d_c - (d_c - b_e)\left(\frac{S_1 + \ell_1 - h_s}{h - h_s}\right) \qquad (3\text{-}6)$$

$$\ell_1 = 2.3\, d_e\left(\frac{d_c^2}{a_1 b_1}\right)^{1/3} \qquad (3\text{-}7)$$

$$\Psi = K_p\,\frac{n+1}{2} = \left(\frac{\rho_p\, d_p^2\, u_{tg}}{18\,\mu_G\, d_c}\right)(n + 1) \qquad (3\text{-}8)$$

where E = fractional collection efficiency of an entrainment separator

C = parameter reflecting the shape of the cyclone

Ψ = size or operating characteristic

n = vortex component

d_c = cyclone diameter, cm

a_1 = height of the entrance to the cyclone, cm

b_1 = width of the entrance to the cyclone, cm

d_e = gas exit pipe diameter in cyclone, cm

S_1 = height of the exit pipe inside the cyclone, cm

ℓ_1 = natural height of vortex in cyclone, cm

h_s = height of vertical cylinder of cyclone, cm

d_ℓ = size parameter, cm

T = temperature, °K

b_e = diameter of bottom part of cone, cm

h = overall cyclone height, cm

K_p = inertial parameter

σ_p = drop density, g/cm^3

d_p = drop diameter, cm

u_{tg} = tangential velocity, cm/sec

μ_G = gas viscosity, poise

Pressure Drop - Because cyclones are operated at higher gas velocities than other entrainment separators, the pressure drop in a cyclone is usually higher than in other devices. Cyclones are sometimes equipped with inlet vanes, which serve to introduce the gas stream to the cyclone more smoothly. The pressure drop in a device with an inlet vane is expected to be lower than in one without. Shepherd and Lapple (1940) derived an equation for a cyclone with inlet vanes for pressure drop as a function of inlet gas velocity and the cyclone inlet and outlet dimensions:

$$\Delta P = 0.00513\ \rho_G \left(\frac{Q_G}{a_1 b_1}\right)^2 \left(\frac{7.5\ a_1 b_1}{d_e^2}\right) \qquad (3\text{-}9)$$

where ρ_G = gas density, g/cm³

Equation (3-9) can be modified by writing it as a function of the geometric average of the gas velocity at the cyclone inlet and outlet:

$$\Delta P = 0.00513 \times 5.89\ \rho_G\ v_{Ave}^2 \qquad (3\text{-}10)$$

Shepherd and Lapple also developed an equation for a cyclone without inlet vanes:

$$\Delta P = 0.00513\ \rho_G \left(\frac{Q_G}{a_1 b_1}\right)^2 \left(\frac{16\ a_1 b_1}{d_e^2}\right) \qquad (3\text{-}11)$$

Packed Bed

Packed beds of standard design with a capacity of up to 65 m³/sec (140,000 CFM) are available. They can remove drops as small as 3 μm in diameter at 80-90% efficiency. Superficial gas velocities range from 75 to 250 cm/sec, and pressure drop is generally low, 0.05 - 0.1 cm W.C. per cm of bed length.

Cross flow beds are claimed to have high drainage efficiency and therefore are less prone to plugging. Upstream washing is recommended to avoid plugging if solids are present in the drops to be removed.

Packing in different materials, shapes and sizes is available. Tellerete rings are claimed to have high collection efficiency and low pressure dorp.

Packed beds are often used for mass transfer because of their high interfacial area. Thus they are sometimes employed when simulatneous mass transfer and entrainment separation are desired.

Primary Efficiency - Jackson and Calvert (1966) and Calvert (1968) have developed a theoretical relationship between particle collection efficiency and packed bed operating parameters by considering the bed to be made of a series of semicircular channels. Their formulation included the following assumptions:

1. The drag force on the drop is given by Stokes Law.
2. The number of semicircular bends, "n_1", is related to the overall height, "Z", of the packed section of the bed, the packing diameter, "d_c", and the channel width, "b_1", when any consistent units may be used, by:

$$n_1 = \frac{Z}{d_c + b_1} \qquad (3\text{-}12)$$

These assumptions led to the following equation for predicting the primary efficiency for a packed bed

$$E = 1 - \exp\left[\frac{2\pi}{2(j + j^2)\,(\varepsilon - H_d)}\ \frac{Z}{d_{c1}}\ K_p\right] \qquad (3\text{-}13)$$

$$j = \frac{b}{d_{c1}} \qquad (3\text{-}14)$$

$$K_p = \frac{u_G\ d_{pa}}{9\ \ G\ d_c} \qquad (3\text{-}15)$$

where j = ratio of channel width to packing diameter
= bed porosity
H_d = fractional liquid hold-up in the bed
Z = bed length, cm
d_{c1} = packing diameter, cm
u_G = superficial gas velocity, cm/sec
d_{pa} = aerodynamic drop diameter, cm(g/cm³)$^{1/2}$

Pressure Drop - Perry (1963) gives a generalized pressure drop and flooding correlation plot which appears as Figure 3-5, where a dimensional group of function $\frac{G^2 F \Psi \mu_L{}^{0.2}}{\rho_G \rho_L g}$, (centipoise)^{02}, is plotted against a dimensionless group of function $\frac{L}{G}\left(\frac{\rho_G}{\rho_L}\right)^{1/2}$, where "G" and "L" refer to the gas and liquid mass flow rates respectively. Values for the packing factor, "F", for dumped pieces, stacked pieces and grids are given in Tables 3-3 and 3-4. If "F" is not known, $\frac{a}{\varepsilon^3}$ may be used instead.

The operation of packed beds is limited by flooding. The flooding lines for dumped pieces, grids and stacked rings are shown in Figure 3-5. Pressure drop should be obtained by using the largest gas and liquid streams.

Zigzag Baffles

Baffles can efficiently separate drops greater than 10 μm in diameter, while some of the better designed devices can separate drop diameters of 5-8 μm. Common gas velocities are 2.0-3.5 m/sec, and the pressure drop for a 6-pass separator is about 2-2.5 cm W.C.

The most common baffle shape is zigzag with 3 or 6 passes. These can be fabricated from a continuous wavy plate or each pass is separated, in which case the separation distance is normally smaller than the width of the baffles. Cross-flow baffles are claimed to have higher drainage capacity than countercurrent flow baffles.

Primary Efficiency - A theoretical equation to predict primary collection efficiency in zigzag baffles is not available. However, Sarokin, Demidova and Kuzman (1968) give the condition for minimum entrainment in the exit stream:

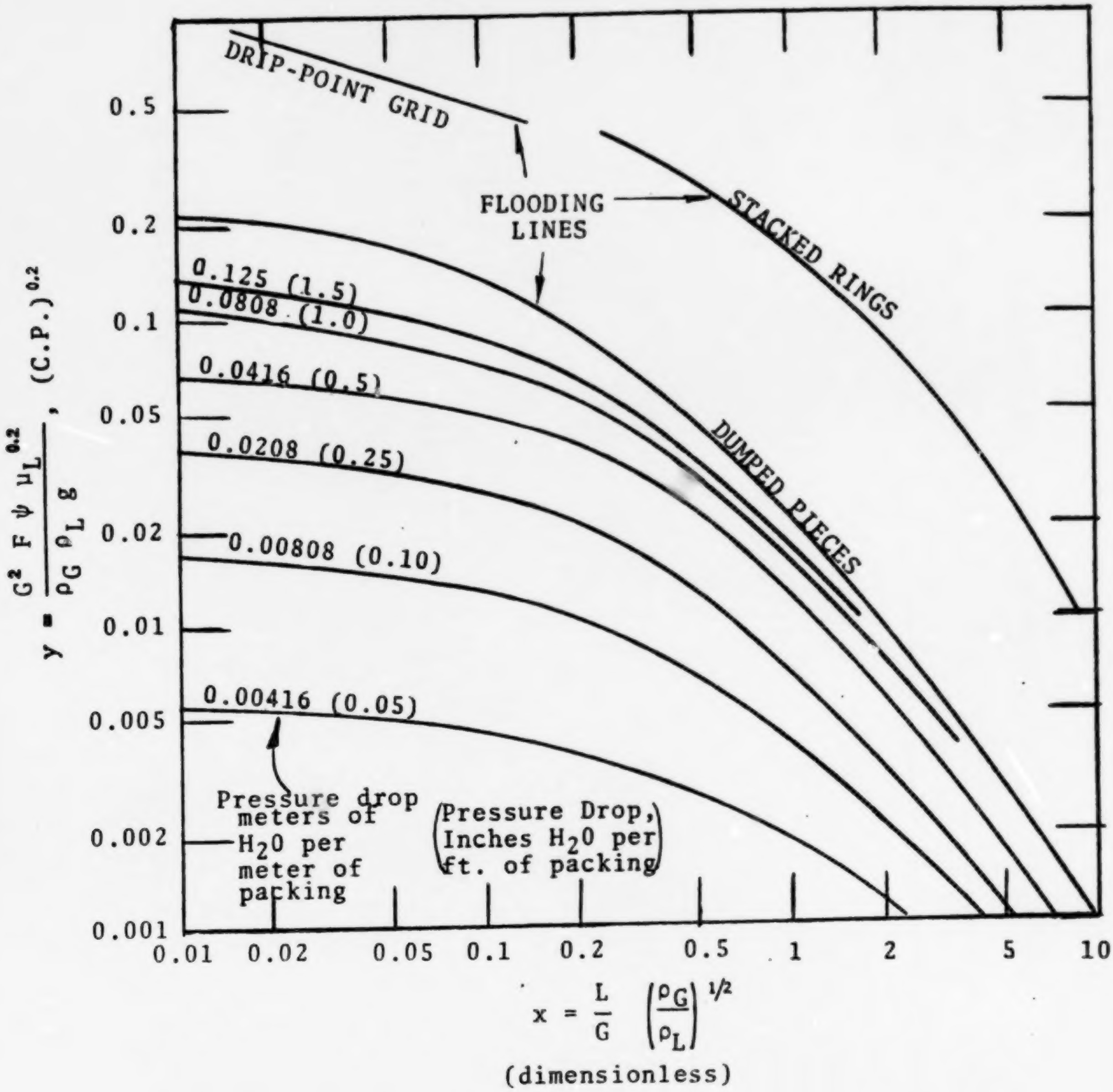

Figure 3-5 - Generalized flooding and pressure drop correlation for packed beds (Perry, 1963).

Table 3-3. PACKING FACTORS, "F", FOR DUMPED PIECES (m^2/m^3)

	Nominal size of packing, cm										
	[0.64]	[0.95]	[1.27]	[1.59]	[1.9]	[2.5]	[3.2]	[3.8]	[5]	[8]	[10]
Raschig rings, ceramic											
.16 cm wall	5,250	3,280									
.32 cm wall						510					
.63 cm wall								430	210		
.95 cm wall										121	98
Raschig rings, carbon											
.16 cm wall	5,250		1,340								
.32 cm wall					920	525					
.63 cm wall								430	210		
.79 cm wall										118	
Raschig rings, metal											
.08 cm wall	2,300	1,280	980	560	510	380					
.16 cm wall			1,340	950	720	450	360	272	187	105	
Lessing rings, porcelain											
.32 cm wall						(800)					
.63 cm wall									(360)		
Lessing rings, metal											
.08 cm wall			(1,060)		(630)						
.16 cm wall						(472)	(387)	(295)	(200)		

Table 3-3. PACKING FACTORS, "F", FOR DUMPED PIECES (m^2/m^3) (continued)

	Nominal size of packing, cm										
	[0.64]	[0.95]	[1.27]	[1.59]	[1.9]	[2.5]	[3.2]	[3.8]	[5]	[8]	[10]
Partition rings										262	190
Pall rings, plastic				318		171		105	82		
Pall rings, metal				230		158		92	66		
Berl saddles	2,950		790		560	360		213	148		
Intalox saddles, ceramic	2,380	1,080	660		475	322		171	131	72	
Intalox saddles, plastic						108			69	52	
Super-Intalox, ceramic						200			100		
Pellerettes									150		

Parentheses denote a value of a/ε^3, rather than empirical F.

Table 3-4. PACKING FACTORS, "F", FOR GRIDS AND STACKED PIECES (m^2/m^3)

	Nominal size of packing, cm							
	2.5	3.8	5	8	10	13	14	15
Wood grid	20	11	8.2	5.9	4.9			
Metal grid	8.2							
Grid tiles						118		
Checker brick, ε=0.55							135	
Raschig rings, ceramic								
.63 cm wall			95	16				
.95 cm wall				36	12.8			
Raschig rings, metal				21				
Partition rings, diameter								
7.6 cm length				(1,200)	(725)			
10.2 cm length					(705)			(410)
15.2 cm length								(375)
Partition rings, square set								
7.6 cm length				(690)	(460)			
10.2 cm length					(450)			(275)
15.2 cm length								(260)

Parentheses denote a value of a/ε^3, rather than empirical F.

$$0.35 < k = 10\ \mu_G \left(\frac{\rho_G}{g^2 \sigma (\rho_L - \rho_G)} \right)^{1/2} < 0.40 \qquad (3\text{-}16)$$

where k = Kutateladze number

This equation was confirmed with experimental data by the authors.

Pressure Drop - No equation for the pressure drop in the zigzag baffle type entrainment separator is available. Mathematical models for predicting primary efficiency and pressure drop in this device will be presented in the next chapter.

Tube Bank

Although tube banks have not been used in entrainment separators, equations predicting primary efficiency and pressure drop have been developed and are presented below.

Primary Efficiency - Calvert and Lundgren (1970) found that the collection efficiency for closely packed rods is given by the equation for rectangular jet impaction. The collection efficiency of each stage of impaction can be found in Figure 3-6. Each row of tubes except the first represents one stage of impaction. "β" is used as a parameter in Figure 3-6 and is defined by:

$$\beta = 2\ \ell / b \qquad (3\text{-}17)$$

where b = jet orifice width
ℓ = distance between orifice and impingement plane

"K_p", the inertia parameter, is defined with drop radius, "r_p", rather than diameter as in Figure 3-2.

Efficiency for the bank of tubes is given by:

$$E = 1 - (1 - \eta_j)^N \qquad (3\text{-}18)$$

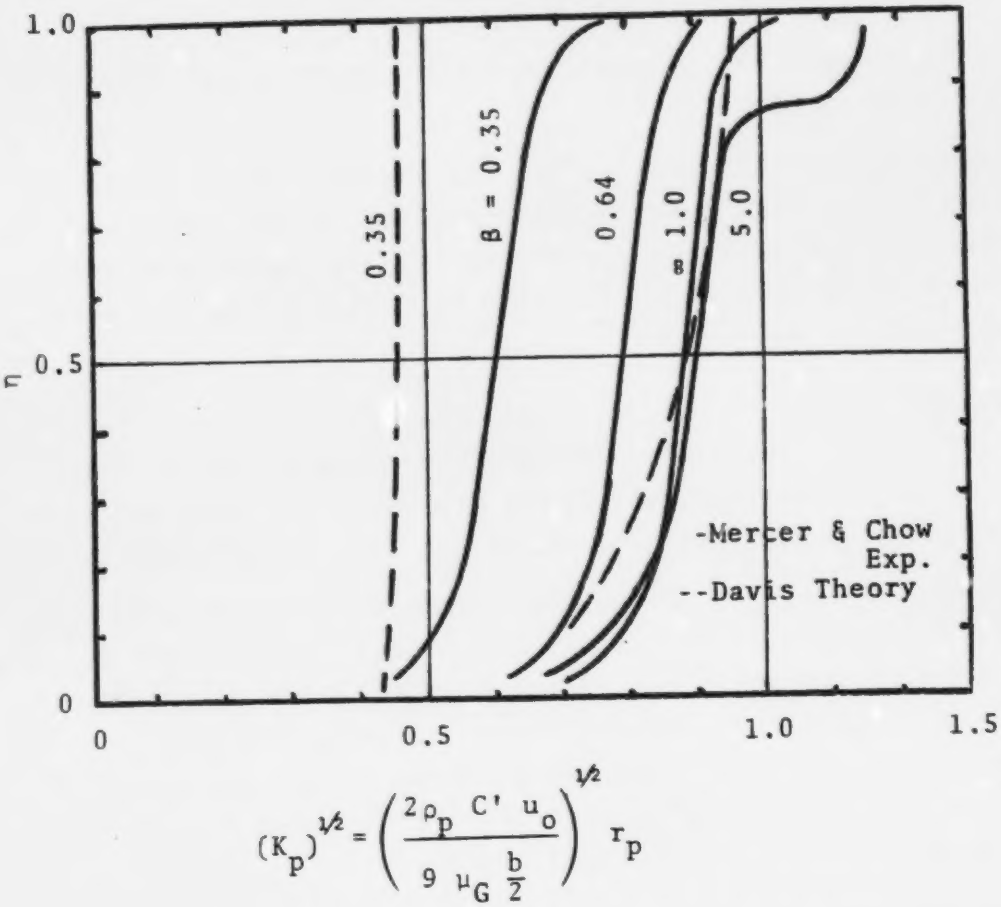

Figure 3-6 - Theoretical and experimental collection efficiencies of rectangular aerosol jets.

where η_j = collection efficiency for a given particle diameter in one stage of rectangular jet impingement

N = number of stages in the tube bank

If the tubes are widely spaced, the target efficiency, "η", can be calculated from Figure 3-2. In this case the efficiency for the entire tube bank is:

$$E = 1 - (1 - \eta \frac{a'}{A})^n \qquad (3\text{-}19)$$

where a' = cross-sectional area of all the tubes in one row

A = total flow area

n = number of rows

Pressure Drop - a properly designed tube bank is claimed to offer low pressure drop. Radford and Houghton (1940) found a lower pressure drop in tests using a bank of tubes than in using zigzag baffles or knitted mesh. Moyers (1960) expressed the pressure drop per row as:

$$\Delta P = 4.95 \times 10^{-5} \rho_G u_G^{2.19} \qquad (3\text{-}20)$$

Mesh

Knitted mesh of varying density and voidage is widely used for entrainment separators. There are basically three different kinds of mesh: (1) Layers with crimp in the same direction - each layer is actually a nested double layer. (2) Layers with crimp in alternate directions - this results in an increase in voidage, reduced sheltering, a decrease in pressure drop per unit length and an increase in target efficiency per layer (3) Spirally wound layers - the pressure drop is lower by about 2/3 than in layers with crimp in the same direction, but the creeping of fluids, which contributes to reentrainment, is expected to be higher.

Standard mesh 10-15 cm thick having a density of about 0.15 g/cm^3 is used to remove drops larger than 5 μm in diameter. Gas velocities range from 0.3 to 5 m/sec and liquid flow rate is limited by the drainage capacity of the mesh to 2.5×10^{-3} g/sec cm^2 of mesh. A lower density mesh made of standard wires is used when 10-20% higher flow rates are desired.

Often two mesh type separators in series are used to remove drops in the 1-5 μm diameter range. The first mesh, normally made of fine wires, coalesces the small drops, and the second mesh, made of standard wires, removes them. The first mesh is operated beyond the flooding velocity and the second under flooding velocity. A major disadvantage with this arrangement is a pressure drop which may reach 25 cm W.C.

Some manufacturers use two or three stages of mesh, the first being coarser and the final being finer, to remove large and small drops successively.

A mesh type separator has the advantage that it can be made to fit vessels of any shape. Any material which can be drawn into the shape of a wire can be used for fabrication. However, mesh separators are limited in application because they plug easily. This can be avoided by upstream washing, which will decrease removal efficiency and increase pressure drop.

Primary Efficiency - Bradie and Dickson (1969) present the following expression for primary efficiency in mesh separators:

$$E = 1 - \exp\left(-\frac{2}{3} \pi a_2 \ell_2 \eta\right) \tag{3-21}$$

where a_2 = specific area of mesh; surface area of wires per unit volume of mesh pad, cm^2/cm^3

ℓ_2 = length of mesh pad in the direction of flow, cm

η = collection efficiency of cylinder wire

The collection efficiency of cylindrical wire "η" can be obtained from Figure 3-2. The factor of 2/3 in the exponential was introduced by Carpenter and Othmer (1955) to correct for the fact that all the wires in the knitted mesh are not perpendicular to the flow. That factor is the ratio of the projected area of wires perpendicular to the flow to the cross-sectional area of wires along the wire length.

The maximum allowable gas velocity in the knitted mesh is calculated from the equation of Souders and Brown (1934):

$$u_{G,max} = 30.5\ a_3 \left(\frac{\rho_L - \rho_G}{\rho_G}\right)^{1/2} \qquad (3\text{-}22)$$

where "a_3" varies with operating conditions and mesh design. For most cases, $a_3 = 0.35$.

Pressure Drop - The additional pressure drop due to the liquid load may exceed the pressure drop in a dry knitted mesh. York and Poppele (1963) have suggested that the total pressure drop in the knitted mesh is the sum of the pressure drop in the dry knitted mesh and the pressure drop due to the presence of liquid:

$$\Delta P = \Delta P_{dry} + \Delta P_L \qquad (3\text{-}23)$$

where ΔP_{dry} = pressure drop in absence of liquid, cm W.C.
ΔP_L = pressure drop due to presence of liquid, cm W.C.

"ΔP_{dry}" can be obtained from an "f" (friction factor) versus "$N_{Re,G}$" (gas Reynolds number) correlation presented in Figure 3-7. Carman (1937) developed the correlation to determine the pressure drop in solid granular materials as a dotted line on the plot. A similar curve is presented for wire mesh by Stasangee (1948) and Shuring (1946). York and Poppele obtained the data for knitted mesh both with

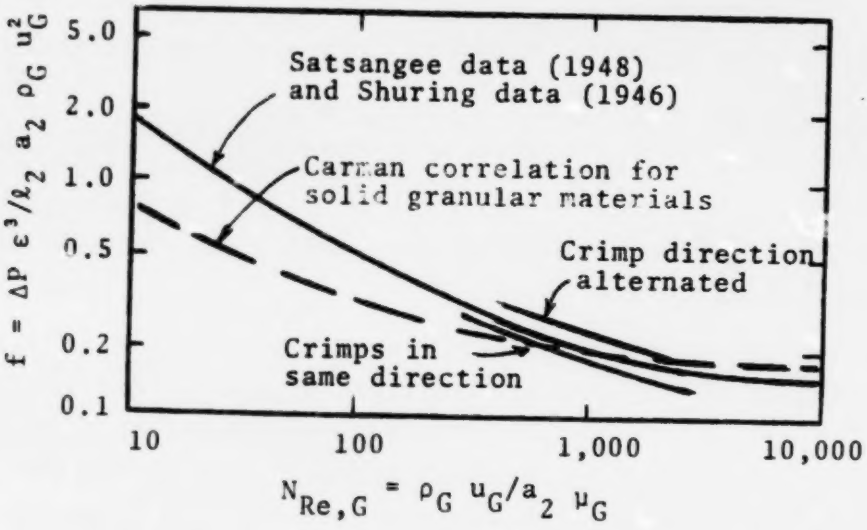

Figure 3-7 - Friction factor, f, versus Reynolds number, N_{Re}, for wire mesh entrainment separator without entrainment load.

the crimps alternated and in the same direction. Their curves are plotted in Figure 3-7 and should be used in determining pressure drop. If the specific area, "a_2", is not specified, it can be determined from the mesh porosity, "ε", and the knitted mesh wire diameter, "d_m":

$$a_2 = \frac{4}{\pi} (1 - \varepsilon)\, d_m \qquad (3\text{-}24)$$

Pressure drop data due to presence of liquid are not available for all operating conditions or for mesh of different styles. Values of "ΔP_L" obtained by York and Poppele are presented in Figures 3-8 and 3-9, with liquid velocity as the parameter. The specifications of the knitted mesh used in the two figures are shown in Table 3-5.

Sieve Plates

Primary Efficiency - Taheri and Calvert (1968) derived an equation for sieve plate primary collection efficiency:

$$E = 1 - \exp(-40\, F_1^2\, K_p) \qquad (3\text{-}25)$$

where $0.30 < F_1 < 0.65$ (3-26)

$$K_p = \frac{\rho_p d_p^2 v_h}{9\, \mu_G d_h} \qquad (3\text{-}27)$$

where F_1 = foam density, ratio of clear liquid height to total foam height

v_h = velocity of gas through hole, cm/sec

d_h = hole diameter, cm

Pressure Drop - Perry (1963) has suggested that the pressure drop in sieve plates can be calculated according to:

$$\Delta P = h_w + h_{ow} + h_{dp} + h_r \qquad (3\text{-}28)$$

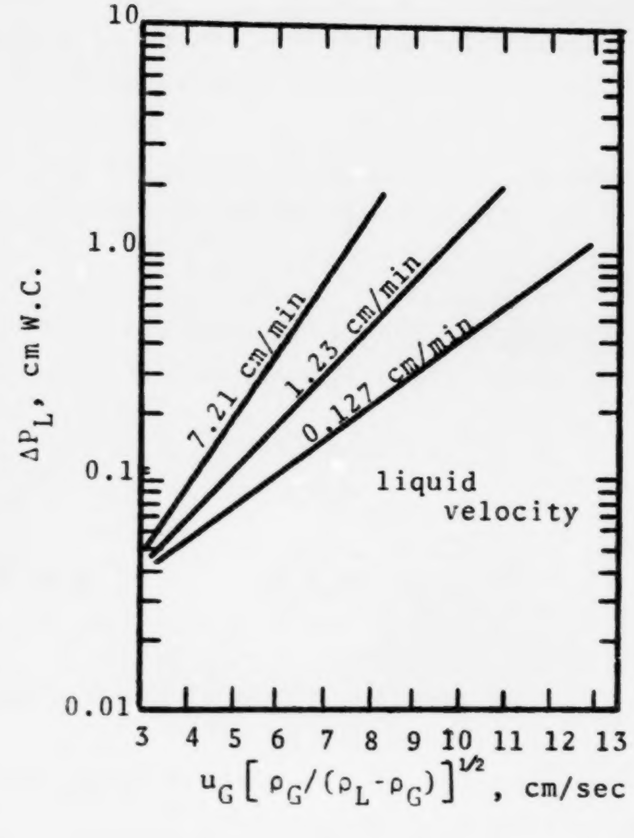

Figure 3-8 - Pressure drop due to presence of liquid in the knitted mesh with the crimps in the same direction

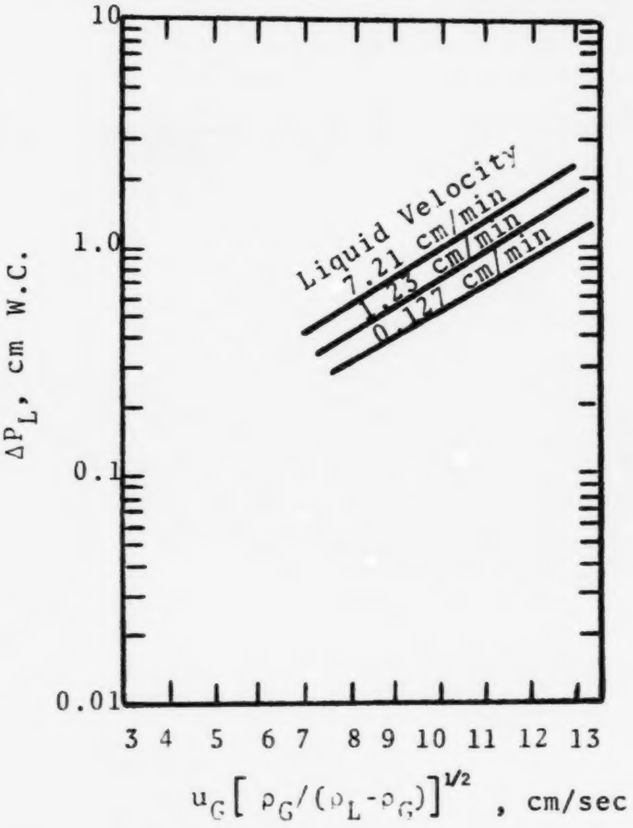

Figure 3-9 - Pressure drop due to presence of d liquid in the knitted mesh with the crimps in the alternate direction

Table 3-5. KNITTED MESH SPECIFICATIONS

	Figure 3-8	Figure 3-9
Direction of crimps	same	alternate
ε	0.977	0.99
a, cm^2/cm^3	3.61	1.51
wire diameter, d_c, cm	0.028	0.028

where h_w = weir height = 4-9 cm, assume 5 cm, if unknown (3-29)

$$h_{ow} = \text{head over the weir} = 0.143\ F_w\ \frac{Q_L}{w_1} \qquad (3\text{-}30)$$

$$h_{dp} = \text{dry plate head loss} = \frac{1}{c^2}\ \frac{\rho_G}{\rho_L}\ \frac{v_h}{2g} \qquad (3\text{-}31)$$

$$h_r = \text{residual pressure drop} = 0.013\ \frac{\rho_{water}}{\rho_L} \qquad (3\text{-}32)$$

$$\frac{1}{c^2} = 1.14\ [0.4\ (1.25 - f_h) + (1 - f_h)^2] \qquad (3\text{-}33)$$

where F_w = column wall curvature correction factor = 1.1
Q_L = liquid flow rate, here in m^3/hr
w_1 = weir length, m
f_h = fraction of the perforated open area in the plate

REENTRAINMENT

As a result of the design equations presented in the previous section, one is able to determine the primary collection efficiency for five types of entrainment separators. However, the overall separator efficiency is found to be less than the primary efficiency because of reentrainment. Increasing overall efficiency means reducing reentrainment, the achievement of which requires a knowledge of the parameters important in determining the extent of reentrainment. Thus, engineering equations describing this process are vital to improved efficiency.

One mechanism of reentrainment results from high gas velocity. In order to avoid this hazard, entrainment separators are operated at lower gas velocities, resulting in the large size and high cost of this equipment.

Another source of difficulty is that the theory of two-phase flow, which can serve as the basis for developing the desired equations, is itself not well developed.

Due to the complexity of the subject and the necessity of starting from the basics of two-phase flow, the following material provides a lengthy but useful base from which equations predicting reentrainment might be developed.

Reentrainment from an entrainment separator may take place by any one or more of the following mechanisms:

1. Transition from separated to separated-entrained flow caused by high gas velocity.
2. Rupture of bubbles at the gas liquid interface and subsequent drop formation.
3. Creeping of the liquid along the solid surface and movement into the gas exit in the entrainment separator.
4. Shattering of liquid drops due to impaction.

The last three mechanisms of reentrainment depend upon the design of entrainment separators. The first mechanism represents the upper limit of the operation of entrainment separators.

Transition from Separated to Separated-Entrained Flow

Reentrainment may occur at high gas velocities due to transition from separated to separated-entrained flow. In simple geometries such as straight tubes, the transition takes place at much higher velocities than those at which entrainment separators are operated. Yet reentrainment is observed in separators at the lower velocity. This is caused by such phenomena as the impingement of the gas stream onto the liquid at an angle and the presence of gas jets. Also the flow pattern in the entrainment separator is not so uniform as in circular tubes. However, due to the limited information available, we must consider two-phase flow in a simple geometry such as the circular tube.

In the operation of entrainment separators, flows may be horizontal, vertically upward or downward, or inclined. The onset of reentrainment depends upon the flow direction, flow geometry and the fluid properties. We will examine reentrainment in the simple geometries for which literature is available.

Horizontal Flow in Circular Tube - The best known and most widely used flow regime map for horizontal flow is that of Baker (1954), which is shown in Figure 3-10. The Baker chart as modified by Scott (1963) is shown in Figure 3-11. where "G_L" and "G_G" stand for the mass flow rates of liquid and gas, respectively, in kg/m² sec. The dimensionless parameters "λ" and "Ψ_1" represent allowances for the fluid physical properties in the system and are defined by the following:

$$\lambda = \left[\left(\frac{\rho_G}{\rho_A}\right)\left(\frac{\rho_L}{\rho_W}\right)\right]^{0.5} \tag{3-34}$$

$$\Psi_1 = \left(\frac{\sigma_W}{\sigma_L}\right)\left[\frac{\mu_L}{\mu_W}\left(\frac{\rho_W}{\rho_L}\right)^2\right]^{0.5} \tag{3-35}$$

where ρ_A = density of air, g/cm³
ρ_W = density of water, g/cm³
σ_W = surface tension of water, dyne/cm
σ_L = surface tension of liquid, dyne/cm
μ_W = viscosity of water, poise

The onset of reentrainment may be considered as a transition from separated flow to entrained flow. The curve separating the two regions is shown in Figure 3-10.

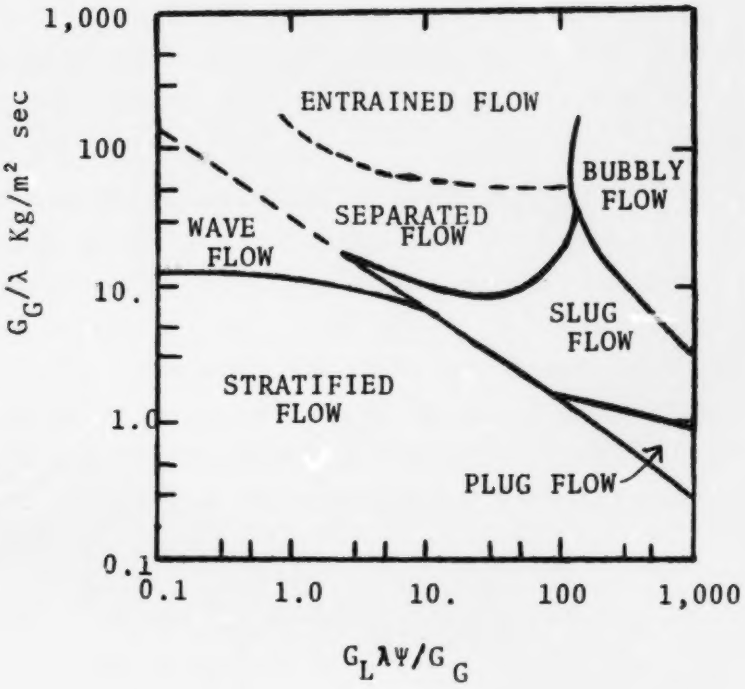

Figure 3-10 - Baker chart

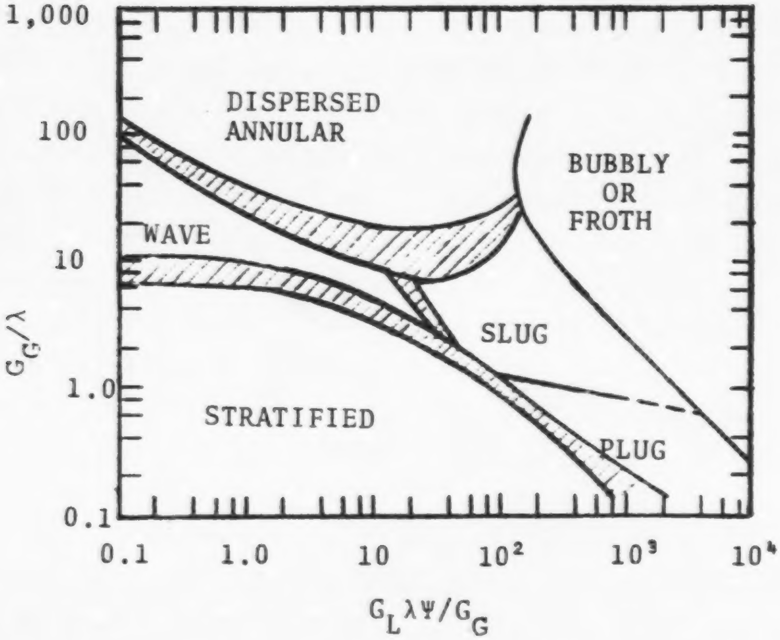

Figure 3-11 - Flow pattern diagram for horizontal flow (After Baker, 1954, as modified by Scott, 1963).

From that figure, it can be calculated that for an air-water system, entrained flow starts at $G_G = 125$ Kg/m^2 sec when $G_L/G_G = 1$ Kg/Kg. If $G_L/G_G = 100$ Kg/Kg, entrained flow starts at $G_G = 37.5$ Kg/m^2 sec. This corresponds to a re-entrainment velocity of 100 m/sec at a liquid loading of 1.33×10^{-3} m^3/m^3. The transition velocity drops to 30 m/sec at a liquid loading of 0.133 m^3/m^3.

Vertically Upward Flow in a Circular Tube - Cousins et al. (1965) studied the transition from separated to separated-entrained flow in a 0.95 cm bore vertical tube. The flow was in the upward direction. Their general conclusion is that for thin liquid films at low liquid Reynolds numbers, the gas velocity for entrainment increases rapidly with decreasing liquid rate, and a limiting liquid flow rate may be reached, below which no entrainment occurs irrespective of further increases of gas rate. At higher liquid flow rates, both gas and liquid flow rates are important in governing the onset of entrainment. Figure 3-12 from the work of Cousins et al. (1965) illustrates this conclusion.

For the asymptotic case of a limiting liquid flow rate, the onset of entrainment corresponds closely to the formation of large disturbance waves in the liquid film. For lower gas flow rates the existence of large disturbance waves is not a sufficient condition for the onset of entrainment. Thus, there is a region in which the gas velocity is sufficient to give rise to large waves on the surface but is insufficient to break these waves into droplets. Zhivaikin (1962) suggested that the onset of droplet entrainment in upward flow can be correlated by the equation:

$$\frac{u_{Gc}\mu_L}{\sigma} = \left(\frac{164}{N_{Re,L}}\right)^{.5} \qquad (3\text{-}36)$$

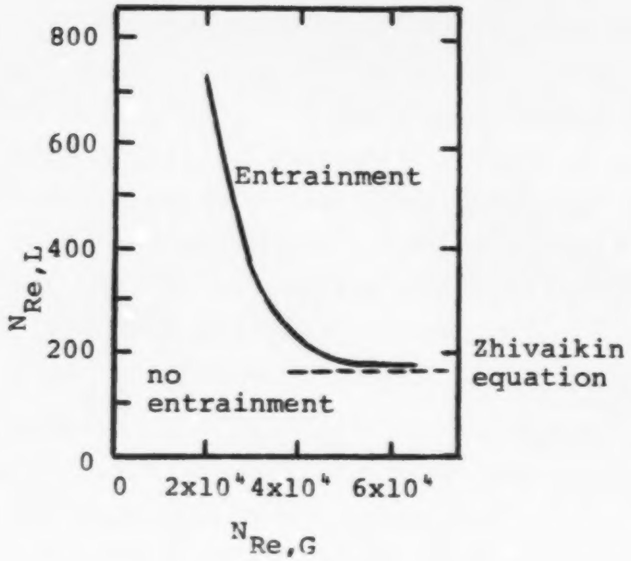

Figure 3-12. Onset of entrainment in air-water flow. (Results of Cousins, et al., 1965)

where u_{Gc} = critical gas velocity for entrainment
$N_{Re,L}$ = liquid Reynolds number

Vertically Downward Flow in Circular Tube - For downward flow the onset of entrainment equations are presented by Chien and Ibele (1962), Steen and Wallis (1964) and Zhivaikin (1962) and appear in Chapter 4. Each investigator defined onset of entrainment differently and thus their predictions for onset of entrainment differ significantly. Their data were obtained in a 2.5 cm bore tube.

Measurements of the amount of liquid entrainment in upward and downward co-current two-phase annular flow are presented in Figure 3-13. It can be seen that for upward flow the quantity entrained passes through a minimum with increasing air flow rate, while for downward flow entrainment increases with total liquid flow rate.

Effect of Impingement of Gas Jets - As mentioned earlier, the gas and liquid phases do not flow parallel in the entrainment separator. Jets of gas are present, which may impinge on the liquid film at various angles. The presence of gas jets, their impingement on the liquid film at various angles, etc. depend upon the entrainment separator design.

Wallis (1962) studied entrainment in ducts with various inlet designs. The reentrainment velocity varies with inlet design, from 1,800 cm/sec to 2,400 cm/sec. The data are shown in Figure 3-14.

Interfacial Waves - The study of interfacial wave behavior is important in the determination of transition from separated flow to separated-entrained flow. Experimental and theoretical studies of wave behavior and its influence on other phenomena are still at a very early stage of development. The most advanced theoretical studies have been concerned

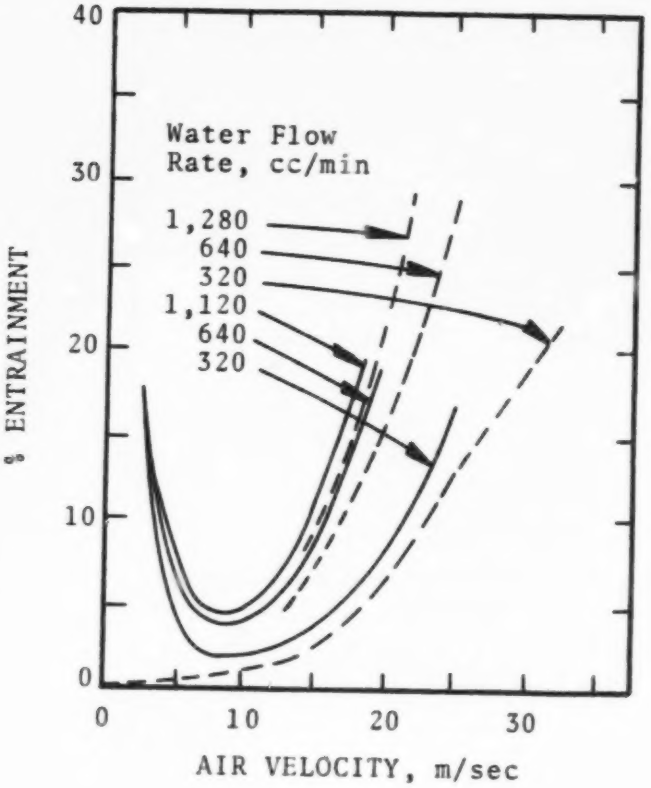

Figure 3-13 - Comparison of entrained fraction in upward and downward cocorrent annular flow in 1.25 cm I.D. tube. Solid line represents upflow and dotted line represents downflow.

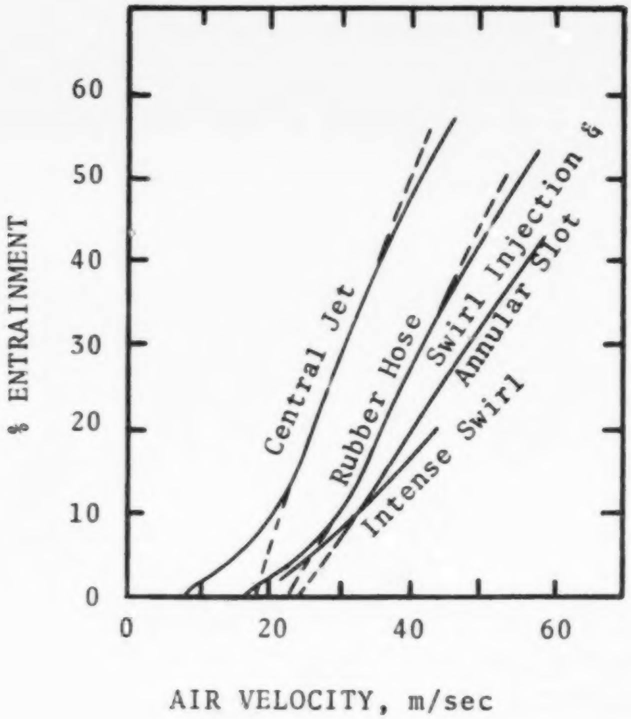

Figure 3-14 - Extrapolation method for determination of point of onset of entrainment for vertical downflow in 2.2 cm I.D. tube. Water flow rate = 1,280 cm^3/min. The curves are shown for different inlet designs. After Wallis (1962)

with the problem of the initial formation of waves, rather than their development and influence. However, the instability of the waves represents the physical phenomenon responsible for transition from separated to separated-entrained flow. Thus, to understand the physical phenomena responsible for reentrainment in entrainment separators, one should look at the interfacial waves, breaking of the waves, drag friction on the film due to gas flow, etc.

A flow map showing different regions of interfacial structure observed in air-water flow at atmospheric pressure is illustrated in Figure 3-15 (Hall-Taylor et al. 1963). As the air velocity is increased, ripple waves and disturbance waves take place. These waves represent instability of the interface. One theory that explains interfacial instability is the Kelvin-Helmholtz theory.

Consider the case of the flow of two inviscid fluids of different densities (say a gas and a liquid), separated by a vertical interface on which a regular train of waves is moving with a velocity, "C". As the gas flows around the curves of the streamlines, centrifugal forces are set up and these must be balanced by a pressure gradient in the direction normal to the streamline:

$$-\frac{\partial p}{\partial n} = \rho_G \frac{1}{r} (\bar{u}_G - C)^2 \qquad (3\text{-}37)$$

where r = radius of curvature, cm
$\bar{u}_G$ = mean gas velocity, cm/sec
n = direction normal to the streamline

The pressure at the interface can be found by integrating this equation between the interface and infinity.

It follows from Equation (3-37) that for surfaces of positive curvature the pressure at the interface will be less than the undisturbed pressure at infinity, whereas for

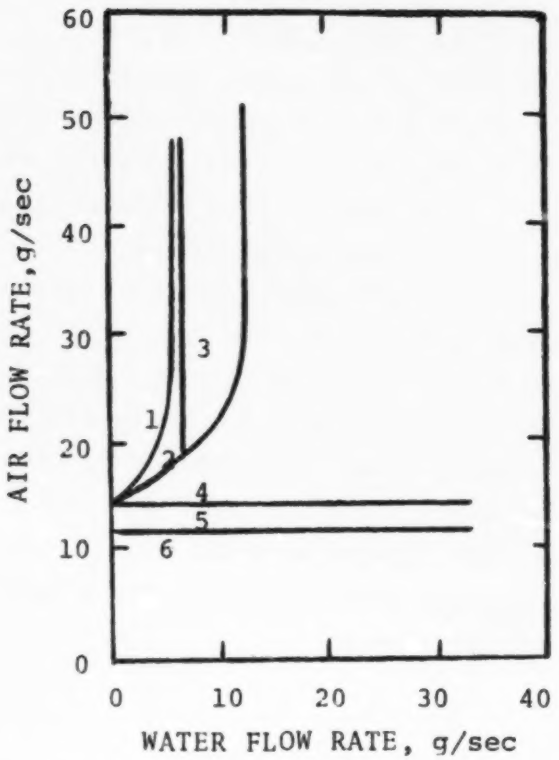

Figure 3-15 - Region of wave flow in air-water flow in a 3.2 cm bore tube. 1. Water not wetting tube. 2. Ripple waves only. 3. Ripple waves with pulses of disturbance waves. 4. Disturbance waves and ripple waves. 5. Churn flow. 6. Plug and churn flow.

surfaces of negative curvature the pressure at the interface will be greater than the value at infinity. Thus, the gas flowing past the wavy interface generates an increased pressure over the troughs and suction over the crests. A similar line of argument obviously applies on the liquid side of the interface, only the liquid exerts an outward pressure at the crests and suction at the troughs.

For vertical flow the only forces opposing these normal stresses are those due to surface tension. For a stable interface condition, the surface tension stresses exactly balance the effects of the normal stress. On the other hand, the wave will grow in amplitude when the sum of the local liquid and gas normal stresses exceeds the surface tension stress. It can be further deduced that the thinner the liquid film the greater the gas velocity needed to cause an increase in amplitude of a given size wave.

It may be expected that the effect of waves will be to increase the friction factor. To determine the liquid flow rate, it is necessary to have interfacial friction factor.

Roberts and Hartley (1961) found, on plotting friction factor as a function of liquid film thickness for a given gas velocity, that the friction factor did not begin to increase with film thickness until a certain value had been exceeded. They were able to correlate the difference between the interfacial friction factor and that for the same gas flow rate in the absence of the liquid phase, by the equation:

$$f_i = f_G + 1.5 \left[\frac{\delta}{d_{eq}} - \frac{5}{N_{Re,G}} \left(\frac{2}{f_G} \right)^{0.5} \right] \qquad (3\text{-}38)$$

and, $$f_i = \tau_i \left(\frac{1}{2} \rho_G {u'_G}^2 \right)^{-1} \tag{3-39}$$

where f_i = interfacial friction factor

f_G = friction factor in the absence of liquid phase

δ = liquid film thickness, cm

d_{eq} = equivalent (hydraulic) diameter, cm

τ_i = interfacial shear stress, gm/cm sec^2

Thus, for very thin liquid films there would be no significant waves on the interface and no effective roughness. For thicker films there would be a minimum instantaneous film thickness corresponding to the troughs of the waves on the surface.

Gill et al. (1963) calculated the equivalent roughness height and plotted it as a function of the film thickness defined by Roberts and Hartley. The correlation is shown in Figure 3-16.

Hanratty and Woodmansee (1965) suggested that the onset of reentrainment may result from suction on the wave by the Kelvin-Helmholtz mechanism. This suction will lead to a tearing of the wave tips.

A number of possible mechanisms have been suggested by which transfer of droplets can be effected by the waves, but at present there is no definite evidence to favor any particular one. Lane (1957) described the mechanism illustrated in Figure 3-17. The gas starts to "undercut" the wave and a round, open ended bubble begins to form. The bubble grows, leaving a thick-ringed filament around its base and eventually breaks up into droplets. Once the breakup occurs, the excess (dynamic) pressure inside the bubble gives rise to a rapid radial transport of the droplets.

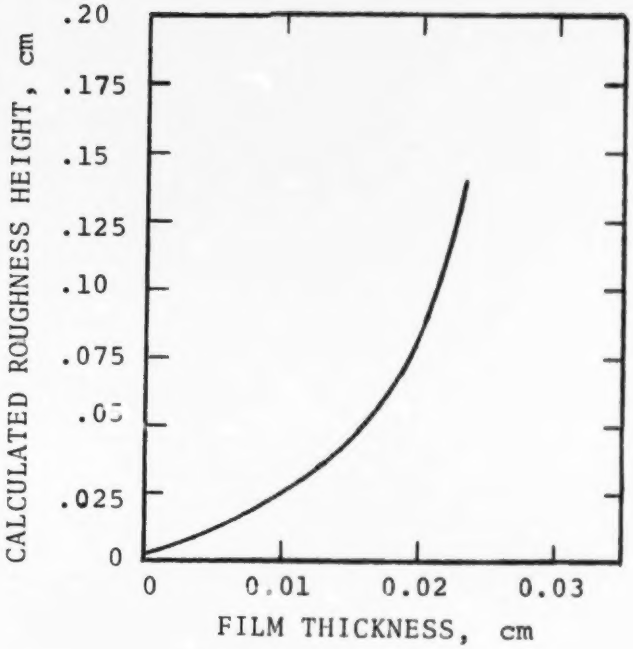

Figure 3-16 - Relationship between effective roughness height and film thickness.

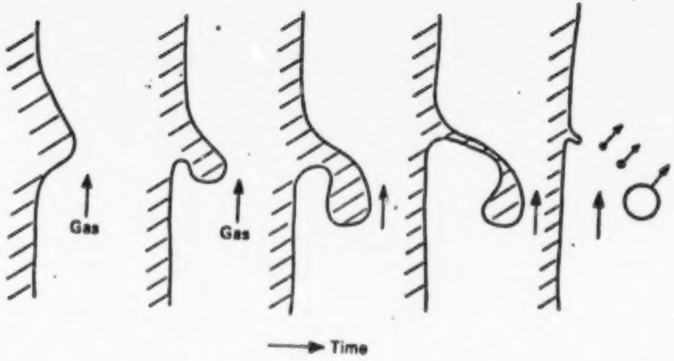
Gas
Gas
Time

Figure 3-17 -
Breakdown of Disturbance Wave by Undercutting

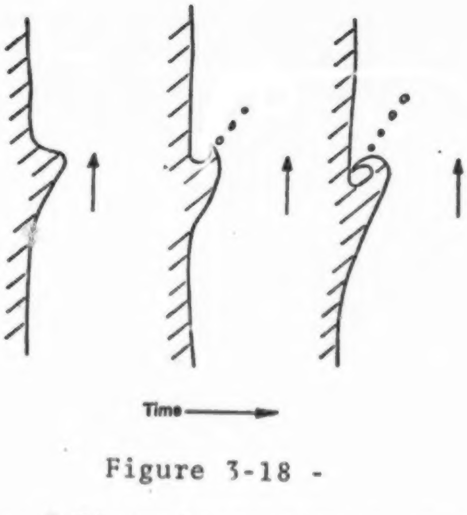

Figure 3-18 -
Breakdown of Disturbance Wave by Rolling

An alternative form of breakup is illustrated in Figure 3-18. A large amplitude wave on a shallow liquid layer tends to steepen at the front and then to form a breaking wave. If the gas velocity is very high, it might be expected that the tips of the waves would be drawn out into thin liquid sheets with subsequent breakup.

Entrained Fraction and Rate of Reentrainment - If the gas velocity is increased beyond the onset of reentrainment, some of the liquid that is collected on the entrainment separator elements will be reentrained. To determine the overall efficiency of a separator, one must know the equilibrium entrainment fraction, rate of reentrainment, and reentrainment drop diameter. In this section we will deal with entrained fraction and the rate of reentrainment.

There are no reliable methods at present for estimating the fraction of liquid flowing as entrained droplets out of an entrainment separator. Geometrical factors, inlet conditions, physical and chemical properties and change of conditions along the entrainment separator can all affect the results obtained. Therefore, any correlations that have been developed for entrained fraction estimation should be treated critically.

Wickes and Dukler (1960) have attempted to correlate the data for entrained droplet flow rate by means of the Martinelli (1949) parameter "X":

$$X = \left[\frac{(dp_f/dz)_L}{(dp_f/dz)_G} \right]^{1/2} \qquad (3\text{-}40)$$

where $(dp_f/dz)_L$ = frictional pressure gradient for liquid flowing alone in a tube, dyne/cm³

$(dp_f/dz)_G$ = frictional pressure gradient for gas flowing alone in a tube, dyne/cm³

A dimensional entrainment parameter "R" was obtained by intuitive reasoning and was defined as:

$$R = \frac{3.8\text{x}10^{3}\ B\ W_{LE}\ u_L/u_G}{(dp_f/dz)_G} \quad . \tag{3-41}$$

where W_{LE} = the flow rate of entrained liquid, g/sec
B = empirical constant, 22 for smooth injection and 13 for shock injection

Collier & Hewitt's (1961) data correlate fairly closely about a line given by the following equation

$$X = 0.069\ R^{0.39} \tag{3-42}$$

Hughmark (1973) correlated the entrainment data of Collier & Hewitt, Alia, et al. (1965) and Wicks and Dukler. The data are plotted in Figure 3-19. Empirical correlating equations are:

$$y_G^+ < 36 \qquad \alpha = 0 \tag{3-43}$$

$$36 < y_G^+ < 42, \quad \alpha = -0.000442 + 0.000013\ y_G^+ \tag{3-44}$$

$$42 < y_G^+ < 60, \quad \alpha = -0.000625 + 0.0000172\ y_G^+ \tag{3-45}$$

$$60 < y_G^+, \qquad \alpha = 5\text{x}10^{-8}\ (y_G^+)^{22} \tag{3-46}$$

where $\alpha = \dfrac{W_L\ \rho_G}{W_G\ \rho_L}$ = volumetric flow ratio

and W_L, W_G are liquid and gas flow rates, g/sec

Anderson, Bollinger & Lamb (1964) obtained the rate of interchange between entrainment and separated flow in horizontal pipes. Their results show that the rate of interchange (% of the total liquid flow per 30.5 cm length of pipe) can be correlated as follows:

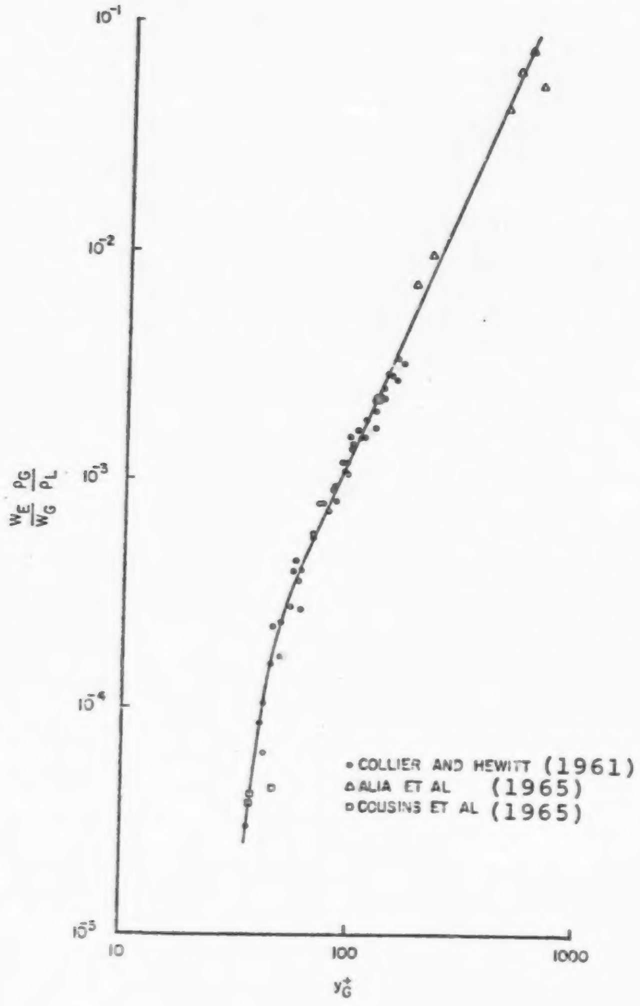

Figure 3-19 - Correlation of entrainment data by Hughmark (1973).

% interchange = 4 for $N_{Re,L} > 2,570$, $N_{Re,G} > 3,000$ (3-47)

% interchange = 0.5 for $N_{Re,L} = 1,150$, $N_{Re,G} > 3,000$ (3-48)

% interchange = 0 for $N_{Re,G} < 3,000$ (3-49)

Drop Diameter of Reentrainment - Another important factor, besides the amount of reentrainment, is the drop diameter of reentrainment. If a secondary entrainment separator is used to remove the reentrained drops, it is necessary to know the drop diameter of reentrainment to design the secondary separator.

Few investigators have measured the drop size distribution arising from separated flow. Wicks and Dukler (1966) obtained data for co-current downward flow in a 15 cm x 1.8 cm rectangular vertical channel. The mass median drop diameter varied between 150 and 450 μm. The smallest drop diameter found in the entrainment was 45 μm.

Cousins and Hewitt (1968) obtained data during experiments on the mass transfer of liquid droplets subsequent to removal of liquid film. Photographs of the droplets were obtained for a zone immediately adjacent to the channel wall. The mass median drop size was between 90 μm to 175 μm. They also found a minimum droplet size of 45 μm. Both sets of data show a decrease in the mass median diameter with increasing gas velocity.

Fraser et al. (1963) studied drop formation from liquid sheets by an air blast at 90°. They observed that the liquid sheet does not break down upon immediate impact with the air stream but is deflected away from it. Waves are initiated at the point of impact and the sheet breaks down into drops through the formation of unstable ligaments. The air velocity was varied between 10^3cm/sec and $6x10^3$cm/sec and the liquid flow rate between 12.5 and 125 g/sec. The liquid drop size varied from 30 μm to 250 μm. They observed that the average drop size increases with increase in liquid flow rate and decreases with increase in air velocity.

Reentrainment Due to Rupture of Bubbles

The second mechanism which leads to reentrainment is rupture of bubbles. Again the important questions are at what velocity reentrainment begins, what is the drop diameter of the reentrainment, what is the amount of liquid in the reentrainment, etc. The effect of operating variables such as gas velocity, liquid flow rate, etc. should also be determined.

The following section deals with the mechanism of bubble rupture, the drop size distribution created by rupture of bubbles, and the trajectory of these reentrained drops.

Rupture of bubbles is the main cause of the reentrainment of liquid drops into the gas phase in devices such as sieve plate, bubble cap plate, packed bed, and mesh type separators. The collapse of a bubble when exiting from the liquid phase is associated with thinning of the liquid film starting at the top part of the bubble. The upper surface thins to the extent of becoming weak enough to rupture. Rupture of the upper part of the bubble film takes place when the film thickness if of the order of 0.1 μm, provided there are no external disturbance forces leading to the rupture of films (Kitchener, 1964; Jashnani, 1971). The collapse of the bubble at the interface leads to the release of surface tension energy which is converted into kinetic energy. The kinetic energy is sufficient to impart high velocities to liquid drops formed during this process.

Drop Diameter of Reentrainment - The liquid drops which are formed during the rupture of bubbles are of two distince diameter ranges. Small drops (about 30 to 40 μm) are formed from the top of the bubble surface, and large drops (about 1 mm) are formed due to the disturbances in the liquid phase following the bubble rupture. Formation of the small drops was observed by Stumpner (1936), and he attributes drop formation to the rupture of the projecting dome of the bubble into fragments.

Davis (1940) cites the work of Edgerton, Germeshausen and Grier (1936) on the rupture of a soap bubble to establish that during collapse, the dome opens and forms an initial perforation near the apex without creating drops. He suggests that large drops are subsequently formed by the breakup of the liquid jet which forms when the surrounding liquid moves inward to fill the depression caused by the bubble. The depth of the depression is a function of the bubble size. Drops are more likely to form from small, rather than large, bubbles. The work of Dombrowski and Frazer (1954) shows that a thin liquid film on the top of the bubble breaks up by the initial formation of a number of perforations which subsequently expand to give a lace-like structure. The liquid ligaments so formed are unstable and break into small drops of varying size.

Drop formation due to bubble burst occurs in three steps. The first step, the lifetime of the bubble at the interface, lasts on the order of 1/100th sec. or longer; the actual bubble burst, the second step, takes a few microseconds; and events subsequent to the bubble burst extend over a few milliseconds.

Newitt et al. (1954) measured the drop size distribution due to the rupture of a bubble, and a typical distribution is shown in Figure 3-20. They also observed that in all cases the Sauter mean diameter of large drops, "$d_{s,\ell}$", decreases nearly linearly and the number of large drops, "N_ℓ", increases with decreasing bubble diameter. Furthermore, both "$d_{s,\ell}$" and "N_ℓ" decrease with rising temperature, and the change in the number of drops produced by the bursting of large bubbles decreases markedly as the temperature is raised. Figure 3-21 shows the variation of the Sauter mean diameter "$d_{s,\ell}$" with the bubble diameter at 25°C, using distance from the interface as parameter.

Large drops are formed from jets of liquids which are formed following bubble rupture. As the liquid surrounding the bubble moves inward to fill the depression caused by the bubble, it usually forms a jet of liquid. As the bubble diameter is reduced, the internal pressure rises and the energy available for jet formation increases. This gives rise to jets of higher initial velocity and hence greater unbroken length. Stuhlman (1932), experimenting with bubbles of 0.25 cm diameter or less, showed that the resulting jets became progressively thinner with decreasing bubble diameter and break down into two or more drops per jet.

Garner, et al. (1954) found that 95% of the droplets entrained in the evaporator were below 20 μm, but because of their low mass they formed only a small fraction (about 2%) of the total weight of the entrained liquid.

Droplets from the rupture of bubbles larger than 0.5 cm diameter were almost entirely produced from the bubble dome. The entrainment resulting from bursting bubbles increased by 20 fold when the bubble diameters were reduced from 0.6 cm to 0.2 cm. Mass median drop diameters of 440 μm, 660 μm and 820 μm were obtained from bubbles having 0.2 cm, 0.3 cm and 0.4 cm diameter, respectively.

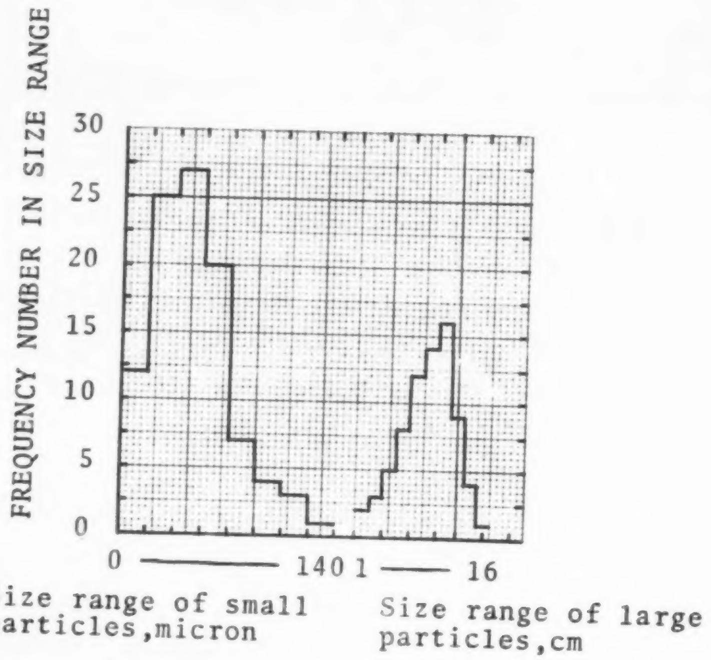

Figure 3-20 - Histogram showing size distribution of large and small drops resulting from bubble burst

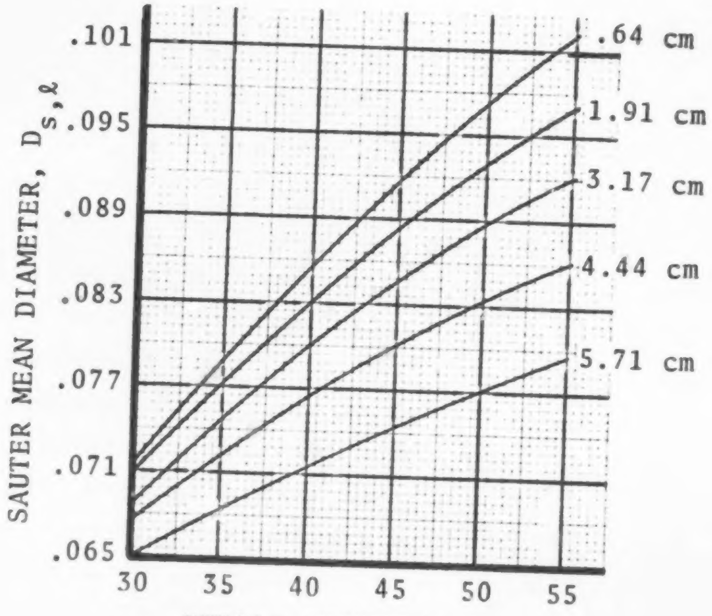

Figure 3-21 - Sauter mean diameter, $D_{s,\ell}$, against bubble diameter at 25°C.

Small drops travel outward from the point of burst at angles of up to 80° from the vertical. Thus, some of the drops will be collected on the walls.

Formation of Jet After Bubble Burst - To determine reentrainment in the gas phase, it is necessary to study the kinetics of the liquid jet formed after the bubble burst. The dimensions of the jet are important, as the instability of jets produces drops which are reentrained in the gas phase. The velocity of rise of the liquid jet will give the large drops their initial velocity.

Davis (1940) gives the following equation for jet velocity based on the pressure pulse following bubble rupture:

$$u = 6 \frac{\sigma t}{\sigma_L d^2} \tag{3-50}$$

where t = time during which the impulse force is applied (about 3×10^{-5} sec)

d = bubble diameter, cm

Equation (3-50) predicts velocities which are very small, about 0.1 cm/sec. According to Newitt et al. (1954), when the rupture of a bubble takes place, a partial vacuum is created due to the impulse force, and therefore the absolute pressure rather than pressure excess should be used as an impulse force:

$$u = \frac{3}{2} \frac{(P_o + \frac{4\sigma}{d})\, t}{\sigma_L d} \tag{3-51}$$

where P_o = pressure outside the bubble, dyne/cm^2

Equation (3-51) assumes no correction for the change in bubble diameter due to the contact with air by part of the bubble surface.

Newitt et al. give the following equation for the height of the jet:

$$h_1 = \left(\frac{2}{(g\ \sigma_L/\sigma) - \frac{1}{a_4}} \right)^{1/2} \tag{3-52}$$

For air water system, $a_4 = 1\ \text{cm}^2$, $\sigma = 73$ dynes/cm, $g = 980\ \text{cm/sec}^2$ and $\rho_L = 1\ \text{g/cm}^3$ give $h_1 = 0.404$ cm. The experimental jet height as obtained from photographs is 0.44 cm.

Weber (1931) has calculated the relationship between the unbroken length of the jet and its velocity. In the range of velocities created by 0.2 to 0.5 cm bubble diameters, the relationship between velocity and length is linear. Haenlein's (1931) experimental values confirm this. The distance, "ℓ_3", of the unbroken jet is given by the expression:

$\ell_3 = t'\ u$

where t' = rise time of the unbroken length of jet, sec

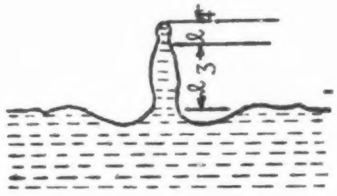

(3-53)

The velocity obtained from Equation (3-51) should be used in Equation (3-53) to calculate the length of the unbroken jet.

If the length of the liquid jet is longer than the perimeter of its cross-section, it becomes unstable and breaks up. The breakup occurs at different lengths along the jet, and it is this broken part which forms the liquid drop.

For non-viscous liquids Weber (1931) gives the most favorable wave length for breakup of a jet as:

$$\ell_4 = \sqrt{2}\ \pi\ d_{jet} = 4.42\ d_{jet} \tag{3-54}$$

where d_{jet} = diameter of the jet, cm

Equating a cylindrical length of jet, equal to $4.42\ d_{jet}$, with the volume of a drop formed, results in:

$$d_p = 1.89\ d_{jet} \qquad (3\text{-}55)$$

Castleman (1931) gives the following expression, based on the work of Rayleigh (1879, 1889) and Weber (1931), for the time of break-up of a liquid jet:

$$t = \frac{2.3}{a_5} \log \frac{\alpha_1}{\alpha_o} \qquad (3\text{-}56)$$

and, $$a_5 \doteq 0.343 \left(\frac{4d}{\rho_G\ d^2_{jet}} \right)^{0.5} \qquad (3\text{-}57)$$

where, d = bubble diameter, cm

α_1 = amplitude of surface disturbance of the jet = $0.5\ d_{jet}$

α_o = initial surface disturbance = 10^{-5} cm

The above equation gives times which are roughly 4 times greater than actually observed.

The total length of jet will be the sum of unbroken and broken parts:

$$h_1 = \ell_3 + \ell_4 = t'\ u + 4.42\ d_{jet} \qquad (3\text{-}58)$$

Trajectory - Reentrainment will depend upon gas velocity, flow direction, terminal and initial velocities of drops and hydrodynamic properties. Large drops which have a terminal settling velocity greater than the upward gas velocity will eventually fall down. However, it is necessary to provide enough height following the mist eliminator, for these drops to reverse direction and start falling.

If the gas velocity is in the vertical direction, the vertical height traveled by the large drops (with diameter "$d_{s,\ell}$") is given by Equation 3-59, from Lapple and Shepherd (1940):

$$h_2 = (1 + u_G) \int_o^{u-u_G} \frac{u\ du}{a_6 u^{1.4} + g} + (1 + u_G) \int_o^{u_G} \frac{u\ du}{a_6 u^{1.4} - g} \qquad (3\text{-}59)$$

where $a_6 = \frac{0.0055}{d_{s,\ell}{}^{1.6}}$. The equation is based on drag coefficient $C_d = 18.5\ N_{Re}{}^{-0.6}$. The time for vertical travel is:

$$t_2 = \int_o^{u-u_g} \frac{du}{a_6 u^{1.4} + g} + \int_o^{u_G} \frac{du}{a_6 u^{1.4} - g} \qquad (3\text{-}60)$$

Figures 3-22 and 3-23 give a plot of time and height versus initial drop velocity with drop diameter as parameter (gas velocity $u_G = 0$).

The drop ballistics for small drops with drop diameter, "$d_{s,s}$", differs from that of the large ones because the initial velocity of the small drops is not necessarily in the vertical direction.

Lapple and Shepherd give integrated forms for this case, based on Stokes Law:

$$t_h = \frac{\rho_L\ d_{s,s}^2}{18\ \mu_G} \ln\left(\frac{u_o}{u}\right) \qquad (3\text{-}61)$$

$$S_h = \frac{\rho_L\ d_{s,s}^2}{18\ \mu_G} \left[1 - \exp\left(\frac{-18\ \mu_G\ t_h}{\rho_L\ d_{s,s}^2}\right)\right] \qquad (3\text{-}62)$$

$$t_v = \frac{\rho_L\ d_{s,s}^2}{18\ \mu_G} \ln\left(\frac{u_t - u_o}{u_t - u}\right) \qquad (3\text{-}63)$$

$$S_v = u_t\ t_v - \left(u_t - u_o\right) \frac{\rho_L\ d_{s,s}^2}{18\ \mu_G} \left[1 - \exp\left(\frac{-18\ \mu_G\ t_v}{\rho_L\ d_{s,s}^2}\right)\right] \qquad (3\text{-}64)$$

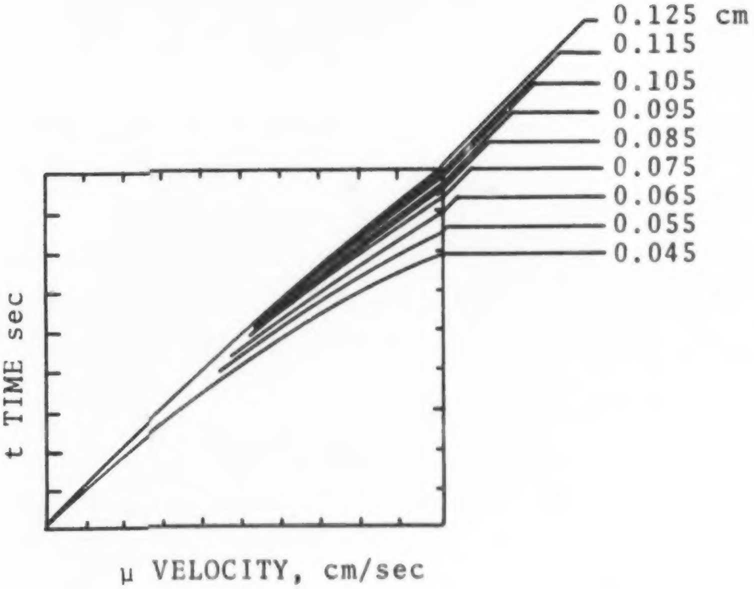

Figure 3-22 - Time against velocity curves for drops of varying degree

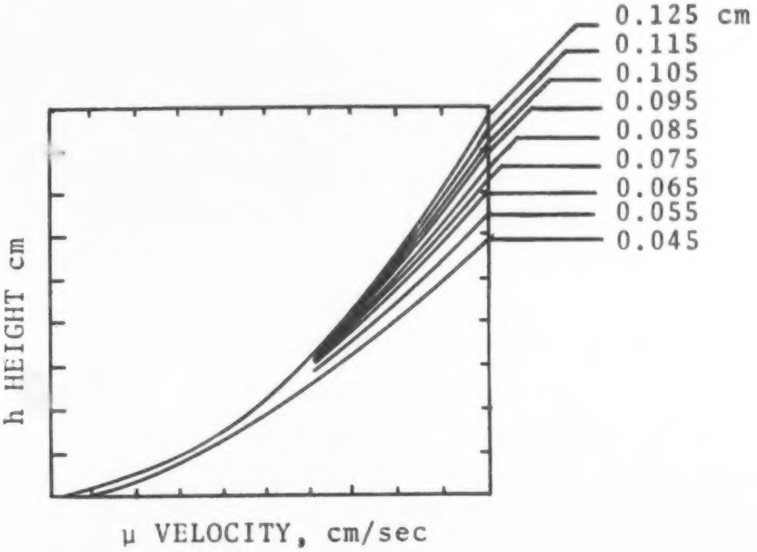

Figure 3-23 - Height against velocity curves for drops of varying diameter

where S = the distance traveled by drop and subscripts "h" and "v" refer to the horizontal and the vertical direction

u_o = the initial velocity in horizontal (Equations 3-61 and 3-62) and in vertical (Equations 3-63 and 3-64) direction

Creeping of Fluids

The presence of drag forces due to gas flow leads to creeping of liquid in the entrainment separator. Creeping may be prevented by providing a proper drainage system. If creeping is not prevented, reentrainment may occur.

In the entrainment separator gas usually flows vertically upward or horizontally. If there is creeping of liquid, it flows as a film or as drops. The liquid and gas flow in the same direction. Thus, to determine the effect of creeping, we need equations to predict liquid flow rate due to drag forces exerted by gas in various directions and in various geometries. Again, we are limited to the theoretical development to predict two phase flow in simple geometries.

Consider liquid and gas flowing in a vertical tube. The gas is flowing vertically upward and liquid is flowing as a film and therefore forming an annulus. The liquid film is subject to various forces: drag force due to gas flow in the vertically upward direction, gravity force in the downward direction and frictional force due to tube wall.

For gas velocity lower than the critical velocity the liquid near the wall flows downward due to gravity. As the gas velocity is increased the liquid at the interface reverses its flow direction and moves with the gas; as a result the liquid film begins to thicken. At a critical gas flow rate the liquid does not flow down any more, and the liquid film thickens rapidly.

Shearer and Nedderman (1965) give the equation for shear stress inside the liquid film:

$$\tau = \left(- \frac{dp}{dz} - \rho_G\, g\right)\left(\frac{D-2\ \delta}{4}\right) + \left(- \frac{dp}{2dz} - \rho_L\, g + \frac{\rho_G}{2}\, g\right)(\delta - y) \qquad (3\text{-}65)$$

where D = the diameter of the tube, cm
τ = shear stress measured at a distance "y" from the wall, dyne/cm²

The velocity profile for the liquid can be obtained by integrating Equation (3-65). The liquid is assumed to be Newtonian and the boundary condition is given by $u_L = 0$ at $y = 0$ for a laminar flow:

$$u_L = \frac{1}{\mu_L}\left[\frac{y(D-2\delta)}{4}\left(- \frac{dp}{dz} - g\rho_G\right) + \left(\frac{dp}{2dz} + g\rho_L - \frac{g\rho_G}{2}\right)\frac{(\delta-y)^2-\delta^2}{2}\right] \qquad (3\text{-}66)$$

Integration of Equation (3-66) gives Equation (3-67):

$$Q_L = \frac{\pi D}{\mu_L}\left[- \frac{dp}{dz}\frac{D\delta^2}{8} + \frac{dp}{dz}\left(\frac{\delta^3}{12}\right) - \frac{g\rho_L\delta^3}{3} - \frac{g\rho_G D\delta^2}{8} + \frac{5}{12}\, g\rho_G\delta^3\right] \qquad (3\text{-}67)$$

However, in the case of a liquid film flowing vertically downward, terms containing "g" should be more important than terms containing "$\frac{dp}{dz}$".

The situation is significantly more complex in the general case when the flow is not steady and part of the film is in turbulent motion. In entrainment separators the situation is further complicated due to entrance effect.

When the flow channel is not vertical, Equation (3-67) should be modified by replacing "g" by "gCosθ"; where "θ" is the angle between the channel direction and the vertical. However, if the effect of gravity is larger than the effect of the pressure gradient, the thickness of the film across the channel will be uneven and separated flow rather than annular flow may form. Equations are not available for the case of cross flow.

Shattering of Drops

Reentrainment may take place due to shattering of drops in two ways.

1. Due to splashing of drops on the solid surface,
2. Due to high relative velocity between gas and liquid drops.

Garner et al. (1954) observed splashing in a 10 cm glass evaporator. The size distribution of the shattered drops showed a large variation. The drops were larger than 200 μm. The splashing was observed in a gas-liquid system where localized areas of high velocity were present.

Shattering of the drops due to high relative velocity between gas and liquid drops does not increase entrainment in the gas phase. However, small drops are more liable to be carried away in the gas phase than large drops and therefore shattering of drops should be avoided.

MANUFACTURERS' SURVEY

The information received from the manufacturers of entrainment separators was reviewed. Cyclone, mesh, fiber bed, packed bed and baffles are commonly used as entrainment separators. Sometimes two or more devices are combined in the entrainment separation process. The description of the available entrainment separators is given in the proceeding paragraphs. The first paragraph gives the code used in the description.

Manufacturer

(Type)	Type of separator
(L)	liquid load, cm^3/cm^3, and drop diameter, μm
(G)	Gas volume, m^3/sec
(U_G)	Gas velocity, cm/sec (maximum operating range)
(E)	Overall separation efficiency, %

(ΔP)	Pressure drop, cm W.C.
(Lim.)	Limitations
(App.)	Application
(Mat.)	Materials of construction
(Com.)	Comments

ACS Industries

(Type)	Mesh
(L)	up to 2.71 g/cm² sec, $d_p > 5$ μm
(G)	$U_G = k \left[(\rho_L - \rho_G)/\rho_G\right]^{1/2}$ k = 0.35 for oil and gas, = 0.25 for steam at 1 atm, = 0.2 for pressure 500 cm Hg, = 0.15 - 0.2 for vacuum
(E)	Figure 3-24
(ΔP)	Figures 3-25 and 3-26, Table 3-6
(App.)	Mists of petroleum, H_2SO_4, caustic, HCl, water soluble dusts
(Mat.)	Steel, SS, MO, Ni, Haste alloy, PP, Teflon

Aerodyne Development Corporation

(Type)	Cyclones, integral part of wet scrubber
(G)	14.1 (30,000 CFM)
(Com.)	Uses secondary air to impart centrifugal action

Aget Manufacturing Company

(Type)	Fiber filter
(G)	0.141 - 1.22 (300 - 2,600 CFM)
(App.)	Mists from screw machine, thread grinders, centerless machines
(Mat.)	Glass wool

Air Purification Methods

(Type)	Cyclone with vanes
(L)	$2.66\text{x}10^{-4}$ $-1.1\text{x}10^{-3}$
(G)	0.19 - 15.5 (400-33,800 CFM)
(U_G)	1,130 - 1,480 cm/sec
(E)	95% for 10 μm and 100% for > 13 μm, See Figure 3-27

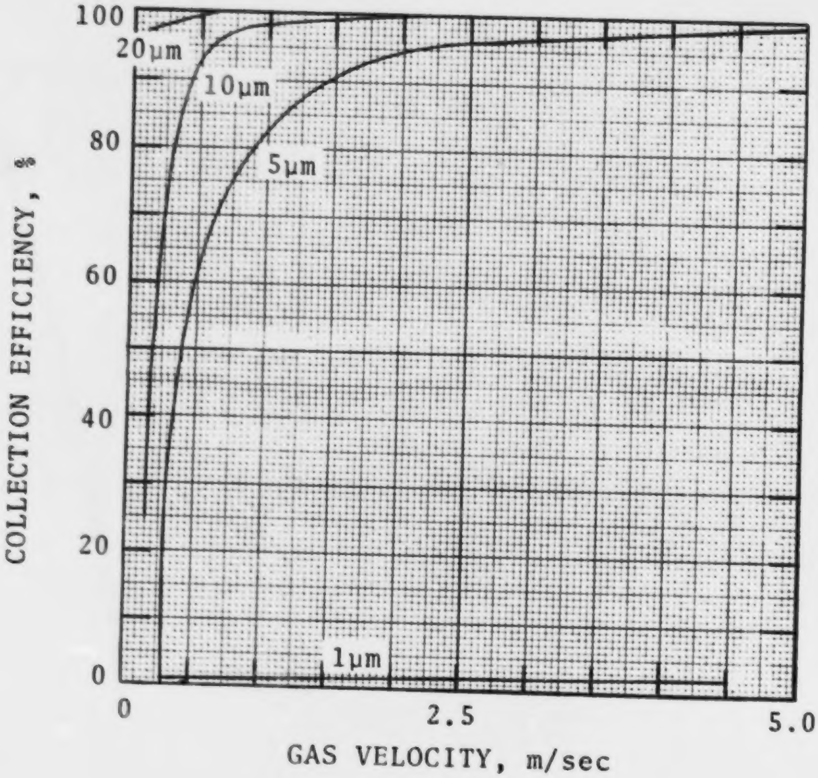

Figure 3-24 - Calculated collection efficiency for water droplets in air for ACS mesh

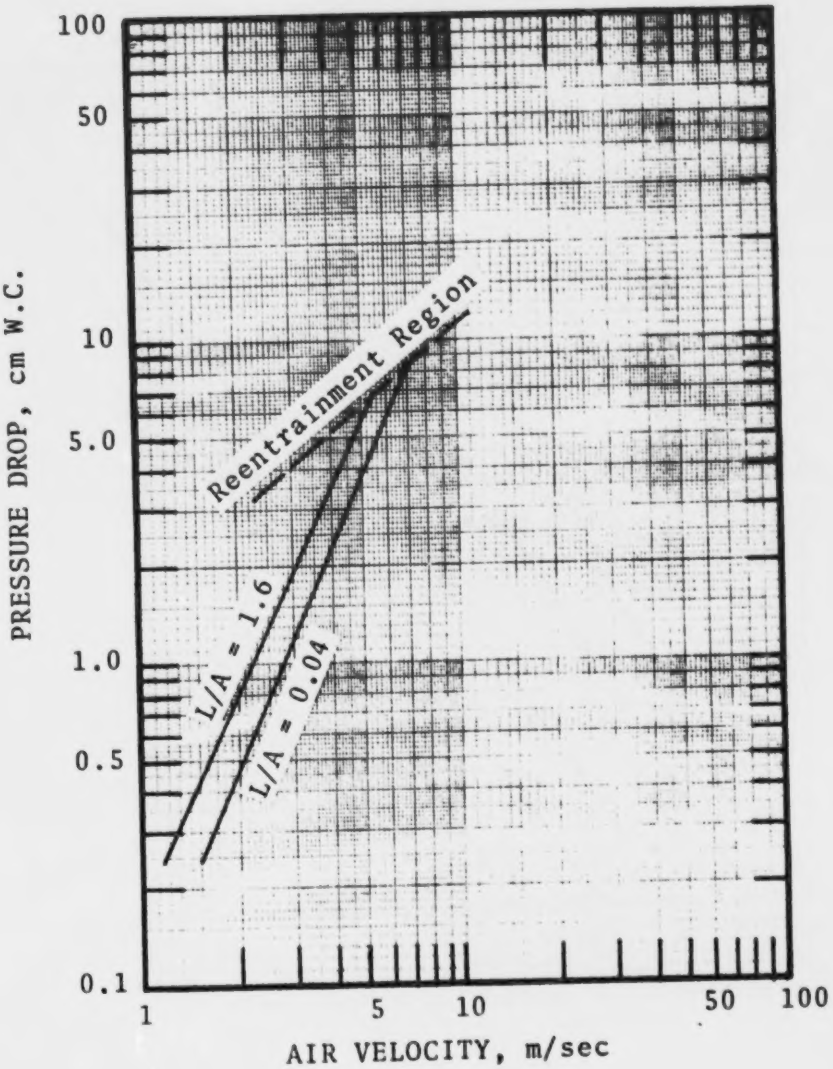

Figure 3-25 - Pressure drop versus air velocity for 10 cm thick ACS style 4CA mesh. L/A = superficial liquid velocity, cm/min.

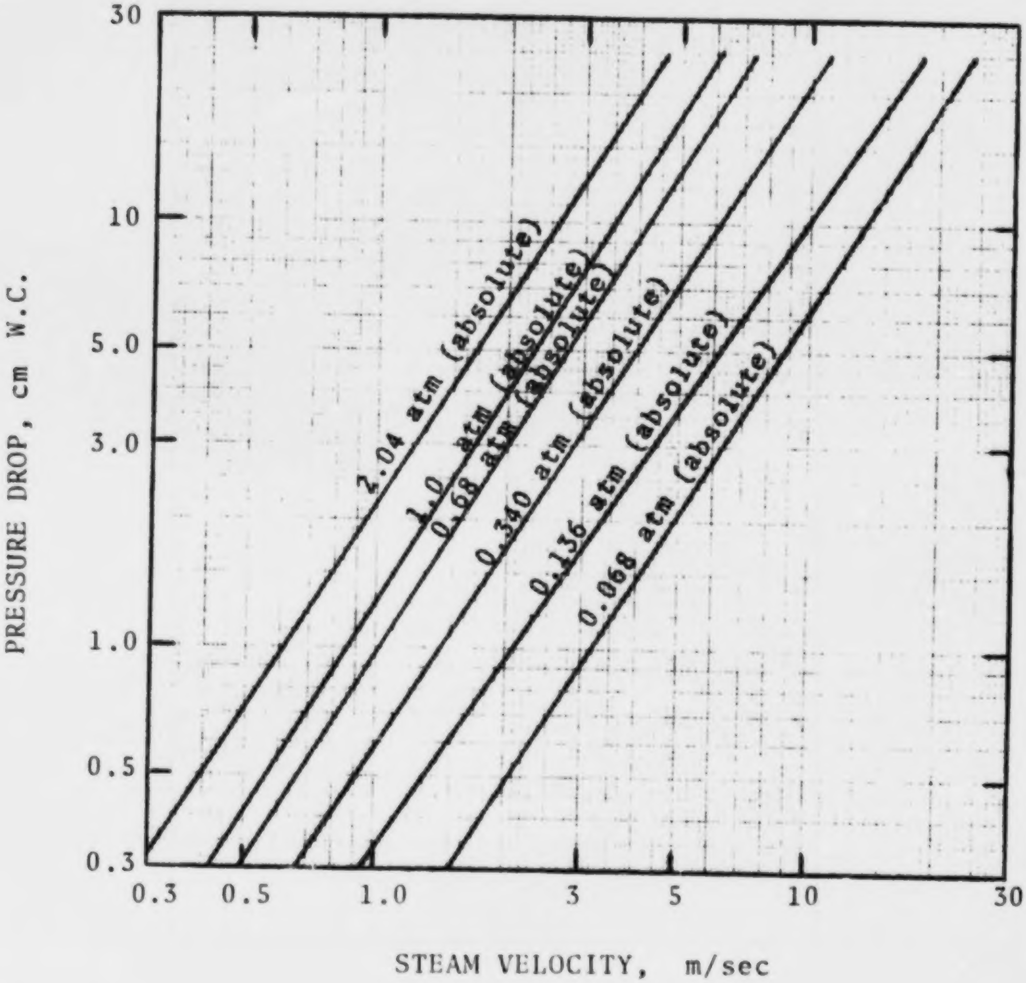

Figure 3-26 - Pressure drop versus steam velocity at various pressures through 10 cm thick ACS mesh.

Table 3-6. MESH PARAMETERS

Mesh Style	Density g/cm^3	Wire Diameter cm	Percent Voids	Wire Surface cm^2/cm^3
4BA	0.192	0.028	97.6	3.77
4CA	0.144	0.028	98.2	2.79
7CA	0.080	0.028	99.0	1.48
3BF	0.115	0.015	98.6	3.93

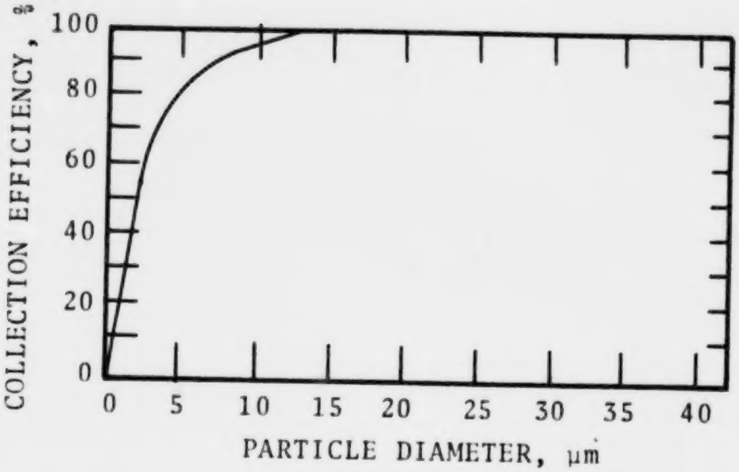

Figure 3-27 - Collection efficiency versus particle diameter for Air Purification Methods cyclone separator with inlet velocity of 16-21 m/sec

Air Purification Methods (continued)

(App.)	in venturi scrubbers and mist removal

Arco Scrubbers (Envirotech)

(Type)	Baffles, packed bed and cyclone
(G)	65 (138,000 CFM)
(Com.)	cross flow in packed bed

B. B. Barefoot & Associates

(Type)	Cyclone, integral part of scrubber
(G)	2.4 - 47.2 (5,000 to 100,000 SCFM)
(App.)	Foundry, furnaces, sinter plants

Balston, Inc.

(Type)	Fiber filters
(G)	0.38 (800 CFM)
(E)	99.99
(ΔP)	351
(App.)	Sterilization of air, air to instruments, laboratory air clean up, breather filters in underground mines
(Mat.)	Glass fiber 90% void

Beco Engineering Co.

(Type)	Packed beds of 1.9 cm x 1.9 cm hexagonal cylindrical pellets from three dimensional bonded fibers
(L)	No limit
(G)	35.2 (75,000 CFM)
(ΔP)	See Figure 3-28
(App.)	Distillation, fume scrubbers, packed towers
(Mat.)	Nylon 6.6 for pH > 4, epoxy bonded polyester for acidic medium

Beetle Plastics

(Type)	Packed bed
(G)	0.16 - 33.6 (350 - 50,000 SCFM)
(U_G)	220
(App.)	Hcl, HF and NH_3 fumes

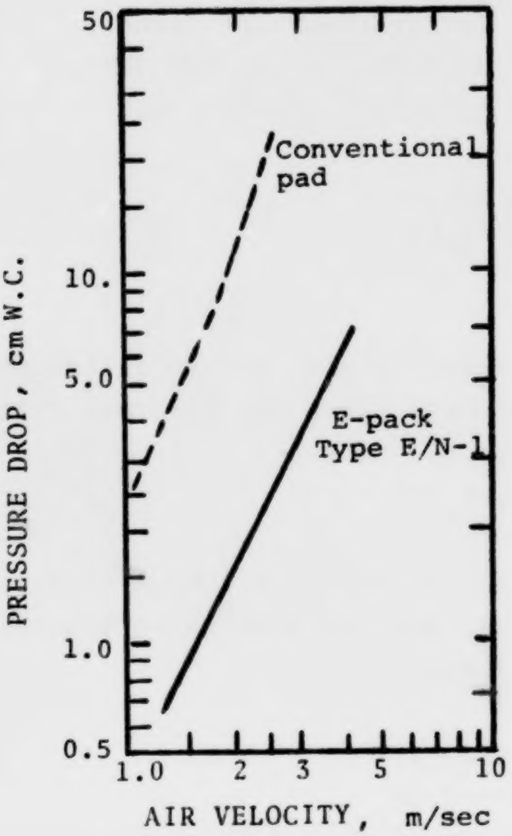

Figure 3-28 - Comparison of pressure drop characteristics of Beco Engineering Type E/N-1 pad and conventional Pad length is 30 cm and air at room temperature and 1 atm pressure.

Burgess Industries (Delta P Division)

(Type)	Centrifugal
(L)	>5 μm, liquid load less than 5% by weight
(E)	99+% See Figure 3-29
(ΔP)	<1% of abs. line pressure
(Lim.)	Maximum pressure 25 atm
(App.)	Compressors, expanders, vacuum pumps
(Mat.)	Carbon steel
(Com.)	Coalescer recommended for below 5 μm
(Type)	Small cyclone tubes
(L)	Maximum 5% load
(E)	95% for 4 μm, 98% for 6 μm
(Mat.)	Carbon steel, stainless steel and alloy steel
(Type)	Zigzag baffles
(L)	liquid load < 5%, drops > 5 μm
(E)	99.99% for 8 μm
(Mat.)	Carbon steel

Cal-Metex

(Type)	Mesh
(U_G)	30-460, 10% higher for hi-thruput
(E)	99.9+%
(ΔP)	$= 0.034\ \rho_G\ u_G^2$ (Figure 3-30) for 10 cm thick standard mesh, $= 0.02\ \rho_G\ u_G^2$ for 15 cm thick hi-thruput mesh
(Lim.)	Sauder Brown constant, a = 0.25 for standard, = 0.23 for hi-thruput and 0.22 for extra dense
(Mat.)	S.S., carbon steel, Ni, Cu, PP
(Com.)	density = 0.145 g/cm^3 for standard, = 0.08 g/cm^3 for hi-thruput and = 0.195 g/cm^3 for extradense. See Figure 3-31 for onset of reentrainment velocities.

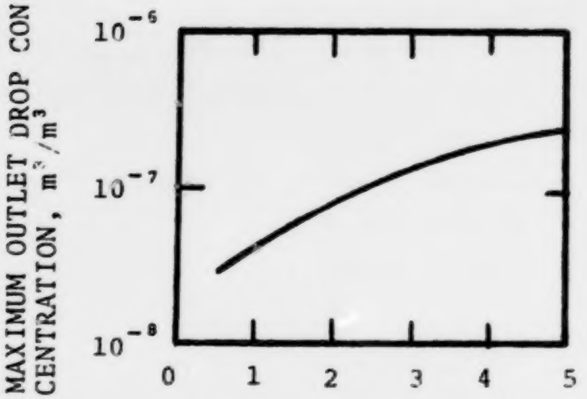

Figure 3-29 - Efficiency curve for Burgess Industries centrifuge. Inlet drop diameter is greater than 5 μm and maximum liquid in inlet is 5% of gas weight.

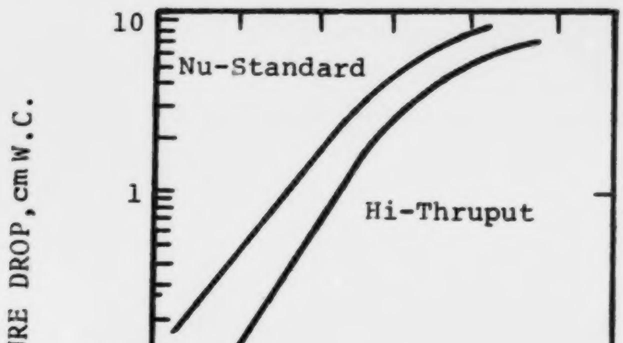

Figure 3-30 - Pressure drop characteristic of 10 cm thick Nu-standard and 15 cm thick Hi-thruput mist eliminators.

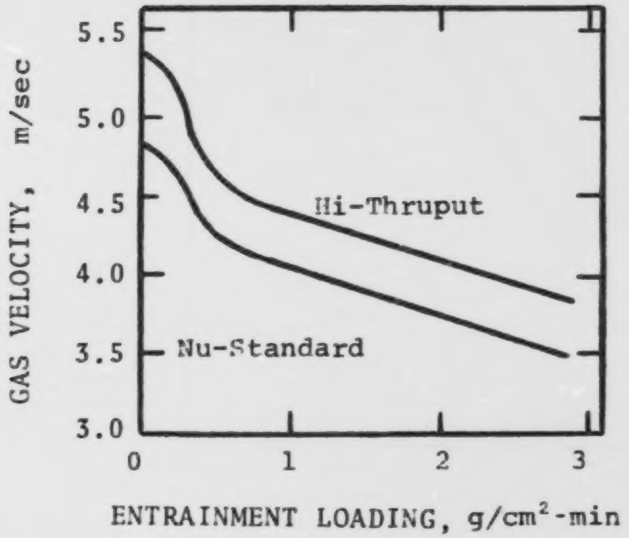

Figure 3-31 - Safe operating limits for Nu-standard and Hi-thruput mist eliminators. Reentrainment will not occur when velocities do not exceed those shown.

Cebeco Manufacturing Company

(Type)	Fiber filter
(L)	0.5 μm
(G)	118 (250,000 CFM)
(E)	99.9% for > 0.5 μm
(ΔP)	17.5-25
(App.)	H_2SO_4 mists, organic plasticizers, oil mists, carbon black
(Mat.)	Glass wool - finer than used in laboratories
(Com.)	5 cm thick, wash may be used for solids

Ceilcote

(Type)	Packed column - crossflow and counterflow
(L)	>3 μm, >8 μm for countercurrent with upstream washing
(G)	0.15 - 23.6 (330-50,000 CFM)
(U_G)	215 (maximum 255 - for lower liquid loads)
(E)	Crossflow: 95+% for > 10 μm and 85-95% for <10 μm. Counterflow: 85-95% for > 10 μm and 50-85% for < 10 μm
(ΔP)	0.008 cm/cm of packing at recommended velocity in crossflow
(Lim.)	If solids are present countercurrent flow is recommended
(Mat.)	Steel, steel lined with flakeline, rubber, etc.
(Type)	Wet cyclone
(L)	>5 μm
(G)	1.4-23.6 (3,000-50,000 ACFM)
(U_G)	1,650
(E)	95%
(ΔP)	5-10

Centri Spray Corporation

(Type)	Zigzag baffles
(G)	14.1 (30,000 CFM)
(U_G)	195
(App.)	Scrubbers in foundry cupolos
(Mat.)	Galvanized steel, PP

Chemico Industry

(Type)	Cyclone
(Com.)	Cyclone is integral part of scrubber

Donaldson Company

(Type)	Multiple cyclone
(G)	26 (55,000 CFM)
(E)	99.97 for > 0.3 μm
(App.)	Air purification in mines
(Com.)	Irrigation with 2.66×10^{-5} - 0.67×10^{-5} L/G recommended

DuPont

(Type)	Fibrous bed, 0.1-0.3 mm diameter fiber
(G)	14.1 (30,000 CFM)
(App.)	Foundry cupolos, mist of H_2SO_4, mists from venturi scrubber
(Com.)	Irrigation with water to avoid plugging, flooding correlation shown in Figure 32

Edwards Engineering Corp.

(Type)	Mesh
(L)	Drops formed by condensation
(App.)	Vapor condensers

Fisher Klosterman, Inc.

(Type)	Cyclones
(L)	Critical drop diameter 6-27 μm
(G)	19.6 (42,000 CFM)
(U_G)	1,400

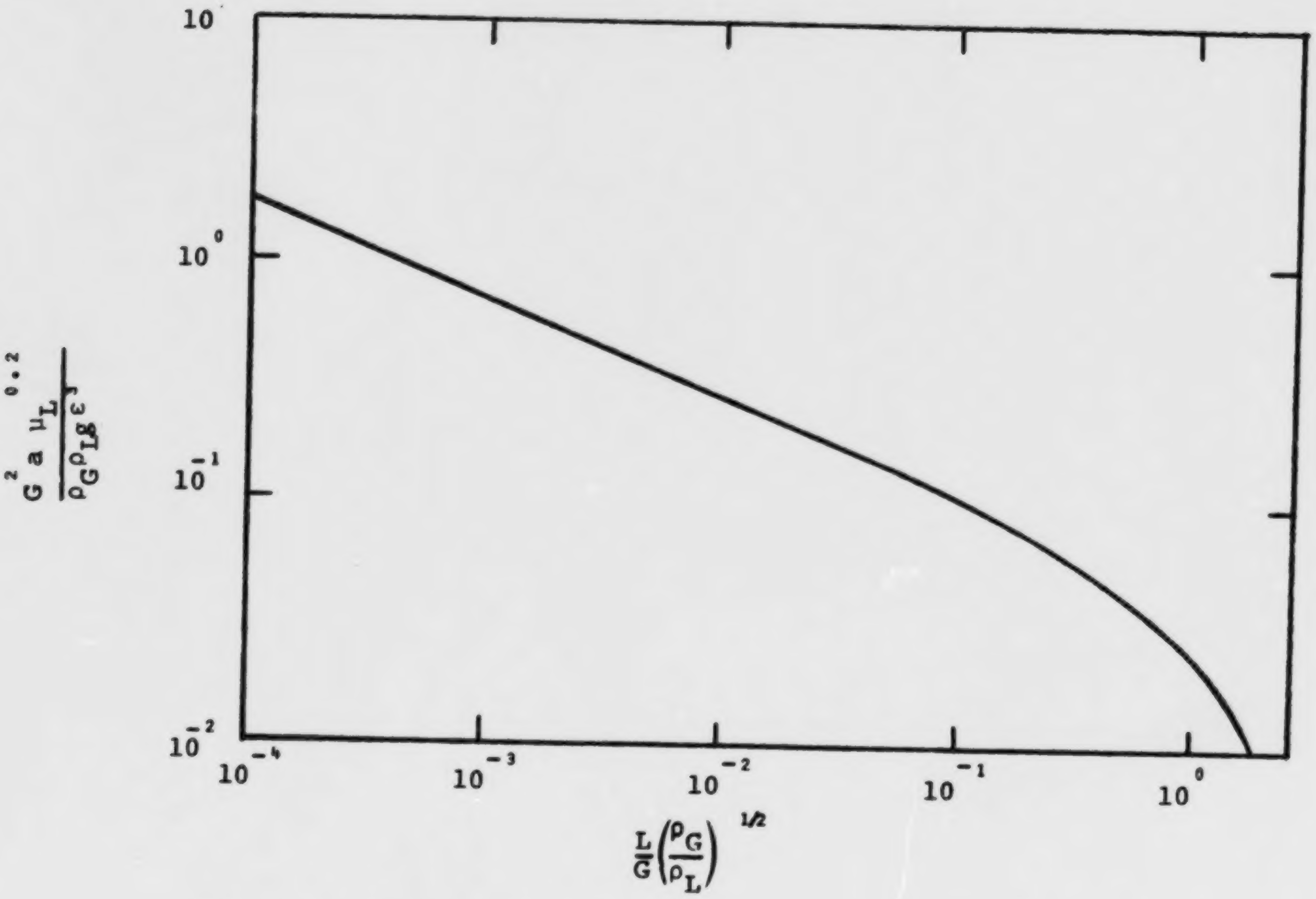

Figure 3-32 - Flooding correlation for fibrous bed structures by Porter and Lucas (1968)

Fisher Klosterman, Inc. (continued)

(E)	100% above critical diameter drops
(ΔP)	15
(Type)	Three stage filter consisting of 14-18 mesh, fiberglass, submicron diameter fiber filter
(G)	15.1 (32,000 CFM)
(ΔP)	0.25 - 7.5, 0.26 at rated capacity
(Lim.)	Filters need replacement
(App.)	Oil mist collection

Industrial Plastic Fabricators

(Type)	Packed bed 15 cm deep or mesh 10 cm deep
(G)	0.23 - 11.8 (500-25,000 CFM)
(E)	90-99% (efficiency of total scrubber)
(Mat.)	Knitted mesh or PP
(Com.)	Integral part of fume scrubber

Koch Engineering Company

(Type)	Cyclone
(G)	1.18-47.2 (2,500 - 100,000 CFM)
(ΔP)	2.5-5
(Com.)	Wall wash available if scaling is expected
(Type)	Zigzag vane 3 or 6 passes
(U_G)	355
(ΔP)	2.5 for 6 passes
(Mat.)	PP
(Type)	Spin vane
(G)	47.2 (100,000 CFM)
(ΔP)	10
(Com.)	Less wear on shell, effective for vessels larger than 400 cm in diameter
(Type)	Fleximesh
(L)	2.7×10^{-3} to 2.7×10^{-2} g/sec cm^2
(U_G)	150-450

Koch Engineering Company (continued)

(E)	See Figure 3-33
(ΔP)	1.25 - 7.5 depending upon liquid load
(Lim.)	Not recommended for high liquid loads ($5x10^{-4}$L/G)
(App.)	In wet scrubbers, removal of acid mist, oil droplets, in distillation columns
(Mat.)	SS, Inconel, Monel, Ni, Ti, PP, Teflon, Hastelloy

Lau, Inc.

(Type)	Centrifugal, mechanical aided and fiber filter
(ΔP)	12.5 maximum
(App.)	Oil mist created by coolent or cutting lubricant
(Mat.)	Polyurethene-filter

Monsanto-Enviro Chem Systems, Inc.

(Type)	Fiber filter, high volume and high efficiency filters
(L)	No limitation on high efficiency, 3 μm on high volume
(U_G)	<30 for high volume, <15 for high efficiency
(E)	See Figure 3-34
(Lim.)	Cannot handle excessive solids, upstream washing recommended to avoid plugging
(Mat.)	Fibers < 10 μm in diameter
(Com.)	Above velocities represent onset of reentrainment

North American Rockwell

(Type)	Mesh, panel filters, two stage on line mesh separators
(G)	up to 4.7 (10,000 CFM) maximum actual volume = 0.47 (1,000 CFM) at 10 atm
(E)	99.96 on 0.3 μm drops - by DOP method
(ΔP)	60-250 when clean, 350-500 at 10 atm
(Lim.)	10 atm, 120°C
(App.)	Removal of mist from compressed air
(Com.)	All the data is for two stage mesh

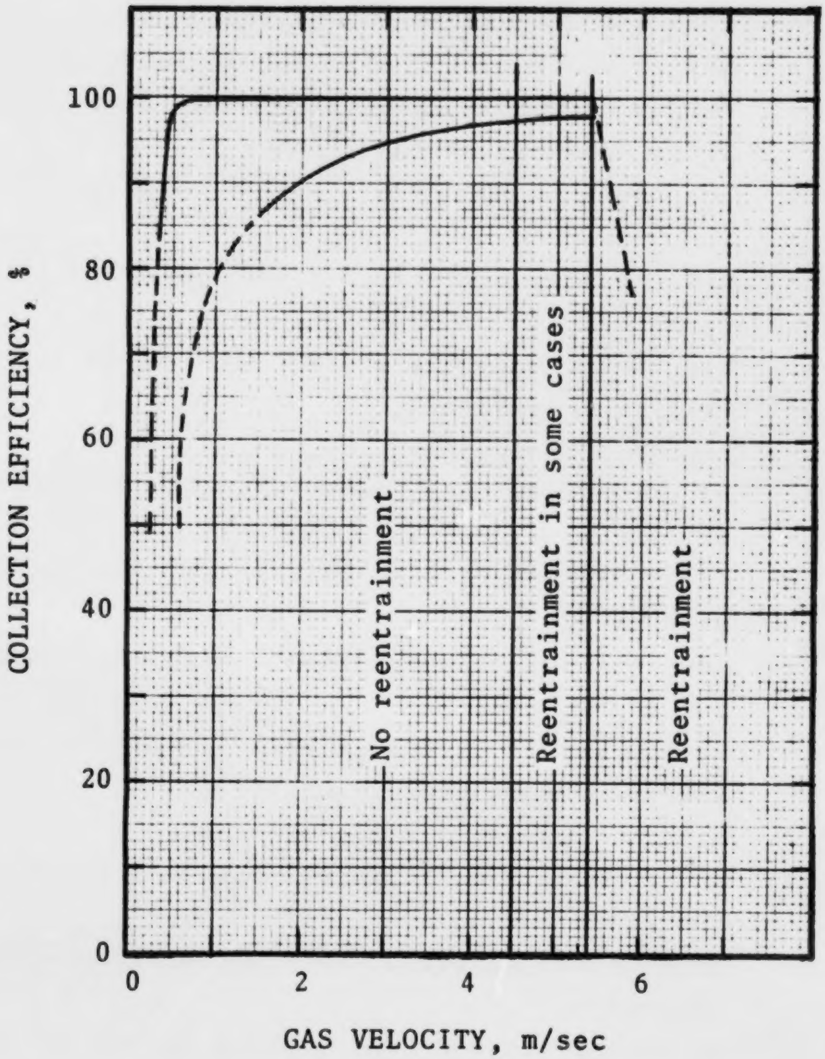

Figure 3-33 - Performance of Koch fleximesh separator

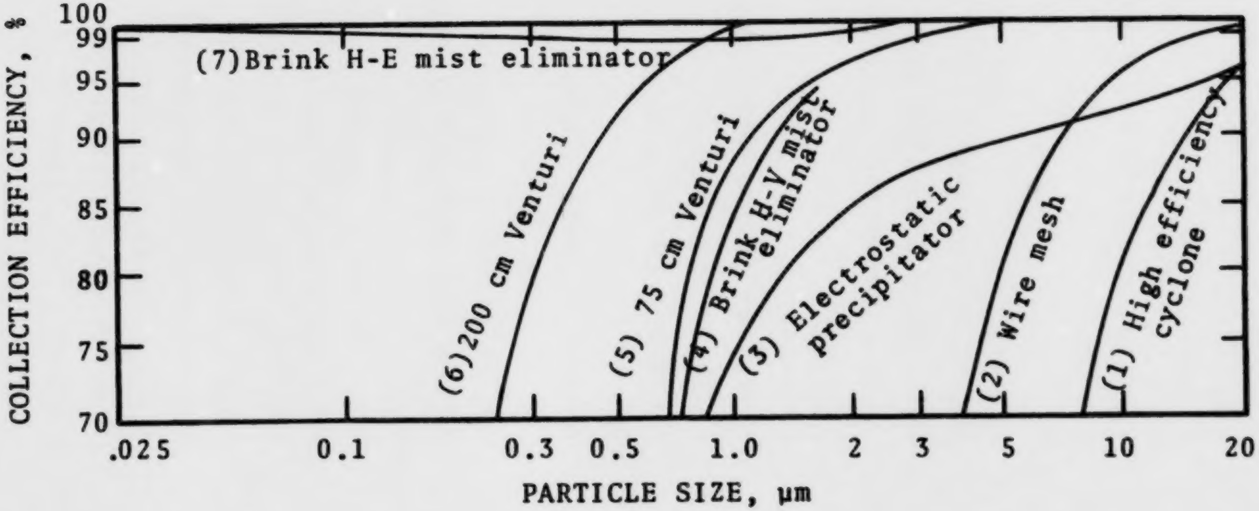

Figure 3-34 - Collection efficiency of particulate collectors.

Research Cottrell

(Type)	Cyclone - integrated with flooded disc wet scrubber
(L)	8-20
(ΔP)	2.5
(App.)	cupolas, electric arc furnace, gas cooling
(Mat.)	316 SS

Tailor & Company

(Type)	Cyclone
(G)	141 (300,000 ACFM)
(E)	exit gas < 2.33×10^{-6} L/G
(Com.)	Cyclone connected to scrubber

Wright Austin Company

(Type)	Cyclone
(G)	0.0025-47 (5-100,000 SCFM)
(U_G)	4,050 no reentrainment up to 7,800
(E)	99% for > 10 μm
(ΔP)	50
(App.)	Removal of drops from wet steam, compressed air and gas
(Com.)	Can be directly connected to steam lines 0.6 cm to 120 cm in diameter

York Separators

(Type)	Mesh single stage and two stage
(L)	5 μm for single stage, 0.3 μm for two stage
(G)	450-540 (950,000-1,040,000 CFM)
(U_G)	Sauder Brown constant for single stage, $k_1 = 0.12$ for 7.5 cm disengaging space and $k = 0.43$ for 38 cm disengaging space
(E)	99.9 for single stage, 100% up to 1 μm for 2 stage - See Figure 3-35

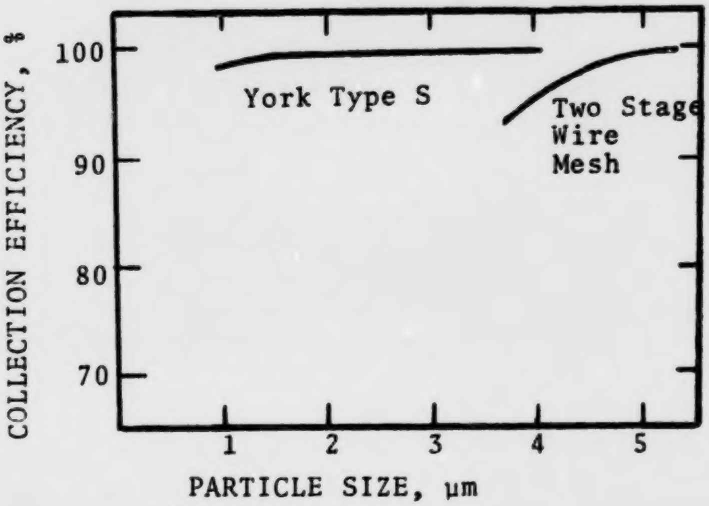

Figure 3-35- Efficiency comparison of York scrubber with two stage wire mesh mist eliminator.

York Separators (continued)

(ΔP)	<2.5 for single stage, 25 for two stage
(App.)	Refinery vacuum towers, distillation equipment, evaporators, absorbers, scrubbers
(Mat.)	SS, Mo, Ni, Inconel, Ti, Ta, Cu, Hastelloy, PE, PP, Teflon

Zurn Industry

(Type)	Impingement separator
(G)	0.57 to 34 (1,200 to 72,000 CFM)
(Type)	Cyclone - integral part of venturi scrubber
(G)	56.3 (120,000 CFM)

THEORY

In the previous chapter equations predicting primary collection efficiency and pressure drop were presented for cyclone, packed bed, tube bank, mesh and sieve plate entrainment separators. Part of this chapter is devoted to the development of mathematical models for primary efficiency and pressure drop in a zigzag baffle separator. In addition, models for reentrainment in both horizontal and vertical baffles and in cyclones are discussed. At this point in the study, these are the only separators for which mathematical models of reentrainment have been formulated.

ZIGZAG BAFFLES

Primary Efficiency

A zigzag baffle section is shown in Figure 4-1. The gas flow pattern in a baffle section is too intricate to be described as a series of gentle bends. The model used to characterize the flow must include the effects of turbulent mixing. One can assume either that mixing occurs after flow through each bend or that mixing occurs continuously throughout the flow path. The latter assumption is made here.

The presumption of turbulence may be verified by calculating the gas Reynolds number as follows:

$$\text{Hydraulic Diameter} = \frac{\text{4x cross-sectional area}}{\text{wetted perimeter}} = 2b' \qquad (4\text{-}1)$$

$$N_{Re,G} = \frac{2b'u'_G\rho_G}{\mu_G} = \frac{2bu_G\rho_G}{\mu_G} \qquad (4\text{-}2)$$

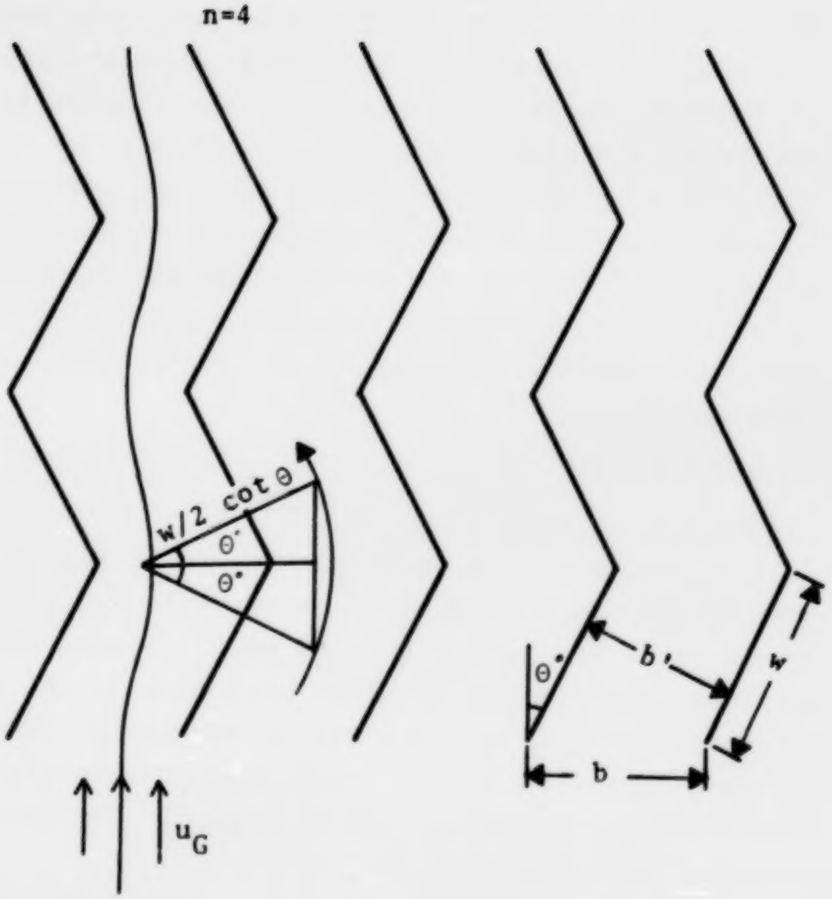
n=4
w/2 cot θ
θ'
θ'
θ'
b'
w
b
u_G

Figure 4-1 - Continuous zigzag baffles

where b' = perpendicular distance between two consecutive baffles in the same row, cm
u'_G = actual gas velocity between the baffles, cm/sec
b = spacing between two consecutive baffles in the same row, cm
u_G = superficial gas velocity based on empty duct, cm/sec = $u'_G \text{Cos}\,\theta$

Under typical conditions used in the pilot plant, $b = 7.25$ cm, $\rho_G = 1.25 \times 10^{-3}$ g/cm^3, $\mu_G = 1.8 \times 10^{-4}$ poise and $u_G = 300$ cm/sec. Therefore, $N_{Re,G} = 3 \times 10^4$ and the flow should be turbulent. The presence of corners and edges in the baffle section should enhance the turbulence.

The gas is assumed to flow as in Figure 4-1. The flow path is a series of alternate bends of angle 2θ, and the total number of bends equals the number of rows of baffles in the entrainment separator.

The terminal settling velocity of a drop, in cm/sec, is:

$$u_t = \frac{d_p{}^2 \sigma_p a}{18 \mu_G} \qquad (4\text{-}3)$$

where d_p = drop diameter, cm
ρ_p = drop density, g/cm^3
μ_G = gas viscosity, centipoise
a = acceleration due to centrifugal force, cm/sec^2

The acceleration due to centrifugal force was approximated on the basis of an average radius of curvature in the baffles, as follows:

$$a = \frac{2(u'_G)^2}{w\ \text{Cot}\,\theta} \qquad (4\text{-}4)$$

Equation (4-3) is based on Stokes law and applies only if the drop Reynolds number $N_{Re,D} < 0.1$. If $N_{Re,D} > 0.1$, an appropriate friction factor should be included in the calculation. Foust, et al. (1959) give a plot of drag coefficient as a function of Reynolds number in Figure 4-2, which can be used to determine "u_t". The effect of surrounding drops on the motion of any individual drop is neglected.

A number balance on the drops entering and leaving an element of fluid $rd\theta$ long, where $r = \frac{w}{2} \cot \theta$ (see Figure 4-1), b' thick and of unit width gives:

$$u'_G b' dc = c u_t r d\theta \qquad (4\text{-}5)$$

where c = number concentration, #/cm³

For the boundary conditions $c = c_o$ (initial concentration) at $\theta = 0$ and $c = c$ at $\theta = 2n\theta$ (where n = number of rows), Equation (4-4) can be integrated to yield:

$$\frac{c}{c_o} = Pt = \exp \ -\frac{u_t}{u'_G}\frac{2nr\theta}{b'} = \exp \ -\frac{u_t}{u_G}\frac{nw\theta}{b \tan\theta} \qquad (4\text{-}6)$$

where Pt = penetration

Figure 4-3 shows penetration versus gas velocity for $n = 6$ with "θ" and "d_p" as parameters. For a single baffle angle penetration is predicted to increase as the drop diameter is lowered. Increasing the angle should result in decreased penetration for a particular drop diameter. In all cases increasing gas velocity is expected to lower the penetration. The effect becomes more pronounced as "θ" and "d_p" are increased.

If drop mixing is neglected, penetration can be expressed as:

$$Pt = 1 - \frac{u_t}{u_G}\frac{nw\theta}{b \tan\theta} \qquad (4\text{-}7)$$

A comparison of the theoretical primary efficiency curves is presented in Figure 4-4. The model based on mixing gives

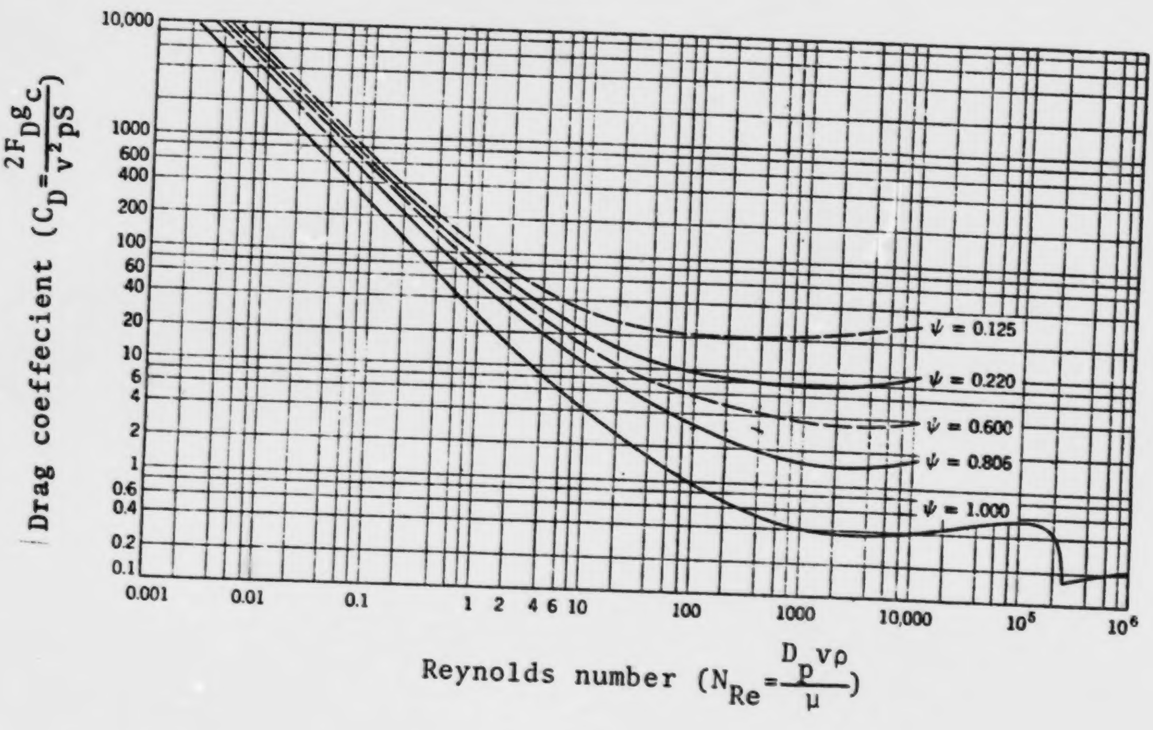

Figure 4- 2 - Drag coefficient versus Reynolds number after Foust et al (1959), with sphericity ψ as the parameter.

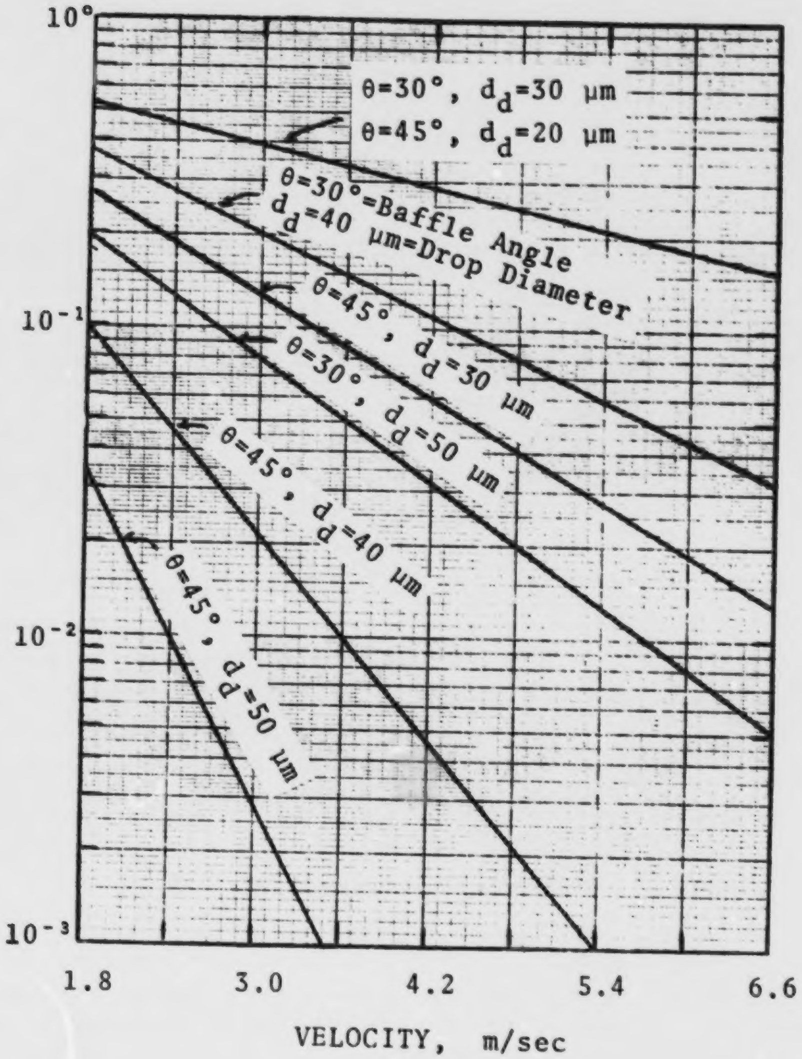

Figure 4-3 - Penetration versus gas velocity for baffle section.

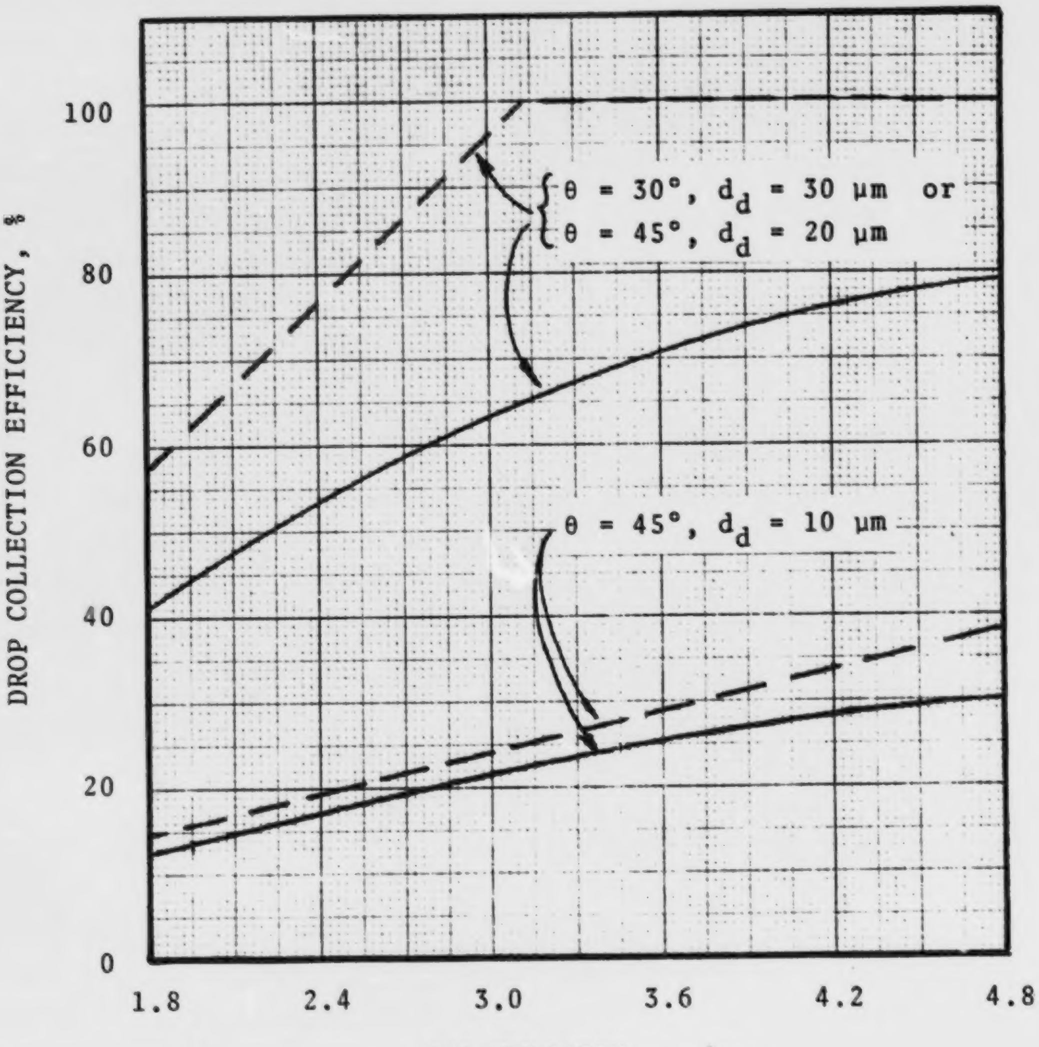

Figure 4-4 - Comparison of primary efficiency curves based on theoretical model for complete mixing (——) and for no mixing (---) models.

an asymptotic increase to 100% efficiency as gas velocity is increased, while the model based on no mixing predicts a linear increase. However, experimental values of primary efficiency in entrainment separators do not show a linear increase with increasing gas velocity. Hence the model based on mixing is considered more valid.

This model was developed for a continuous baffle system. If the baffles are discontinuous and staggered, the efficiency will be higher than that predicted from the present model.

Pressure Drop

Determination of the pressure drop is based on the drag coefficient, "f_D", for a single plate held at an angle "θ" to the flow as presented in Figure 4-5 (Fage and Johanson, 1927). Neglecting the effect of neighboring plates, pressure drop may be expressed as:

$$\Delta P = \sum_{i=1}^{n} f_D \rho_G \frac{u_G'^2}{2} \qquad (4\text{-}8)$$

where the summation is made over the number of rows of baffles.

The actual gas velocity,"u_G'", in the baffle section should be used in Equation (4-8). Note that the angle of incidence for the second and subsequent rows of baffles will be twice the angle of incidence for the baffles in the first row.

Reentrainment

The following sections are devoted to a theoretical development of equations describing the conditions necessary for the occurrence of reentrainment in baffle-type entrainment separators. The first section deals with reentrainment

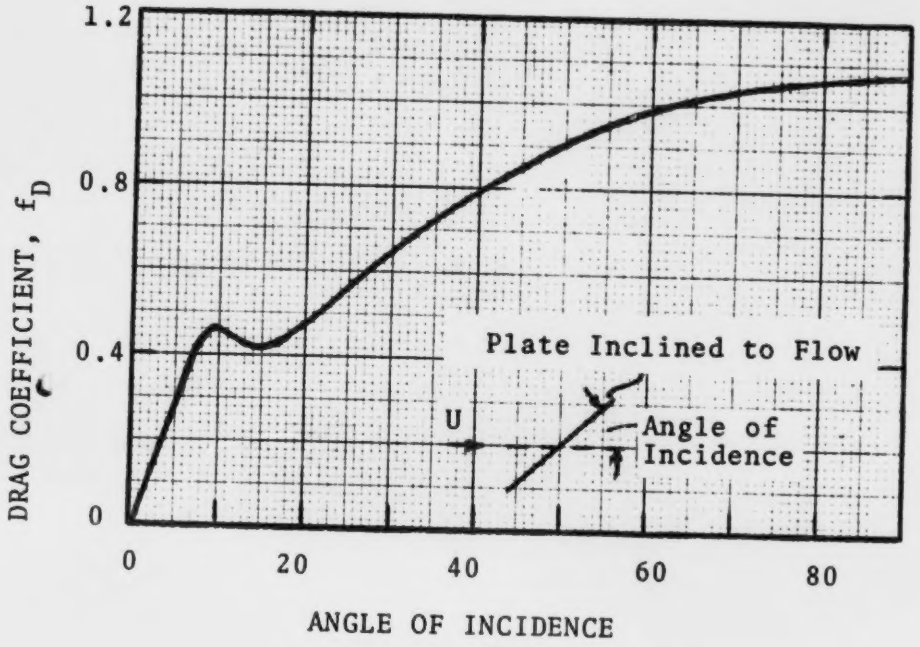

Figure 4-5 - Drag coefficients for flow past inclined flat plates (data from A. Fage & F. C. Johansen, (1927).

in horizontal baffles, and the second with the same phenomenon in vertical baffles.

The significant difference between vertical and horizontal baffles is that in horizontal baffles:

1. Prior to the onset of reentrainment conditions, liquid flows on both sides of the baffles.
2. The wetted perimeter for gravity flow is in proportion to the length of the baffle.
3. Depending upon baffle angle to vertical, only the "g cos θ" component of "g" is available for flow due to the gravity.
4. All the liquid has to flow through the bottom row of baffles.
5. The drag force due to gas velocity and the force due to the gravity are acting in opposite directions.

Whereas in the vertical baffles:

1. Liquid flows on only one side of the baffle.
2. The wetted perimeter for gravity flow is proportional to the width of the baffle.
3. Gravity is acting in the optimum direction for liquid collection.
4. Liquid can be collected on each baffle.
5. The drag force due to gas velocity and the force due to gravity are acting at right angles.

The effects of corners, capillaries and film detachment have not been accounted for. Thus, it is possible for reentrainment to occur before the conditions the model predicts. Nevertheless, the model can be used to determine the upper limit of operating conditions.

Horizontal Baffles - The goal of this section is to derive a relationship which gives the theoretical maximum liquid load, "Q_L/Q_G", at a given air velocity, "u_G", with no re-entrainment. The gas flow rate, "Q_G", can be expressed as:

$$Q_G = bu_G\ell \qquad \text{cm}^3\text{/sec} \qquad (4\text{-}9)$$

where ℓ = baffle length, cm

The liquid flow rate, "Q_L", cm³/sec, is made up of flow due to drag force between the gas and the liquid film and flow due to gravity. The derivation of "Q_L" which follows, results in a system of six equations in nine variables. At that point two additional equations will be formulated in order to determine the desired relationship. For certain selected values of "u_G", the maximum "Q_L/Q_G" can then be found. A diagram of the results is presented.

Derivation of Q_L - The following assumptions are made in considering liquid flow in horizontal baffles:

1. Prior to liquid reentrainment, circulation of the liquid on the baffles takes place, i.e., both sides of the baffle are wet.
2. Interfacial stress is the same on both sides of the baffle, i.e., film thickness is the same on both sides of the baffle.
3. Film flow takes place on the baffle.

The derivation begins by considering the forces acting on a liquid film of thickness,"δ", as shown in Figure 4-6 & 4-7. A force balance on the liquid film bounded by the planes at a distance, "δ" and "Y", from the baffle surface gives:

$$\tau\ell dz + (\delta - Y)\, dz\rho_L g\cos\theta + \left(P + \frac{dP}{dz}dz\right)(\delta - Y)\ell$$
$$= \tau_i\ell dz + P(\delta - Y)\ell \qquad (4\text{-}10)$$

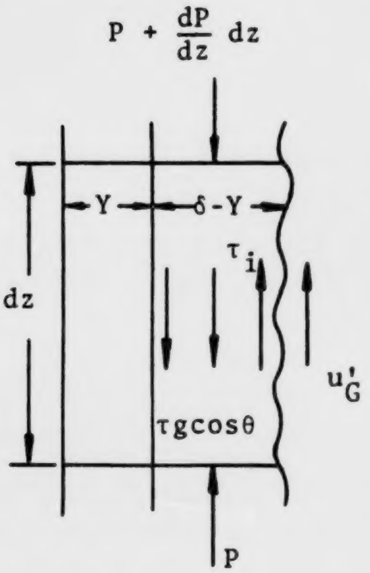
$P + \frac{dP}{dz} dz$
Y
δ-Y
τ_i
dz
u_G'
τgcosθ
P

Figure 4-6 - Forces on an element of liquid film on baffle

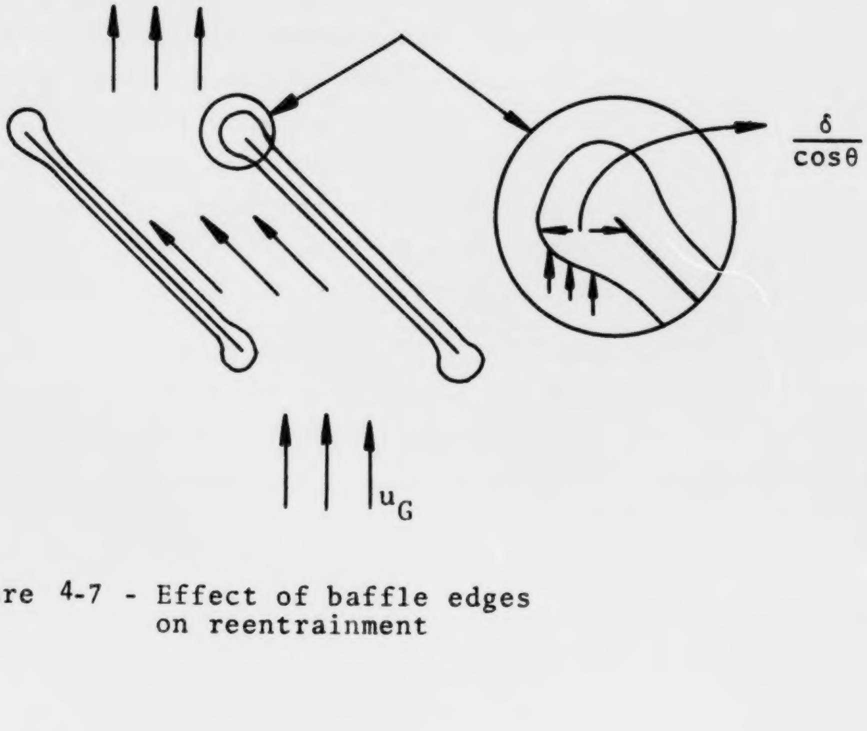
$\frac{\delta}{\cos\theta}$
u_G

Figure 4-7 - Effect of baffle edges on reentrainment

where τ = shear stress, dyne/cm^2
Y = distance from baffle to any point in the liquid film, cm
g = acceleration of gravity, $\frac{\text{cm}}{\text{sec}^2}$
P = pressure, dyne/cm^2
τ_i = interfacial shear stress, dyne/cm^2

Equation (4-10) can be rearranged to:

$$\tau = \tau_i - (\delta - Y)(\rho_L g\cos\theta + \frac{dP}{dz}) \tag{4-11}$$

A force balance on the gas core gives:

$$2\tau_i \ell = -(b' - 2\delta)\ell \frac{dP}{dz} \tag{4-12}$$

For laminar flow in the liquid layer:

$$\tau = -\mu \frac{du}{dY} \tag{4-13}$$

Substitute the value of "τ_i" from Equation (4-12) and the value of "τ" from Equation (4-13) into Equation (4-11) and rearrange to yield:

$$du = \frac{1}{\mu} \left[\frac{(b'-2\delta)}{2} \frac{dP}{dz} + (\delta - Y)(\rho_L g\cos\theta + \frac{dP}{dz})\right] dY \tag{4-14}$$

Integrate over the limits 0 to "u" and 0 to "Y" (no slip flow) to obtain the velocity profile:

$$u = \frac{1}{\mu} \left[\frac{(b'-2\delta)}{2} Y\frac{dP}{dz} + (\delta Y - \frac{Y^2}{2})(\rho_L g\cos\theta + \frac{dP}{dz})\right] \tag{4-15}$$

"Q_L" can now be determined by substitution into its defining equation:

$$Q_L = 2\int_o^{\delta} u\ell dY \qquad (4\text{-}16)$$

which results in:

$$Q_L = \frac{\ell}{\mu} \left[(b'-2\delta)\frac{\delta^2}{2}\frac{dP}{dz} + \frac{2}{3}\delta^3 \left(\rho_L g\cos\theta + \frac{dP}{dz}\right)\right] \qquad (4\text{-}17)$$

Neglect the term containing "$\delta^3 \frac{dP}{dz}$" as compared to "$\delta^2 \frac{dP}{dz}$" (to check: effect of neglecting = $\frac{1/3\delta}{b'/2}$. If δ = 0.1 cm and b' = 5 cm, effect = $\frac{0.1 \times 2}{5 \times 3} < 2\%$) to obtain:

$$Q_L = \left[\frac{\ell}{\mu} \quad \frac{b'\delta^2}{2}\frac{dP}{dz} + \frac{2}{3}\rho_L g\delta^3\cos\theta\right] \qquad (4\text{-}18)$$

Equation (4-18) expresses the liquid flow rate as the sum of its pressure gradient and gravity components. However, it is valid only for laminar flow. Sherwood and Pigford (1952) and Grimley (1948) give the following conditions for determining the flow regime:

Laminar flow without rippling, $N_{Re,L} < 4$ to 25

Laminar flow with rippling, 4 to 25 < $N_{Re,L}$ < 1,000 to 2,000

Turbulent flow, 1,000 to 2,000 < $N_{Re,L}$

where $N_{Re,L} = \frac{4Q_L}{\ell\nu}$

Near the onset of reentrainment conditions, ripples are observed, so the liquid flow due to gravity will be less than predicted for purely laminar flow. Fairs (1944) gives the following equation for gravity flow as:

$$Q_{L,g} = \frac{1}{2.43}\,\frac{2}{3}\,\frac{\ell}{\mu}\,\rho_L g \cos\theta\delta \qquad (4\text{-}19)$$

Therefore, the expression for total liquid flow rate with rippling is:

$$Q_L = \frac{\ell}{\mu}\left[\frac{b'\delta^2}{2}\,\frac{dP}{dz} + \frac{1}{2.43}\,\frac{2}{3}\,\rho_L g \cos\theta\delta^3\right] \qquad (4\text{-}20)$$

Additional Equations - Having derived an equation for "Q_L", we now have two equations, (4-9) and (4-20), in five unknowns, "Q_L", "Q_G", "u_G", "δ", and "$\frac{dP}{dz}$". To narrow the gap, we return to Equation (4-12):

$$\tau_i = -\frac{(b'-2\delta)}{2}\,\frac{dP}{dz} = -\frac{b'}{2}\,\frac{dP}{dz} \qquad (4\text{-}21)$$

if $\delta = 0$ at the gas-liquid interface. By Equation (4-39):

$$\tau_i = \frac{f_i \rho_G u_G'^2}{2} \qquad (4\text{-}22)$$

Substitute (4-22) into (4-21) and solve for $\frac{dP}{dz}$:

$$\frac{dP}{dz} = -\frac{\rho_G}{b'}\,f_i\,u_G'^2 = -\frac{\rho_G\,f_i\,u_G^2}{b\cos\theta} \qquad (4\text{-}23)$$

where $b = b'\cos\theta$ and $u_G = u_G'\cos\theta$.

Equation (4-23) introduces a sixth unknown, "f_i", the interfacial friction factor. Equation (3-38) states:

$$f_i = f_G + 1.5\left[\frac{\delta}{d_{eq}} - \frac{5}{N_{Re,G}}\sqrt{\frac{2}{f_G}}\right] \qquad (4\text{-}24)$$

The two new quantities which appear in Equation (4-24), "$N_{Re,G}$" and "f_G", can be related by commonly available graphs correlating them. "$N_{Re,G}$" can be expressed as:

$$N_{Re,G} = \frac{d_{eq}\ u'_G\ \rho_G}{\mu_G} = \frac{2b\ u_G\ \rho_G}{\mu_G} \qquad (4\text{-}25)$$

At this point we have six equations in eight unknowns, and we need an expression for δ. The pressure on the liquid film due to gas velocity, assuming a drag coefficient of 1, is:

$$P_1 = \frac{\rho_G\ u^2_{Gc}}{2} \qquad (4\text{-}26)$$

where P_1 = pressure due to gas velocity, dyne/cm²

u_{Gc} = reentrainment velocity, cm/sec

Since gas is flowing on both sides of the baffles, a force balance on the liquid film yields:

$$\left(\frac{\rho_G\ u^2_{Gc}}{2}\right) \frac{2\delta\ell}{\cos\ \theta} = 2\sigma\ell \qquad (4\text{-}27)$$

or

$$u^2_{Gc}\ \delta = \frac{2\sigma\ \cos\ \theta}{\rho_G} \qquad (4\text{-}28)$$

Now we have seven equations (4-19, 4-20, 4-23, 4-24, 4-25, 4-28) and the correlation between "$N_{Re,G}$" and "f_G" in nine unknowns (Q_L, Q_G, u_G, δ, $\frac{dP}{dz}$, f_i, f_G, N_{Re}, u_{Gc}). Setting $u_G = u_{Gc}$ gives an eighth equation, enabling us to calculate the maximum liquid load, "Q_L/Q_G", at a given air velocity, "u_G". Baffle angle "θ" is used as a parameter and the result is plotted in Figure 4-8.

Vertical Baffles - The objectives of this section are similar to those for the horizontal baffle section. An equation for

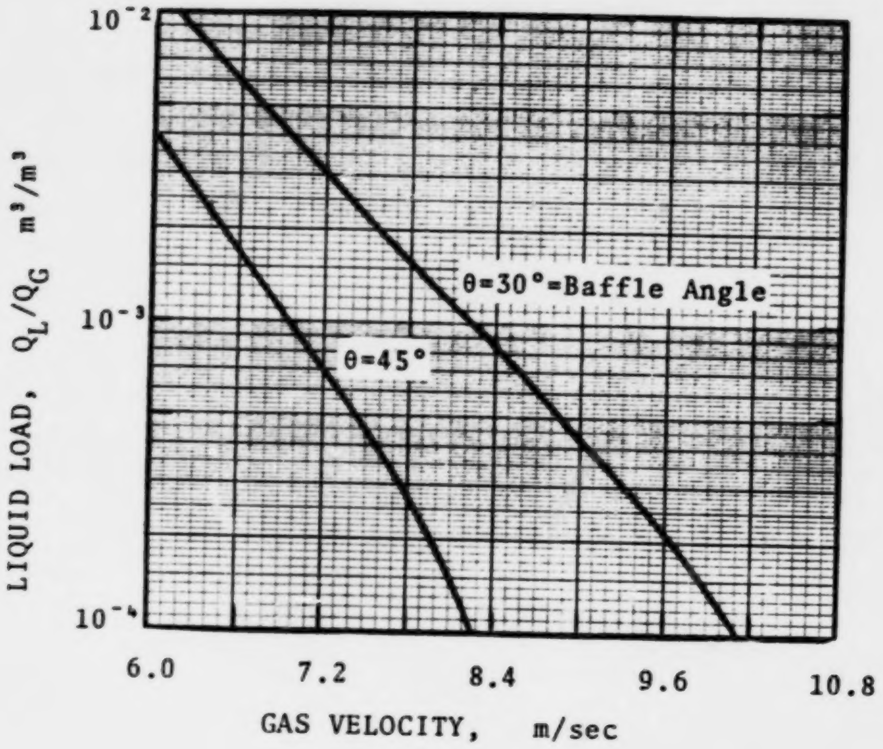

Figure 4-8 - Maximum liquid load, Q_L/Q_G versus gas velocity in horizontal baffle section.

liquid flow on the baffles, "Q_L", will be derived. Combined with other equations, we will be able to construct a diagram for theoretical reentrainment.

Liquid Flow Due to Pressure Gradient - The following assumptions are made in the derivation of "Q_L":

1. Reentrainment takes place only on the edges of the baffles.
2. Film flow takes place on the baffle surface.
3. Liquid collected per unit area of the baffle surface is the same everywhere on a given baffle.
4. Laminar flow with rippling is present everywhere on the baffle.

Consider Figures 4-6 and 4-7, which show a portion of the baffle with liquid film thickness, "δ". A force balance on the film bounded by planes at a distance "δ" and "Y" from the baffle surface gives:

$$\tau \ell dz + \left(P+\frac{dP}{dz}dz\right)(\delta-Y)\ell = \tau_i \ell dz + P(\delta-Y)\ell \qquad (4\text{-}29)$$

which can be rearranged to:

$$\tau = \tau_i - (\delta-Y)\frac{dP}{dz} \qquad (4\text{-}30)$$

Assume laminar flow:

$$\tau = -\mu\frac{du}{dY} \qquad (4\text{-}31)$$

Substitute and rearrange:

$$du = -\left[\frac{1}{\mu}\tau_i - (\delta-Y)\frac{dP}{dz}\right]dY \qquad (4\text{-}32)$$

A force balance on the gas core gives:

$$2\tau_i \Delta\ell = -(b'-2\delta)\Delta\ell\frac{dP}{dz} \qquad (4\text{-}33)$$

Substitute the value of τ_i from Equation (4-21) into Equation (4-32):

$$du = \frac{1}{\mu}\left[\frac{(b'-2\delta)}{2}\frac{dP}{dz} + (\delta-Y)\frac{dP}{dz}\right] dY \qquad (4\text{-}34)$$

Integrate over limits "u" from 0 to "u" and "Y" from 0 to "Y" (no slip flow):

$$u = \frac{1}{\mu}\left[\frac{(b'-2\delta)}{2}\, Y\, \frac{dP}{dz} + (\delta Y - \frac{Y^2}{2})\, \frac{dP}{dz}\right] \qquad (4\text{-}35)$$

The volumetric flow rate of liquid is:

$$Q_L = \int_0^{\delta} u\, \Delta\ell\, dY \qquad (4\text{-}36)$$

where the integrand must be a small section of the baffle length, "Δℓ", rather than the entire length "ℓ". Integration yields:

$$Q_L = \frac{\Delta\ell}{2\mu}\left[(b'-2\delta)\,\frac{\delta^2}{2}\,\frac{dP}{dz} + \frac{2}{3}\,\delta^3\,\frac{dP}{dz}\right] \qquad (4\text{-}37)$$

If the term containing "$\delta^3\frac{dP}{dz}$" is neglected compared to "$\delta^2\frac{dP}{dz}$":

$$Q_L = \frac{\Delta\ell}{\mu}\,\frac{b'\delta^2}{4}\,\frac{dP}{dz} \qquad (4\text{-}38)$$

Substitute the value of "$\frac{dP}{dz}$" from Equation (4-23) to obtain the liquid flow rate in the horizontal direction:

$$Q_L = -\frac{\Delta\ell\,\delta^2 f_i\, u_G'^2\, \rho_G}{4\mu} \qquad (4\text{-}39)$$

Liquid Flow Due to Gravity - As in horizontal flow a section of the baffle must be considered rather than the entire baffle. Ripple flow on a vertical surface of width "Δw" is of the same form as Equation (4-19):

$$Q_L = \frac{1}{2.43}\,\frac{1}{3}\,\frac{\Delta w}{\mu}\,\rho_L\, g\, \delta \qquad (4\text{-}40)$$

The differences in Equation (4-40) from Equation (4-19) are caused by flow on only one side of the baffle and $\theta = 0$ for vertical flow, making $\cos \theta = 1$.

The total flow rate is the sum of the individual flow rates.

Additional Equations - Equations for "δ" and "f_i" have been detailed in the derivation for horizontal baffles. The expressions to be used for this case are identical.

In order to solve the system of equations for vertical baffles, a stepwise calculation on a digital computer must be carried out. In this instance, intervals of $\Delta w = w, w/2, w/3$ and $w/4$ were used with $\Delta \ell = \ell, \ell/2, \ell/3, \ell/4$, respectively. In the present calculations reentrainment was determined using $\Delta w = w/4$ and $\Delta \ell = \ell/4$.

Figures 4-9 and 4-10 show the results of these calculations, with gas velocity as the parameter. Both give reentrainment as a function of liquid loading. Figure 4-9 utilizes a baffle angle of 30°, while for Figure 4-10, $\theta = 45°$.

A comparison of the two figures shows that reentrainment is higher and starts at lower superficial gas velocities for $\theta = 45°$. This is due to the fact that at the same superficial velocity, the actual velocity in the baffle section with $\theta = 45°$ is higher than the actual velocity in the baffle section with $\theta = 30°$.

CYCLONE

Primary Efficiency

The following derivation gives primary efficiency of a cyclone as a function of the average residence time of a drop in the cyclone. The derivation is based on the following assumptions:

1. Drop motion is not influenced by neighboring drops.
2. There is no coalescence of liquid drops in the gas phase.

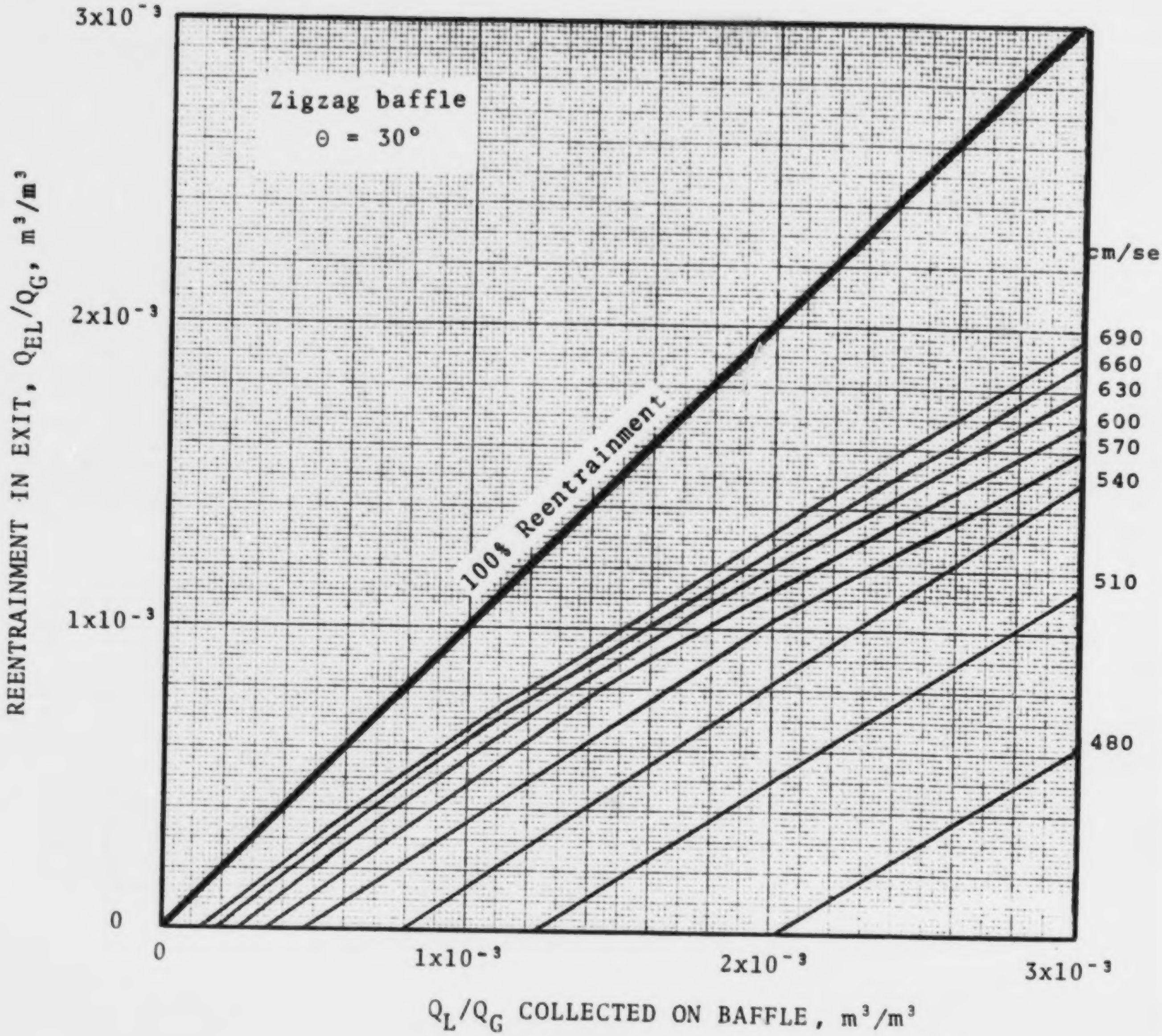

Figure 4-9 - Predicted effect of liquid loading in inlet on reentrainment from vertical baffles. Gas velocity is the parameter.

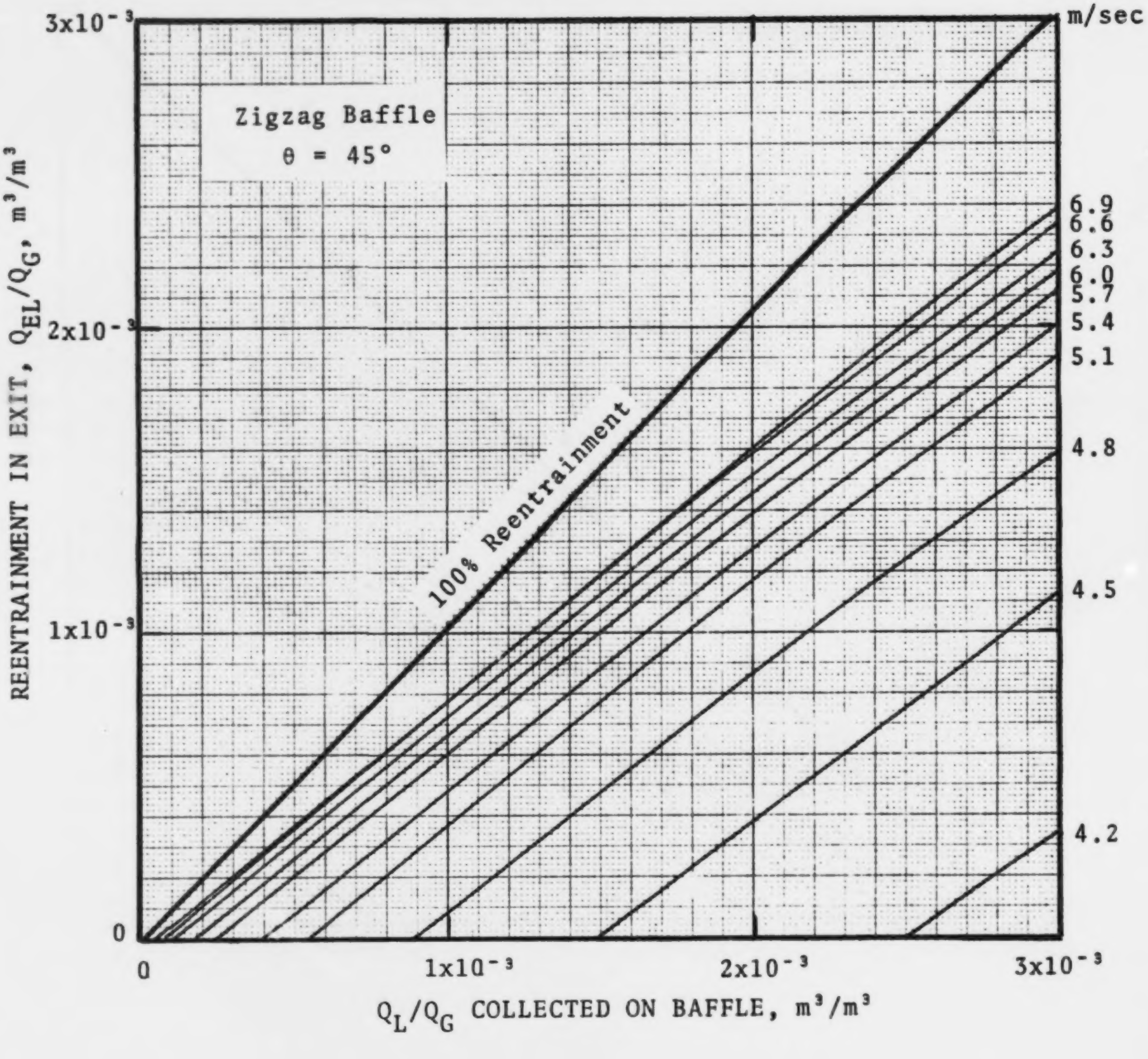

Figure 4-10 - Predicted effect of liquid loading in inlet on reentrainment from vertical baffles. Gas velocity is the parameter.

3. The radial velocity of the gas is zero.
4. The tangential velocity component of the drop is the same as that of the gas stream, i.e., there is no slip in the tangential direction between the drops and the gas.
5. The tangential velocity component is related to the radial position by a modified form of the equation for a free vortex in an ideal fluid.

$$u_{tg}\ r^{n} = \text{constant} \tag{4-41}$$

where u_{tg} = tangential gas velocity, cm/sec

r = radius, cm

n = vortex exponent, defined by Equation (3-5).

6. The drag force, turbulent mixing, and drop bouncing or reentrainment are sufficiently prevalent to insure that a uniform concentration of uncollected drops is maintained in the gas flowing through any horizontal cross-section of a cyclone, i.e., that back-mixing is complete.
7. Reentrainment takes place only in the cylindrical part of the cyclone.
8. The gas velocity near the vortex wall inside the cyclone is equal to the gas velocity in the cyclone inlet.
9. The gas enters the exit core (below the cyclone exit) only in the conical portion of the cyclone.

A force balance on a drop in the cyclone yields:

$$\frac{d^2 r}{dt^2} + \frac{18\ \mu}{\rho_L\ d_\rho^2}\frac{dr}{dt} - u_{tg}^2\ r^{2n}\ \frac{1}{r^{(2n+1)}} = 0 \tag{4-42}$$

From Equation (4-41):

$$u_{tg}\ r^{n} = u_{1}\left(\frac{d_{c}}{2}\right)^{n} \qquad (4\text{-}43)$$

where u_1 = cyclone inlet velocity, cm/sec
d_c = cyclone diameter, cm

Neglecting the second order differential from Equation (4-42) and combining Equations (4-42) and (4-43):

$$\frac{dr}{dt} = \frac{d_{p}\ u_{1}^{2}\ \rho_{L}}{18\mu}\left(\frac{d}{2}\right)^{2n+2}\ \frac{1}{r^{2n+1}} \qquad (4\text{-}44)$$

If the drop just reaches the cyclone wall in time "Δt", then $r = d_c/2$ and from integration of Equation (4-44):

$$\Delta t = \frac{9\mu}{(n+1)\rho_{L}}\left(\frac{d_{c}}{2u_{tg}d_{p}}\right)^{2}\left[1 - \left(\frac{2r}{d_{c}}\right)^{2n+2}\right] \qquad (4\text{-}45)$$

Consider a horizontal cross-section of a cyclone, as shown in Figure 4-11. In time "dt", all drops a distance "dr" or less from the cyclone wall will move to the wall and be collected. Meanwhile the drops will travel a distance "$rd\theta$" tangentially and "dh" vertically. The number of drops removed, "dn_i", will be:

$$-\ dn_{i} = \frac{d\theta}{2}\left[\frac{d_{c}^{2}}{4} - \left(\frac{d_{c}}{2} - dr\right)^{2}\right]c\ dh \qquad (4\text{-}46)$$

where c = number concentraion of drops, #/cm³

The total number concentration of drops in the sector from which drops are removed is:

$$n_{i} = \frac{d\theta}{8}\ d_{c}^{2}\ c\ dh \qquad (4\text{-}47)$$

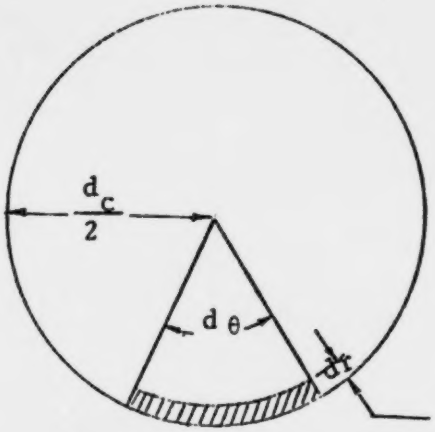
$\frac{d_c}{2}$
d θ
dr

Figure 4-11 - Cross section of a cyclone.

The fraction of drops removed in time "dt" is therefore:

$$-\frac{dn_i}{n_i} = \frac{d_c\ dr - dr^2}{d_c^2/4} \approx \frac{4dr}{d_c} \tag{4-48}$$

neglecting the second order differential.

In order to relate the fraction of drops collected to the average residence time, it is necessary to express Equation (4-48) in terms of time. This may be done through Equation (4-44):

$$\frac{dr}{dt} = \frac{\rho_L}{18\mu}\left(\frac{2d_p u_{tg}}{d_c}\right)^2 \frac{d_c}{2}\left[\frac{\rho_L(n+1)}{9\mu}\left(\frac{2d_p u_{tg}}{d_c}\right)^2 t\right]^{\frac{(2n+1)}{(2n+2)}} \tag{4-49}$$

Combining Equations (4-48) and (4-49):

$$\int_{n_i}^{n_{i+1}} \frac{dn_i}{n_i} = -\int_0^{\Delta t} \frac{\rho_L}{9\mu}\left(\frac{2d_p u_{tg}}{d_c}\right)^2 \left[\frac{\rho_L(n+1)}{9\mu}\left(\frac{2d_p u_{tg}}{d_c}\right)^2 t\right]^{-\frac{(2n+1)}{(2n+2)}} dt \tag{4-50}$$

Integrating up to the average residence time "t" we obtain the equation for primary collection efficiency:

$$\ln\left(\frac{n_{i+1}}{n_i}\right) = -2\left[\frac{\rho_L}{9\mu}\left(\frac{2d_p u_{tg}}{d_c}\right)^2 (n+1)\Delta t\right]^{\frac{1}{2n+2}} \tag{4-51}$$

Reentrainment

Onset of Reentrainment - There is great disagreement among results for the onset of reentrainment obtained by different investigators. This is indicative of the problem of defining the onset of reentrainment. Zhivaikin's (1962) equations will be used here for the onset of reentrainment:

$$P = 29.2\, N_{Re,L}^{-0.75} \quad \text{if} \quad N_{Re,L} \leq \frac{0.085}{\nu_L^{\,2}} \tag{4-52}$$

$$P = 100\nu_L\, N_{Re,L}^{-0.25} \quad \frac{0.085}{\nu_L^{\,2}} \leq N_{Re,L} \leq \frac{28.8}{\nu_L} \tag{4-53}$$

$$P = 43.2\, \nu_L^{\,1.25} \quad N_{Re,L} \geqq \frac{28.8}{\nu_L} \tag{4-54}$$

where $$P = \frac{u_{Gc}\mu_L}{\sigma} \tag{4-55}$$

It is assumed that reentrainment does not take place if the onset of reentrainment conditions are not met. The liquid Reynolds number used to determine onset of reentrainment is based on the liquid flowing in the film. It is assumed that the diameter of the inner core of the vortex is the same as the diameter of the exit pipe, d_e. Thus, the hydraulic diameter is $(d_c - d_e)$.

Drop Diameter of Reentrainment - The drop diameter of the reentrained liquid has a size distribution which varies with gas flow rate, liquid flow rate, fluid properties and perhaps pipe diameter. The average drop diameter decreases with increase in gas flow rate. On the other hand, the liquid flow rate has only a weak and ambiguous effect. When the gas velocity exceeds 6,000 cm/sec, high liquid flow rate has no effect on the drop size distribution.

Rate of Reentrainment - It is believed that reentrainment takes place due to penetration of liquid waves into the turbulent zone of the gas. The amplitude of the waves increases exponentially with liquid flow rate. Therefore, reentrainment is assumed to take place in proportion to $\exp(K_1\ N_{Re,L})$ where "K_1" is a constant.

The rate of reentrainment depends upon gas flow rate, liquid flow rate and fluid properties. According to Anderson et al. (1964), the rate of reentrainment is approximately 4% for $N_{Re,L} > 2,750$ and is seen to increase slightly with $N_{Re,G}$ (3.5% for $N_{Re,G} = 3 \times 10^4$, 4% for $N_{Re,G} = 1.6 \times 10^5$). Below $N_{Re,L} = 2,750$, the only data available are for $N_{Re,L} = 1,150$, at which point reentrainment is 0.5%.

Reentrainment Calculation - In order to determine reentrainment in a cyclone, a stepwise calculation was carried out with the aid of a digital computer. Each step represented 30 cm of gas travel. The primary collection efficiency, reentrainment velocity, reentrainment and secondary collection were calculated, and a material balance was carried out at the end of each step. Some of the results appear in the following four figures.

Figure 4-12 shows the predicted reentrainment from a cyclone as a function of gas velocity with inlet drop diameter as the parameter. Reentrainment is seen to be insensitive to drop diameter at velocities greater than about 37.5 m/sec.

Figure 4-13 gives the theoretical reentrainment as a function of liquid loading. A gas velocity of 30 m/sec and an inlet drop diameter of 50 μm was used to plot this curve. As expected, increased liquid loading should increase the reentrainment under the stated conditions.

Figure 4-14 is a comparison of the primary and overall efficiencies of a cyclone. The effect of the drop size distribution is seen to be small. The overall efficiency curves are obtained by subtracting reentrainment from the primary efficiency curve.

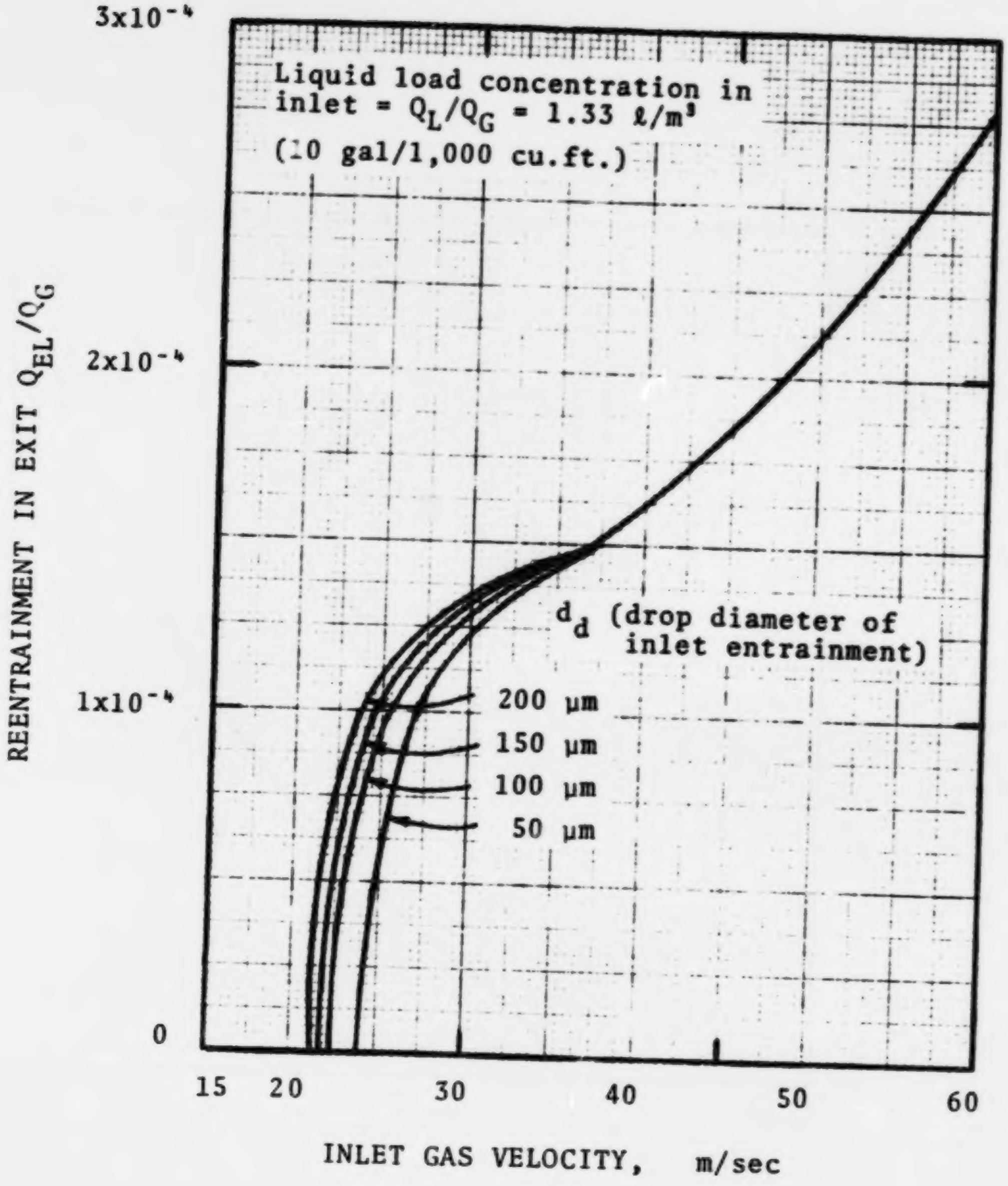

Figure 4-12 - Predicted effect of inlet gas velocity on reentrainment in cyclone with a=9.2 cm, b=28 cm, d_c=127 cm, h_s=132 cm, and d_e=67 cm.

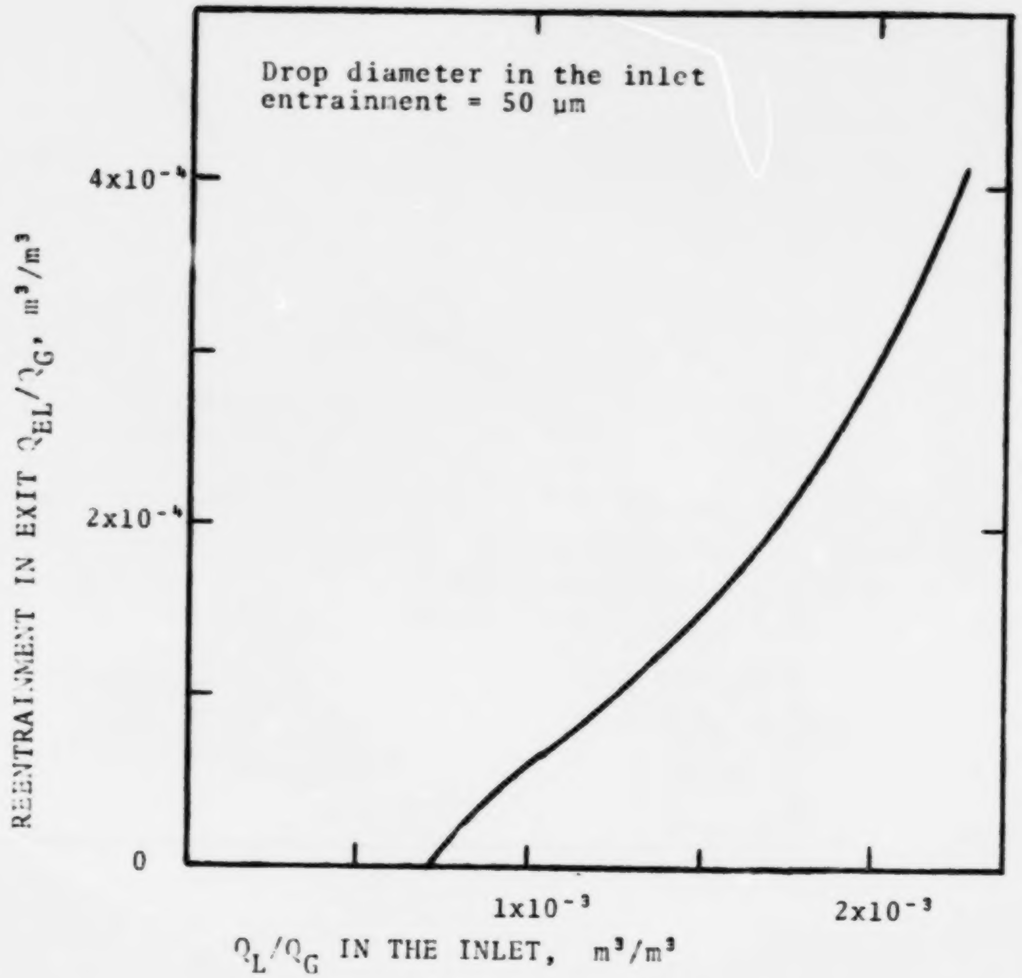

Figure 4-13 - Predicted effect of liquid loading in inlet on reentrainment in cyclone with a=9.2 cm, b=28 cm, d_c=127 cm, h_s=132 cm and d_e=67cm.

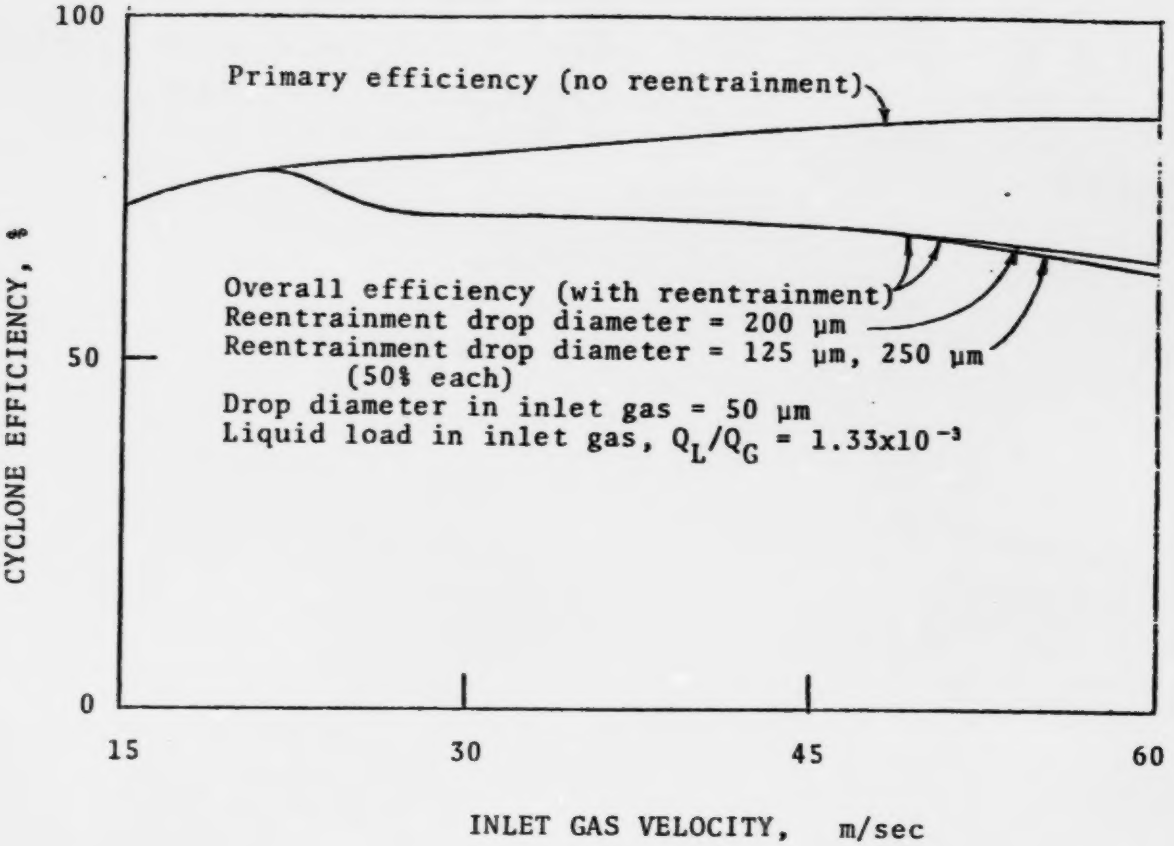

Figure 4-14 - Predicted effect of inlet gas velocity on efficiency of cyclone with a=9.2 cm, b=28 cm, d_c=127 cm, h_s=132 cm and d_e=67 cm.

Figure 4-15 gives the predicted efficiency for an efficient or long cyclone. A height of 381 cm for the cylindrical part of the cyclone is used instead of 127 cm as in Figure 4-14. Reentrainment is predicted to cause a sharper drop in the overall efficiency for the longer cyclone, despite the fact that overall efficiency is higher.

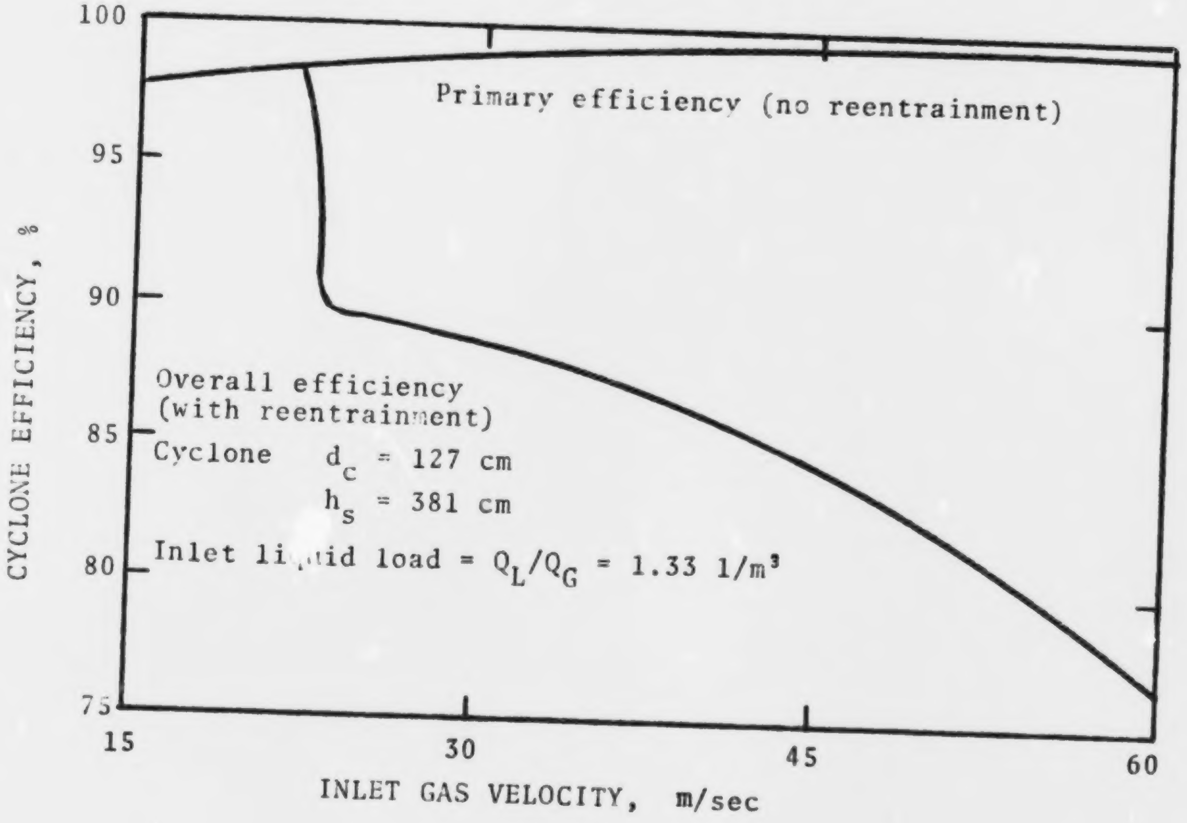

Figure 4-15 - Predicted collection efficiency with and without reentrainment for cyclone with a=9.2 cm, b=28 cm, d_c=127 cm, h_s=381 cm, and d_e=67 cm.

AUXILIARY EXPERIMENT

As discussed in Chapter 3, the first mechanism for reentrainment, i.e. transition from separated to separated-entrained flow caused by high gas velocity, represents the theoretical upper limit of entrainment separator operation. However, in actual practice reentrainment takes place at much lower velocities due to the fact that gas and liquid do not flow in a simple geometry as in annular flow. For instance, jets of the gas stream may strike the water film at an angle, resulting in entrained droplets.

In view of our need for additional information, a small scale experiment was carried out to make visual observations of the transition from separated flow to separated-entrained flow, including the following:

A. Observe the effect of duct dimensions.

B. Study entrainment velocities as a function of the liquid flow rate.

C. Study drop size distribution created by the above transition.

D. Study the effect of impingement angle between air and water phase on entrainment velocities.

For design purposes it is necessary to know the effect of duct dimensions and liquid flow rate on the transition from separated to entrained flow. The drop size created by reentrainment will govern the efficiency of separation of any later stages. For example, a series of two entrainment separators can be used so that the first stage acts as a high-velocity coalescer, while the second is a low-velocity, efficient separator. Thus, the drop size of the reentrainment in the first separator will play an important role in the overall efficiency.

Cousins and Hewitt (1968) and Wicks and Dukler (1966) studied the drop size distribution obtained in the separated-entrained flow. Chien and Ibele (1962), Steen and Wallis (1964) and Zhivaikin (1962) studied the onset of entrainment in separated flow. Most of this work was done on small diameter tubes and there are some differences in the results. Thus, it is necessary to check their results and obtain further information for design of entrainment separators. No work has been reported on the effect of impingement angle.

Figure 5-1 shows the apparatus used to study two-phase flow. It consisted of an open channel 6.5 cm wide and inclined at 30° from the horizontal connected to an overflow tank at the top and a collection funnel at the bottom. The channel was 77 cm long and made of aluminum. Air was blown through a nozzle 5.4 cm x 1.9 cm directly on the water film in the channel at various angles from 0° (parallel to water flow) to 40°. A pitot tube connected to an inclined manometer was used to measure air velocity.

The liquid was introduced into the channel from the overflow tank. Air was introduced with the air inlet nozzle positioned slightly above the liquid film so as not to disturb it. Visual observation and a technique utilizing chemically treated filter paper were used to determine the transition from separated to separated-entrained flow.

SAMPLING FOR DROPLET SIZE DISTRIBUTION

Due to its simplicity, the chemically treated filter paper technique was used to obtain drop size distribution of the entrainment. The method is described by Chilton (1952) and utilizes Whatman filter paper #1 treated with alkali fast green for sampling. The blot diameter is

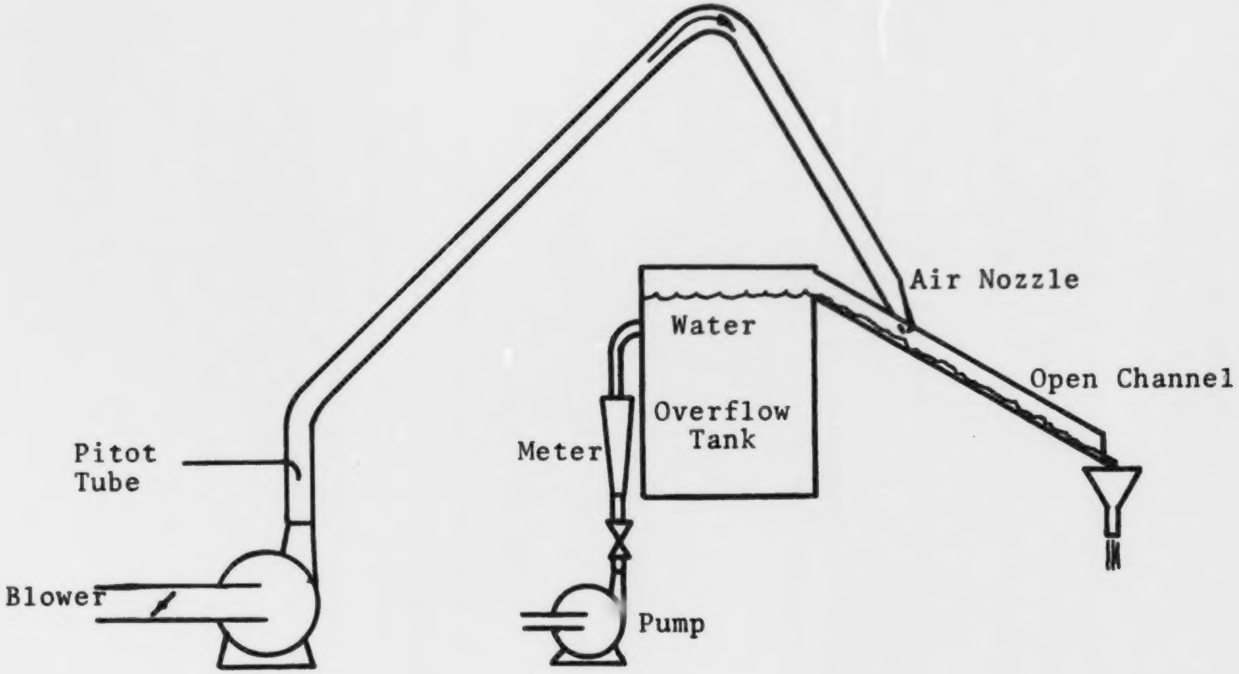
Air Nozzle
Open Channel
Water
Overflow Tank
Meter
Pitot Tube
Blower
Pump

Figure 5-1 - Apparatus to study onset of entrainment velocities

usually larger than the drop diameter due to expansion, and the correlation between the diameters is given by Chilton. It has been determined that there is no effect of using different chemicals, except that chemicals affecting surface tension will have a different correlation.

Some errors in the sampling of drop diameters by filter paper are discussed below:

(1) If the concentration of the blots on the filter paper is high, a few of the blots will overlap. A correction is necessary if the area occupied by the blots exceeds 10% of the area of the filter paper.

During the sampling, drops spread in the filter paper. It is assumed that the blots in the filter paper all have thickness "t_1" which is independent of the blot size in the range of diameters measured on filter paper. Then, by material balance:

$$\frac{\pi}{4} d_b^2 t_1 = \frac{\pi}{6} d_p^3 \qquad (5\text{-}1)$$

where, t_1 = blot thickness, cm

d_b = blot diameter, cm, if blots do not overlap

$$\therefore d_p \propto d_b^{2/3} \qquad (5\text{-}2)$$

The 2/3 slope in the correlation between blot diameter and drop diameter by Chilton (1952) confirms Equation (5-2). Thus, even if the drops overlap, the area occupied by the blots on the filter paper will be the same.

Sauter (1952) showed by statistical analysis that if drops in air are projected onto a plane, the measured value of the fractional area occupied by the shadows, "A'", is related to the actual value of fractional area, "A", by:

$$A = -\ln(1-A') \qquad (5\text{-}3)$$

where A = the fractional area of the shadows if the drops do not overlap. Thus, in the present case:

$$A \ \alpha \ N d_b'^2 \tag{5-4}$$

and

$$A' \ \alpha \ N' d_b'^2 \tag{5-5}$$

where N' = number of blots in a given area

N = number of blots in a given area if blots do not overlap.

d_b' = measured blot diameter, cm

$$\therefore N = N' \frac{A}{A'} \tag{5-6}$$

$$N = N' \left(\frac{A}{1-e^{-A}} \right) \tag{5-7}$$

Since, $N d_b{}^2 = N' d_b'^2$: (5-8)

$$d_b = d_b' \sqrt{\frac{1-e^{-A}}{A}} \tag{5-9}$$

This is the average correction and should be applied to the mean diameter of the blots.

The fractional area can be obtained by simply measuring the blot diameters in a unit area and using the following relationship:

$$A = \Sigma \ \frac{\pi}{4} \ N' \ d_b'^2 \tag{5-10}$$

(2) While measuring the blot diameters, care should be taken not to repeat or leave out some blots. This error possibility may be reduced by using the same technique used to count blood cells.

(3) The capture efficiency of the filter paper is not 100%. A correction is necessary to obtain the actual size distribution.

To determine the error in the sampling, Figure 5-2 was constructed. Drop collection efficiency of a filter paper is plotted against drop diameter, with gas velocity as a parameter. Drop collection efficiency was obtained from the correlation between impaction efficiency and inertial parameter by Golovin and Putnam (1962). The adhesion of the particle to the collector is assumed to be 100% in this case. As seen in Figure 5-2, the error in measuring drop size distribution at the gas velocities and drop diameters used for these experiments is quite small.

DISCUSSION

The liquid film was about 1-3 mm thick and was quite smooth, with no pulsation except when the entrainment velocity was approached. The liquid film thickness was constant in the bottom of the channel in the absence of the air flow. With air flowing, the liquid film thickness in the corners of the channel was higher than in the center of the channel. This increase in the flow rate of the liquid in the corners increases with increase in the total liquid flow rate.

The liquid film thickness at the point of air impingement was much smaller than the thickness upstream from that point (for impingement angle >0°). At a certain distance downstream from the point of air impingement, the liquid film regained its former thickness. Entrainment was observed to take place near the downstream spot where the liquid film rose.

The air velocity measured is the actual air velocity and should be distinguished from the superficial air velocity used by other investigators. If the liquid film is 1-3 mm thick and the tube diameter 2.5 cm, the difference between actual and superficial velocities may be 10 to 40%.

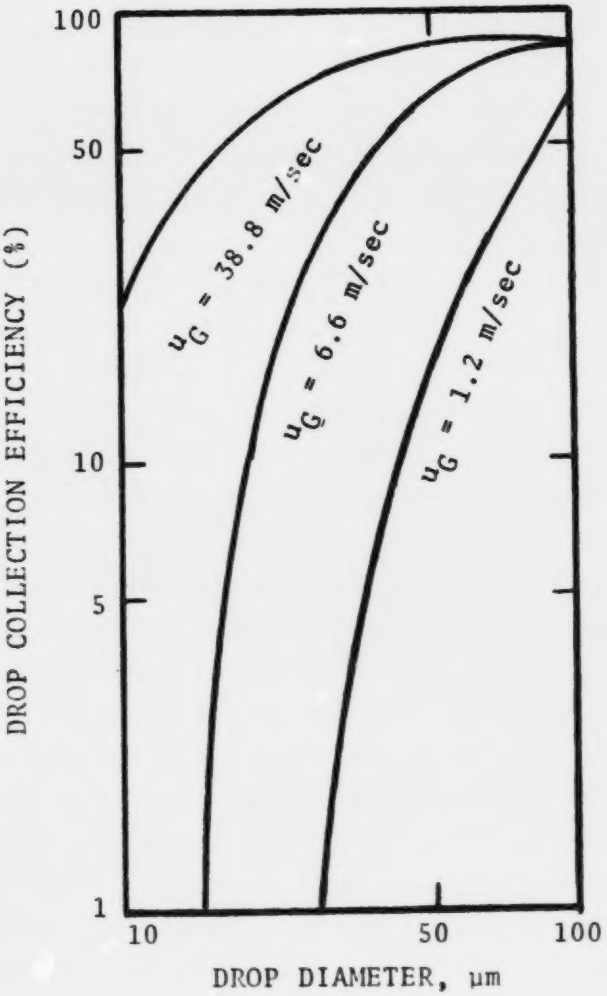

Figure 5-2 - Predicted effect of drop diameter on capture efficiency by 5 cm diameter filter paper held perpendicular to the air velocity.

RESULTS

Figure 5-3 shows the drop size distribution in the separated-entrained flow. The drop size distribution was measured by increasing the air velocity to the point where measurable entrainment was first observed on the coated filter paper. There is no significant effect of different flow rates on the drop size distribution. The average drop diameter is about 250 μm. The distribution of the drop sizes is such that the majority of the drops are small, but these contribute relatively little to the total volumetric drop flow.

Figure 5-4 represents, on a log-probability diagram, the same size distribution as shown in Figure 5-3. It is log normal with mass median drop diameter of 250 μm and geometric standard deviation of 1.5.

A comparison of drop size distributions obtained by various investigators with the present results is shown in Figure 5-5. The data of Cousins and Hewitt (1968) were obtained during experiments on the mass transfer of liquid droplets subsequent to the removal of the liquid film. Photographs of the droplets were obtained for a zone immediately adjacent to the channel wall, and the images on the photographs were measured to produce drop size data.

The Wicks and Dukler (1966) data were obtained by a technique using variable spaced needles. The liquid was injected using a porous wall section. These data should be treated with some reservations, since the reliability of the method of measurement is still uncertain. Figure 5-5 shows that all the distributions are similar in form with slight variation from present results near the end of the curve.

In the present runs the effect of gas velocity on the drop size distribution was found to be negligible. However, the data of other investigators, as shown in Figure 5-5,

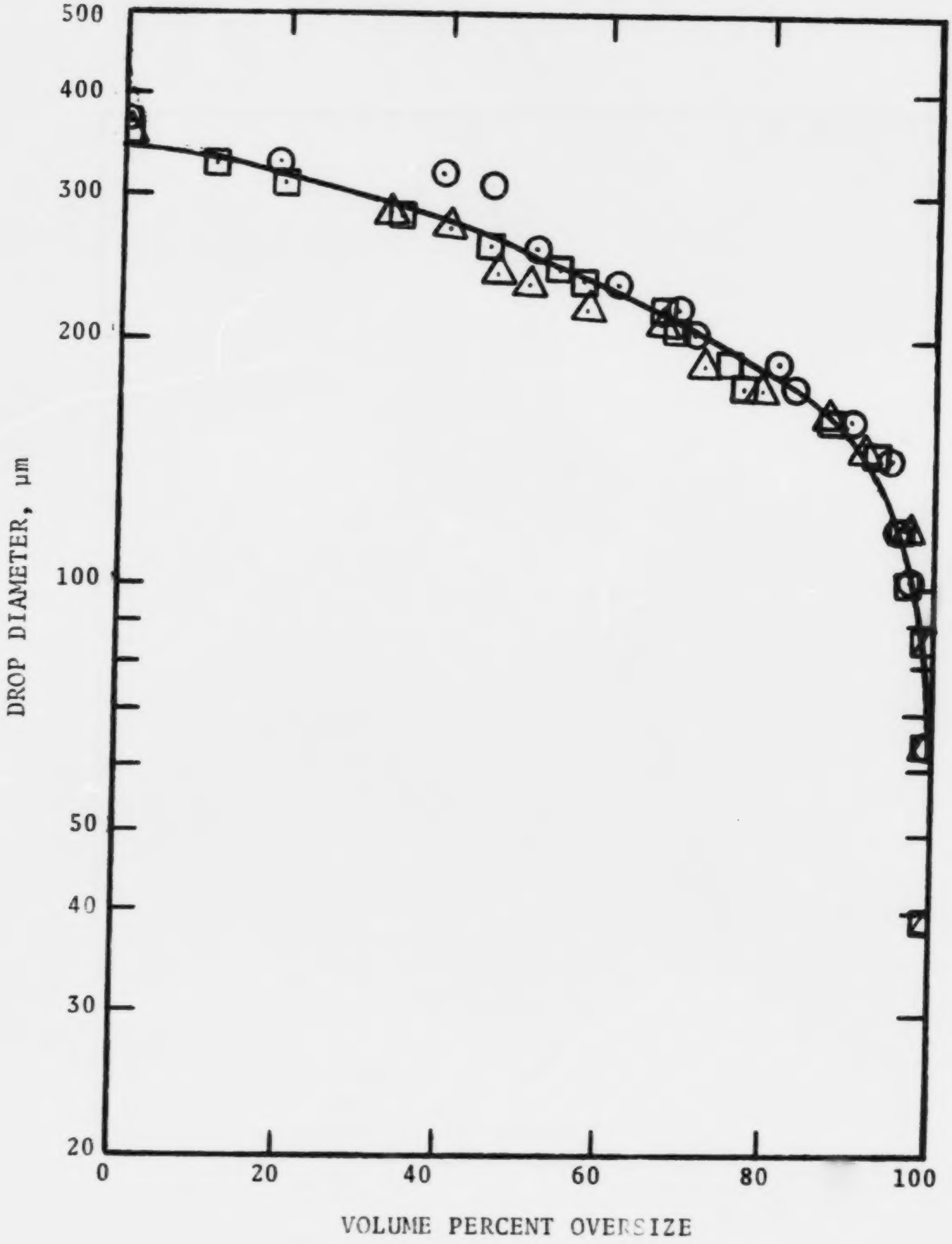

Figure 5-3 - Distribution of droplet size in air-water entrained-separated flow.

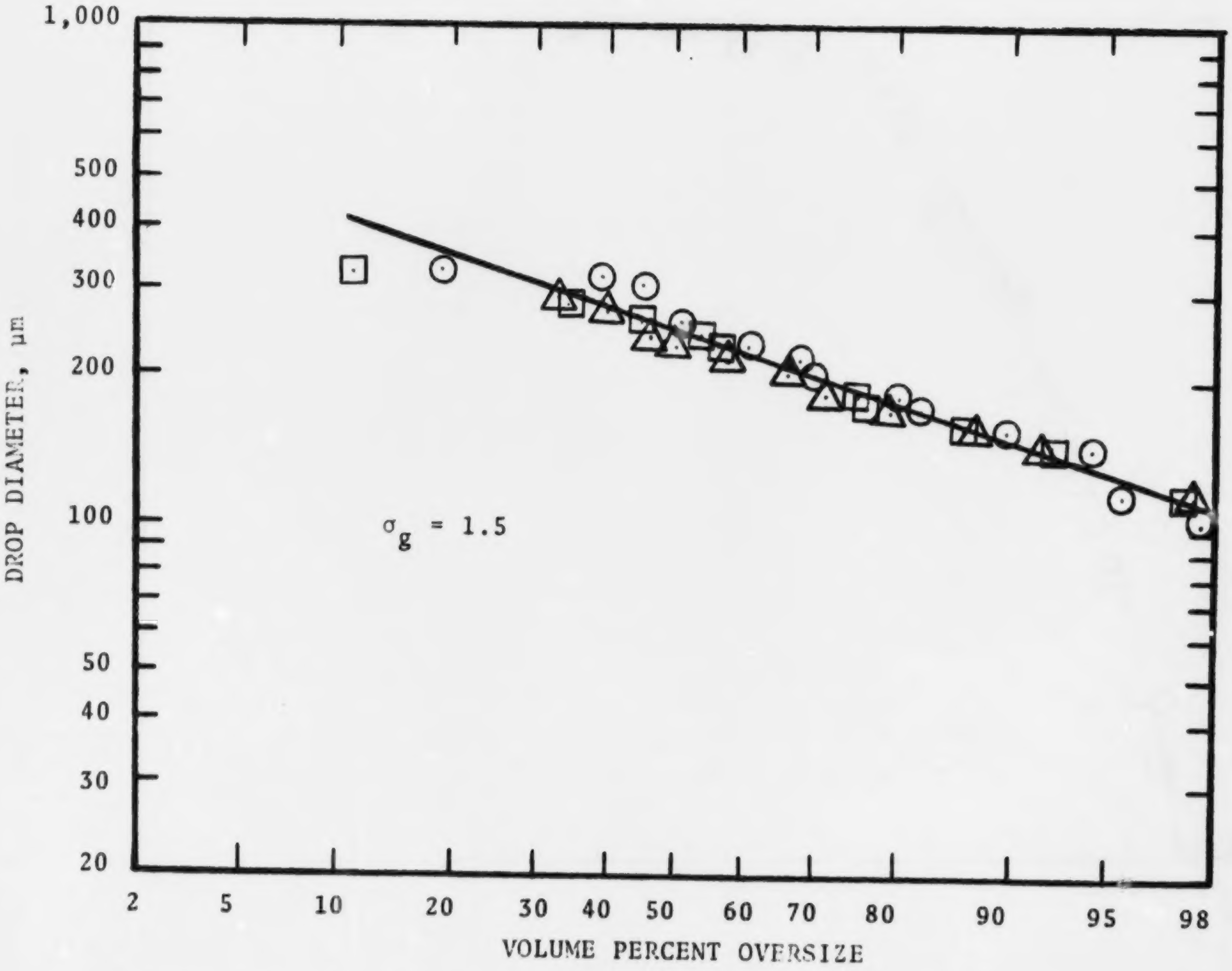

Figure 5-4 - Distribution of droplet size in entrained-separated flow on log-probability graph

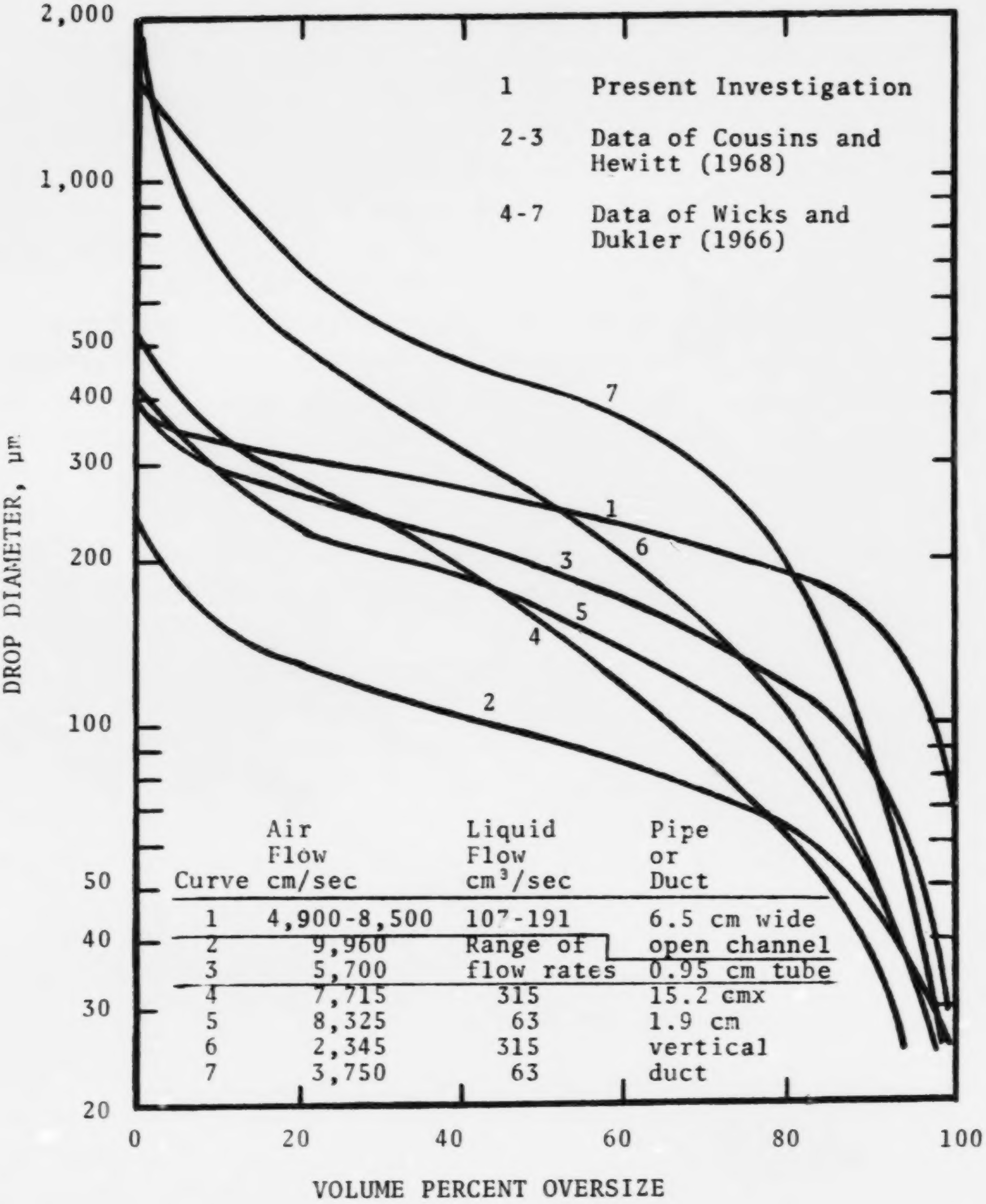

Curve	Air Flow cm/sec	Liquid Flow cm³/sec	Pipe or Duct
1	4,900-8,500	107-191	6.5 cm wide open channel
2	9,960	Range of flow rates	
3	5,700		0.95 cm tube
4	7,715	315	15.2 cmx 1.9 cm vertical duct
5	8,325	63	
6	2,345	315	
7	3,750	63	

Figure 5-5 - Comparison of drop size by different investigators

indicate that increasing gas velocity tends to reduce the mass median diameter. In the velocity range depicted in Figure 5-5, the mass median diameter decreases by roughly 40% when the gas velocity is doubled.

The effect of impingement angle between the gas and the liquid stream is shown in Figure 5-6. It shows the drop diameter versus volume percent oversize in separated-entrained flow. Impingement angle is used as a parameter and was varied for a given water flow rate until entrainment was detected. These data were obtained with air velocity of 38 m/sec through the nozzle outlet, a velocity smaller than the critical velocity needed for entrainment in parallel flow. Thus, the effect of impingement angle (>0°) is a reduction in entrainment velocity. From Figure 5-6 a slight effect of impingement angle on the drop size distribution is seen.

The effect of liquid flow rate on the impingement angle needed to produce entrainment is shown in Figure 5-7. Air velocity was 38.8 m/sec during these runs. The effect of increasing the impingement angle is to reduce the liquid velocity required for entrainment.

Figure 5-8 compares the results for entrainment velocities obtained by various investigators. Here u_{Gc} = gas velocity causing entrainment and the liquid Reynolds number, "$N_{Re,L}$", is the superficial liquid Reynolds number based on the empty cross-section of the duct:

$$N_{Re,L} = \frac{4Q_L}{d_o \nu_L} \qquad (5\text{-}11)$$

where ν_L = kinematic viscosity of the liquid, cm²/sec
d_o = duct width, cm

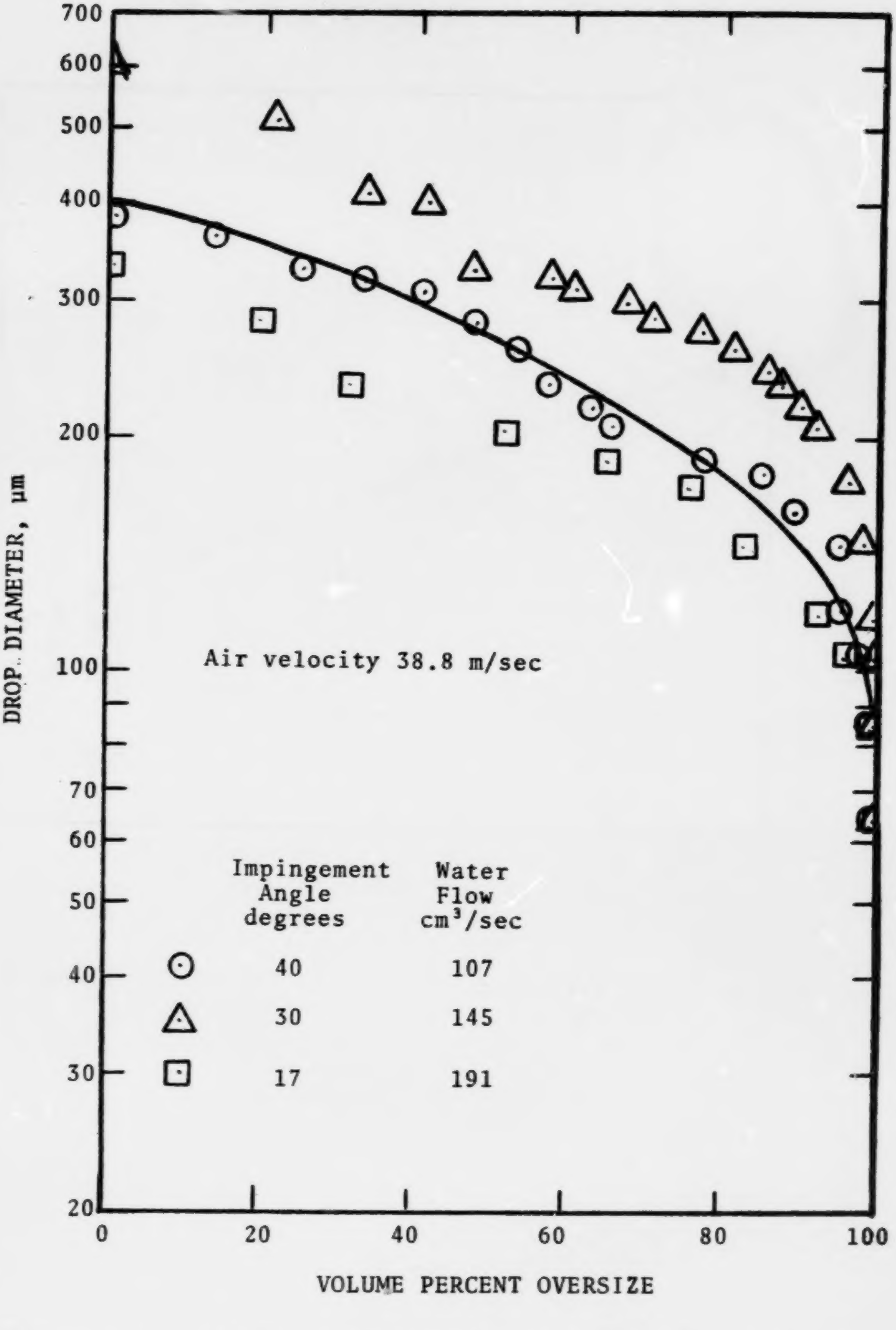

Figure 5-6 - Effect of impingement angle on drop size

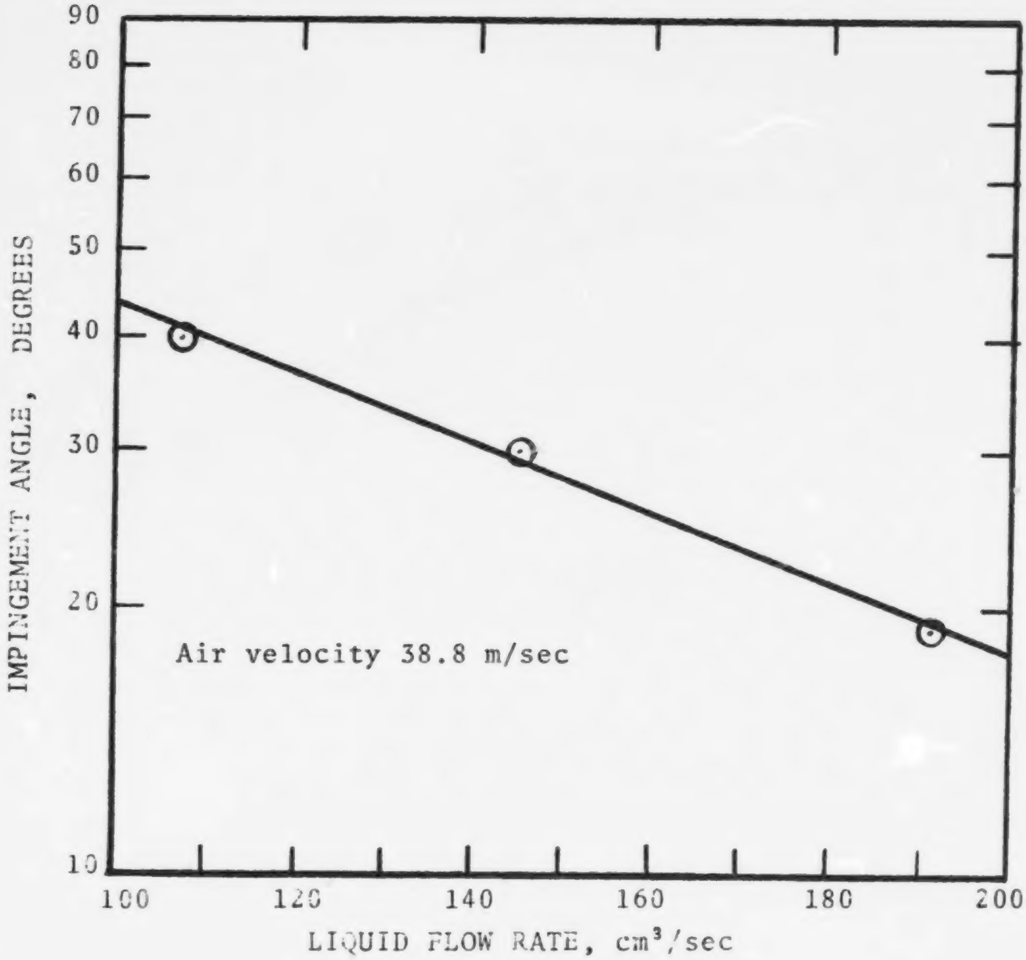

Figure 5-7 - Effect of liquid flow rate on impingement angle for onset of entrainment.

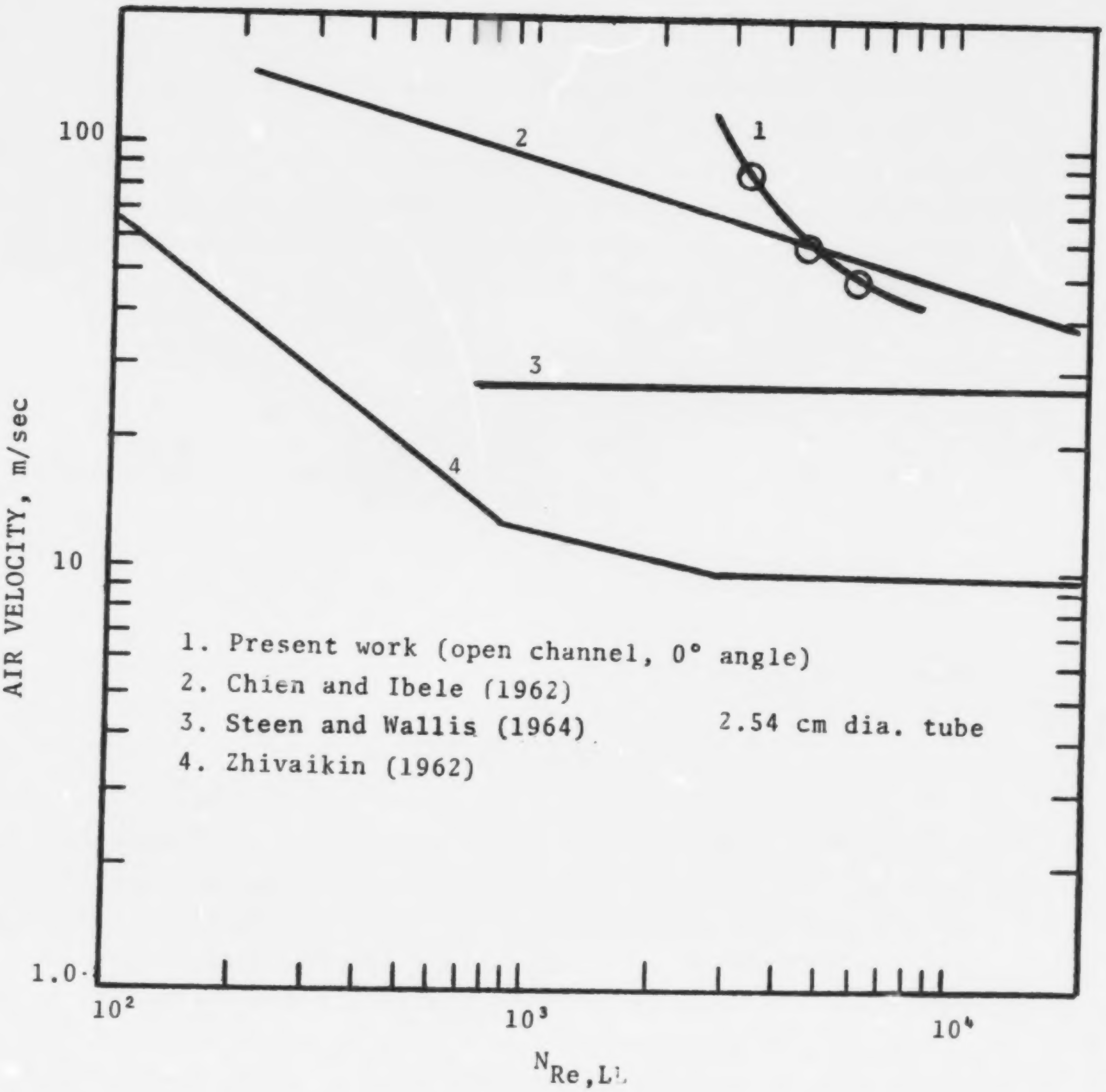

Figure 5-8 - Comparison of entrainment onset velocity by different investigators.

The results differ significantly due to the problem of defining the onset of entrainment. Zhivaikin (1962), who defined the onset of entrainment as occurring when it is first detectable, expressed his results in terms of the following empirical equations for the critical gas velocity "u_{Gc}" for the onset of entrainment:

$$P = 29.2\, N_{Re,L}^{-0.75}, \qquad \text{if} \quad N_{Re,L} \leq \frac{0.085}{\nu_L^2} \tag{5-12}$$

$$P = 100\, \nu_L\, N_{Re,L}^{-0.25}, \qquad \text{if} \quad \frac{0.085}{\nu_L^2} \leq N_{Re,L} \leq \frac{28.8}{\nu_L} \tag{5-13}$$

$$P = 43.2\, \nu_L^{1.25}, \qquad \text{if} \quad N_{Re,L} \geq \frac{28.8}{\nu_L} \tag{5-14}$$

where "P" is defined by:

$$P = \frac{u_{Gc}\mu_L}{\sigma} \tag{5-15}$$

Steen and Wallis (1964) defined the onset of entrainment as that air velocity which represents the extrapolation of the straight line portion of a graph of entrainment percentage versus air velocity. Since the increase in entrainment with air velocity is similar to the exponential function, their results lie considerably above those of Zhivaikin. Steen and Wallis also obtained an expression for "P", when viscous forces in the liquid film can be ignored, as:

$$P = 2.46 \times 10^{-4}\, (\mu_L/\mu_G)(\rho_L/\rho_G)^{1/2} \tag{5-16}$$

Chien and Ibele (1962) defined the transition on the basis of pressure drop versus gas flow rate curves. A change in the slope of the curve was taken to indicate the onset of gross entrainment. Their results apply to conditions where a large fraction of the total liquid flow is entrained, so their prediction of "u_{Gc}" is even higher than that of Steen and Wallis. Chien and Ibele correlated their data by the following equation:

$$N_{Re,Gc} = 1.2 \times 10^{+6} (N_{Re,L})^{-0.3} \qquad (5\text{-}17)$$

where $N_{Re,Gc}$ = gas phase Reynolds number with $u_G = u_{Gc}$

Equation (5-17) can be rearranged as:

$$P = 1.2 \times 10^{6} \left[\frac{\mu_L \ \mu_G}{d_o \sigma \rho_G}\right] (N_{Re,L})^{-0.3} \qquad (5\text{-}18)$$

The present results are comparable with those of Chien and Ibele. In this study we defined the onset of entrainment as when the entrained drops made an impression on the treated filter paper. The present results may be slightly higher due to the fact that actual air velocity in the inlet nozzle rather than the superficial velocity in the channel was measured.

CONCLUSIONS

A. Because our results were comparable with others in terms of entrained drop diameter despite differences in duct dimensions, it is concluded that duct size does not affect the reentrained drop size distribution.

B. Entrainment velocity depends upon liquid Reynolds number as shown in Figure 5-8. The Chien and Ibele curve is recommended for determining the onset of reentrainment.

C. Increased impingement angles result in decreased entrainment velocities as shown in Figure 5-7. Thus, sharp angles in the entrainment separators should be avoided.

EXPERIMENTAL PILOT PLANT

An experimental pilot plant for the study of entrainment separators was designed and built. The purpose of the pilot plant was to do the following:

1. To obtain reliable data over a wide range of operating variables to provide a basis for improved or new methods
2. To check presently available design equations for entrainment separators
    - A. Efficiency of separation
    - B. Pressure drop
3. To determine the effect of higher gas velocity on reentrainment, bouncing of drops and impaction mechanism
4. To study liquid drainage and flooding
5. To study problems associated with entrainment separators
6. To study vertical and horizontal sections

DESCRIPTION OF THE PILOT PLANT

The maximum capacity of the wet scrubber entrainment separator is 85 m^3/min (3,000 CFM). This capacity was selected based on the following consideration. The entrainment separator cross-section was selected to be 30.5 cm x 61 cm. This section is sufficiently large to have minimal wall effects for separators and provides a fairly long (61 cm) collection element when cross-flow effects are important. Normally, the maximum air velocity in industrial separators is around 3.0 m/sec. If velocities 2.5 times higher are studied, the maximum air velocity will be 7.5 m/sec. This will give the maximum capacity of 85 m^3/min.

A block diagram of the pilot plant is shown in Figure 6-1. The equipment consists of a filter, blower, heater, spray sections, observation sections, entrainment separator test sections, liquid tanks, pumps, etc. The top view of the pilot plant is shown in Figure 6-2. Figure 6-3 shows the connections between various tanks at the bottom of the platform.

A description of the equipment in the pilot plant is given below.

Air Prefilter

Automotive air filters were used to clean the incoming air. The air supply was taken from outside the building and was connected to a box containing prefilters with a 48 cm diameter galvanized duct. The prefilter consisted of 5 filters in parallel, each having a capacity of 18.5 m^3/min. The pressure drop at this capacity is 0.25 cm W.C.

Blower

A Western Blower size 122 B1 and Class III was used. It has a capacity rating of 88 m^3/min at 30.5 cm W.C.(static pressure), a 7.5 KW (10 HP) motor, rotatable housing and an opposed blade discharge damper. The blower was supported on a hard rubber base to prevent vibrations, and it had a flexible duct connected at the outlet. The blower was insulated with accoustical fiberglass and concrete blocks to reduce the noise level.

Air Heater

A gas-fired air heater rated at 30 kcal/hr (120,000 Btu/hr) was used to heat the air.

Spray Section

The spray section served to humidify the incoming air stream and to generate entrainment for the test section. It

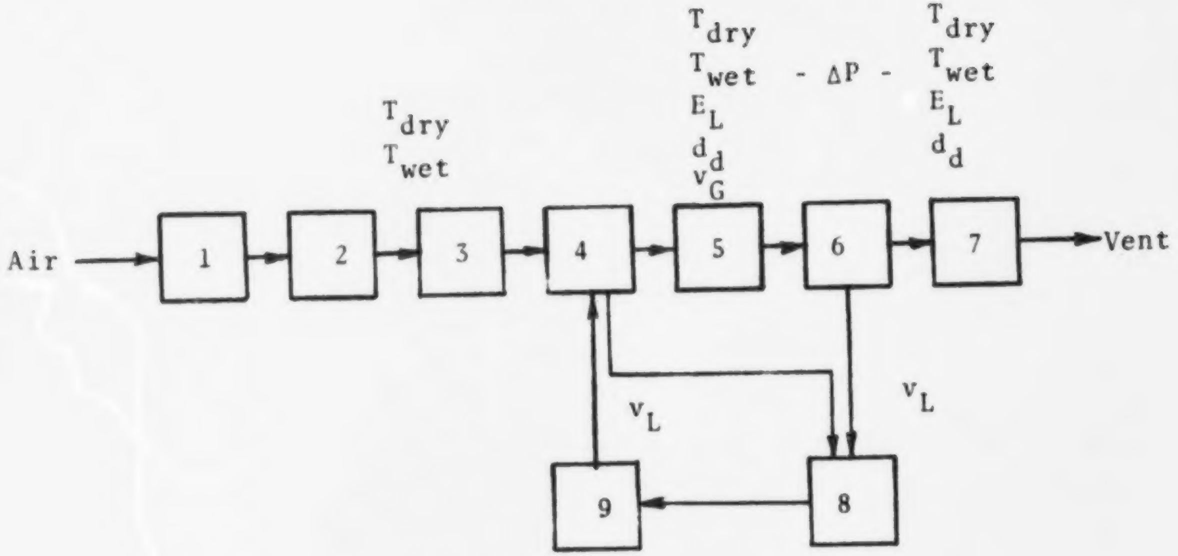
Air
1
2
3
4
5
6
7
8
9
Vent
T_{dry}
T_{wet}
T_{dry}
T_{wet}
E_L
d_d
v_G
- ΔP -
T_{dry}
T_{wet}
E_L
d_d
v_L
v_L

1. Filter 2. Blower 3. Heater 4. Spray Section
5. Observation 6. Test Section 7. Observation
8. Liquid Catch Tanks 9. Liquid Feed Tanks

Figure 6-1 - Block diagram of experimental apparatus.

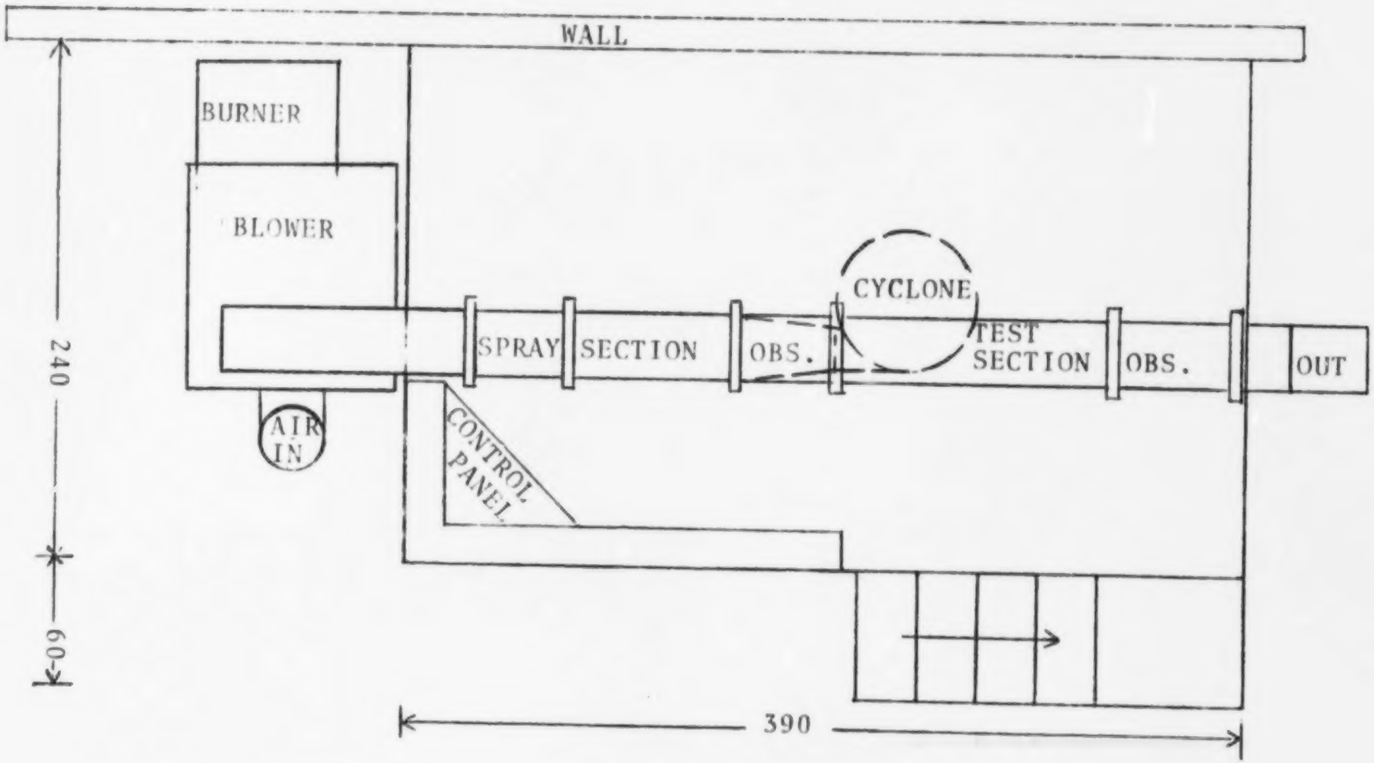
WALL
BURNER
BLOWER
AIR IN
CONTROL PANEL
SPRAY
SECTION
OBS.
CYCLONE
TEST SECTION
OBS.
OUT
240
60
390

Figure 6-2 - Top view of the entrainment separator pilot plant. All dimensions in cm.

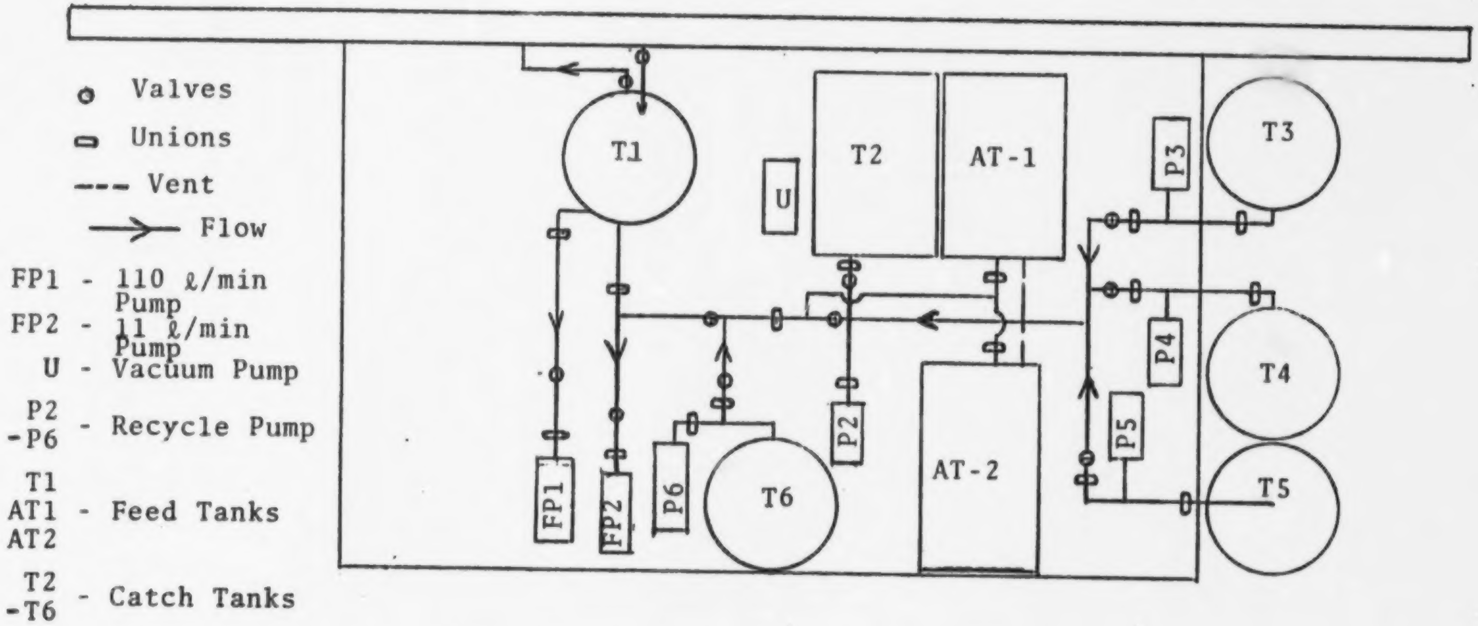
Valves
Unions
Vent
Flow
FP1 - 110 ℓ/min Pump
FP2 - 11 ℓ/min Pump
U - Vacuum Pump
P2 -P6 - Recycle Pump
T1 AT1 AT2 - Feed Tanks
T2 -T6 - Catch Tanks
T1
U
T2
AT-1
T3
P3
P4
T4
P5
T5
AT-2
P2
T6
P6
FP1
FP2

Figure 6-3 - Flow diagram showing connection between various tanks and pumps.

was equipped with various nozzles from Spraying Systems Co. The nozzle specifications are given in Table 6-1. In any section the nozzles were equispaced as shown in Figure 6-4 to generate uniform flow.

The 1/4 M6 nozzle, a single fluid hollow cone nozzle with a 0.105 cm orifice, was operated at 3.4 atm line pressure and produced drops of about 250 μm in diameter, in agreement with the manufacturer's claim. If operated at 13.6 atm, it is expected to produce drop diameters ranging from 40 to 100 μm.

The 1/4 M6SS nozzles were connected with 1.25 cm iron pipe. The remaining nozzles were connected with 2.5 cm p.v.c. pipe. Two spray sections were used in the pilot plant. The 1/4 M6 nozzles were installed in the first spray section, which had inside dimensions of 30.5 cm x 61 cm cross-section and 46 cm length.

The second spray section, 76 cm in length, was equipped with 1/4 M26 nozzles, and arrangement was made to accommodate any of the remaining nozzles. There was considerable reduction in the cross-sectional area due to the presence of 2.5 cm p.v.c. pipes. The reduction was compensated by enlarging the cross-section to 46 cm x 61 cm. Whenever 1/4 M6 nozzles were used to generate spray, the second spray section was replaced by a blank section having a cross-section 30.5 cm x 61 cm.

The spray section was equipped with a drain at the bottom to catch the liquid collected on the walls of the spray section.

Observation Sections

Two observation sections were used, one at each end of the entrainment separator test section. They had dimensions of 30.5 cm x 61 cm cross-section and 50 cm length. Two plexiglass windows, 30 cm x 30 cm, were installed on opposite sides on each observation section. A door was provided for sampling of entrainment and drop diameters.

Table 6-1. NOZZLES USED IN SPRAY SECTION

Type of Nozzle	Model # (Spray Systems)	Pressure atm	# of Nozzles	Flow rate cm^3/sec nozzle
Hollow cone	1/4 M6SS	13.6	12	14.2
Fogjet Nozzle	1-11 1/2 F18	2.7	1	1140
	1 1/2-11 1/2 F35	2.7	1	2200
Full Cone	1/8 GG3	2.7	12	63.0
Hollow Cone	1/4 M26	2.7	12	27.2

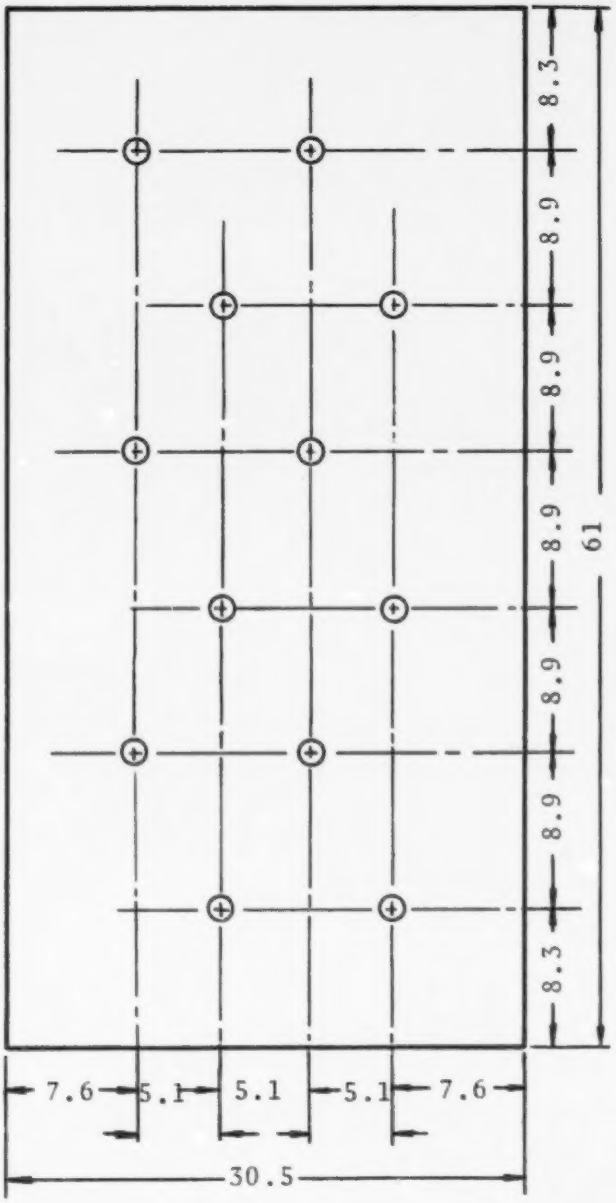
8.3
8.9
8.9
8.9
8.9
8.9
8.3
61
7.6
5.1
5.1
5.1
7.6
30.5

Figure 6-4 - Nozzle positions in the 30.5cmx61cm duct. All dimensions in cm.

Drainage of Liquid in the Test Section

Liquid drainage is important in the design of entrainment separators. The original drainage system in the test section consisted of 20 equispaced openings, 0.6 cm in diameter, per 30 cm length of the test section and a false bottom, giving a space of 1.8 cm height, which was filled with Raschig Rings. It was observed that the drainage in the test section was not 100% effective. The bottom surface was coated with hydrophobic resin, and the collected liquid had a tendency to flow around the holes and thus creep along the length of the test section.

To solve this problem the holes were enlarged to 0.8 cm diameter, and the number of holes was increased from 20 to 40 per 30 cm length of the test section. To avoid creeping of fluids at the bottom of the test section, notches 0.6 cm wide and 28 cm long (perpendicular to the air flow direction) were made at 30 cm intervals in the test section bottom. The number of Raschig Rings was reduced to about 1/3 under the false bottom. This drainage system was quite efficient for low liquid loads.

The theoretical maximum air flow (without Raschig Rings in the false bottom) through the false bottom is 2% of the total flow. The presence of liquid and Raschig Rings in the false bottom should lower this percentage significantly. No reentrainment from the false bottom was observed. At higher liquid flow rates (57 ℓ/min and higher), the liquid built up to 3-4 mm in height for drainage. The total drainage capacity of the test section was more than 150 ℓ/min. However, most of the liquid was collected in the first two drainage sections of the test section.

The notch dimensions were increased to 2.5 cm width since it was observed that a notch is more effective than a hole in drainage. This change resulted in efficient drainage. In a few runs a problem was observed. When the air flow rate is high and the liquid load is small, some reentrainment is caused from the notch.

Liquid Catch Tanks

Four 0.2 m^3 (55 gal) drums were used as catch tanks. These were connected to the test section to collect separated liquid alont the length of the test section. One additional 0.2 m^3 drum was used to collect liquid from the bottom of the spray section. Each tank was connected to a water meter and a pump with liquid level controller for recirculation of the liquid.

Liquid Supply Tanks

Three 0.2 m^3 (55 gal) drums were used as supply tanks. These tanks were connected to receive fresh water and recirculated water. On the outlet side were located rotameters for flow measurement and pumps.

Control Panel for Equipment

The control panel was equipped with the following:

1. Electrical connections
    - A. Magnetic starter for 88 m^3/min blower
    - B. Switches for pumps, heater, sampling pump, observation lights, etc.
    - C. Temperature recorder
2. Non-electrical connections
    - A. Rotameters and water meters
    - B. Dry gas meter
    - C. Pressure gauges
    - D. Needle valve, diaphragm valve, globe valves, and gate valves
    - E. Manometers to measure pressure drop.

Electrical Supply Panel

A 110 V, 3 phase, 100 amp/phase electrical supply panel was installed near the equipment site.

Water Supply

The maximum fresh water supply was 50 ℓ/min (13 gpm).

Water supply to fine spray nozzles:

Piston pump - 1P741 (Grainger catalog)
Maximum pressure - 34 atm (500 Psi)
Flow rate at maximum pressure - 11.4 ℓ/min (3 gpm)
Motor rpm - 1,725
Motor KW 1.1 (1.5 HP)

A rotameter with ± 2% accuracy was used to measure flow rate. A needle valve and auxiliary line near the pump were used to control flow rate. A pressure gauge was used to measure static pressure.

Water supply to coarse spray nozzles:

Centrifugal pump - Model 165U (Barnes Pump)
Maximum pressure - 3.4 atm (50 Psi)
Flow rate at maximum pressure - 120 ℓ/min (31 gpm)
Motor rpm - 3,450
Motor KW 1.1 (1.5 HP)

A rotameter with ± 2% accuracy was used to measure flow rate. A diaphragm valve and auxiliary line near the pump were used to control flow rate. A pressure gauge was used to measure pressure.

TEST SECTION

Five different types of entrainment separators were studied:

1. Mesh
2. Packed bed
3. Zigzag baffles
4. Cyclone
5. Tube bank

Entrainment separators 1 through 4 were selected because they are the most common separators used in industry. The fifth separator, the tube bank, was studied to verify claims that it operates with a low pressure drop, gives high efficiency, and has a high reentrainment velocity.

The design of the test section was kept flexible to facilitate any changes which may be necessary. The housings used for the mesh, packed bed, zigzag baffles and tube bank had the same dimensions, and thus it was a simple matter to interchange the test sections.

The test sections were provided with a 50 cm x 90 cm plexiglass window in front and a 25 cm x 90 cm plexiglass window at the top for observation. The dimensions of the test section were 30.5 cm x 61 cm cross-section and 122 cm in length. A false bottom was provided along the length of the test section. The spacing of 1.9 cm height along the length of the test section was loosely packed with Raschig Rings and was divided into four parts to segregate for later measurement, the collected liquid along the length of the test section. A 5 cm diameter p.v.c. drainage pipe was provided in each section. A 30 cm liquid seal was provided in each catch tank.

The five entrainment separators are described below.

Mesh

Model-4CA (ACS Industries)
Type - layered (with layers crimped in alternate directions)
Density - 0.144 g/cm^3
Wire diameter - 0.028 cm
Percent voids - 98.2
Mesh surface area - 2.8 cm^2/cm^3
Thickness - 10 cm

Material of construction - AISI 304

Separation efficiency - Figure 6-5

Pressure drop data - Figure 6-6

The mesh was supported by a grid made from 0.16 cm wire with 1.25 cm width and 2.5 cm height of spacing. The mesh was located in the first 30 cm of the test section.

Packed Bed

Packing - 2.5 cm pall rings

Specific surface - 1.9 cm^2/cm^3

Density - 0.088 g/cm^3

Material of construction - Polypropylene plastic

Packing was supported by the same grid which is used to support the mesh.

Some experiments were conducted using a 90 cm long bed. Later the bed length was reduced to 30 cm. In both cases the support grid at the upstream of the packing was located at the beginning of the test section.

Zigzag Baffles

Baffle dimension - 7.5 cm width and 61 cm height
thickness 0.16 cm

No. of rows - 6

Spacing between rows - 2.5 cm

Angle between baffle and air flow direction - 30°

Spacing between baffles in a row - 6.9 cm

For details see Figure 6-7.

Cyclone

Diameter - 61 cm

Overall height - 244 cm

Inlet height - 30.5 cm

Inlet width - 15 cm

Maximum inlet velocity - 30 cm/sec, higher using an
inlet vane

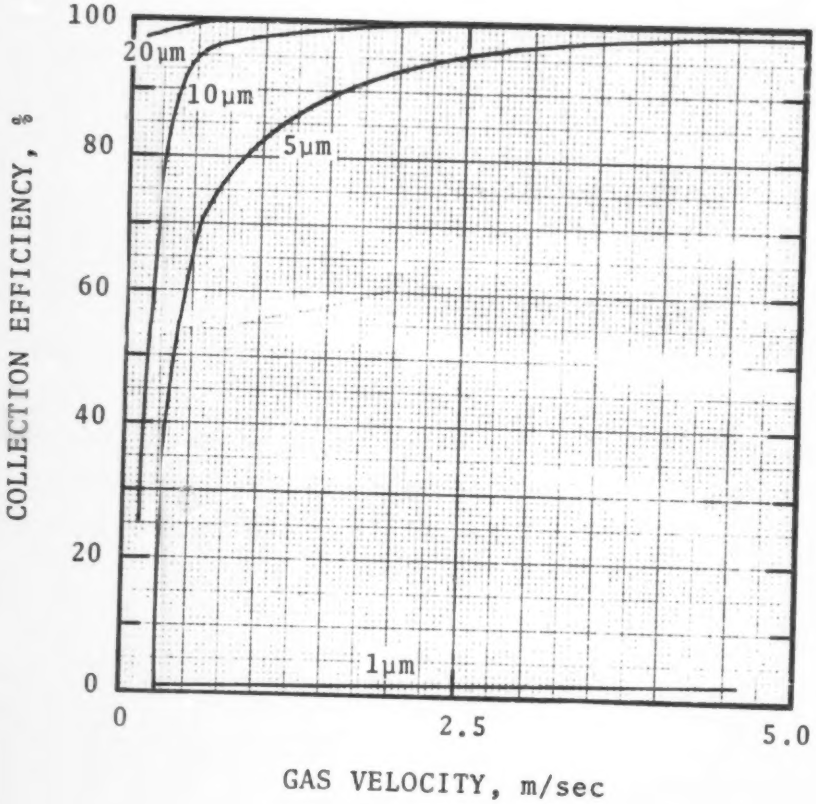

Figure 6-5 - Calculated collection efficiency for water droplets in air. (ACS Industries)

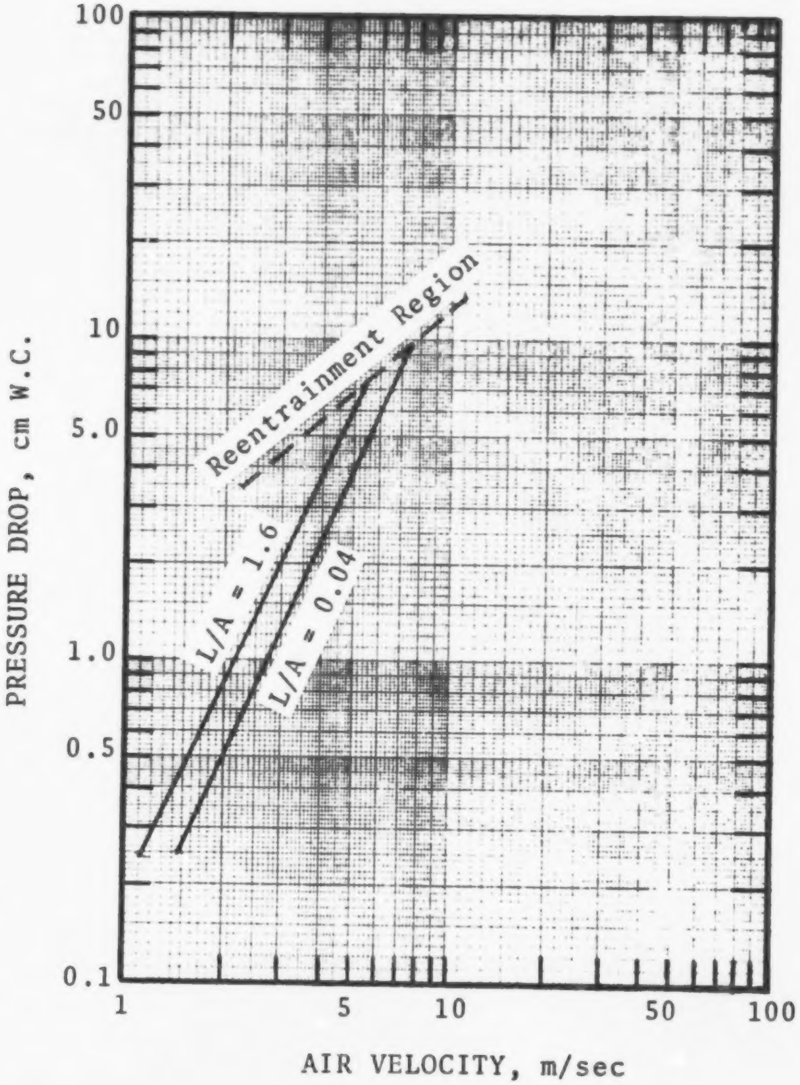

Figure 6-6 - Pressure drop versus air velocity for 10 cm thick ACS style 4CA mesh. L/A = superficial liquid velocity, cm/min (ACS Industries)

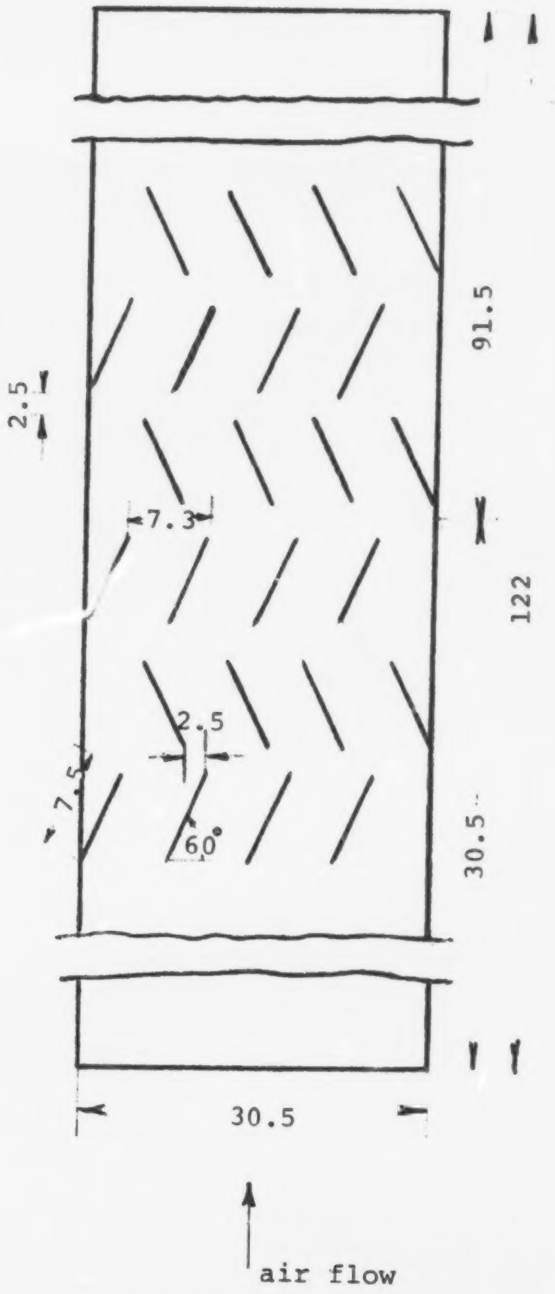
91.5
2.5
7.3
122
2.5
7.5
60°
30.5
30.5
air flow

Figure 6-7. Baffle Section. All dimensions in cm. Aluminum baffles are 0.16 cm thick, 7.5 cm wide, and 61 cm long.

For details see Figure 6-8 and Stearman and Williams (1971).

Tube Bank

Number of rows - 6
External diameter - 1.9 cm
Length - 61 cm
Number of tubes in a row - 8
For details see Figure 6-9.

CALIBRATION

1. Thermocouples: All the thermocouples were calibrated using thermometers. Ice-water, boiling water and room temperature were used. It was found that thermocouples give some errors in reading temperatures.

2. Liquid level in the tank: The liquid level as a function of liquid height in the 0.2 m³ drums was determined by measuring the liquid level and the weight of the tank. The liquid level in the catch tanks was controlled within 5 cm during the experiment. Tanks T_1, T_3, T_4, T_5, T_6 contained 2.55 ℓ/cm of height, and tanks T_2, AT_1, AT_2 contained 5.06 ℓ/cm of height (see Figure 6-3).

3. Water Meters: Water meter number 1 (on tank T_1) was calibrated using a rotameter and a calibrated 0.2 m³ drum. Calibration was done at flow rate intervals of 3.79 ℓ/min (1 gpm).

Water meter Numbers 2 to 6 were connected to the outlets of catch tanks Numbers 2 to 6. To calibrate any water meter, e.g., number 3, the outlet from water meter Number 1 was connected to the inlet of tank 3. Tank 3 was filled with water so that the liquid level was between an arbitrary upper and lower limit. The pump was kept on to control the liquid level in tank 3. The calibration was done by comparing the readings

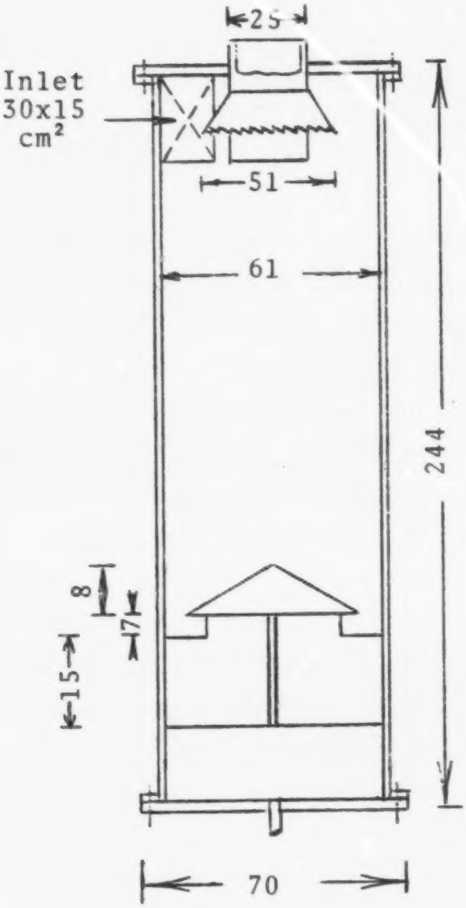
25
Inlet
30x15
cm²
51
61
244
8
7
15
70

Figure 6-8 - Cyclone assembly. All dimensions are in cm.

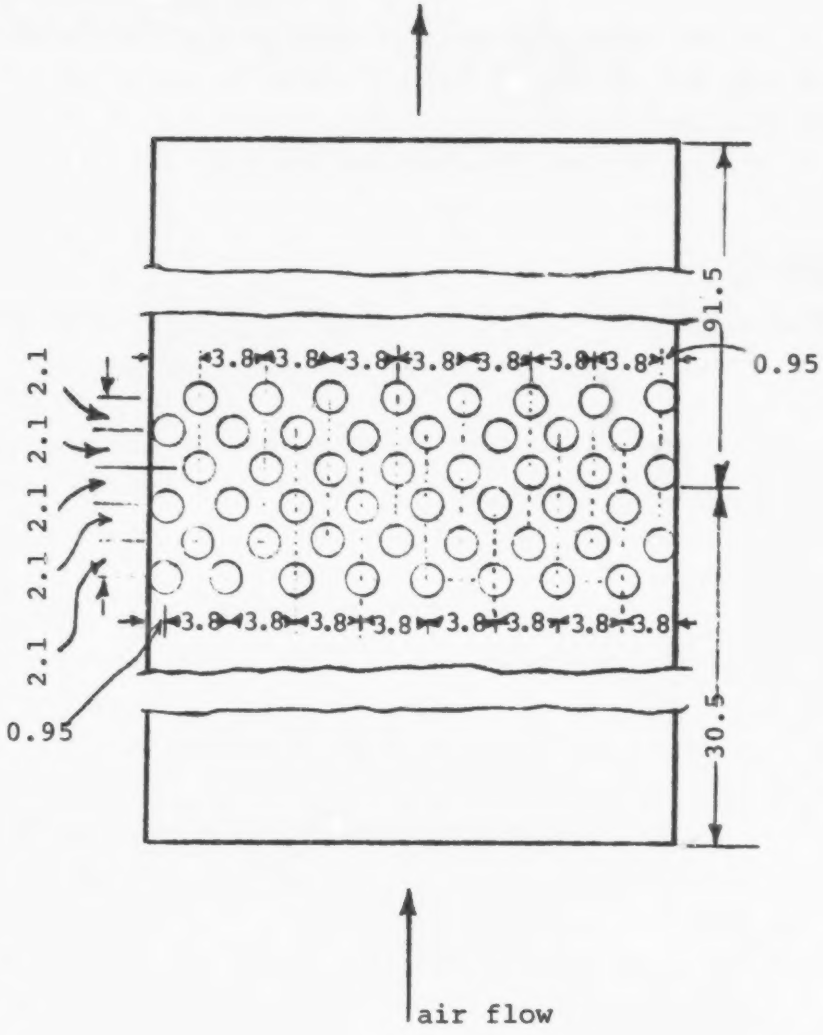
3.8
3.8
3.8
3.8
3.8
3.8
3.8
0.95
91.5
2.1
2.1
2.1
2.1
2.1
2.1
3.8
3.8
3.8
3.8
3.8
3.8
3.8
3.8
0.95
30.5
air flow

Figure 6-9 - Test section with bank of tubes.
All dimensions in cm.

on water meter numbers 1 and 3. Appropriate correction was applied for the change in liquid level in tank number 3 and for the calibration of water meter number 1. To avoid the dynamic error, the calibration was done at flow rates of 3.79 ℓ/min (1 gpm) intervals.

EXPERIMENTAL PROCEDURE

The major points of the experimental procedure are described below. The procedure was modified as required for individual runs.

1. All the tanks were emptied before starting the experiment in order to avoid rust in the water.
2. All the wet bulb thermometers were checked for water.
3. All the valves were checked so that the required valves were kept open and the rest closed.
4. All the recycle pumps were kept on to maintain the liquid level in the tanks between the upper and lower limits.
5. All the catch tanks were filled with liquid until the level was between the upper and lower controlled limits.
6. The feed supply tank was filled to the overflow line. Fresh water was continuously added to the system during the experiment to supplement the water loss in the exit air and to introduce fresh water to the system.
7. The zero position of the inclined manometer was adjusted.
8. Readings were noted for all the water meters and the liquid levels in the catch tanks.
9. The desired air flow was started.

10. Pressure drop across the test section was measured.
11. The desired water flow rate was started.
12. About 1-5 minutes were needed to reach steady state. The experiment was continued for 2 hours.
13. Air flow rate, water flow rate, etc., were checked every few minutes.
14. Visual observations of penetration, flooding, liquid drainage, bouncing of drops, liquid flow on elements of the entrainment separator, etc., were made for the duration of the experiment.
15. Readings were taken of temperature (each hour), entrainment drop size, pressure drop, entrainment loading, etc. (once during each run).
16. At the end of the experiment, liquid and air flow were shut down. Readings were noted for water levels in the tanks and water meter readings.

The blank forms used for the experiments are shown in Figure 6-10.

SAMPLING PROCEDURE

Drop size determination: The drop diameter in the experiments varied between 40 to 2,000 μm. Chemically treated filter papers were used to determine the drop diameters. The grain size of the chemicals normally limits the lower diameter by this method to 5-10 μm. Filters coated with the following chemicals were studied for drop size measurement.

Potassium permanganate
Lissamine green
Erio green
1% potassium ferricyanide and ferrous ammonium sulfate.

Entrainment Separation Project

Experiment #______________ Date ______________________

Test Section:_____________

Air velocity _______________cm/sec, Pitot tube - ____________ft/min

Water flow rate ___________gal/min, Water pressure ____________psi

Time on: ________________, Time off: ______________________

Types of nozzles ________________, Number of nozzles _________

Water flow = __________ $\frac{\text{gal}}{\text{min}}$ x _______min x 3.79x10^3 $\frac{\text{cc}}{\text{gal}}$ = cc

Thermocouples	1	2	3	4	5	6	7	8	9
Before									
_____°F									
After									
_____°C									

Total liquid level	2	3	4	5	6
After					
Before					
Net					
cc					

Water meter	1	2	3	4	5	6
After						
Before						
Net						
x10^3x						
cc						
Total						

ΔP = Dry = _____+0.05 = cm Wet = ________+0.05 = cm

ΔPx0.826 = Dry ______cm, Wet ___________ cm

Abs. Pressure = ___________________cm Hg.

Drop diameter in inlet = mass average __________________μm

Geom. Standard deviation = ___________________________

Water overflowing _________1-2 ___________2-3 ___________3-4

Figure 6-10 - Form for recording test data.

Reentrainment & Penetration

Approximate drop size of large drops __________ mm

Vertical distance ________cm Horizontal distance _______cm

Height of flooded section __________cm

Reentrainment present in observation
Section ______yes ________no

Vertical height in which reentrainment
Present ___________cm

No. of seconds sample taken ____________

No. of drops on the filter paper ___________

Isokinetic sample taken _______yes _______no

Drop diameter __________ave. (mass) μm

Geometric Standard Deviation

COMMENTS:

Figure 6-10 - continued.

Individual drops were most easily seen when 1% potassium ferricyanide and ferrous ammonium sulfate were used as the coating. A correlation given by Chilton (1952) Figure 6-11, was used to convert blot diameter on filter paper to actual drop diameter.

In a few runs isokinetic sampling through a filter holder containing a treated filter was used to measure entrainment drop diameter. This method gave good results when the entrainment load was sufficiently small for individual drops to be seen, or the gas velocity or drop diameter was such that the collection efficiency of filter paper held in air is poor.

Determination of entrainment load:

1. Initially, the arrangement shown in Figure 6-12,was used for liquid load measurement at the inlet and outlet ends. Isokinetic sampling was used. It was observed that all of the liquid was collected in the inlet nozzle and none in the gravity separator, cyclone or filter holder. The results obtained were poor, which may be attributed to:
    A. Entrainment may not be evenly distributed in the cross-section of the duct.
    B. Some liquid may have collected or drained down from the sampling nozzle to the collection flask during sampling.
2. The second method used to obtain entrainment loadings was by material balance. The entrainment in the inlet was obtained by subtracting liquid collected on the walls before the test section from the liquid feed and applying a correction for the humidity of the ambient air. The entrainment in the outlet was obtained by subtracting the liquid collected in various parts of the test section from the inlet entrainment.

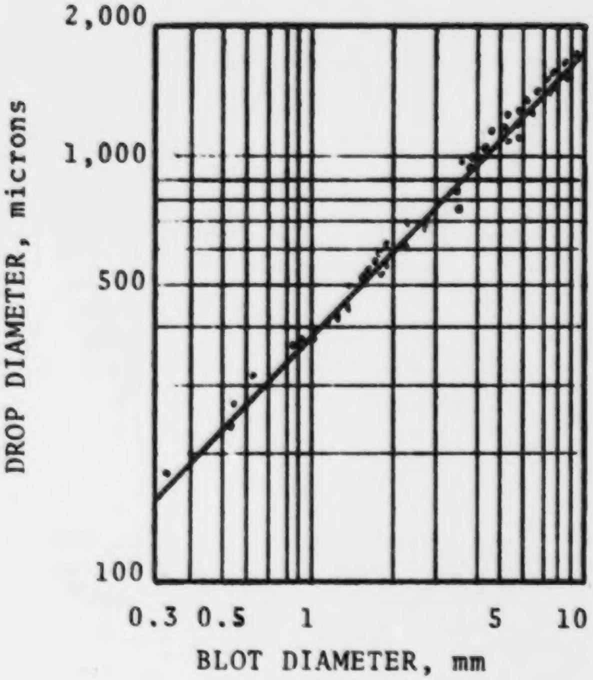

Figure 6-11 - Calibration of Whatman No. 1 filter paper.

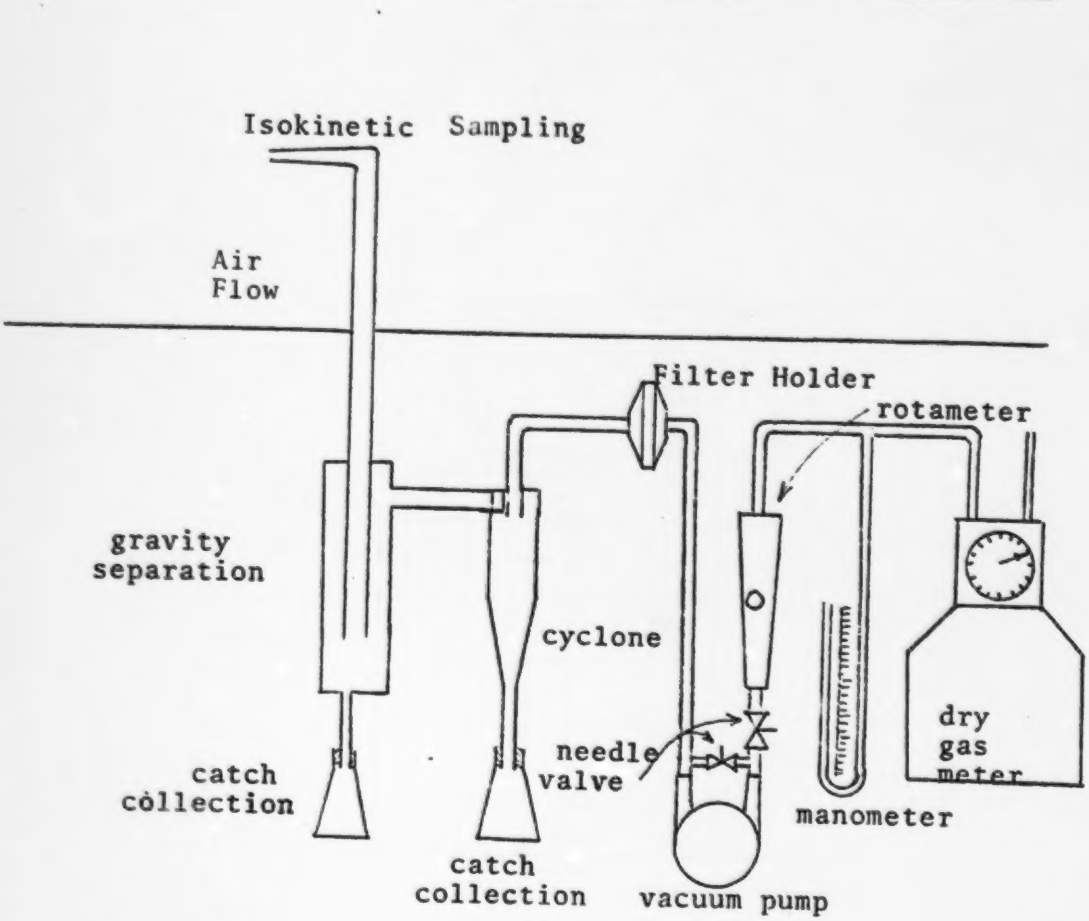
Isokinetic Sampling
Air
Flow
Filter Holder
rotameter
gravity
separation
cyclone
dry
gas
meter
needle
valve
catch
collection
manometer
catch
collection
vacuum pump

Figure 6-12 - Liquid load sampling

This method was discarded due to errors in the liquid balance caused by a fluctuation in the inlet feed rate during the experiment. The fluctuation may have been caused by the nozzles. These errors may have been 5 to 10%. However, in some experiments they may have been magnified because liquid collected on the walls before the test section was as high as 80% of the feed. Also, some errors were found in the humidity correction due to erroneous functioning of the thermocouples.

3. A third method was based on counting the number of drops collected on a filter paper. The entrainment load could be determined if the mass average drop diameter and the sampling time were measured. This method has the following disadvantages:
    A. As shown in the previous chapter, the drop collection efficiency by the filter paper varies with the entrainment drop diameter and gas velocity and is not 100%.
    B. The error which is introduced in the measurement of drop diameter is magnified when the volume of the drop is calculated to determine the entrainment load.
    C. An error is introduced in inserting and removing the filter paper from the duct because of the short sampling time. When the entrainment load is high, the sampling time is one second or less.
    D. The sample represents entrainment load at a single sampling point in the duct which may not represent the average entrainment load.

E. Some error is also introduced due to overlapping of blots on the filter paper.

4. A method based on measuring the entrainment by converting it to vapor and measuring the humidity of the gas was selected for use in all experiments. An isokinetic sample was drawn through a nozzle which was heated to evaporate the entrainment. The air sample humidity was measured by dry and wet bulb thermometers following the nozzle. A thermostat was used to control the heating so that the gases are partially saturated at the end of the nozzle. Traverse sampling was done to get average value of entrainment. A horizontal symmetry was assumed. Fifteen samples at 4 cm intervals were measured along the vertical center line of the duct.
When the liquid loading was large, a specially designed impactor was used upstream of the nozzle. Sampling for two minutes was done at each traverse point in the duct. The liquid collected in the impactor was added to the humidity measured to obtain the entrainment loading.
Figure 6-13 shows the sampling device with impactor. The impactor specifications are given below.
Inlet nozzle diameter - 0.5 cm
Impactor plate dimension - 1.8 x 1.8 cm^2
Distance between nozzle and the impactor plate - 1.2 cm

Problems and Possible Errors in the Experiments

1. Leaks. The equipment was operated under pressure and this led to water leaks. The equipment ducting was made of wood. The wood surface was coated with resin wherever it came in contact with water. Leaks developed near the joints due to expansion and contraction of the wood. The maximum leakage

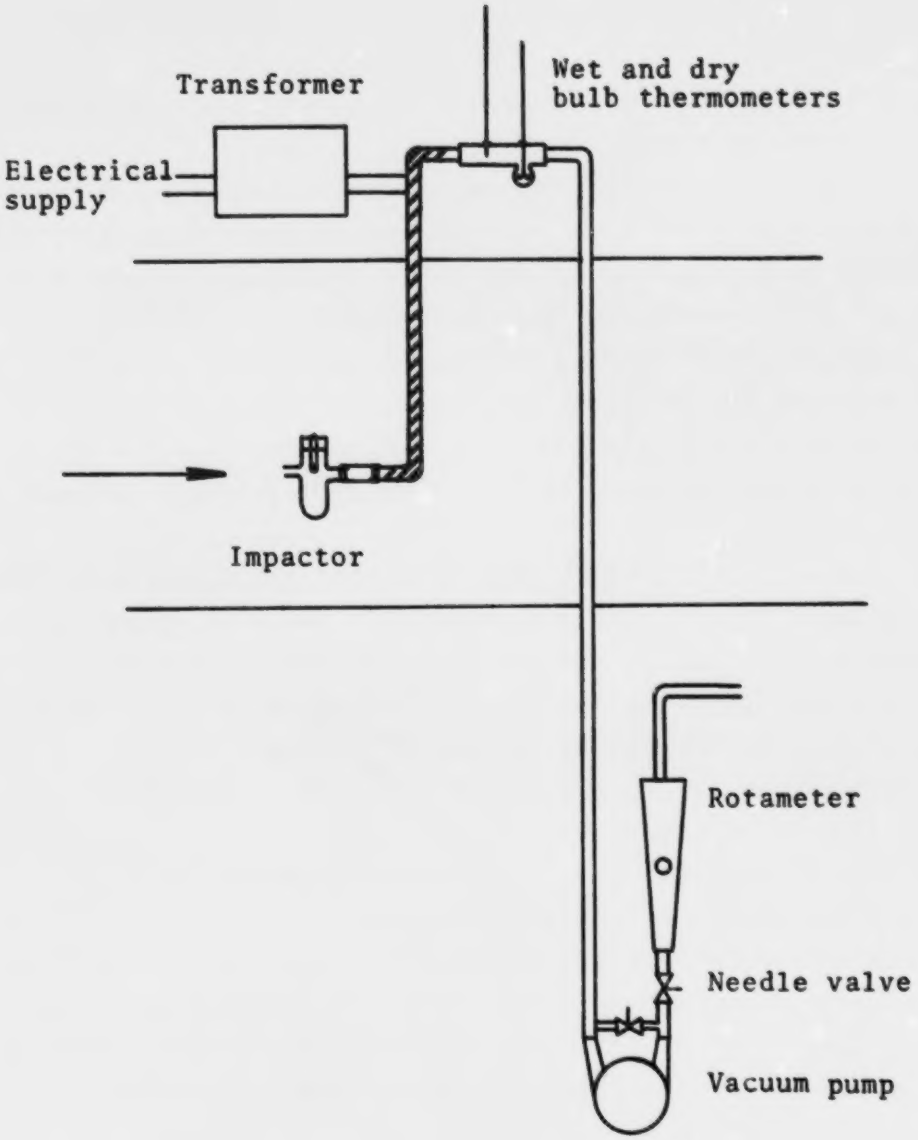
Transformer
Wet and dry
bulb thermometers
Electrical
supply
Impactor
Rotameter
Needle valve
Vacuum pump

Figure 6-13 - Sampling device consisting of impactor, heated inlet probe, dry and wet bulb thermometer and accessories

was 3.8 ℓ (1 gal.) per experiment, a maximum error of about one half of one percent.

2. Liquid level. The maximum error in reading the liquid level was about 2 mm, or one half of one percent. This corresponds to 500 cm^3 of liquid in catch tanks numbers 3 to 6 and 1 ℓ of liquid in catch tank number 2.

3. Water meter reading. All the water meters were calibrated as a function of average flow rate (continuous in water meter #1 and discrete flow in the rest of the water meters). However, reproducibility was poor and the maximum error was 5%.

4. Rotameter reading. The rotameter error was specified as less than 2% of the maximum reading. However, additional errors may have resulted during the experiments due to fluctuation and drift in the flow. The two rotameters have a maximum capacity of 8.4 ℓ/min and 84 ℓ/min.

5. Temperature. The maximum error in temperature reading with a thermometer was 1°C.

6. Air flow rate. Air flow rate was measured with a pitot tube connected to an inclined manometer. The inclined arm of the manometer was scaled to give velocity. Two types of error were present: a) Error due to fluctuation in the air flow rate, and b) Error due to change in fluid density caused by a temperature change. The maximum error due to temperature change was 50 cm/sec or 3-4%, corresponding to change of air velocity of 20 cm/sec in the test section.

EXPERIMENTAL RESULTS AND DISCUSSION

At the time of writing, experiments had been run on the pilot plant with horizontal gas flow through packed bed, zigzag baffle, tube bank and mesh entrainment separators. In each run air was used as the gas, water was the liquid, and no solids were present. Results on overall collection efficiency, pressure drop, reentrainment and liquid flow patterns are presented and discussed in this chapter. However, before the performance of various test sections can be considered, the size distribution of the inlet entrainment must be determined.

INLET ENTRAINMENT

Various nozzles were used in the experiments, although only one type of nozzle was used in any given experiment. A description of the nozzles is given in Table 7-1. A complex relationship among the characteristics of the individual spray nozzles, the interaction of multiple nozzles, the configuration of the experimental duct and the air velocity determines the inlet entrainment size distribution.

The spray generated from the M6 nozzles was analyzed under experimental conditions by filter papers coated with 1% potassium ferricyanide and ferrous ammonium sulfate, as described in Chapter 5. The drop diameter generated from the other nozzles was greater than 100 μm. For these, the manufacturer's data were used to determine drop diameters.

The effect of gas velocity on mass median drop diameter generated from M6 nozzles is shown in Figure 7-1. There is no definite trend. The mass median diameter varies from 76 to 102 μm and averages 84 μm, with an average geometric standard

Table 7-1. NOZZLES USED IN SPRAY SECTION

Type of Nozzle	Model # (Spray Systems)	Pressure, atm gauge	# of Nozzles	ℓ/m/nozzle
Hollow cone	1/4 M6SS	13.6	12	0.853
Fogjet Nozzle	1-11 1/2 F18	2.7	1	68
	1 1/2-11 1/2 F35	2.7	1	133
Full Cone	1/8 GG3	2.7	12	4
Hollow Cone	1/4 M26	2.7	12	2

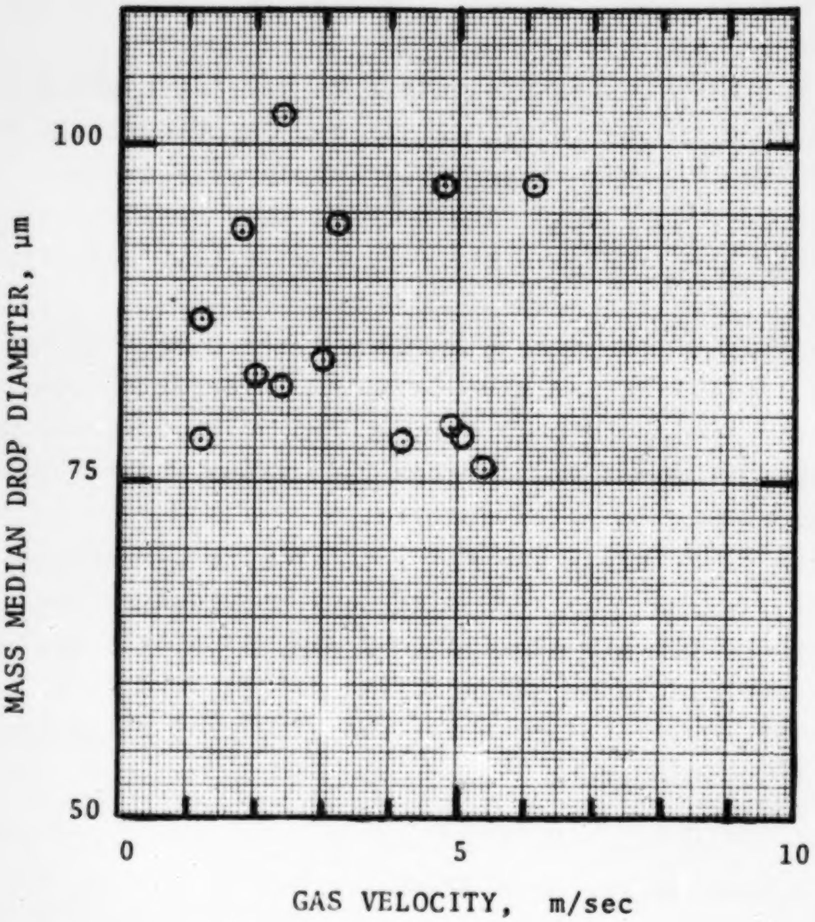

Figure 7-1 - The effect of gas velocity on drop diameter for M6 nozzles

deviation of 1.32. The minimum drop diameter found in the inlet was 30 μm.

Inlet entrainment measurements were made at a point 75 cm downstream of the spray nozzles and 30 cm upstream of the test section. The average water supply pressure was 13.6 atm. gauge (200 psig). The nozzles were oriented toward the downstream side and gave the drops an initial velocity of 51 m/sec.

An analysis of the drop diameters created by each nozzle is given in Table 7-2, and more detailed information concerning the size distribution curves, as provided by the manufacturers, is presented in Figures 7-2 through 7-4. These distributions were measured 30 cm from the nozzles.

In these experiments the M26 nozzles were operated at 2.7 atm pressure, but the drop size data provided by the manufacturer are for 6.8 atm and 10.2 atm. The mass median drop diameter produced by M26 nozzles was obtained from fitting the following relation for the effect of operating pressure on drop diameter:

$$d_{mm} = c_1 \left(\Delta P\right)^{c_2} \qquad (7\text{-}1)$$

where d_{mm} = mass median drop diameter, cm
ΔP = pressure drop at nozzle, atm
c_1, c_2 = constant

The mass median drop diameter for an operating pressure of 2.7 atm was 380 μm. The geometric standard deviation was 1.52 and did not significantly vary with operating pressure.

The nozzles often plugged, due to formation of rust in the water tanks. This resulted in a decreased water flow rate and also may have caused some variation in the drop diameter and standard deviation.

Table 7-2. DROP SIZE ANALYSIS

Source of Data	Type of Nozzle	Operating Pressure atm gauge	Mass Median Diameter, µm	Minimum Drop Diameter, µm	Geometric Standard Deviation
Manufacturer	M6	6.8	127	45*	1.5
Manufacturer	M6	10.2	110	45*	1.5
This Study	M6	13.6	84	30	1.3
Manufacturer	M26	6.8	295	110*	1.5
Manufacturer	M26	10.2	265	102*	1.5
Predicted From Equation (7-1)	M26	2.7	380	-	1.5
Manufacturer	GG3	2.7	1,230	450*	1.8

*2% of the drops are smaller than this diameter.

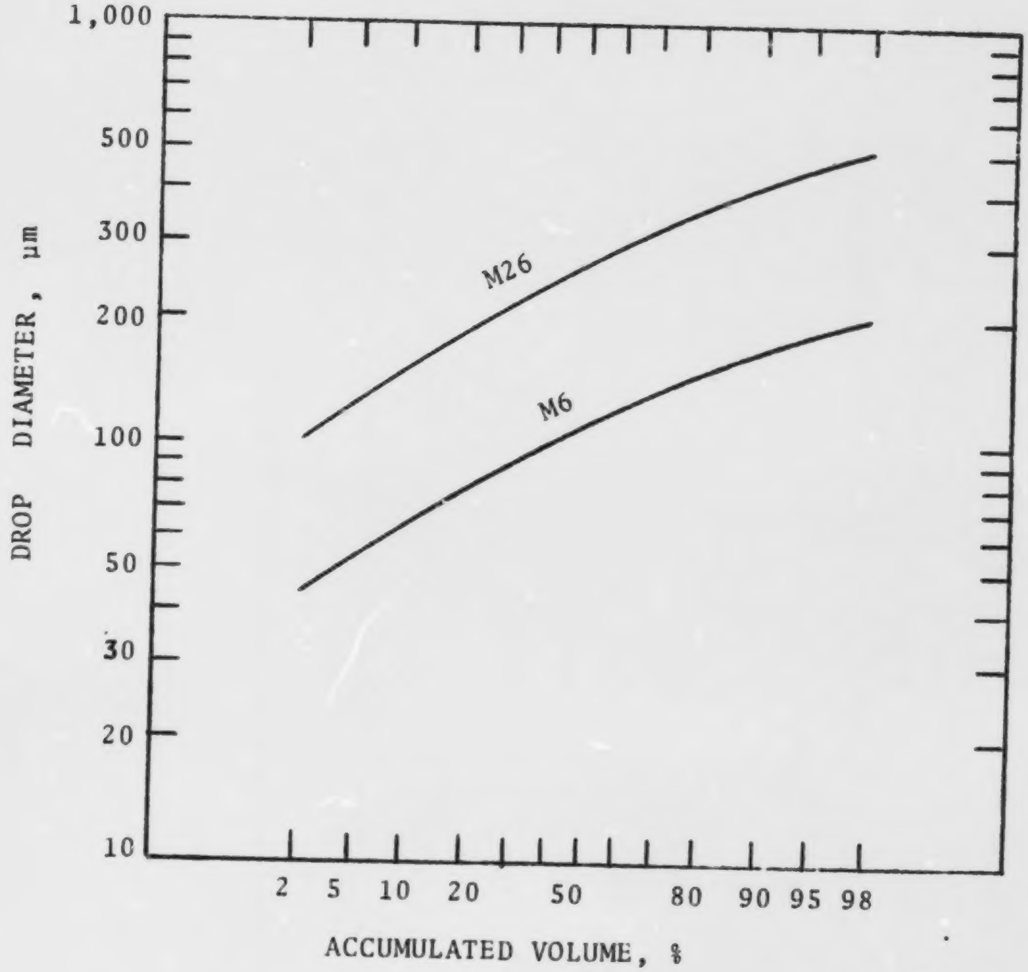

Figure 7-2 - Drop diameter versus volume percentage for hollow cone nozzle spraying water at 10.2 atm gauge pressure. (Manufacturer's data)

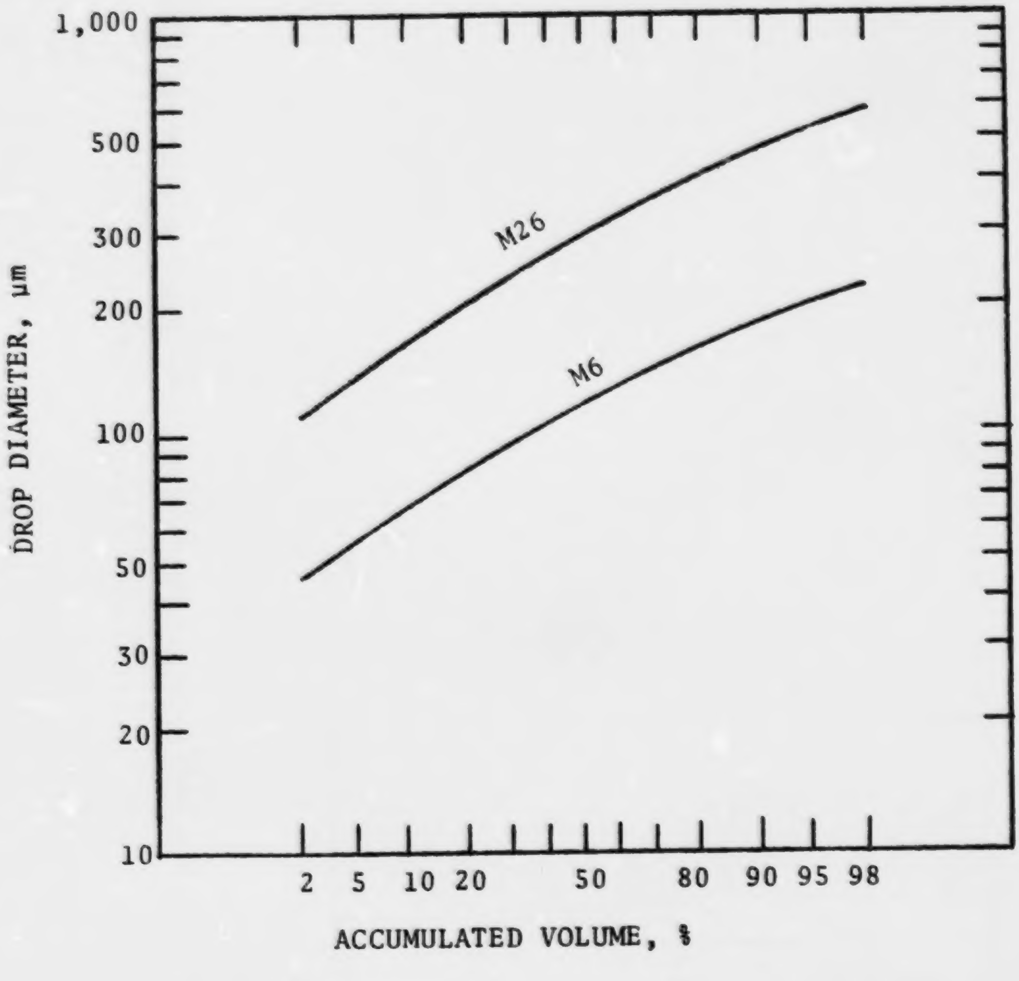

Figure 7-3 - Drop diameter versus volume percentage for hollow cone nozzle spraying water at 6.8 atm gauge pressure. (Manufacturer's data)

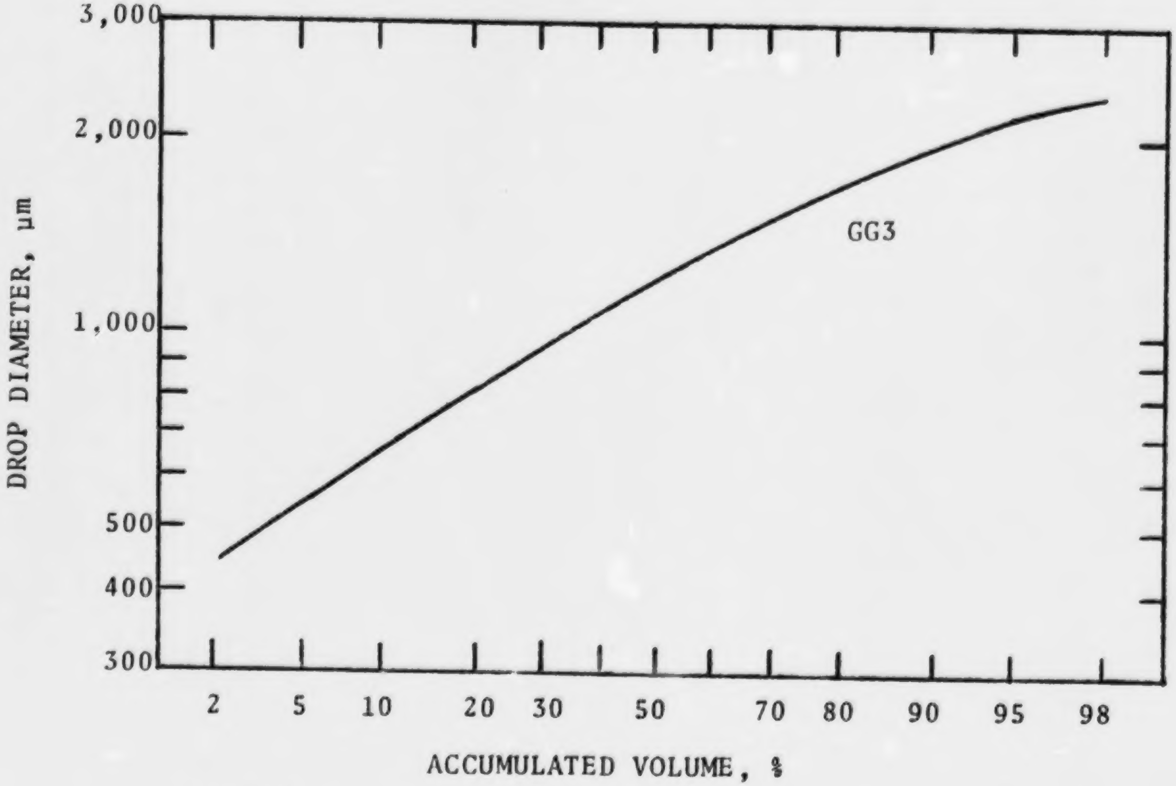

Figure 7-4 - Drop diameter versus volume percentage for fulljet nozzles spraying water at 2.7 atm gauge pressure. (Manufacturer's data)

It was observed that the entrainment flow rate reaching the entrainment separator decreased with decreasing air velocity. This is due to an increase in collection by the walls of the spray section.

EXPERIMENTAL RESULTS

Experimental data (see Appendix) for 153 runs are given in Tables A-1 to A-4. Table A-1 gives the overall performance of the entrainment separator. Liquid to gas volumetric ratio and the entrainment mass median drop diameter are measured at the inlet of the test section. Collection efficiency is the overall efficiency and represents the effect of primary efficiency, reentrainment and secondary collection. Similarly, pressure drop is the overall pressure drop for the test section.

Table A-2 gives the drop diameters of the entrainment entering and leaving the test section. Since the water feed rate, water pressure and type and number of nozzles affect drop diameter in the inlet, these variables are included in this table. The entry type and number of nozzles give the nozzle model number followed in brackets by the number of nozzles. The details of these nozzles are given in Table 7-1.

Table A-3 gives the liquid material balance in the system. As explained in the details of the equipment, the liquid collected in the test section is divided into four parts along the length of the test section. Liquid collected on the side of the spray section and the observation section upstream of the test section is also measured.

In some experiments liquid flowing as entrained drops after the test section is determined by material balance, i.e., [water in air after test section] = [total water supplied] - [total water collected]. In the rest of the experiments, liquid flowing as entrained drops was measured directly by measuring the humidity of a heated outlet gas sample.

Table A-4 gives pressure drop data for the system. "ΔP_{dry}" and "ΔP_{wet}" represent the pressure drops in the test section at the experimental condition without and with liquid flowing.

Packed Bed

Overall Efficiency - Efficiency data for packed beds are presented in Figure 7-5. Runs at gas velocities (Note: All gas velocities are superficial.) lower than 6.0 m/sec did not show any penetration. The theory for primary collection efficiency, shown as a solid line, is based on Equation (3-13) and predicts 100% primary efficiency over the range of gas velocities studied. The data for overall efficiency agrees well with the theory for primary efficiency, which indicates that little or no reentrainment is taking place.

Pressure Drop - Figures 7-6 and 7-7 show the pressure drop in packed bed separators. There is no effect of liquid load on pressure drop. The slope of the straight line on the log-log graph is 1.94.

Reentrainment - According to Figure 7-8, there is no direct dependence of the maximum outlet drop diameter on the gas velocity in a packed bed. Figure 7-9 shows that the geometric standard deviation increases with increasing outlet mass median drop diameter. In both figures, the inlet mass median drop diameter is used as a parameter, but no trends can be detected as it is varied.

The minimum and maximum outlet drop diameters are important in consideration of design criteria for a second

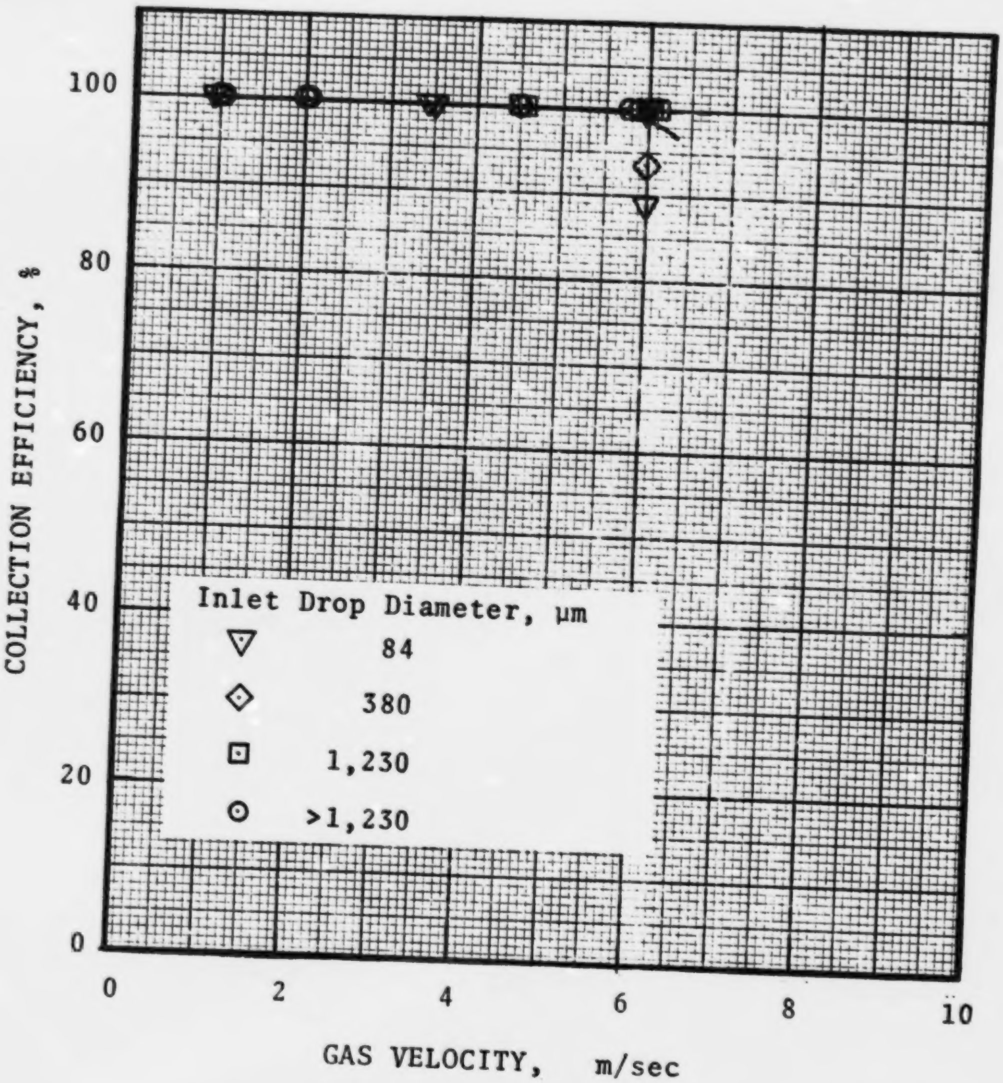

Figure 7-5 - Experimental collection efficiency of a packed bed as a function of gas velocity with horizontal flow.

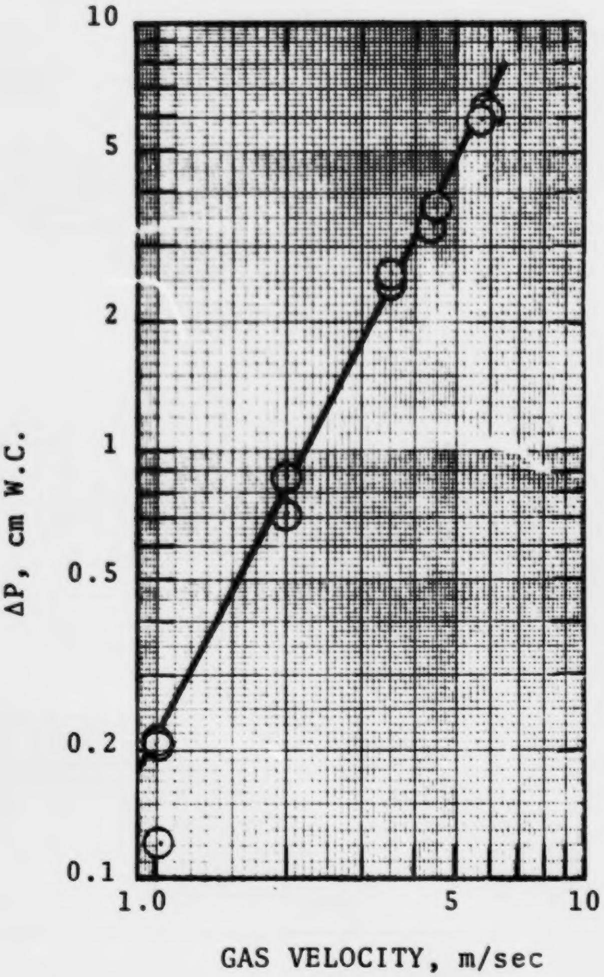

Figure 7-6 - Dry pressure drop in packed bed versus gas velocity

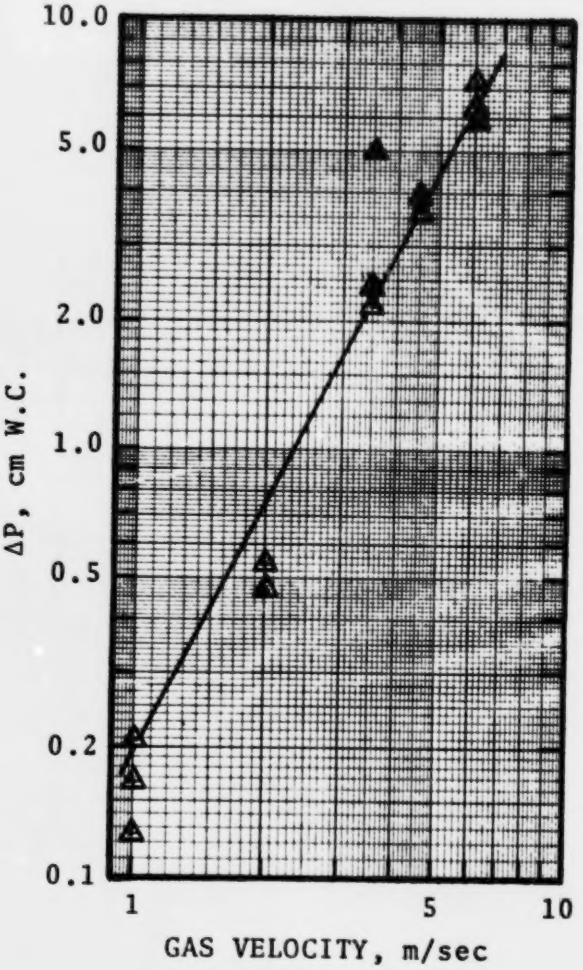

Figure 7-7 - Wet pressure drop in packed bed versus gas velocity

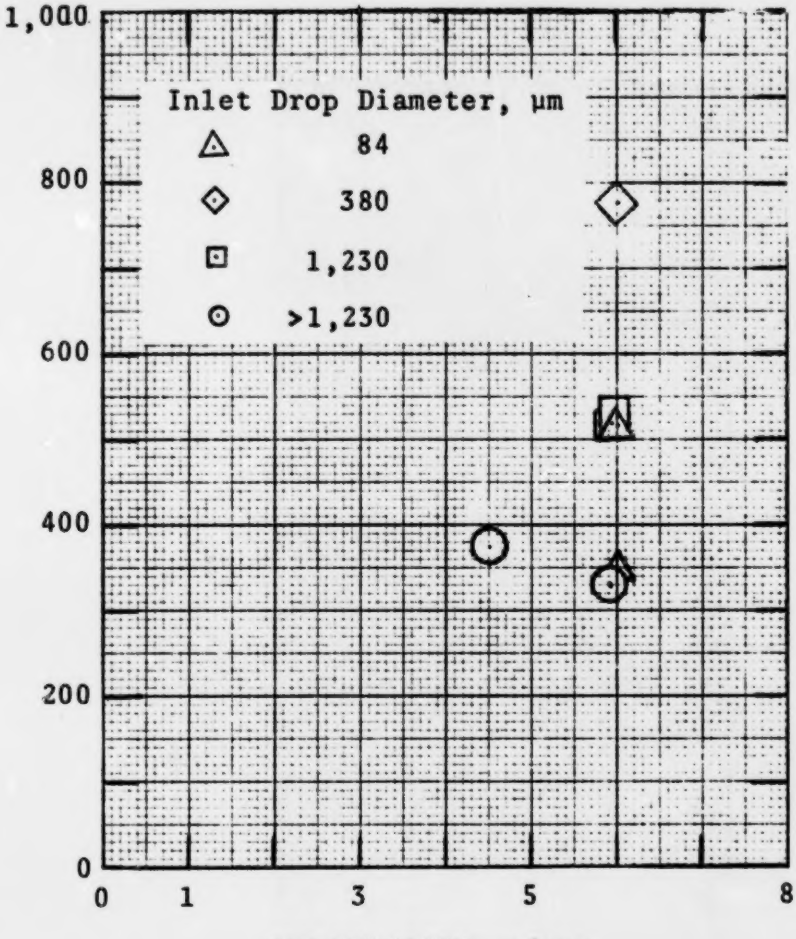

Figure 7-8 - Maximum drop diameter in the entrainment versus gas velocity for 30 cm packed bed

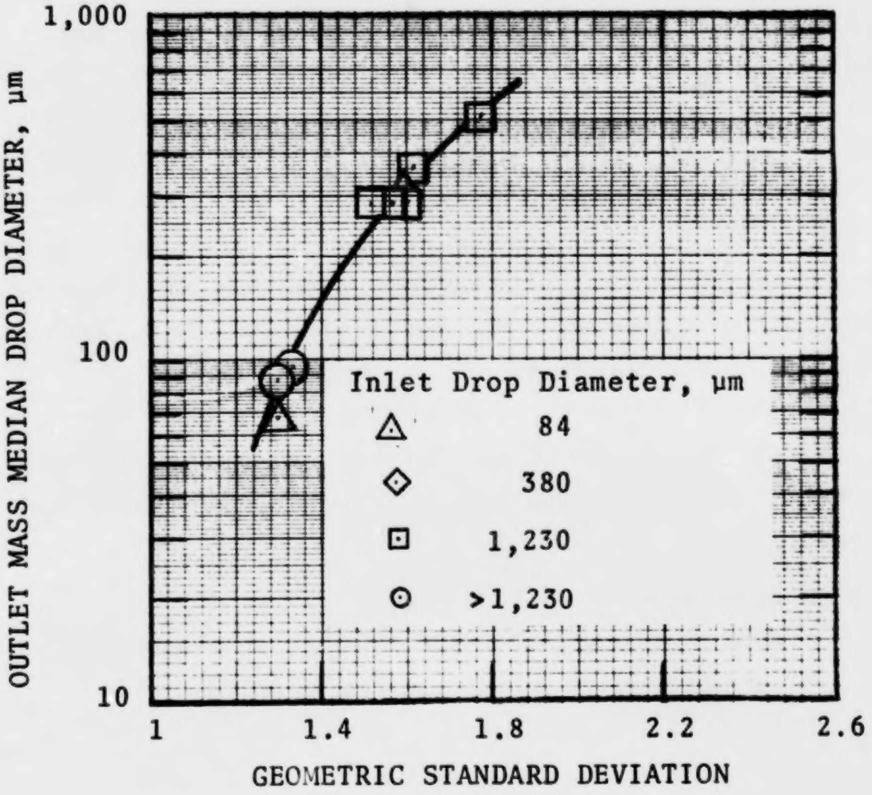

Figure 7-9 - Mass median drop diameter versus geometric standard deviation downstream of 30.5 cm packed bed

stage entrainment separator. For packed beds the minimum outlet drop diameter ranged from 40 to 60 μm.

Zigzag Baffles

Overall Efficiency - The overall collection efficiency for horizontal gas flow through vertical zigzag baffles was determined as a function of gas velocity. Figures 7-10 through 7-12 are plotted for different drop diameters in the inlet entrainment. The separator attains 100% efficiency for gas velocities between 3.0 and 6.0 m/sec. The efficiency falls sharply for gas velocities below 3.0 m/sec for experiments in which the inlet entrainment consisted of drops with 84 μm mass median diameter. Figure 7-13 shows data for all the runs with zigzag baffles.

A theoretical curve for collection efficiency for liquid droplets which have a median drop diameter of 90 μm and geometric standard deviation of 1.35 is also shown in Figure 7-10, where:

n = number of rows
θ = angle between the superficial and actual air flow directions in the baffles
d_{pg} = inlet mass median drop ciameter, cm
σ_g = geometric standard deviation of inlet entrainment

Experimental results reported by Bell and Strauss (1973) for zigzag baffles are plotted in Figure 7-10 along with points obtained in this study for d_{pg} = 380 μm and a line representing the data of Houghton and Radford (1938). The inlet entrainment of the Bell and Strauss experiments was comparable to this study, but their overall efficiency was much lower. This is probably due to the differences in separator design as reported in Table 7-3.

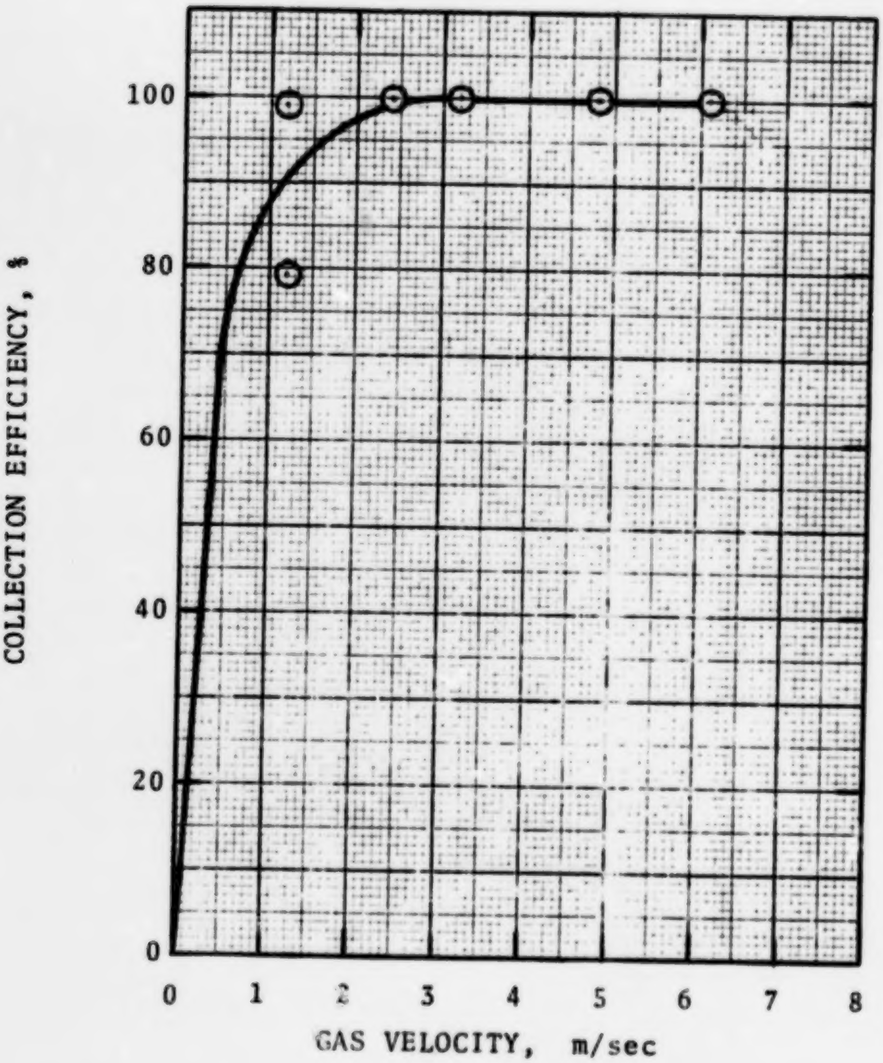

Figure 7-10 - Collection efficiency versus gas velocity in the zigzag baffle device with $n = 6$ and $\theta = 30°$. The solid line represents theoretical curve for $d_{pg} = 90$ μm and $\sigma_g = 1.35$.

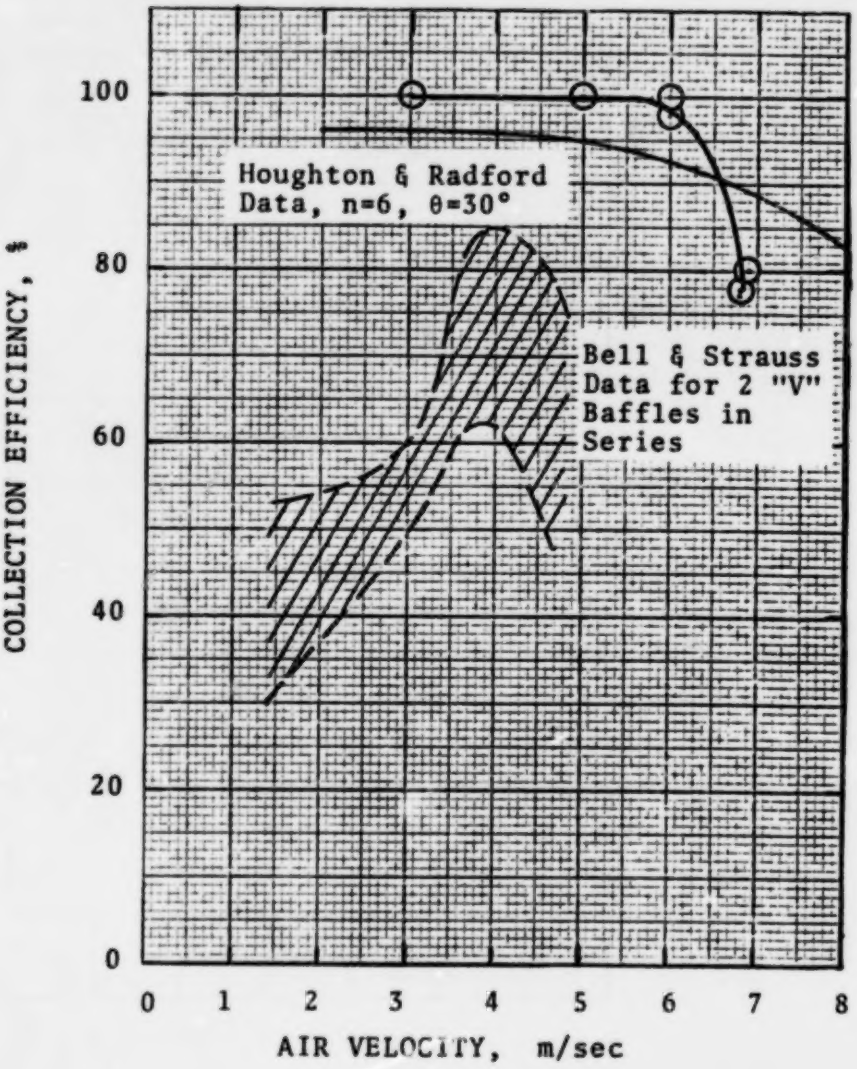

Figure 7-11 - Collection efficiency versus gas velocity in the zigzag baffle device with $n = 6$, $\theta = 30°$, $d_{pg} = 380\ \mu m$ and $\sigma_g = 1.52$.

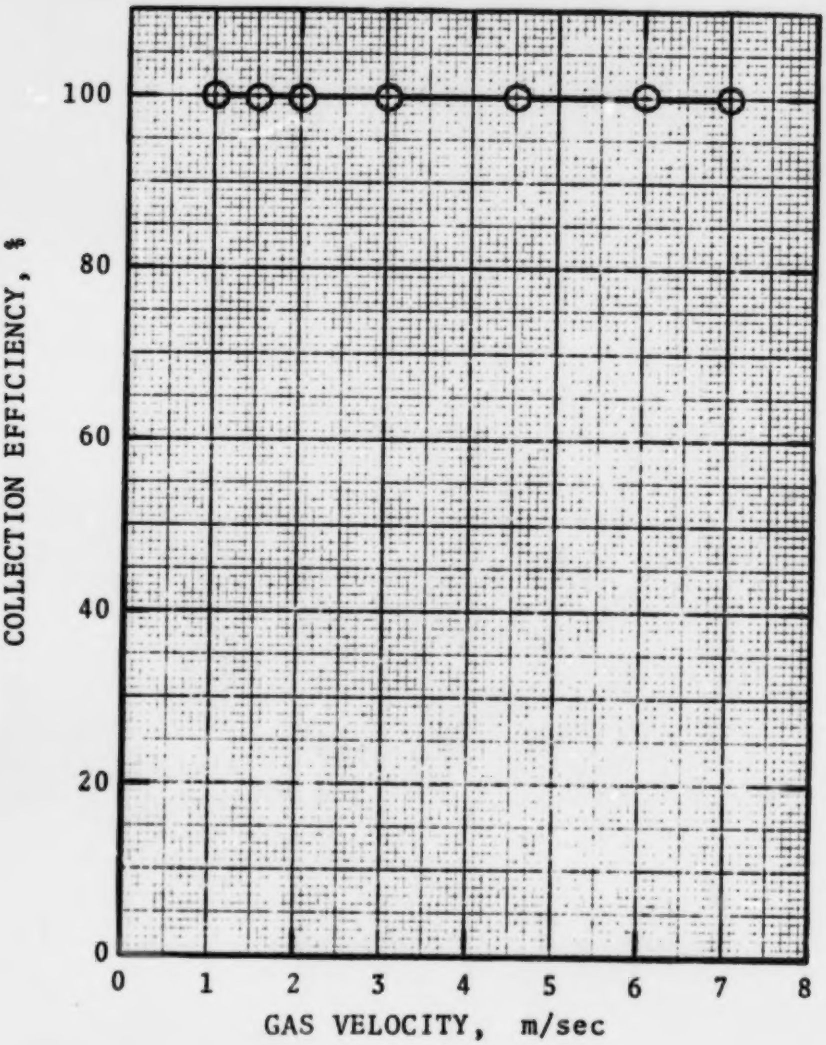

Figure 7-12 - Collection efficiency versus gas velocity in zigzag baffle device with $n = 6$, $\theta = 30°$, $d_{pg} = 1{,}230\ \mu m$ and $\sigma_g = 1.8$. Theory predicts 100% efficiency.

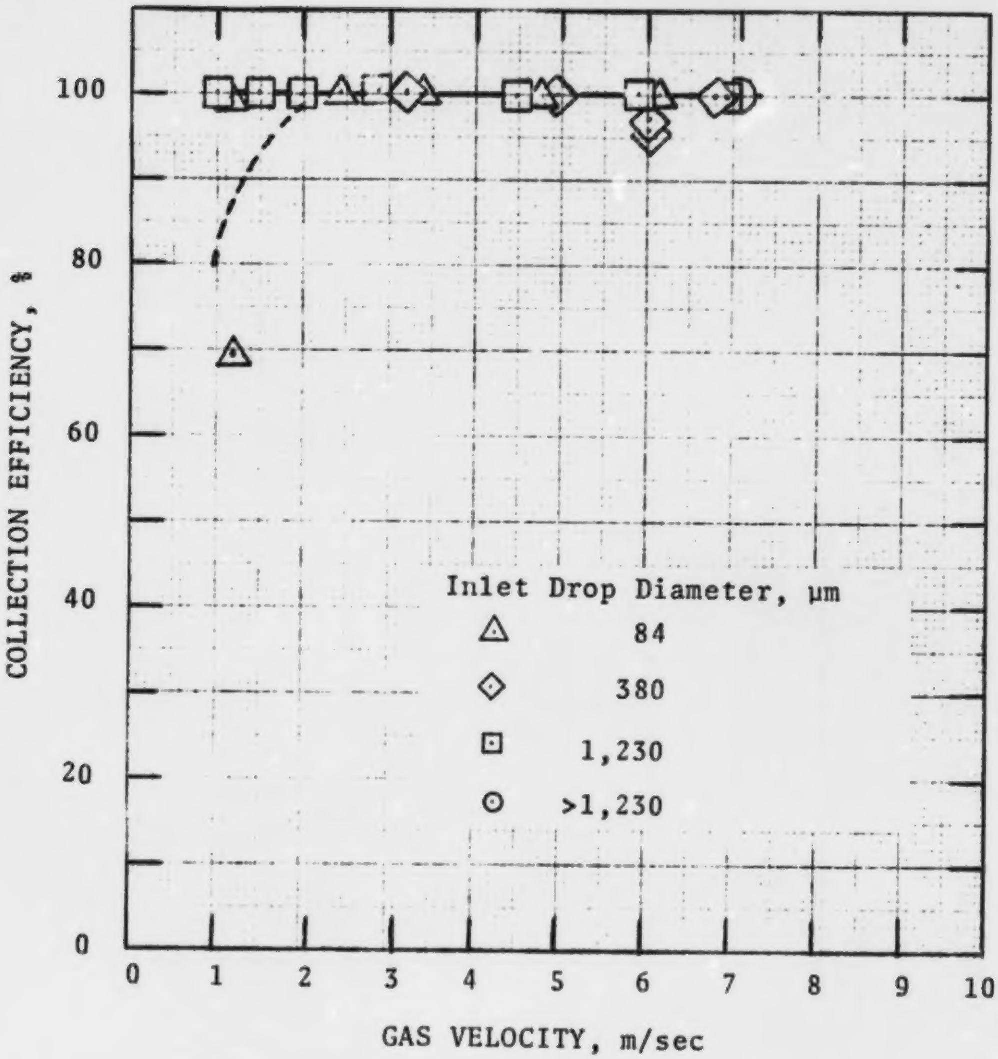

Figure 7-13 - Experimental collection efficiency as a function of gas velocity in the vertical baffles. Solid line represents theory.

Table 7-3. COMPARISON OF BAFFLE TYPE ENTRAINMENT SEPARATORS

	Present Design	Bell & Strauss (1973)	Houghton & Radford (1938)
Number of rows	6	4	6
θ°	30	45	30
Lip to prevent reentrainment	none	1.9 cm on 1st & 3rd row only	0.5 on 4th & 5th row only
Staggering of rows	2.5 cm	none	none
Distance between rows	2.5 cm	3.1 cm between 2nd & 3rd row only	0
Spacing between baffles in a row	6.9 cm	8.8 cm	2 cm
Width of baffles	7.5 cm	6.2 cm	5 cm

Houghton and Radford's experiments were conducted under two operating conditions: (1) Liquid flow rate = 38 cm^3/min and spray drop diameter ranging from about 1 to 60 μm, the predominant size being 40 μm, and (2) Liquid flow rate = 12.3 ℓ/min and spray drop diameter ranging from 2 to 800 μm, the predominant size being about 300 μm. The results obtained under both conditions were similar and were comparable with the present results due to similarities in the design, as summarized in Table 7-3.

Pressure Drop - Experimental dry and wet pressure drop versus gas velocity for baffles is plotted in Figures 7-14 and 7-15, respectively. In both figures the solid lines represent the theoretical prediction of pressure drop as presented in Equation (4-8). The liquid load does not have a significant effect on the pressure drop in the baffle section. This should be expected as liquid holdup in the baffles is small because of the high drainage rates.

Reentrainment - Figures 7-16 and 7-17 show the experimentally determined dependence of the outlet mass median drop diameter on the gas velocity. For an inlet drop diameter of 280 μm, the outlet drop diameter increases with rising gas velocity, as pictured in Figure 7-16. However, Figure 7-17 reveals that no pattern is in evidence for an inlet drop diameter of 1,230 μm.

The size distribution of drops leaving a zigzag baffle separator is depicted in Figure 7-18, with liquid flow rate as the parameter. The two curves have nearly identical slope on the log-probability diagram, but the lower liquid flow rate resulted in larger reentrained drops.

The maximum drop diameter found in the outlet of a baffle separator is graphed versus gas velocity for two inlet drop diameters in Figure 7-19. A correlation can

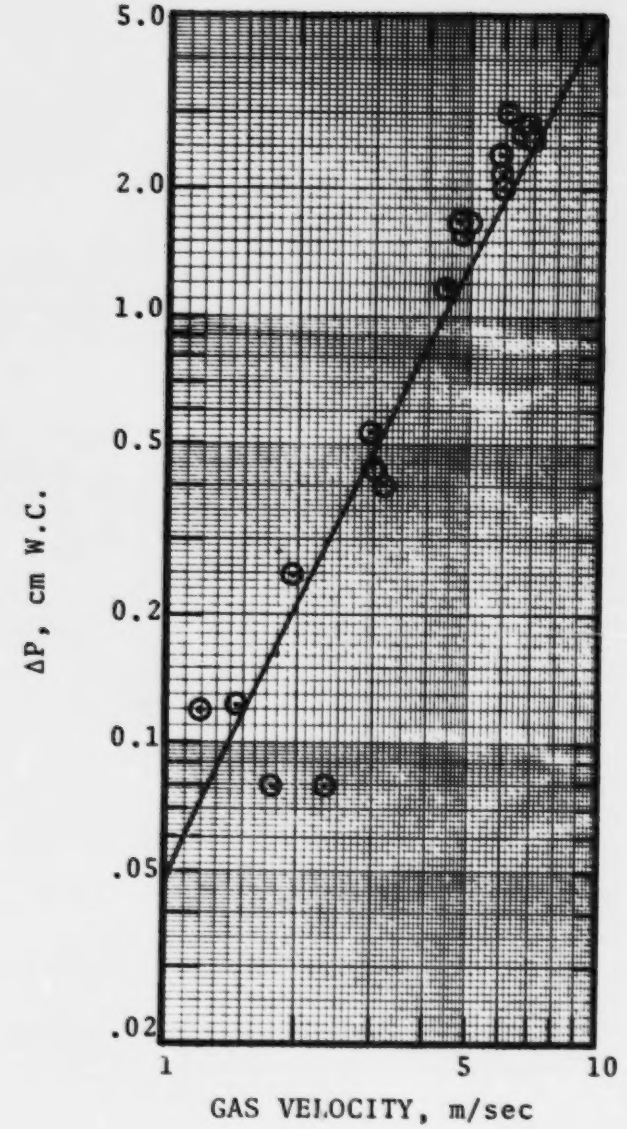

Figure 7-14 - Dry pressure drop in baffles versus gas velocity

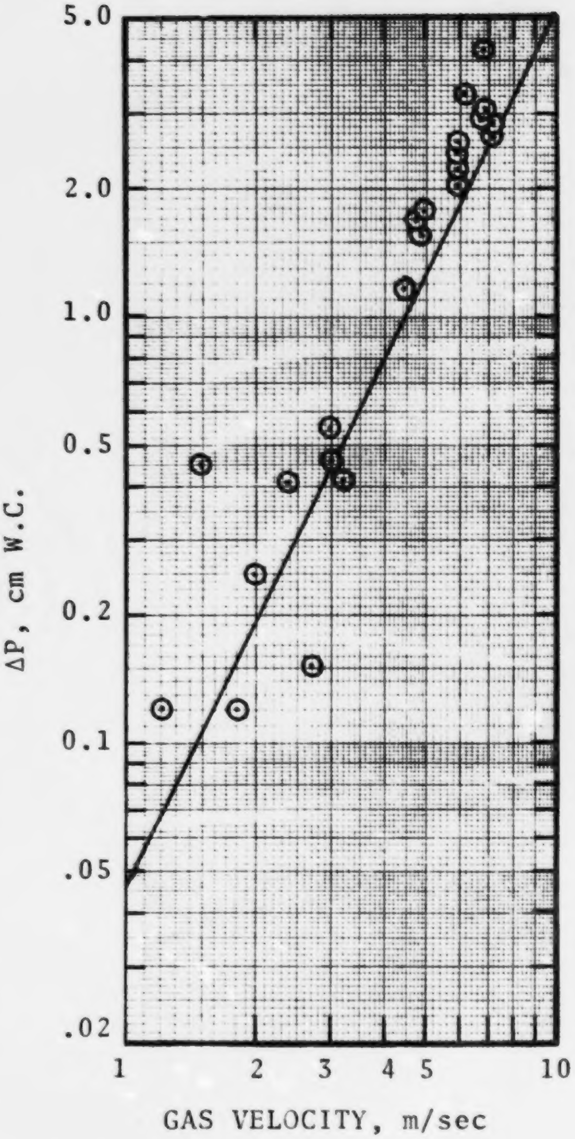

Figure 7-15 - Wet pressure drop in baffles versus gas velocity.

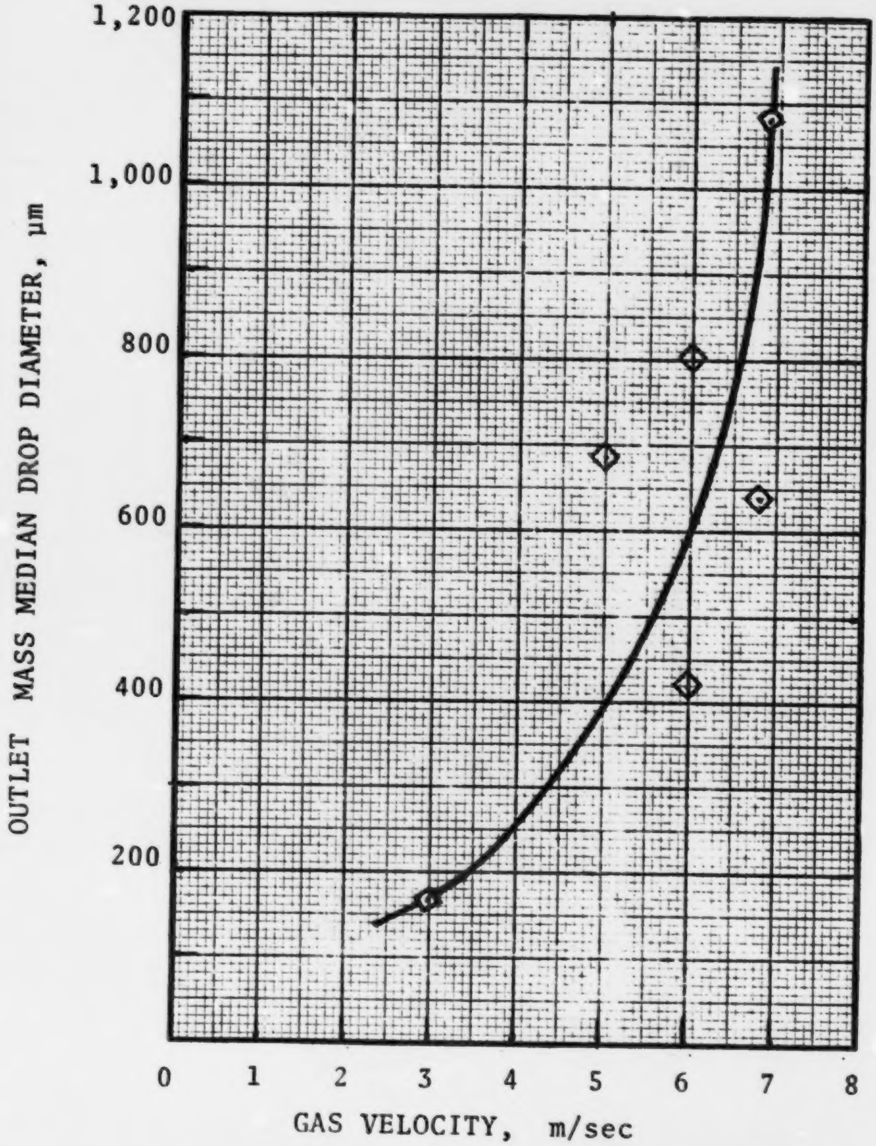

Figure 7-16 - Outlet drop diameter versus gas velocity for zigzag baffles with inlet mass median diameter of 380 µm.

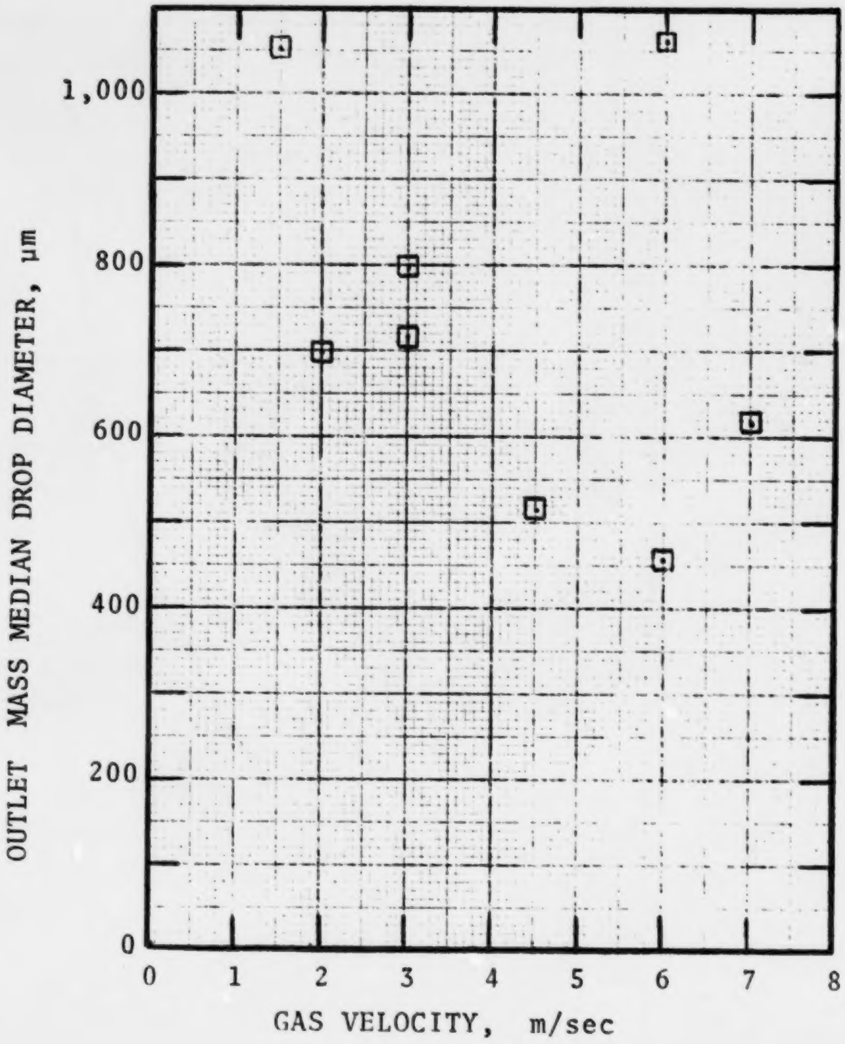

Figure 7-17 - Outlet drop diameter versus gas velocity for zigzag baffle with 1,230 μm inlet mass median drop diameter.

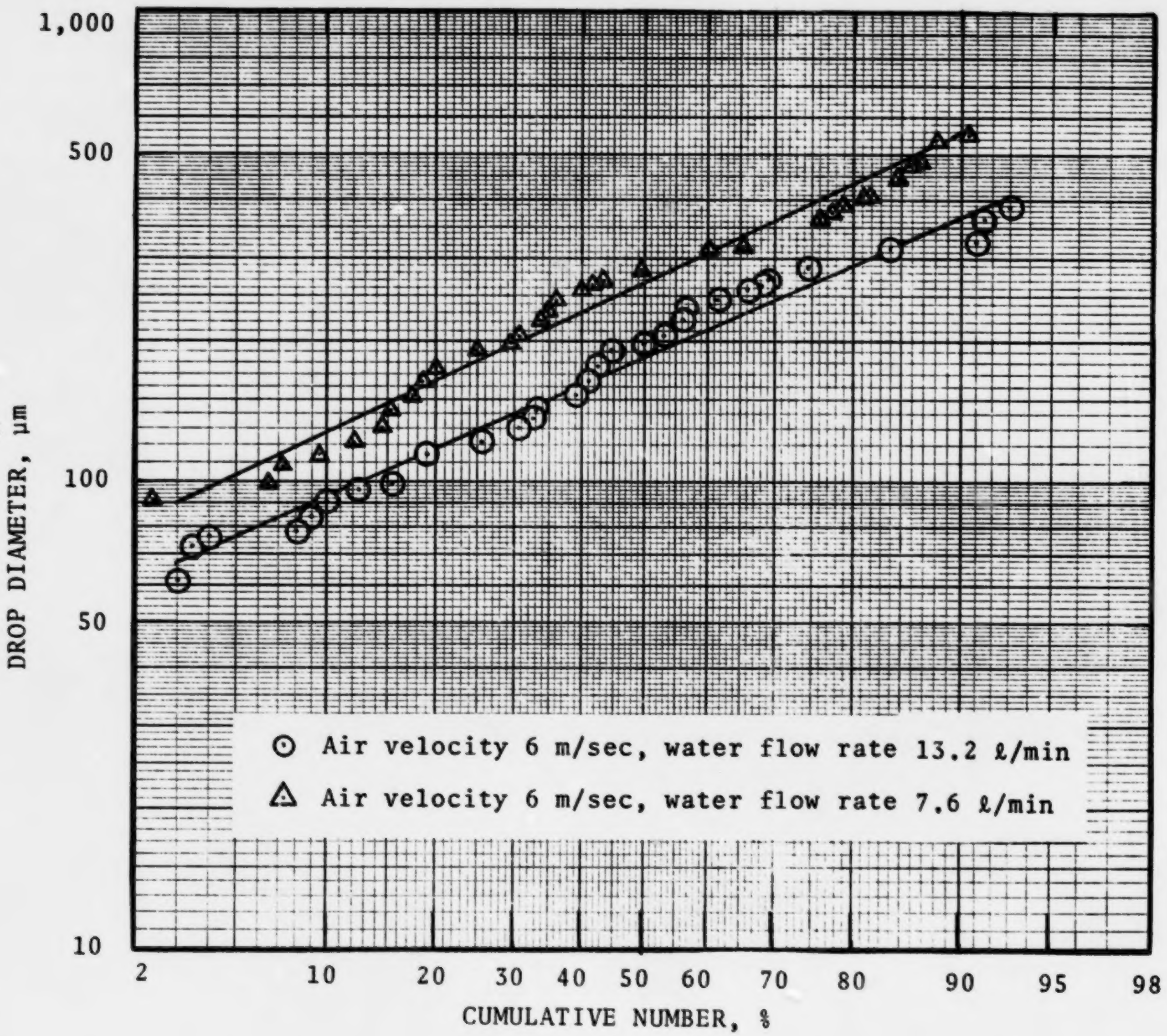

Figure 7-18 - Size distribution of drops leaving baffle entrainment separators

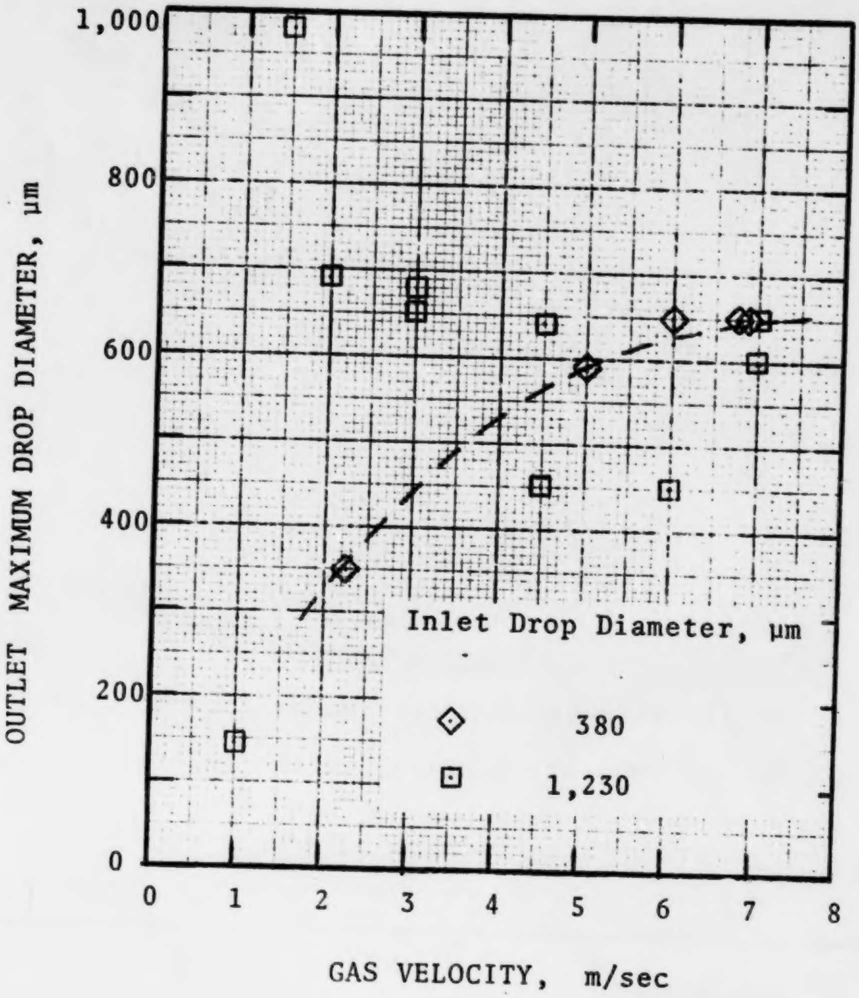

Figure 7-19 - Maximum outlet drop diameter in the entrainment versus gas velocity for zigzag baffles.

be established for 380 μm drops but not for the large 1,230 μm drops. The minimum drop size in the reentrainment was observed to range from 50 to 80 μm.

The geometric standard deviation gets larger as the outlet mass median increases, as seen in Figure 7-20.

Two very important parameters for determining reentrainment are gas velocity and the liquid to gas ratio. The combination of these two which results in reentrainment as observed experimentally is shown in the shaded region in Figure 7-21. The reentrainment observed is 0.5 - 1% of the inlet entrainment.

Liquid Flow on the Baffles - Flow of liquid on the baffle surface was observed in some of the runs. As the flow increases, the film thickness of the liquid near the downstream edge increases. The gas stream forms a wake at the back side of the baffle, which tears away some of the liquid at the downstream edge. The approximate shape of the wake is shown in Figure 7-22. The wake formation becomes more pronounced with increasing gas velocity. The flow of liquid film on the back side of the baffle is shown in the same figure.

If the liquid flow on the baffle surface is small, only drop flow takes place on the back side of the baffle. Some of these drops reach the upstream edge of the baffle, where they are reentrained. The reentrained drops splash on the adjacent baffle in the same row and disintegrate. Some of these small drops are reentrained in the air. The drops normally splash on the third quarter width of the baffles as measured from the upstream. The drops flowing on the back side of the baffles are 3-4 mm in diameter.

Reentrainment from the downstream edge of the baffle was more significant compared to reentrainment from the

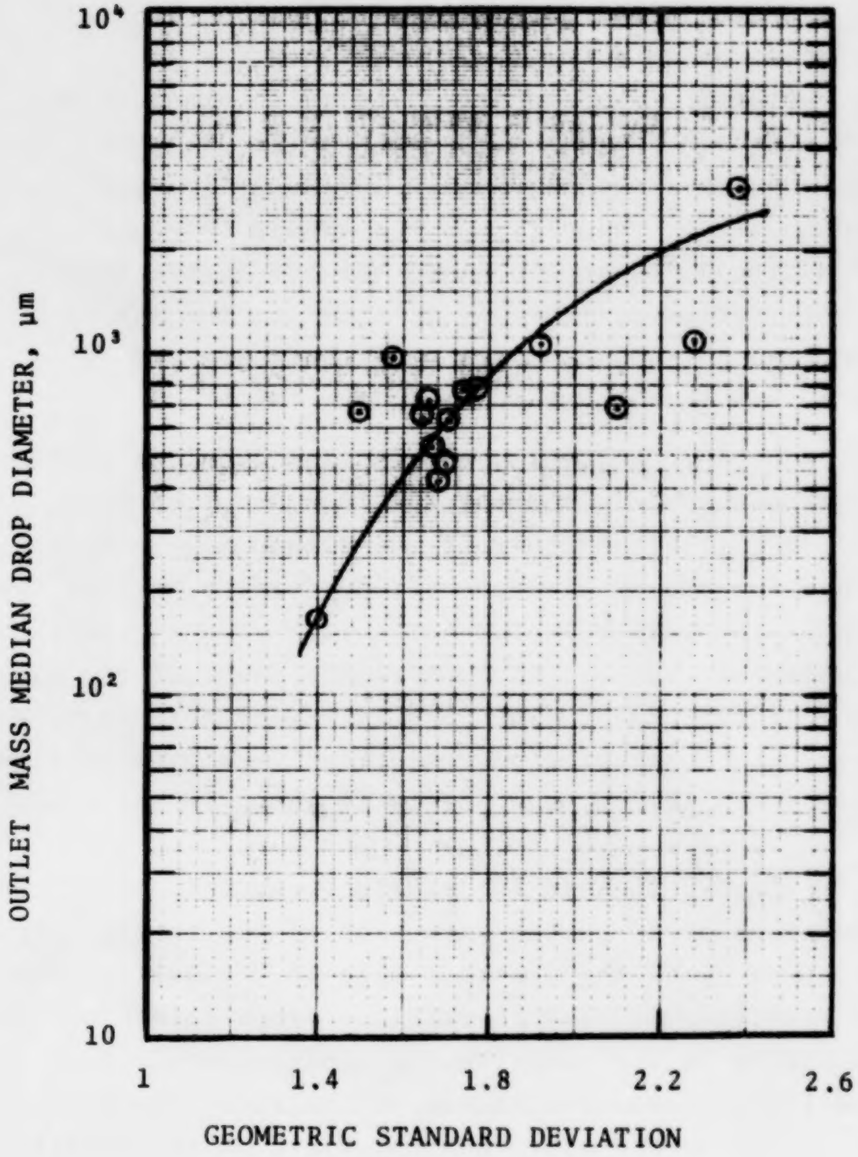

Figure 7-20 - Drop diameter versus geometric standard deviation at zigzag baffle outlet.

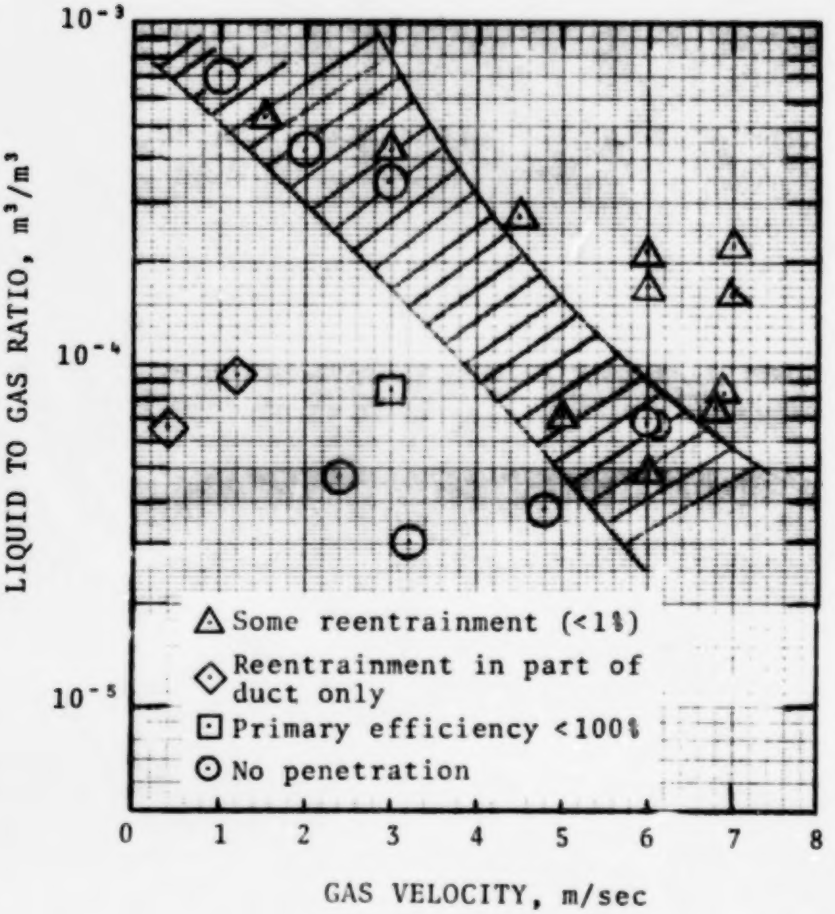

Figure 7-21 - Effect of gas velocity and liquid load on performance of baffle type separator.

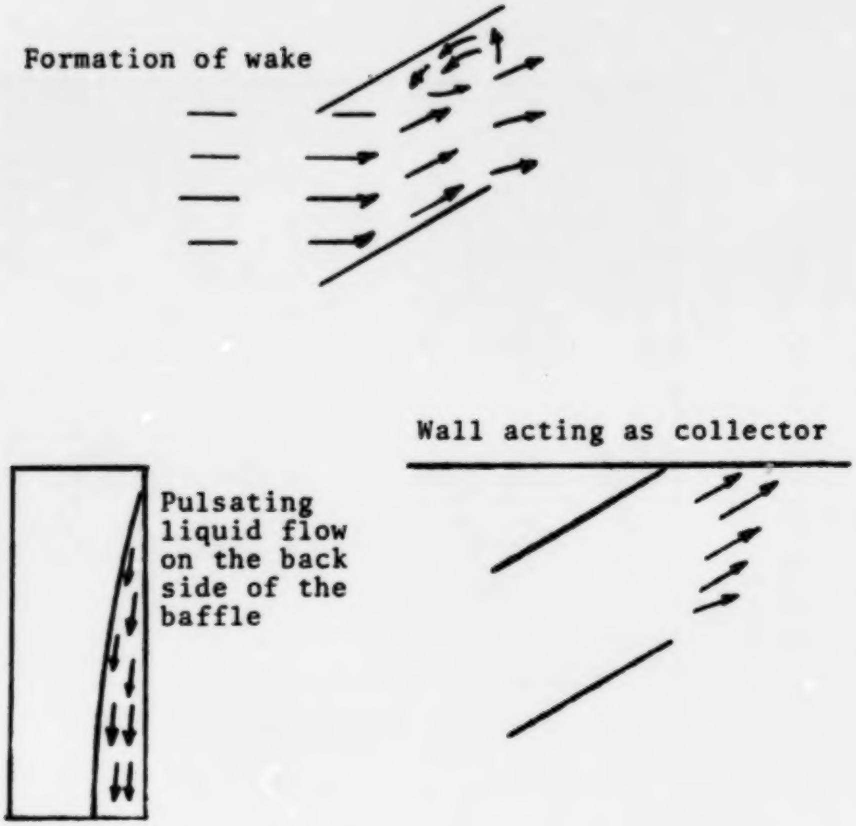
Formation of wake
Pulsating liquid flow on the back side of the baffle
Wall acting as collector

Figure 7-22 - Some observed phenomena in entrainment separator (a) formation of wake (b) liquid flow on the back side of the baffle (c) wall effect

upstream edge. If the liquid flow on the baffle surface was drop flow, some of these drops reached the downstream edge and (1) were reentrained, (2) were turned to the back side of the baffle, (3) fell down at the edge due to gravity, or (4) stayed at the edge of the baffle until they grew by coalescing with other drops. Most of the drops were collected by the third or fourth step. If the liquid was flowing as a film on the baffle, part of the film was torn and reentrained at the downstream end. The drops reentrained from the downstream edge of the baffle were 3-5 mm in diameter. These drops were normally collected on the baffles of the second row, i.e., drops reentrained from the second row were collected on the baffles in the fourth row.

Some wall effect was observed in the baffle section. There were four baffles in a row and the side walls of the test section acted as collectors for the entrainment. This effect is shown in Figure 7-22.

The liquid flow pulsated whenever reentrainment took place and occurred in film flow and in drop flow. It was difficult to determine the amplitude of the pulsating film which may have been of the order of 0.05 cm. The frequency of the wave was not measured.

Mesh

Overall Efficiency - The overall collection efficiency data for horizontal flow through wire mesh are plotted in Figure 7-23. No penetration was observed in experiments at low gas velocity, less than 3.0 m/sec. At higher velocities penetration due to reentrainment was observed. The dotted line, predicting 100% efficiency, represents the theoretical curve based on Equation (3-21). In the range of experimental data, the curve given by the manufacturer

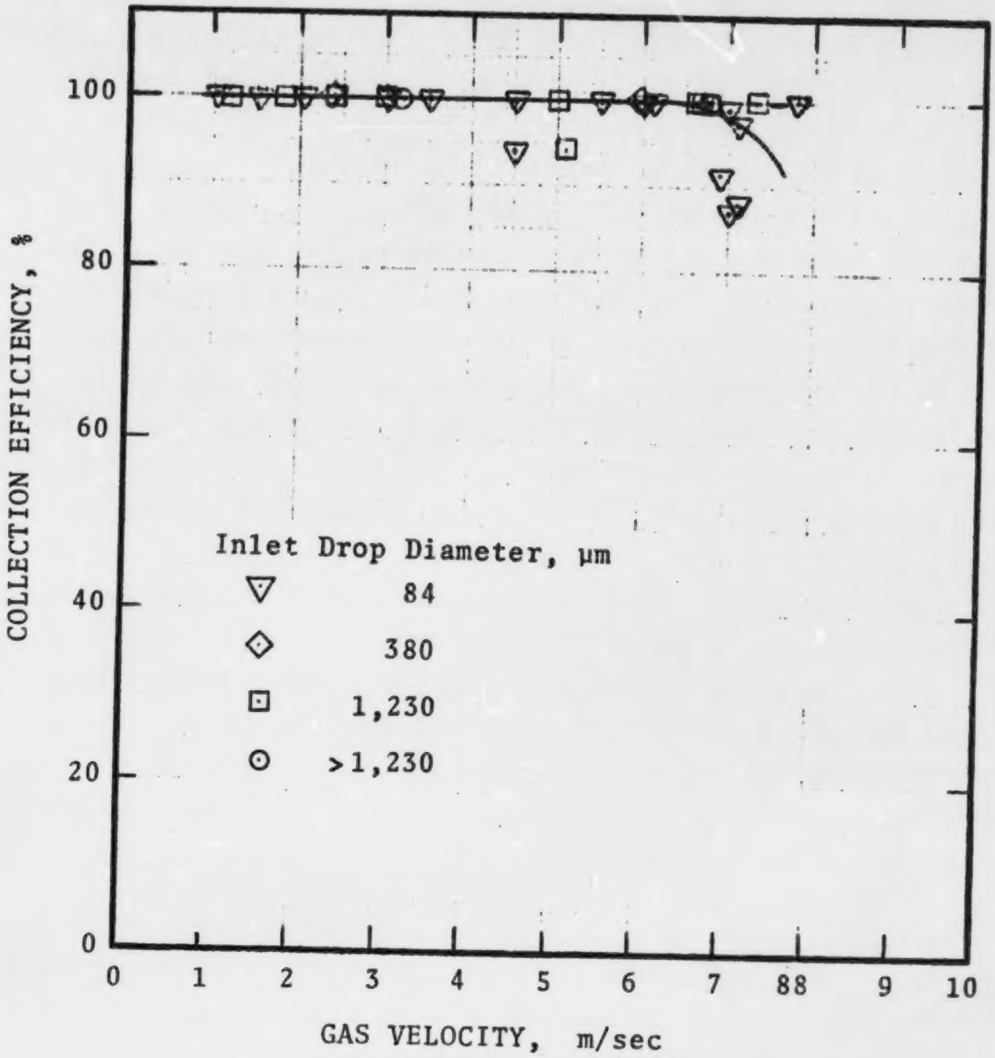

Figure 7-23 - Experimental collection efficiency of wire mesh as a function of gas velocity.

(ACS Industries) for mesh efficiency corresponds to the theoretical curve.

Pressure Drop - In contrast to the results for packed beds and zigzag baffles, the pressure drop in wire mesh separators is affected by liquid load, as seen in Figure 7-24. The slope of the straight lines on the log-log plot is 1.65; thus, "ΔP" can be represented as a function of "$u_G^{1.65}$". In Figure 7-24, $L/A = 0$ represents the dry pressure drop "ΔP_{dry}" through the mesh. For $0 < L/A < 1$ the pressure drop is $1.5\ \Delta P_{dry}$, and for $1 < L/A < 5$ the pressure drop is $2.3\ \Delta P_{dry}$.

Reentrainment - The outlet mass median drop diameter is plotted as a function of gas velocity in both Figures 7-25 and 7-26. Each curve shows a dependence in the range of gas velocities studied, but it is more pronounced for inlet drop diameters of 82 μm than for large drops of 1,230 μm diameter.

Figure 7-27 demonstrates that no trend can be detected relating gas velocity with the maximum drop diameter in the reentrainment. However, the minimum drop diameter was found to range from 40 to 80 μm. As seen in Figure 7-28, there is a positive straight-line correlation between geometric standard deviation and the mass median drop diameter in the outlet.

Figure 7-29 shows the combination of gas velocity and liquid to gas ratio which will result in reentrainment in mesh separators. The shaded area is the region where onset of reentrainment was observed.

Buerkholz (1970) collected reentrainment data for sulfuric acid mist 150 cm downstream of a mesh separator. He found that reentrainment increased from 1.6 to 4.0% (0.3 to 1.3 mg/m^3) as the gas velocity was increased from

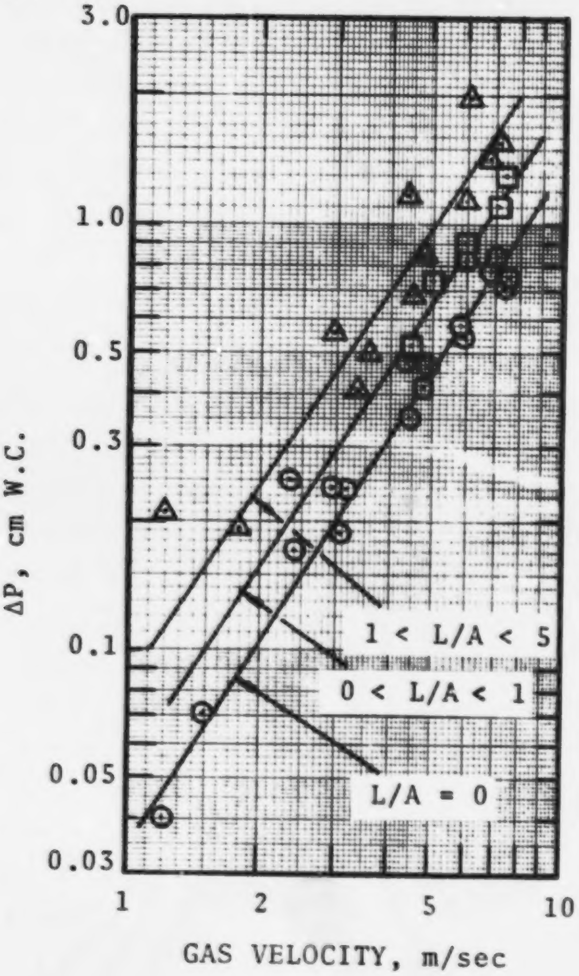

Figure 7-24 - Pressure drop in wire mesh versus gas velocity with liquid load as parameter
L/A = Superficial liquid velocity, cm/min

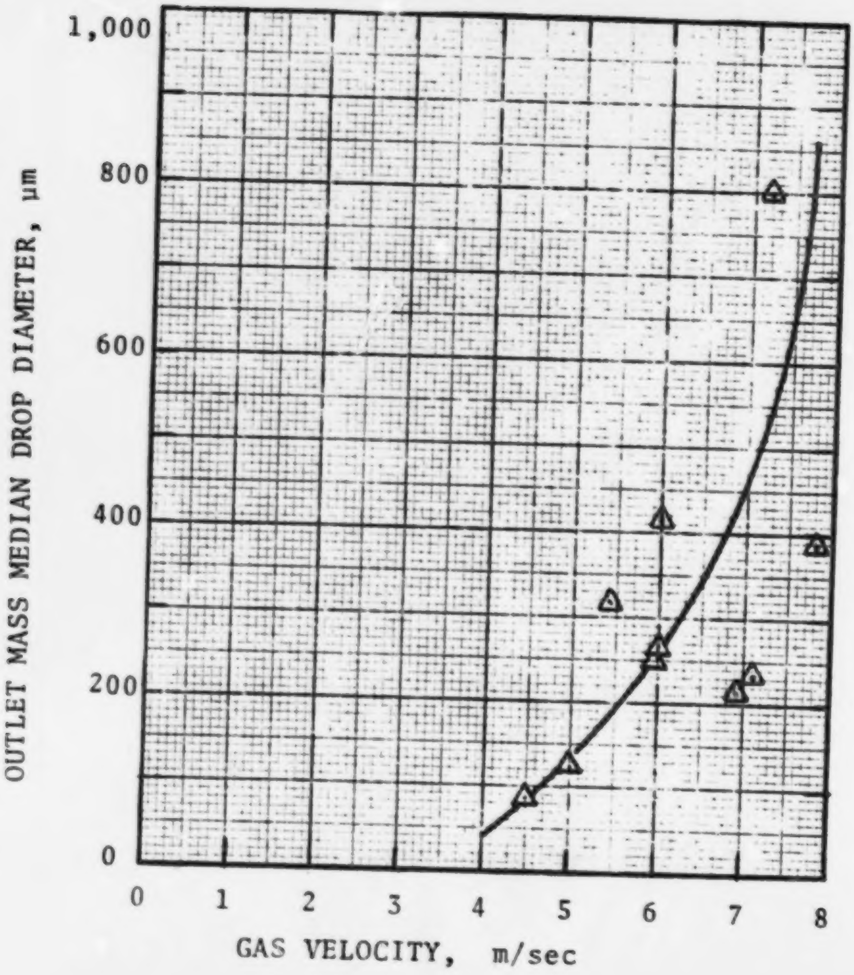

Figure 7-25 - Outlet drop diameter versus gas velocity for mesh with 82 µm inlet drop diameter.

Reproduced from best available copy.

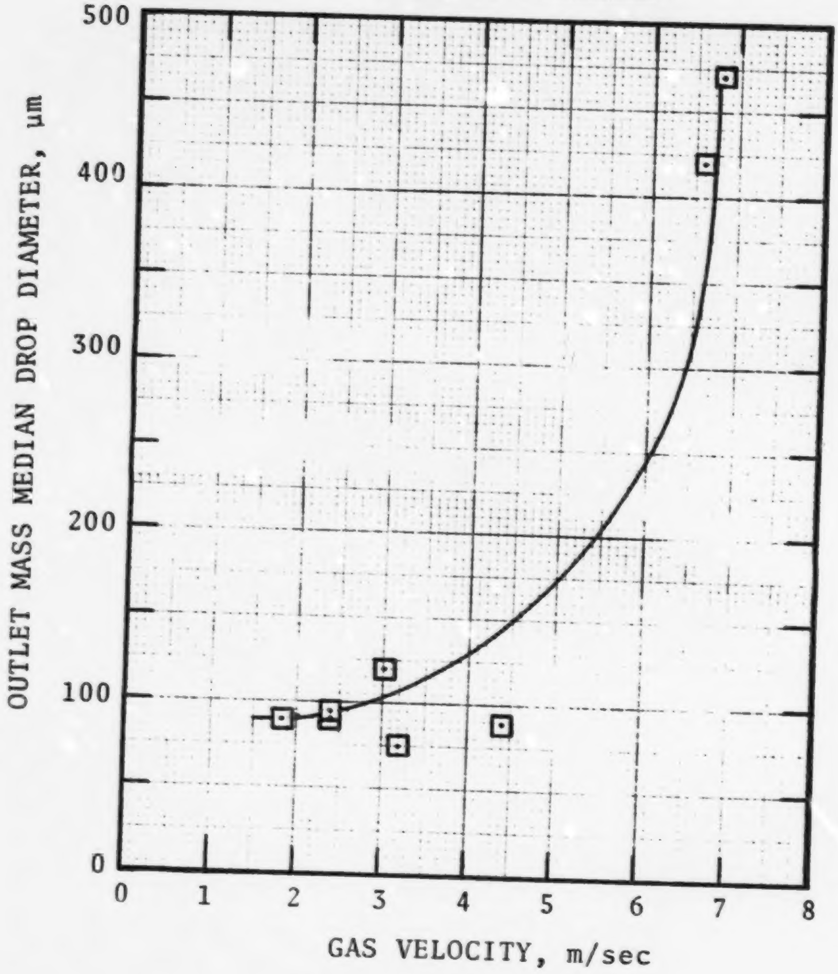

Figure 7-26 - Outlet drop diameter versus gas velocity for mesh with 1,230 μm inlet drop diameter

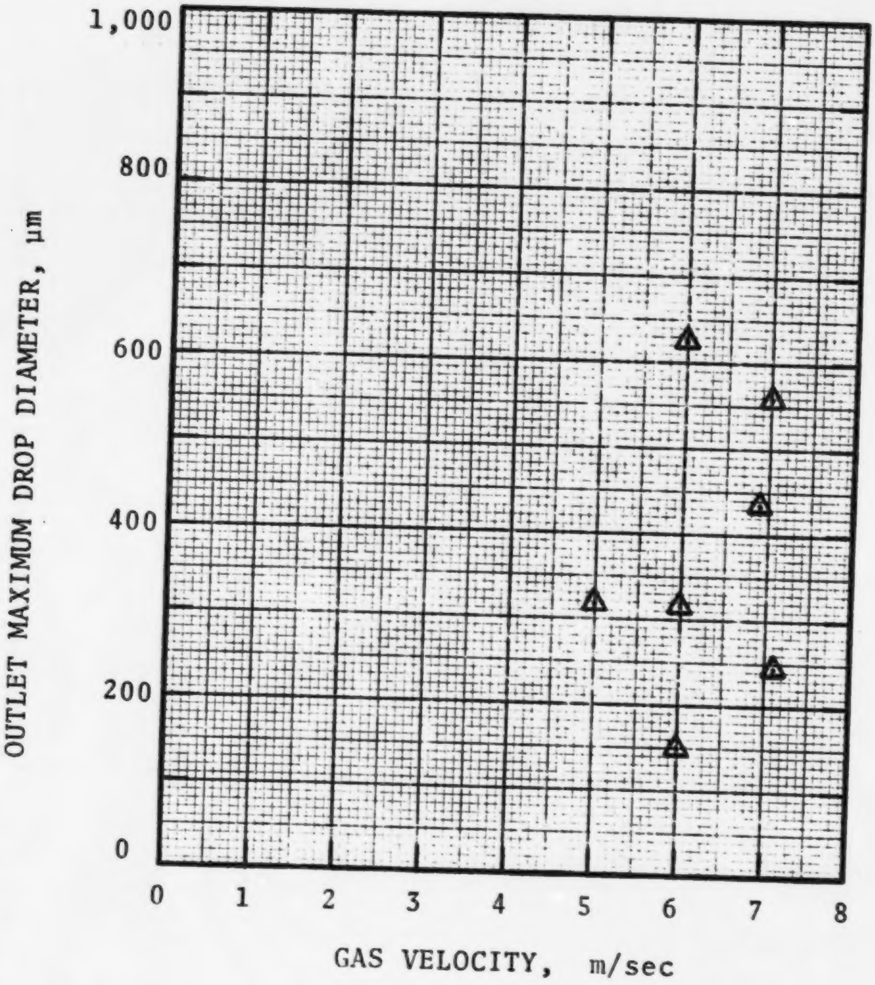

Figure 7-27 - Maximum outlet drop diameter in the entrainment versus gas velocity for mesh

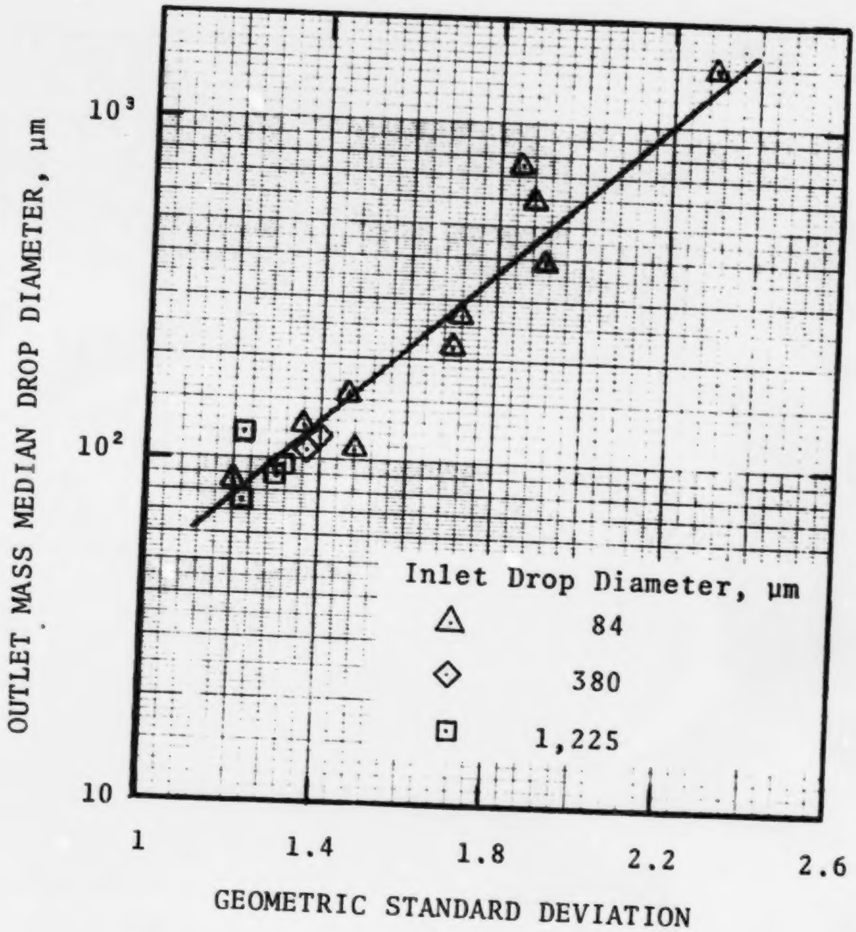

Figure 7-28 - Drop diameter versus geometric standard deviation for mesh.

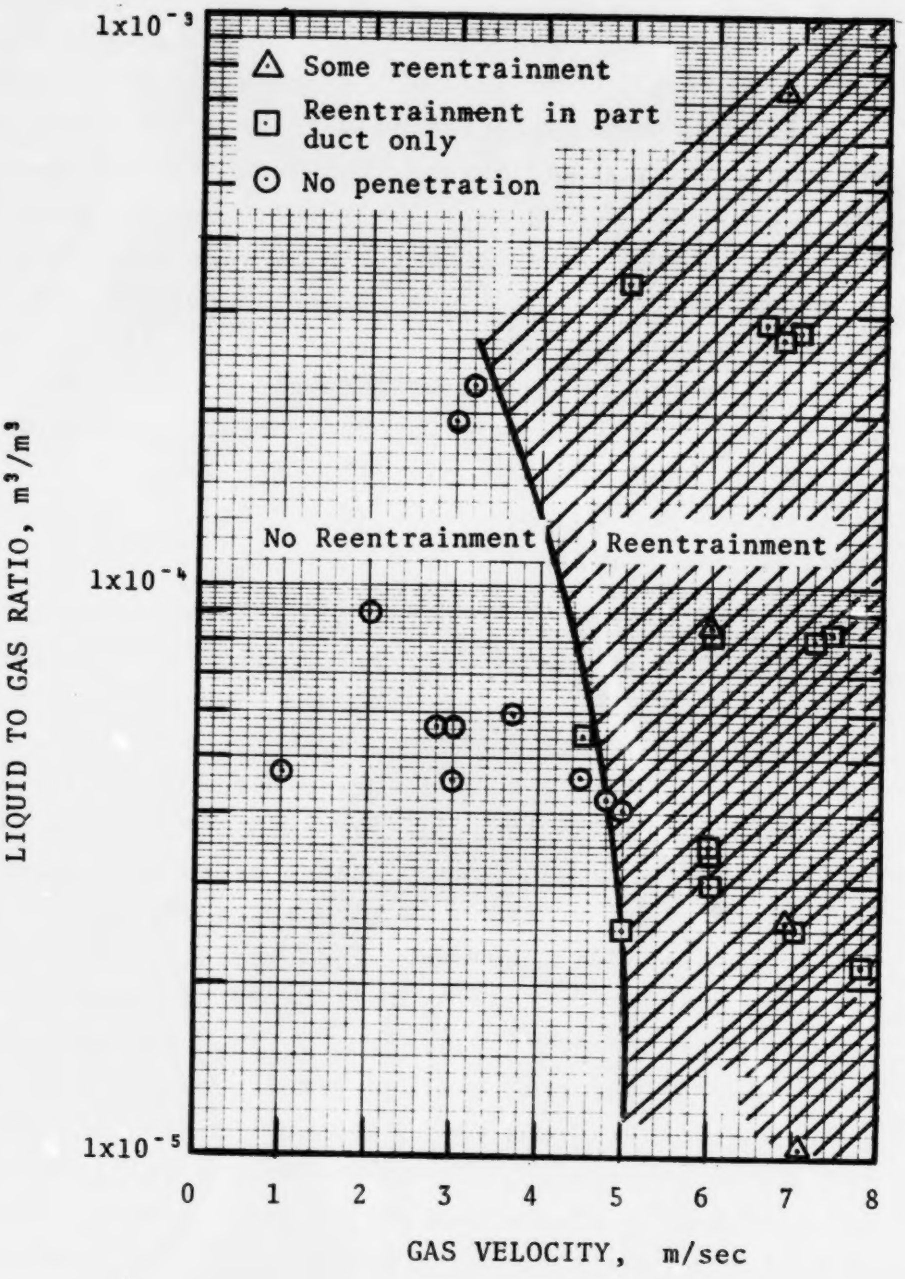

Figure 7-29 - Effect of gas velocity and liquid load on performance of mesh

4.7 to 8.2 m/sec. The outlet mass median drop diameter also increased from 150 to 750 μm. Buerkholz' data, plotted in Figure 7-30, were collected on a 15 cm x 15 cm mesh with sedimentation present between the mesh and the sampling point. The solid line in Figure 7-30 is the onset of reentrainment curve obtained in the present study. The data show good agreement in determining the reentrainment velocity of 5 m/sec at very small liquid loads.

The reentrainment curve obtained from the manufacturer also appears in Figure 7-30. The manufacturer predicts higher reentrainment velocity than the present results. The differences may be due to the fact that the manufacturer used vertical gas flow.

Visual Observation of Reentrainment - Reentrainment in the mesh section was observed to take place in the following ways:

1. At low liquid loads the mesh operated without flooding. Apparently, the drops that are collected on the mesh wires grew to 3-5 mm diameter before they drained down. If the air velocity is high, the path of the drop is not vertically downward. Some of these drops were airborne and struck the wires of the grid supporting the mesh. Normally, the drop shattered into one large drop slightly smaller than the original size and 2-4 satellite drops which were reentrained.

Some of the drops collected on the grid wire drained at once, whereas the rest drained after growing to a larger size. There were other drops which missed striking any wires and emerged from the mesh. These drops were collected at the downstream side of the mesh. The drops passing through the mesh without striking any wires were carried farther downstream of the mesh than others. All these reentrained drops were 4-5 mm in diameter and upon reaching the bottom, they shattered into a few (3-4) satellite drops. The rest of the liquid in the original drop was mixed with the liquid film

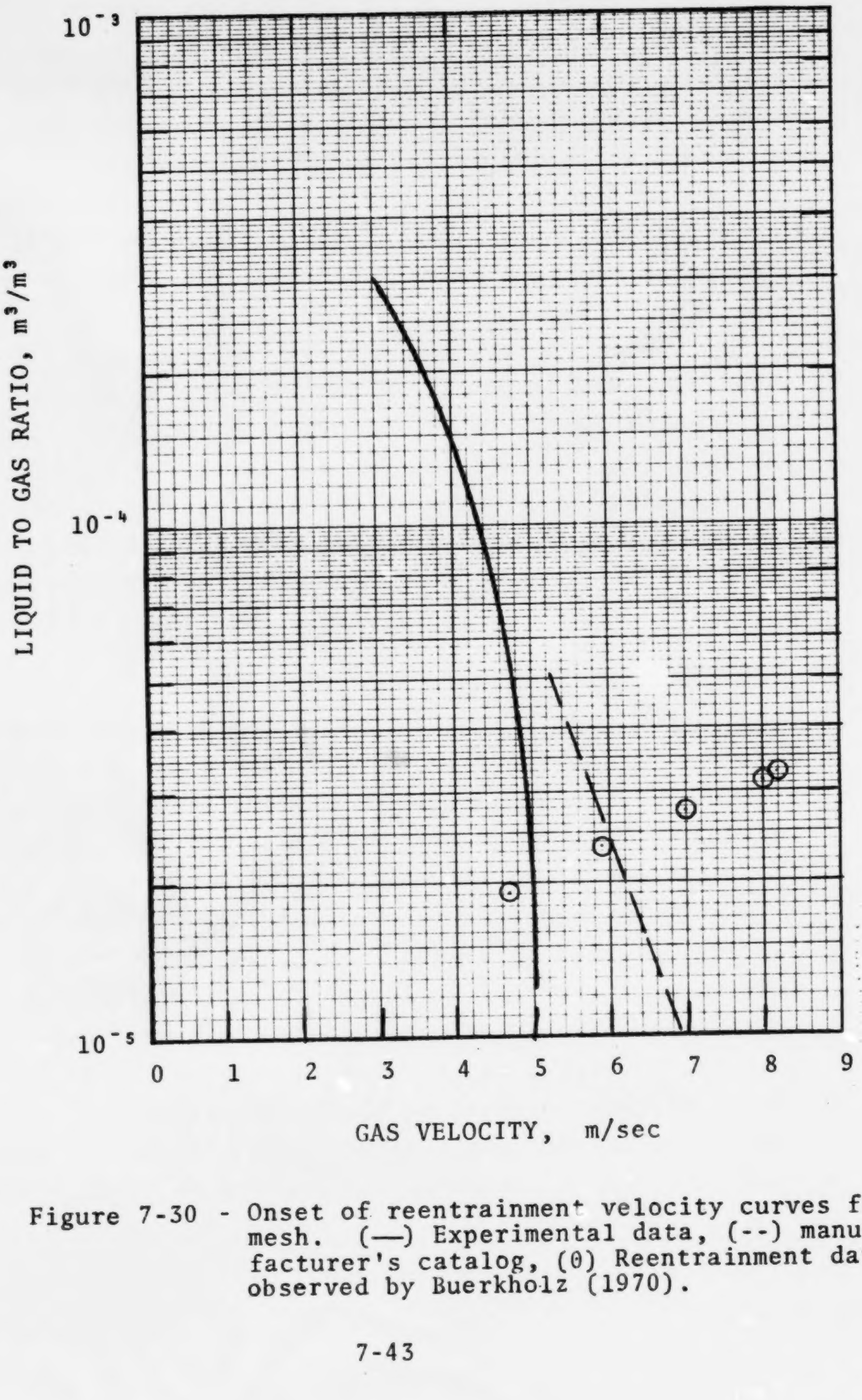

Figure 7-30 - Onset of reentrainment velocity curves for mesh. (—) Experimental data, (--) manufacturer's catalog, (θ) Reentrainment data observed by Buerkholz (1970).

at the bottom. These satellite drops flew into the air due to kinetic energy, and their initial trajectory formed a cone along a vertical axis. The angle of the cone was dependent upon initial drop velocity and was observed to range from 0° to 90°. Some of these satellite drops were reentrained while others fell down.

2. Some drops were reentrained inside the mesh, and the process of reentrainment could not be observed; it is assumed to be the same as described in the earlier part of the first method.

3. When the liquid load was high, partial flooding was observed. Reentrainment by methods 1 and 2 took place above the flooded zone. In the flooded section the air flow rate was low. The flooded section was partially covered by the falling drops from above on the downstream side of the mesh. The reentrainment mechanism was rupture of bubbles, but it could not be observed properly. Reentrainment by the above mechanisms was observed in runs 43 and 46.

Tube Bank

Overall Efficiency - Collection efficiency versus gas velocity data for horizontal flow through tube banks are plotted in Figures 7-31 through 7-33 for various inlet drop diameters. Penetration due to primary efficiency of less than 100% was observed for velocities lower than 3.0 m/sec.

Houghton and Radford's (1938) data for strut separators are also plotted in Figure 7-32. They found a constant collection efficiency of 96.2% for gas velocities from 1.25 to 17.5 m/sec. The inlet entrainment contained drops as small as 1 μm. However, no increase in penetration at lower velocities or reentrainment at higher velocities was observed. A comparison between the configuration used in the present study and that of Houghton and Radford is given in Table 7-4.

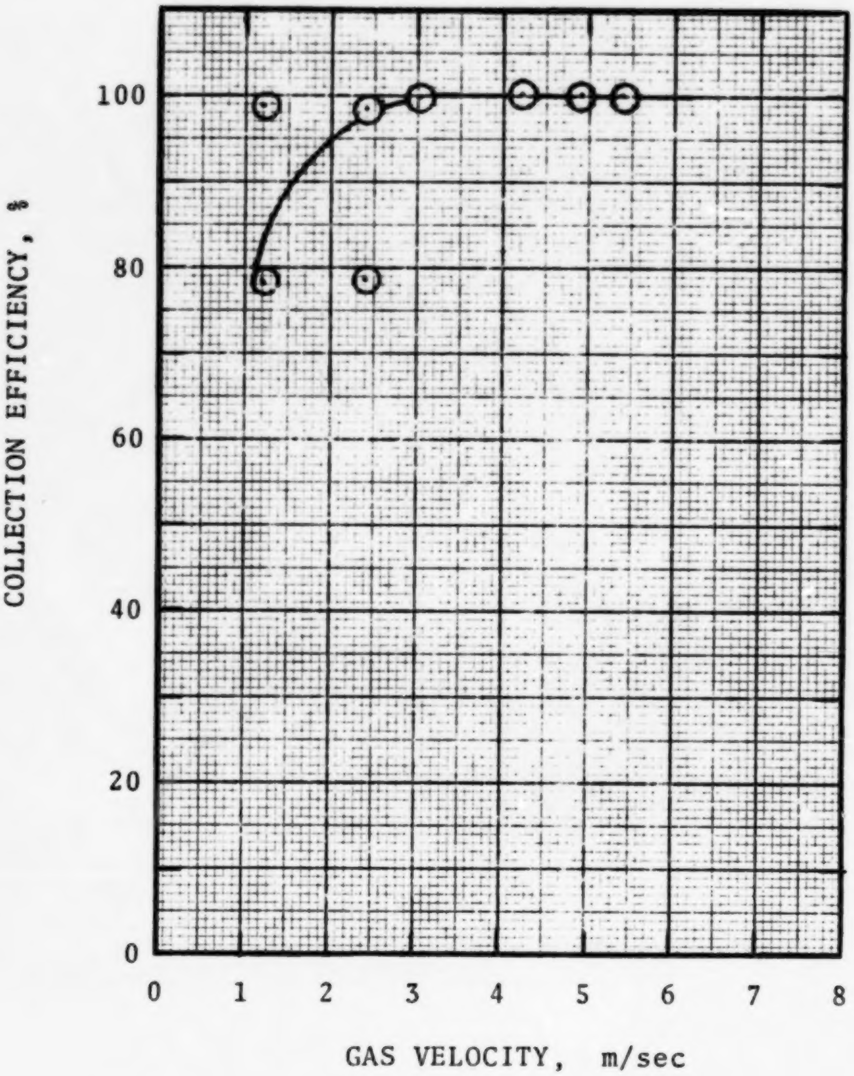

Figure 7-31 - Collection efficiency versus gas velocity in tube bank with $n = 6$, $d_{pg} = 84\ \mu m$ and $\sigma_g = 1.32$.

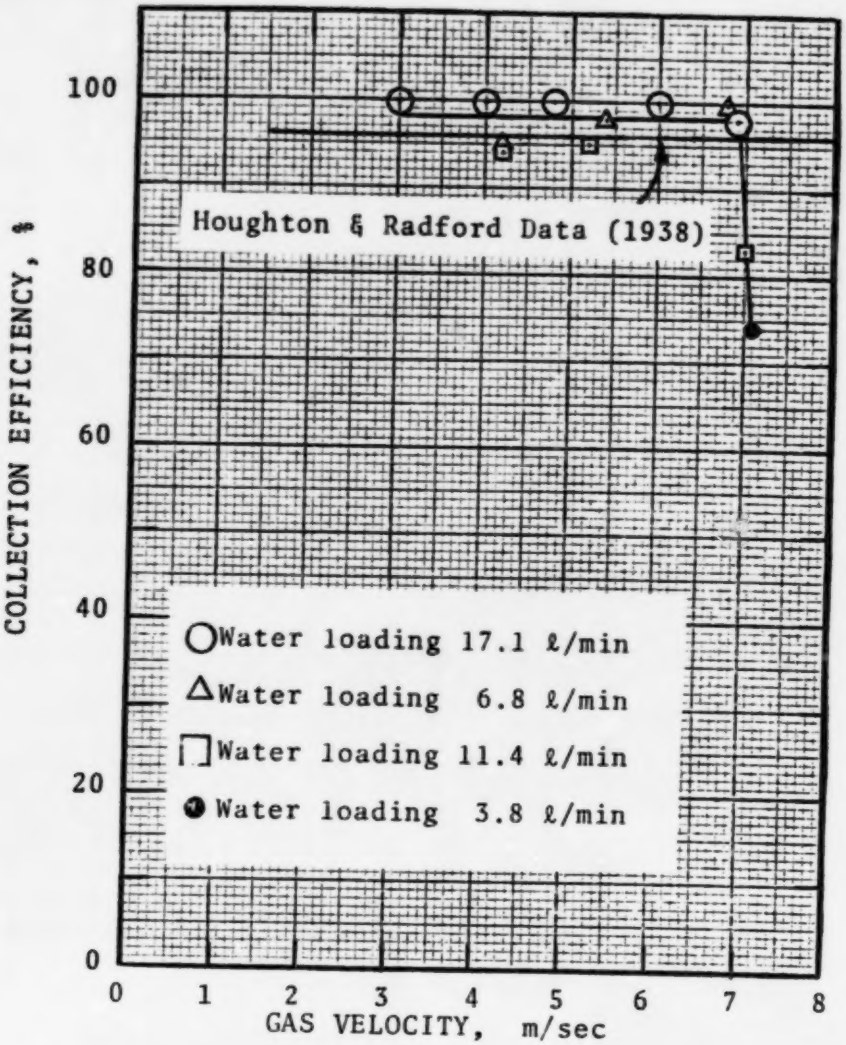

Figure 7-32 - Collection efficiency versus gas velocity in tube bank with d_{pg} = 380 μm and σ_g = 1.5

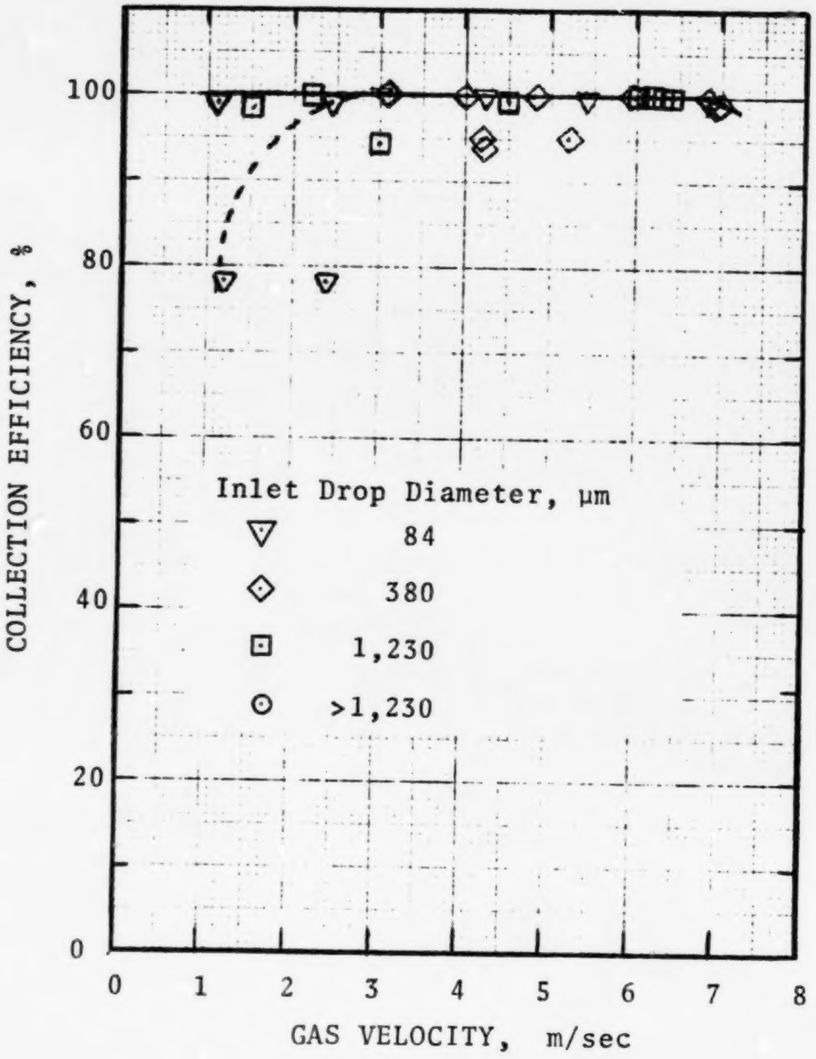

Figure 7-33 - Collection efficiency versus gas velocity in tube bank. Solid line represents theory.

Table 7-4. COMPARISON OF TUBE BANKS

	Present Study	Houghton & Radford (1938)
Tube (minor-major axis) diameter, cm	1.9	1.25x3.2
Spacing between tubes, center to center, cm	3.8	2.5
Spacing between rows, center to center, cm	3.3	5
Number of rows	6	6
Material of tubes	Al	

Pressure Drop - Dry and wet pressure drop through the tube bank is plotted in Figures 7-34 and 7-35. There is no effect of liquid load on the pressure drop; the slope of both curves is 2.33. Therefore the data may be correlated by the following equation:

$$\Delta P = 1.2.\text{x}10^{-5}\ n\ \rho_G\ v_G'^{2.33} \qquad (7\text{-}2)$$

where n = number of rows (6 in present experiments)
v_G' = actual gas velocity near the tubes

The actual gas velocity "v_G'" is twice the superficial gas velocity, which is shown on the horizontal axes of Figures 7-34 and 7-35. An average value of $1.17\text{x}10^{-3}$ g/cm^3 is used for "ρ_G".

Manufacturer's data (Union Carbide Corporation for M.V. separator) for banks of streamlined struts of 2.2 cm equivalent diameter gave the following empirical equation for pressure drop:

$$\Delta P = 2.33\text{x}10^{-6}\ n\ \rho_G\ v_G'^{2.19} \qquad (7\text{-}3)$$

A comparison of Equations (7-2) and (7-3) shows that the former equation gives 5-8 times higher pressure drops for cylindrical tubes with 1.8 cm equivalent diameter than for streamlined struts with larger equivalent diameter.

Grimison (1937) has presented friction factor as a function of tube bank configuration at various Reynolds numbers. For the configuration studied in the pilot plant, friction factor versus superficial gas velocity is plotted in Figure 7-36. Substituting the value of friction factor into the pressure drop relation results in:

$$\Delta P = 4.33\text{x}10^{-4}\ n\ \rho_G\ v_G'^{1.9} \qquad (7\text{-}4)$$

Equation (7-4) predicts pressure drop twice as high as that observed in the present study for v_G = 6.0 m/sec.

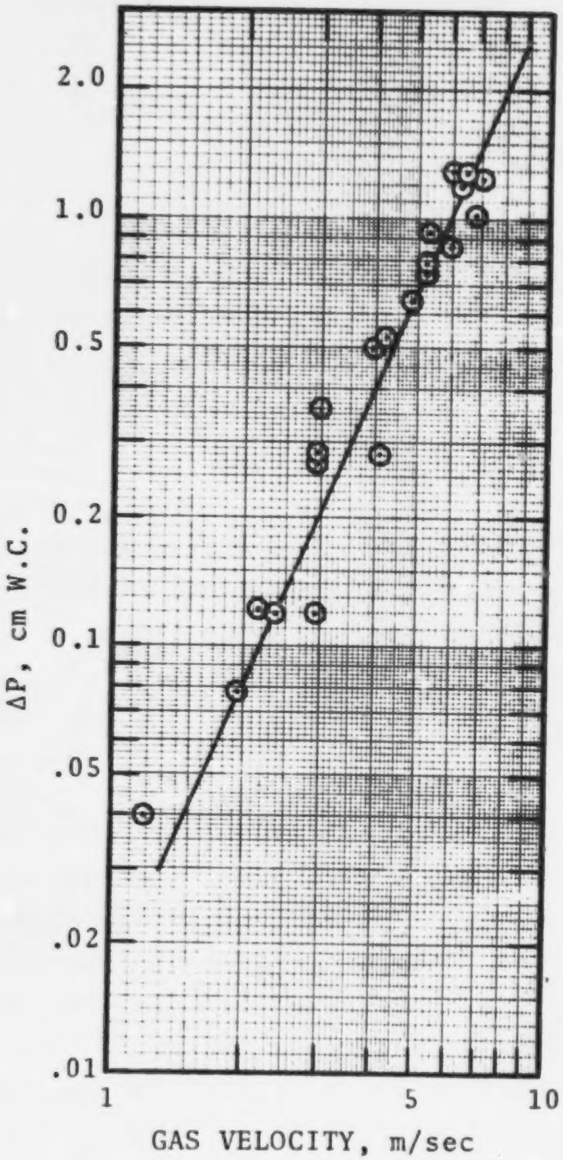

Figure 7-34 - Dry pressure drop in tube bank versus gas velocity

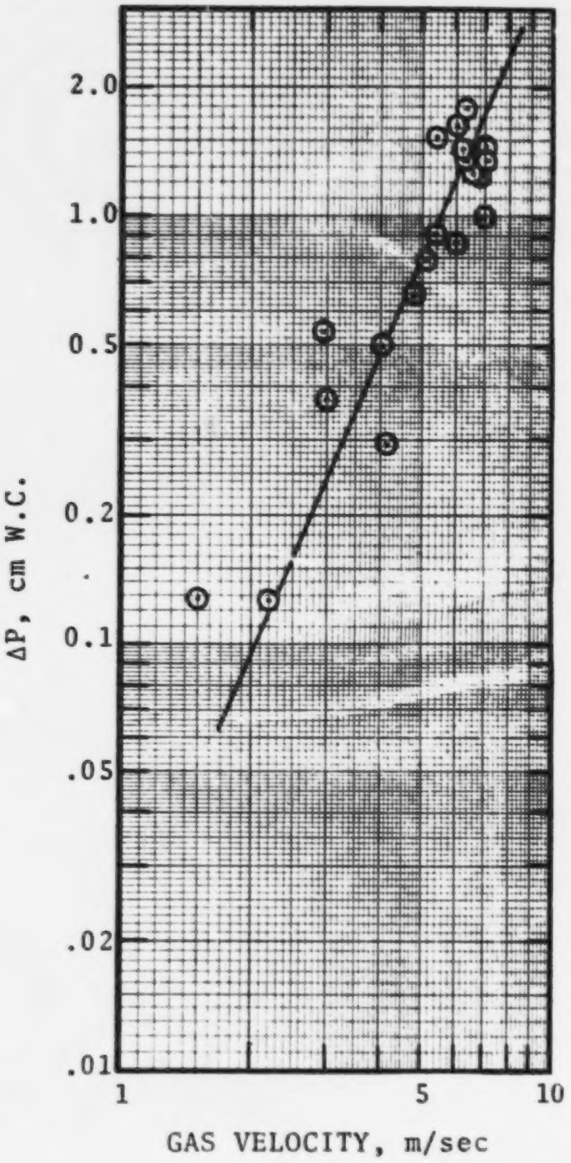

Figure 7-35 - Wet pressure drop in tube bank versus gas velocity

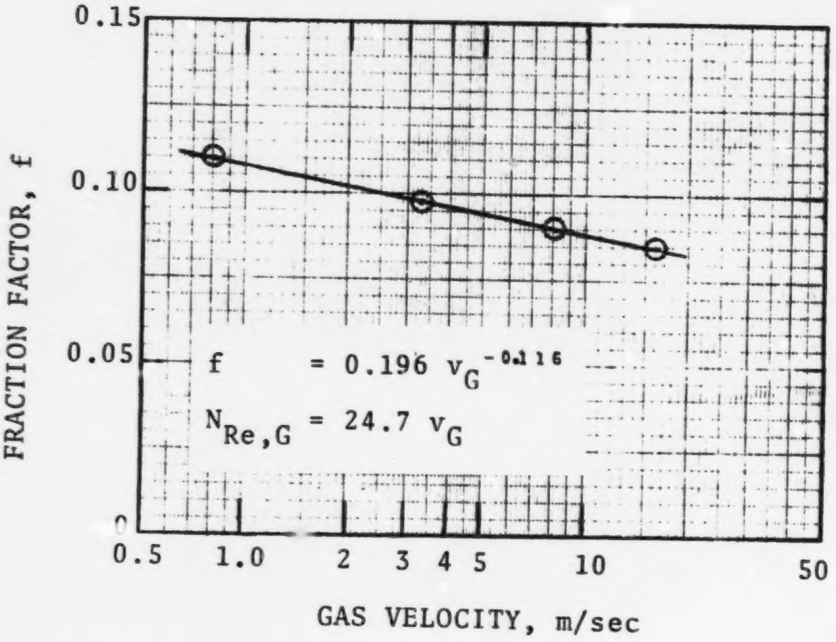

Figure 7-36 - Friction factor versus gas velocity in the bank of tubes

Reentrainment

Figures 7-37 and 7-38 reveal no definite relationship between gas velocity and outlet mass median drop diameter. However, the size distribution curves shown in Figure 7-39 are similar to those obtained from zigzag baffles in Figure 7-18. For both types of separators, a higher liquid flow rate caused smaller drops to be formed.

Figure 7-40 gives a similar relationship between geometric standard deviation and outlet mass median drop diameter as seen for each of the other three types of separators studied. The maximum outlet drop diameter rises with increasing gas velocity, according to Figure 7-41, to a peak of about 350 µm at 7.0 m/sec gas velocity. The minimum drop diameter at the outlet, on the other hand, ranged between 40 and 70 µm.

Figure 7-42 depicts the values of gas velocity and liquid load observed as being necessary for reentrainment. As in the case of zigzag baffles (Figure 7-21), the reentrainment region has an upper and lower gas velocity boundary for a given liquid load, whereas for the mesh (Figure 7-29) there is only a lower boundary.

GENERAL OBSERVATIONS

Pressure Drop

The pressure drop in the empty test section housing as a function of gas velocity is plotted in Figure 7-43. The housing for each separator studied thus far has the same dimension. When the pressure drop is less than 1 mm W.C., it is essentially negligible. Therefore, there is no significant pressure drop for a gas velocity less than about 5.0 m/sec.

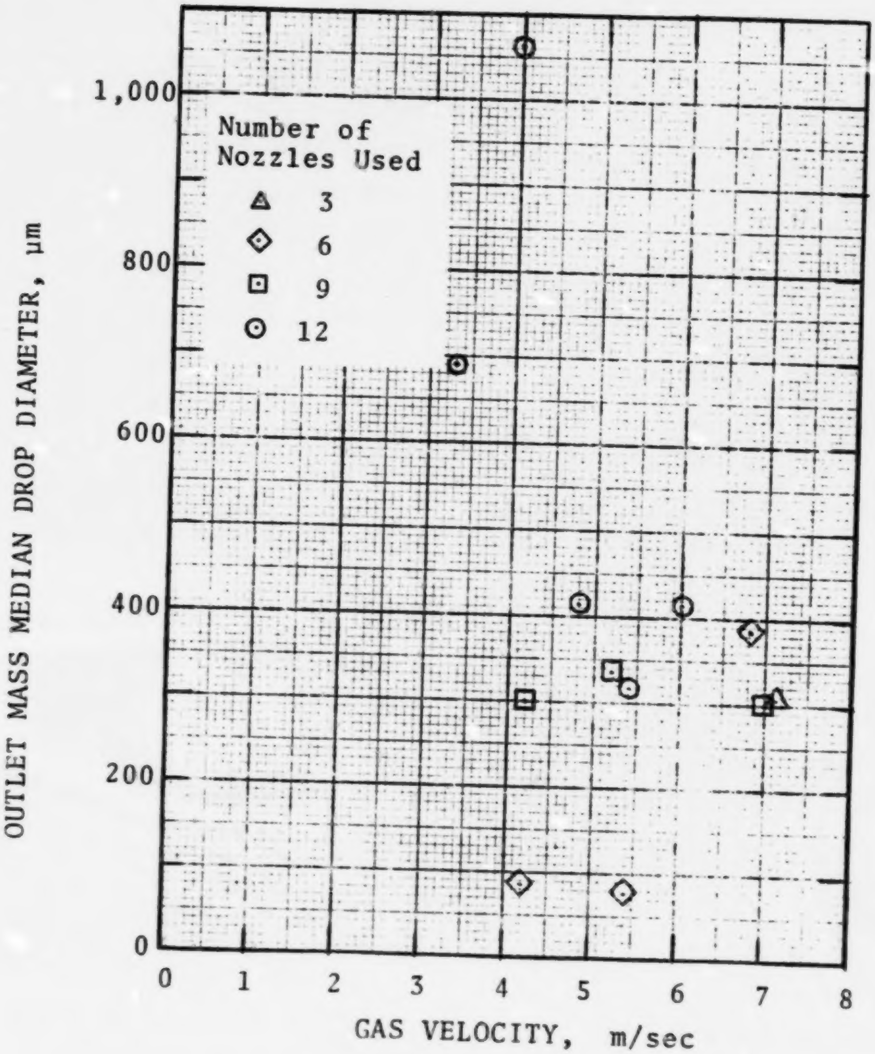

Figure 7-37 - Outlet drop diameter versus gas velocity for tube bank with 380 μm inlet drop diameter.

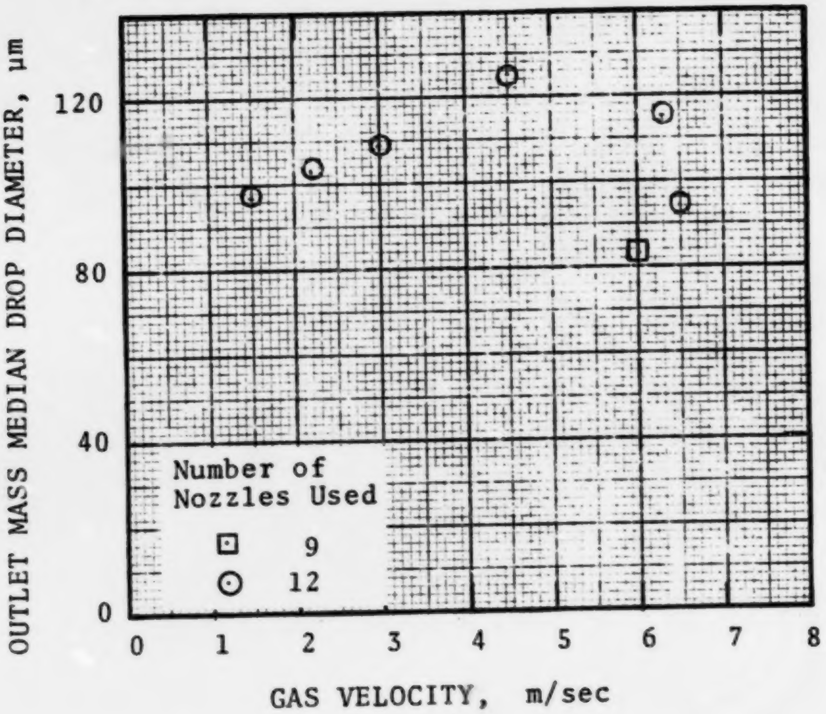

Figure 7-38 - Outlet drop diameter versus gas velocity for tube bank with 1,230 μm inlet drop diameter.

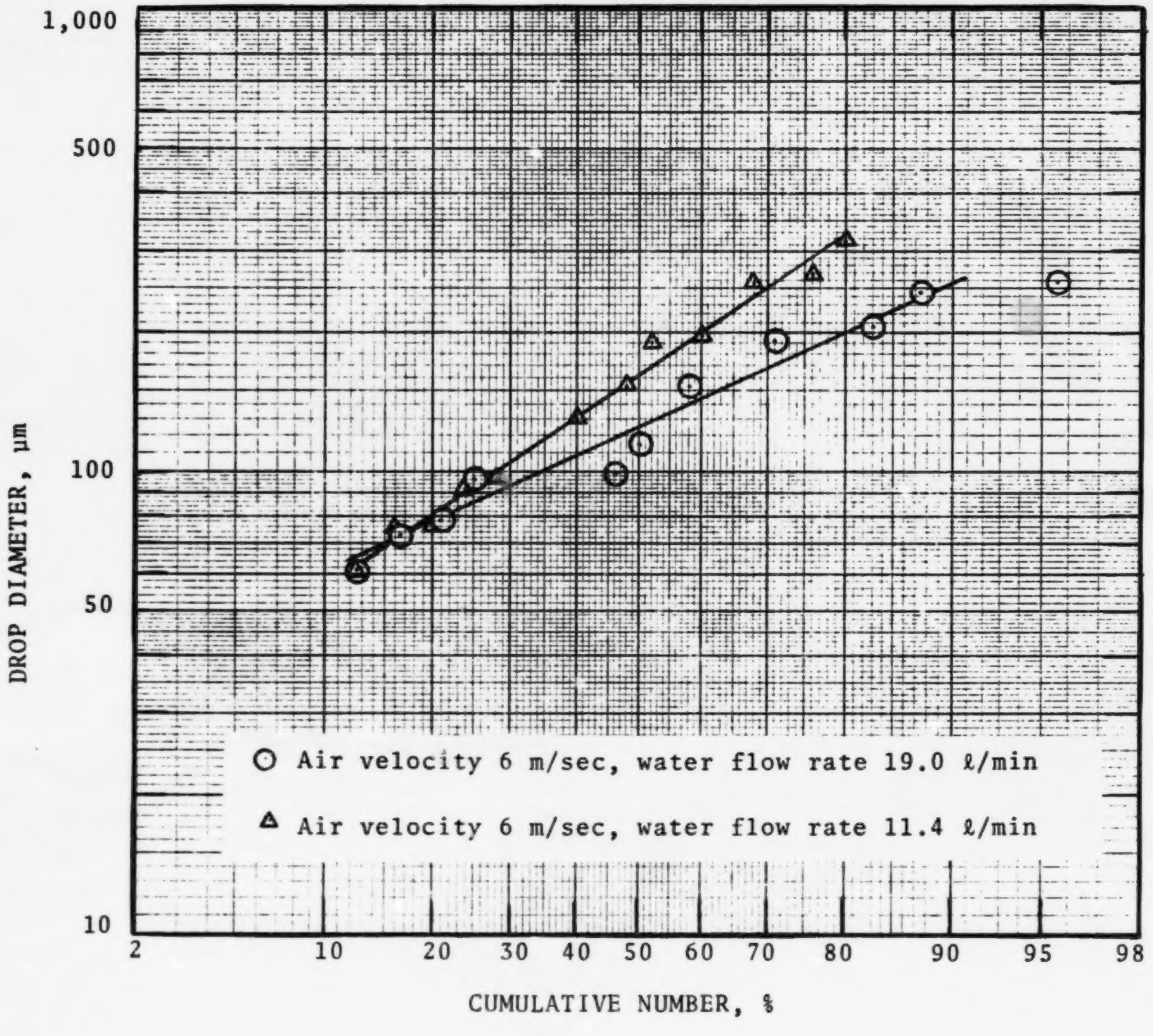

Figure 7-39 - Size distribution of drops leaving tube bank entrainment separators.

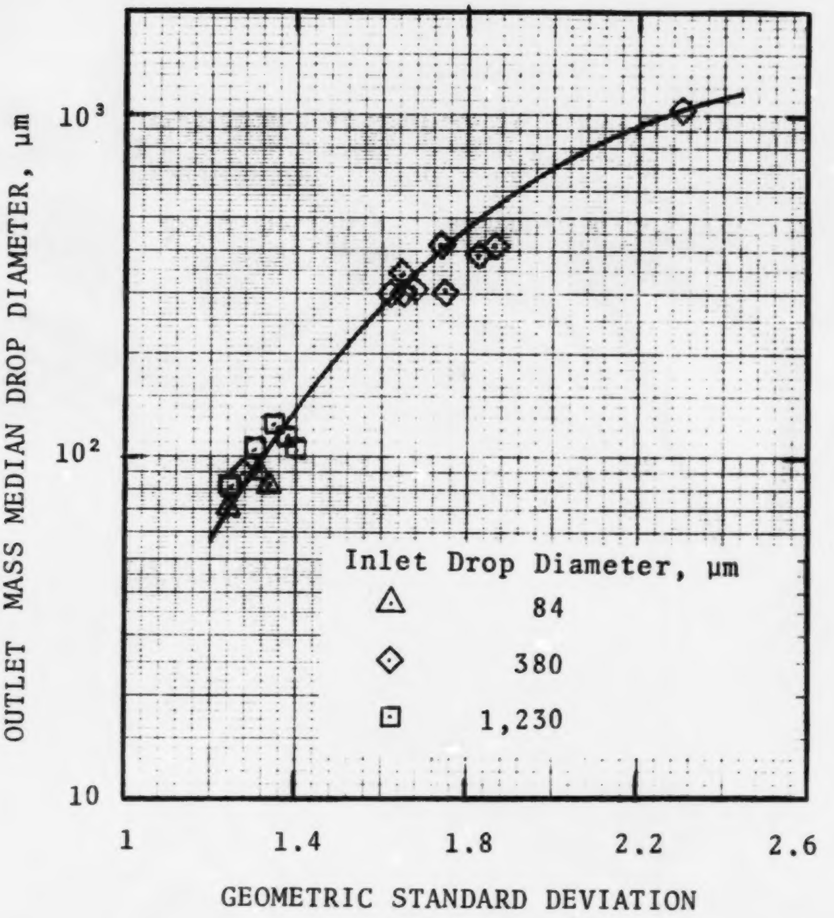

Figure 7-40 - Outlet mass median drop diameter versus geometric standard deviation for tube bank.

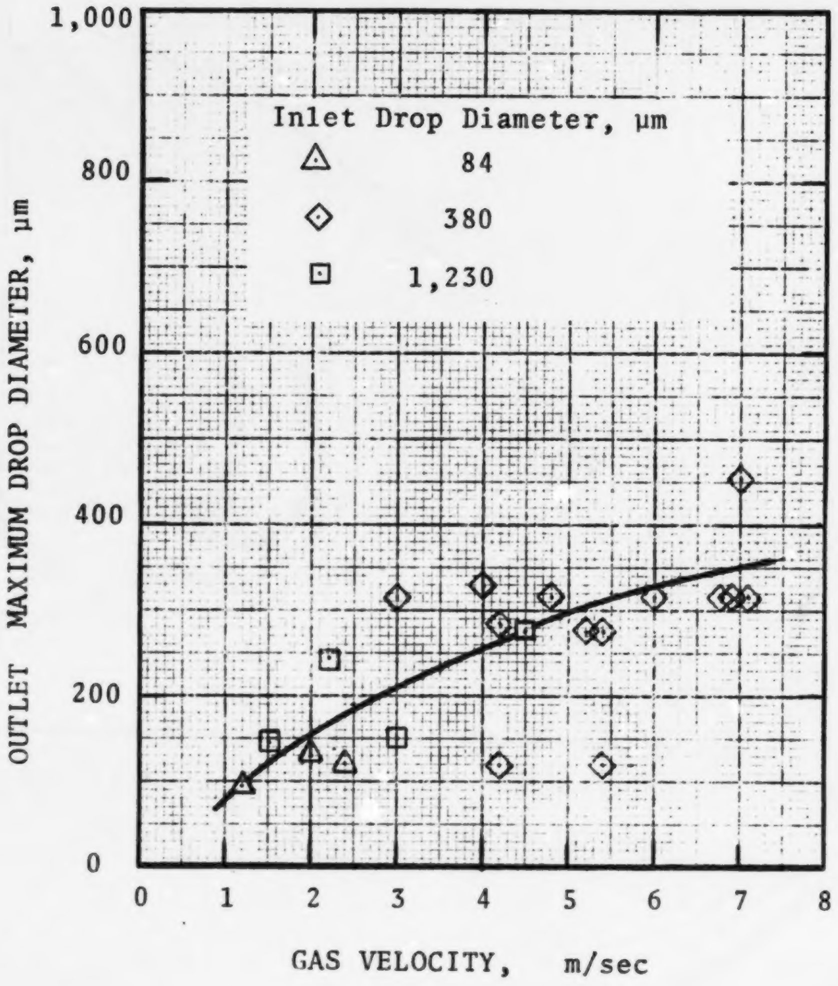

Figure 7-41 - Maximum drop diameter in the entrainment versus gas velocity for tube bank.

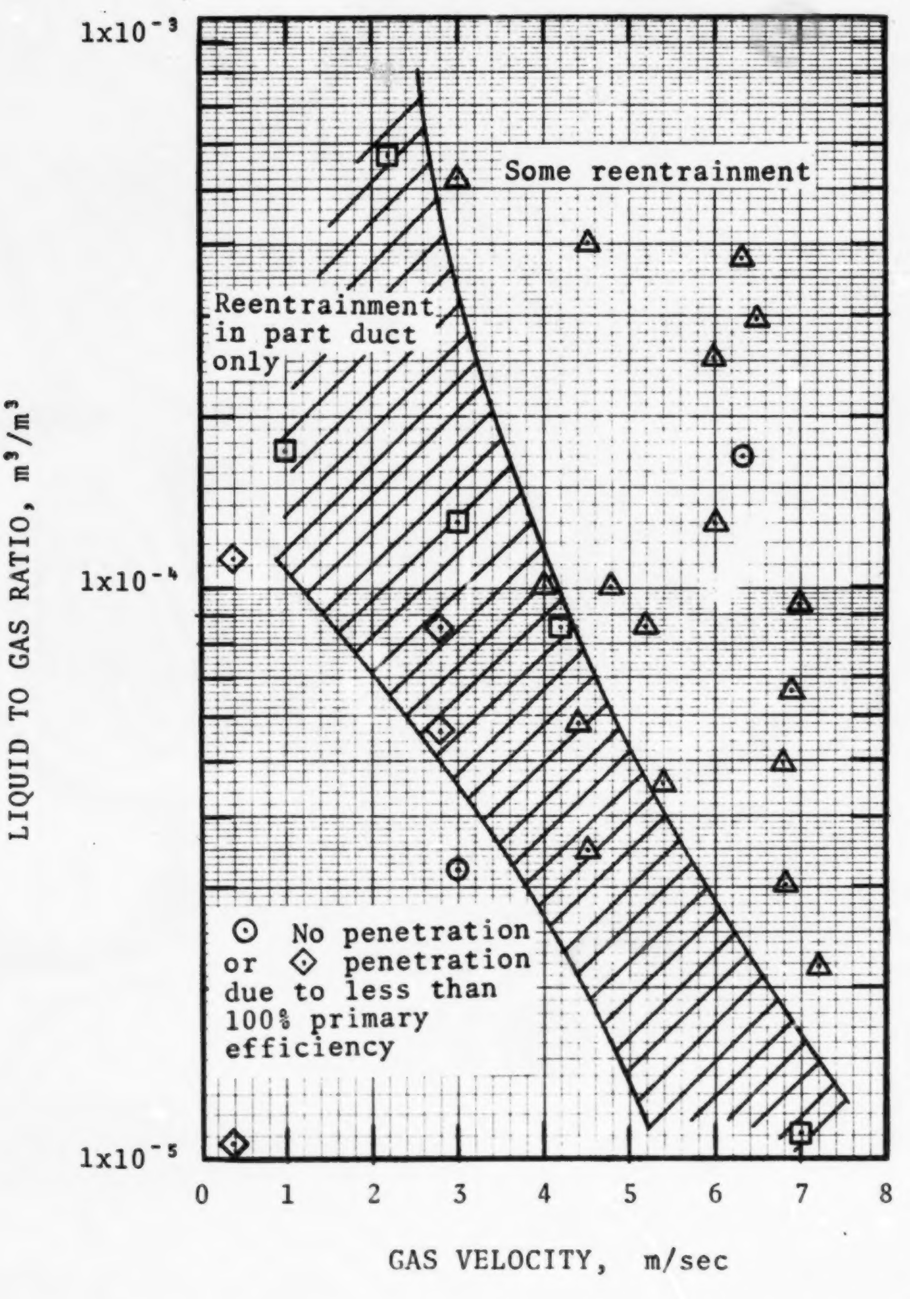

Figure 7-42 - Experimental results showing the effect of gas velocity and liquid load on performance of tube bank.

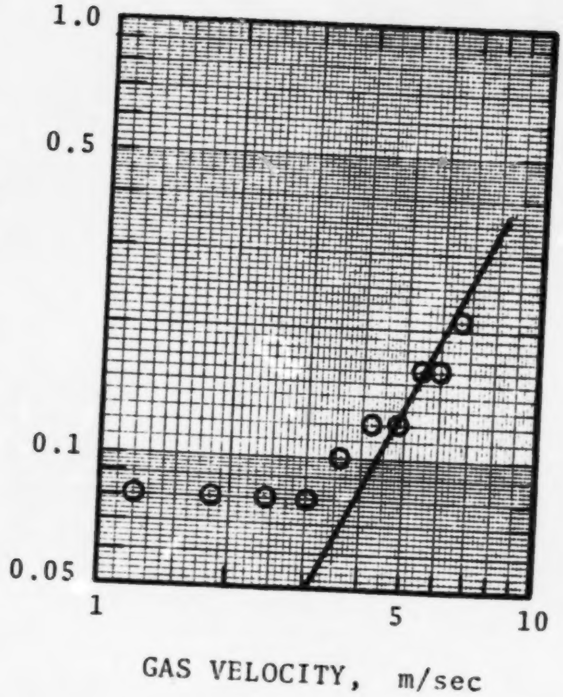

Figure 7-43 - Pressure drop in the empty section versus gas velocity

During the operation of the entrainment separator, the velocity distribution changes due to the presence of the separator. Thus, the wall effects measured by the above method may not represent the true wall effect. However, the presence of the separator does reduce the wall effect. Also, the pressure drop in the empty test section is 10-20% of the pressure drop with entrainment separator. Hence, the effect of the walls on the total pressure drop is small.

The dry pressure drop versus gas velocity relationships for different entrainment separators are shown in Figure 7-44. The packed bed is seen to have the greatest pressure drop. It should be noted that the efficiencies of different separators at a given velocity are not the same.

Bell and Strauss' pressure drop data for baffles are compared with present results for baffles and tubes in Figure 7-45. The high pressure drop found by Bell and Strauss can be explained by the variations in design, differences in "θ" and the distance between rows and the use of lips.

The pressure drop data of Houghton and Radford are compared with the present results in Figure 7-46. The results show good agreement. The small differences in the pressure drops may be explained as below.

The differences in the design are given in Tables 7-3, 7-4, and 7-5. The higher pressure drop in the baffle section obtained by Houghton and Radford may be due to lips on the fourth and fifth row of baffles and no spacing between the rows.

Houghton and Radford's pressure drop data in the tube section give comparable results at velocities lower than 500 cm/sec. At higher velocities the present study gives higher pressure drops, which may be due to smaller spacing between rows and to the use of tubes with circular cross-section rather than struts with streamlined cross-section.

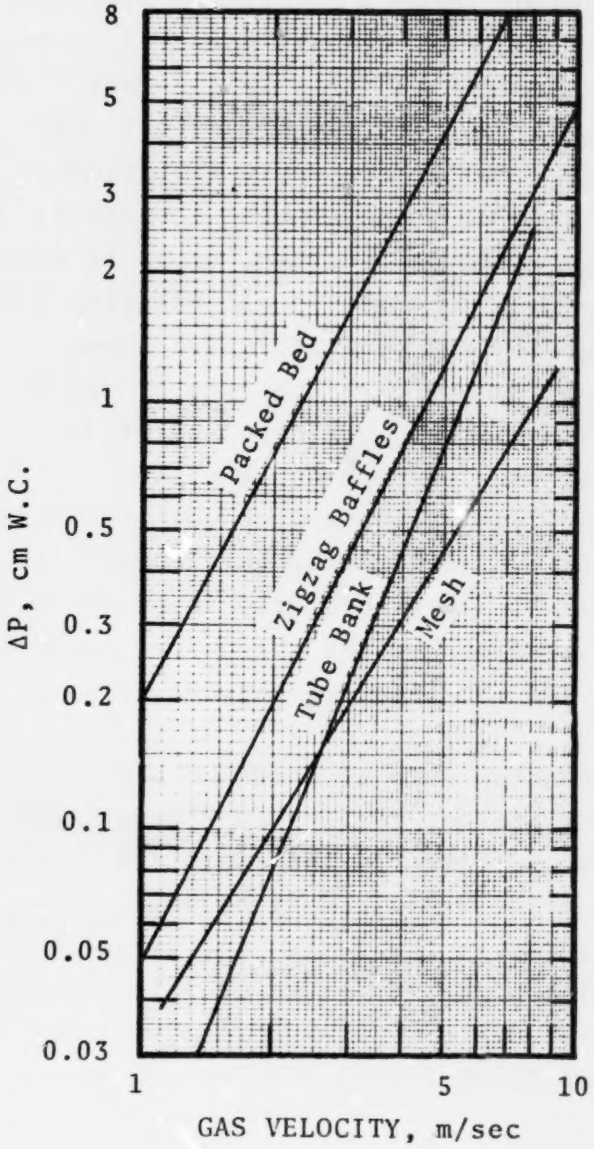

Figure 7-44 - Dry pressure drop versus gas velocity used in pilot plant

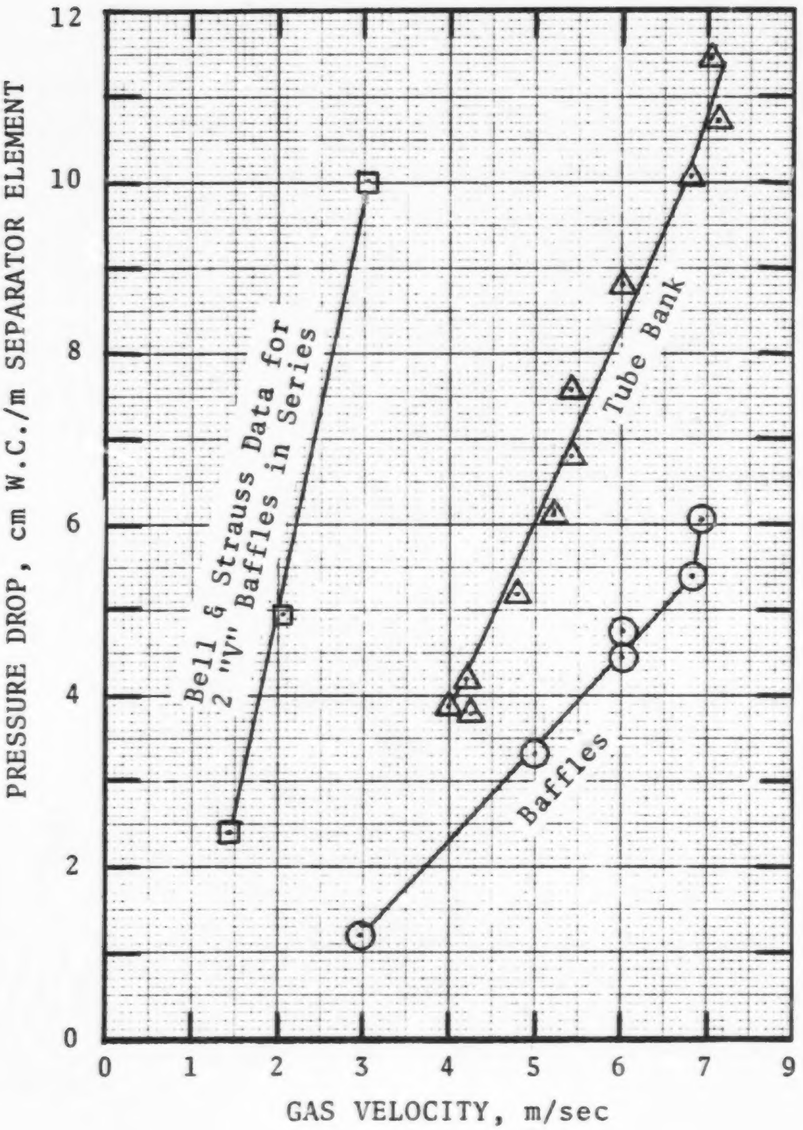

Figure 7-45 - Pressure drop through entrainment separator as a function of superficial gas velocity

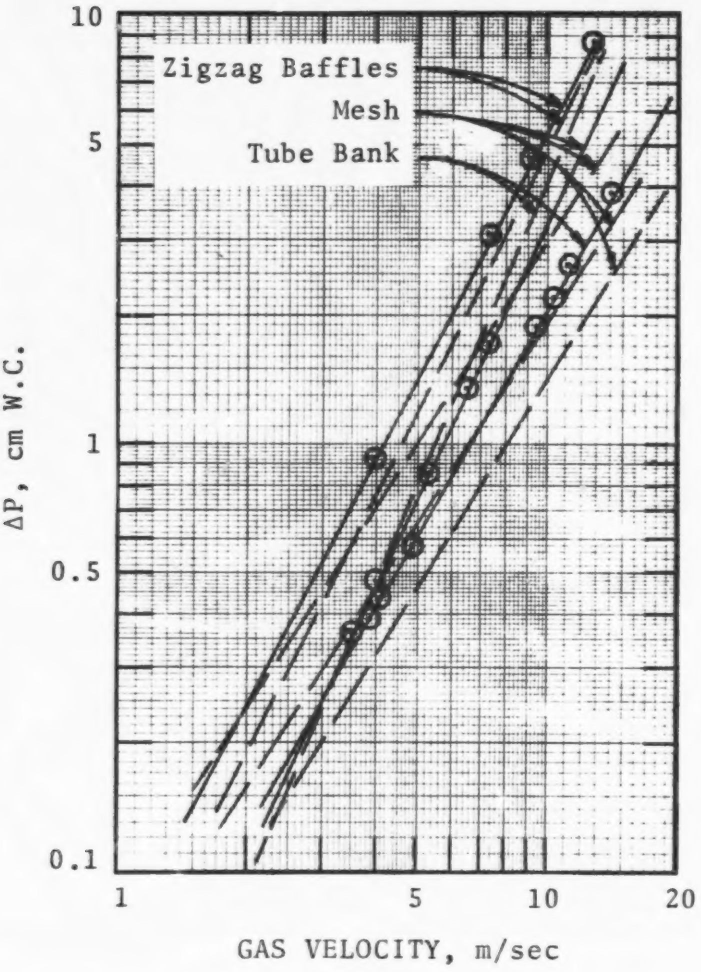

Figure 7-46 - Comparison of pressure drop data of Houghton & Radford (1938) with present results. The dashed lines represent the present results. The three curves for the mesh represent L/A = 0, $0 \leq L/A \leq 1$, $1 \leq L/A \leq 5$. Here, "L/A" is superficial liquid velocity, cm/min.

Table 7-5. COMPARISON OF WIRE MESH DEMISTER

	Present Results	Bell & Strauss (1973)	Houghton & Radford (1938)
Mesh Density, g/cm^3		0.16	
Void space	98.2		
Wire diameter, cm	0.028	0.025	
Bed length, cm	10	10	
Material	SS	SS	
Miscellaneous			Number 4 mesh layers kept 5 cm apart

Reentrainment

Entrainment in the outlet is due to less than 100% primary efficiency or reentrainment. In some runs at low gas velocity, 1.2-2.4 m/sec, entrainment occurred because primary efficiency was less than 100%. Increasing the gas velocity caused the entrainment to disappear in the outlet. Entrainment due to low primary efficiency occupied the entire cross-section of the duct and was observed in runs 5, 146, 147, and 152.

The mass median drop diameter of the reentrainment varied between 70 and 1,000 μm with a geometric standard deviation of 1.2 to 2.4. Some drops settled by gravity between the test section and the position downstream where drop diameters were measured. These measurements were taken at the estimated middle of the cross-section in which entrainment was present, resulting in a variation of the sampling point elevation. No correction for these two effects has been made in the analysis of drop diameters.

As noted earlier in this chapter, the mass median drop diameter increases with increase in geometric standard deviation. Thus the drop diameter distribution becomes broader as the median diameter increases. Similar results were obtained by Garner et al. (1954). They attribute large values of geometric standard deviation to reentrainment caused by shattering of drops. The resulting drops are larger than 200 μm with mass median diameter between 250 and 1,000 μm.

The effect of liquid feed rate on the typical outlet mass median drop diameter and on the reentrainment velocity for different separators is summarized in Table 7-6. The typical diameter and reentrainment velocity are both seen to rise as the liquid feed rate is decreased. Figures 7-38 and 7-39 confirm the data of Table 7-6 for baffles and tube

Table 7-6. EFFECT OF LIQUID LOAD ON REENTRAINMENT IN DIFFERENT ENTRAINMENT SEPARATORS.

Test Section	Typical Outlet Mass Median Diameter	Average Liquid Feed cm^3/sec	Reentrainment Velocity m/sec
Tube Bank	90 μm	4×10^2	1.5
Tube Bank	350 μm	2.7×10^2	3.5
Mesh	170 μm	4×10^2	1.8
Mesh	260 μm	1.5×10^2	4.5
Zigzag Baffles	700 μm	4×10^2	1.5
Zigzag Baffles	700 μm	2.7×10^2	3.0

banks, respectively. In the case of mesh, experimental data show that the mass median drop diameter increases with liquid load.

The minimum diameter of reentrainment for each type of separator is given in Table 7-7, which is a distillation of the data plotted in Figure 7-47. In a few experiments with baffles, the minimum size was as high as 190 µm. As shown in Figure 7-47, most data points lie between 40 and 80 µm.

Kotov (1972) has summarized reentrainment from various separators (Table 7-8). Reentrainment velocities in the present study were much higher than those obtained by Kotov. However, the experimental details of his work are not available, and it is difficult to make comparisons.

Table 7-7. OBSERVED MINIMUM DROP SIZE IN THE REENTRAINMENT

Separator	Minimum Drop Diameter μm
Baffles	50 - 80
Mesh	40 - 80
Packed Bed	40 - 60
Tube Bank	40 - 70

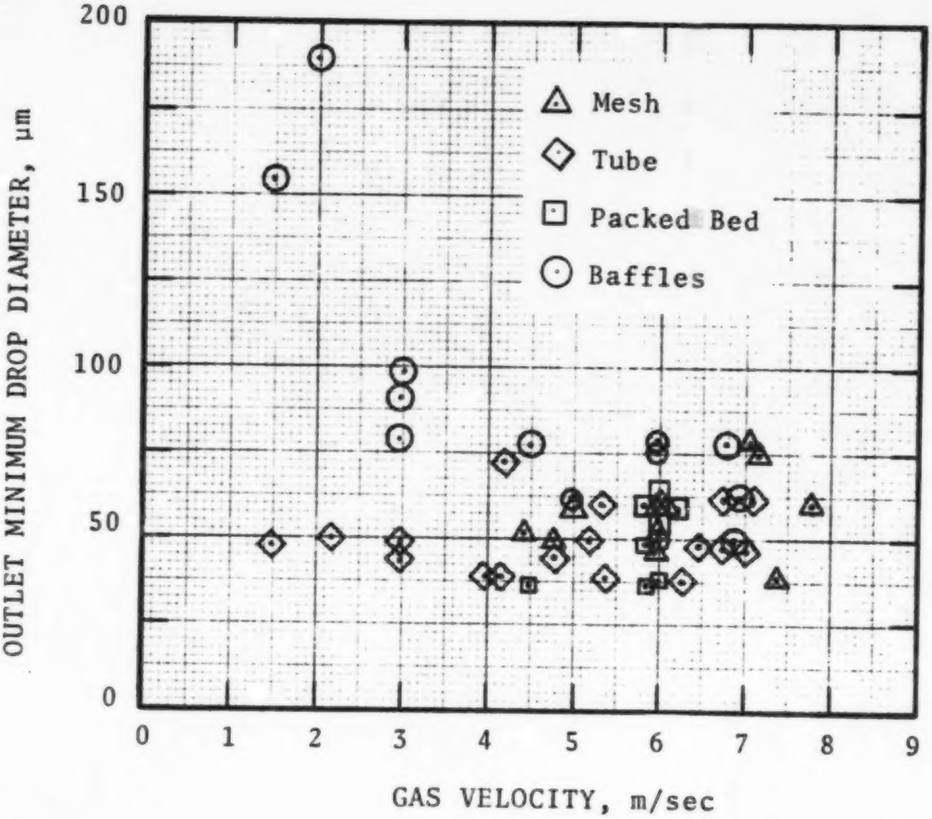

Figure 7-47 - Minimum outlet drop diameter versus gas velocity

Table 7-8. REENTRAINMENT OBSERVED BY KOTOV

Device or Mechanism	Liquid Load In Outlet m^3/m^3	Gas Velocity m/sec
Screen or Mesh	$0.4 - 0.8 \times 10^6$	>1.5
Ceramic Rings	$0.83 - 1.15 \times 10^6$	>1.5
Bubble Break Up	$0.7 - 8 \times 10^6$	<2.8
	$14 - 19 \times 10^6$	2.8 - 3.0

FUTURE RESEARCH AND DEVELOPMENT RECOMMENDATION

The primary objectives of the present research were to evaluate the available technology on wet scrubber entrainment separators, advance theoretical development and design a pilot scale entrainment separator based on the above information. It is also important to define the areas where additional work is needed. At this time, the present contract is in progress and the recommendations made in the following paragraphs are subject to modification as more is learned during the course of the research program.

REENTRAINMENT

One of the problems which present day entrainment separators suffer is their large size which is due to low operating velocities. The gas velocities are limited by reentrainment velocities and flooding conditions. Reentrainment may take place due to various mechanisms, depending on flow rates and geometry.

While the present program will provide information on the conditions under which reentrainment occurs in several separator configurations, it would be helpful to have more detailed knowledge of this phenomenon. It is quite possible that a fundamental study of the mechanisms of reentrainment from different geometric arrangements would enable one to develop more efficient separator designs. At least the results of such a study would delineate the limits of performance possible and save effort which might otherwise be expended in unprofitable directions.

The study needed is onset of reentrainment conditions, rate of reentrainment, equilibrium constant between entrainment and liquid in film, drop size distribution, smooth and shock type contact of gas and liquid, effect of duct dimensions, etc. The application to entrainment separator will include improving design methods to determine reentrainment under operating conditions, effect of higher gas velocities and improvements in design to reduce reentrainment.

SOLID DEPOSITION

Solids deposition and consequent plugging is a major operational problem in scrubber systems. It would be very helpful to have insight into the mechanism(s) by which suspended and dissolved solids deposit and the effects of operating and design parameters. Given a clearer picture of how solids deposit, it should be easier to conceive of and design for conditions which would minimize deposition.

It is probably unavoidable that some deposition will take place in a high efficiency entrainment separator. Therefore, means for removing deposits are required. Washing, either intermittently or continuously, is the most common method used and it has the undesirable feature of introducing liquid where it is not wanted. Research on methods of washing and flow rate required would be worth doing, with the objective of finding the optimum way to use the least liquid.

FIELD TESTING OF INDUSTRIAL ENTRAINMENT SEPARATORS

Performance data on industrial entrainment separators are generally not available. The industrial data are collected to evaluate the overall performance of the scrubber and it is assumed that the entrainment separators have 100% efficiency. Also, all the liquid introduced in the wet scrubber is assumed to be removed by entrainment separator. The effects of sedimentation, bends in the duct carrying entrainment, etc. are neglected. The distance between sampling point and entrainment separator elements is important. Also, the effects of industrial operating conditions on performance of entrainment separators should be determined.

The aim of development of entrainment separators is to improve performance of separators under industrial conditions. Thus, it is necessary to collect data on industrial separators. The data, when compared with theoretical models, will represent possible problems resulting from industrial conditions and will help in designing future entrainment separators.

DEMONSTRATION PLANT

From the present contract work, it is felt that we can determine the performance of an entrainment separator with reasonable accuracy. It is possible to obtain improvement in the performance due to better design. We would like to move from the present research and development to a demonstration of an improved design in the field. The capacity of the present pilot plant is 85 m^3/min. Therefore, the next size should be around 1,000 m^3/min (35,000 CFM).

The demonstration plant operation will involve selecting an organization which operates a suitable plant having entrainment separation problems and which is willing to participate in the demonstration plant program. The design effort will include obtaining the necessary data concerning the source of entrainment, preparing overall design and selecting a final design. The fabrication and start up will involve selection and negotiation with subcontractors, procurement of components and supervision of subcontractor efforts. The test program will be to determine performance, observe the effect of change in variables and compare the performance with theoretical developments.

TO STUDY COMBINATIONS OF ENTRAINMENT SEPARATORS

It seems that if more than one entrainment separator is used, the combined series unit will offer a synergistic effect. It is possible to combine two different entrainment separators to include the best features of each. Some examples are as follows:

1. The maximum gas velocity in the entrainment separator is limited to the onset of reentrainment velocity. It is generally the case, however, that a separator which has high primary drop collection efficiency will have a low reentrainment velocity, while one with high reentrainment velocity will have low primary collection efficiency. If a combined unit is used with the first unit being used for primary collection and coalescence of drops and the second one for collection of large drops while being below the onset of reentrainment velocity, increased capacity will result. The combination of efficiency and capacity will exceed what either unit can do alone.

Because the size of the entrainment separator will be smaller, the initial capital cost will be lower. The minimum drop size that can be separated in the entrainment separator is limited by the operating velocity. This problem can be solved by using a combination of entrainment separators.

2. Sometimes the entrainment load is high and constituted of particles in a wide size range. A single entrainment separator may be inefficient, flooded or may present reentrainment in this situation. A combined unit may be used in this case. The first separator is a precleaner with low pressure drop, which removes large particles constituting a significant fraction of the entrainment. The second separator will be an efficient device.

Table A-1. OVERALL PERFORMANCE OF ENTRAINMENT SEPARATOR

Exp. No.	Test Section	Air Velocity m/sec	Liquid to Gas Ratio m^3/m^3	Median Drop Diameter μm	Collection Efficiency %	Pressure Drop cm W.C.	Reentrainment Present in Observation Section
1	Baffle	4.8	3.4×10^{-5}	97	≈100	1.7	-
2	Baffle	3.2	2.97×10^{-5}	94	≈100	0.41	-
3	Baffle	6.1	5.65×10^{-5}	97	≈100	3.3	-
4	Baffle	2.4	4.66×10^{-5}	102	≈100	0.41	-
5	Baffle	1.8	4.95×10^{-5}	93.6	N.A.	0.12	-
6	Baffle	1.2	9.14×10^{-5}	87	69.2	0.12	-
8	Baffle	4.9	1.213×10^{-4}	79	≈100	1.5	-
9	Tubes	5.4	1.133×10^{-4}	76	≈100	0.82	-
11	Tubes	4.2	N.A.		≈100	0.29	-
12	Tubes	3.0	3.224×10^{-5}	84	≈100	0.16	-
13	Tubes	2.0	N.A.	83	N.A.	0.08	-
14	Tubes	2.4	5.609×10^{-5}	82	78.8	0.12	-
15	Tubes	1.2	1.122×10^{-4}	78	78.6	0	-
17	Tubes	6.3	1.676×10^{-4}	1225	≈100	1.3	-
18	Tubes	6.4	N.A.	1225	≈100	1.4	-
19	Tubes	6.2	3.06×10^{-4}	1225	100	1.5	-
20	Mesh	6.1	1.36×10^{-4}	1225	94	2.2	-
21	Mesh	4.4	1.83×10^{-4}	1225	N.A.	1.3	-
22	Mesh	3.0	2.1×10^{-4}	1225	>99.9	0.62	-
23	Mesh	2.4	2.5×10^{-4}	1225	>99.9	0.54	-

Table A-1. OVERALL PERFORMANCE OF ENTRAINMENT SEPARATOR (continued)

Exp. No.	Test Section	Air Velocity m/sec	Liquid to Gas Ratio m^3/m^3	Median Drop Diameter μm	Collection Efficiency %	Pressure Drop cm W.C.	Reentrainment Present in Observation Section
24	Mesh	1.8	2.72×10^{-4}	1225	>99.9	0.21	-
25	Mesh	2.4	2.37×10^{-4}	1225	N.A.	0.45	-
26	Mesh	.2	3.87×10^{-4}	1225	100	0.21	-
27	Mesh	1.2	7.46×10^{-4}	1225	100	0.29	-
28	Mesh	2.4	4.55×10^{-4}	1225	90.3	0.54	-
29	Mesh	3.2	3.57×10^{-4}	1225	87.8	0.78	-
30	Tubes	6.0	2.53×10^{-4}	1225	N.A.	1.6	-
31	Tubes	6.3	3.78×10^{-4}	1225	91	1.8	-
32	Tubes	6.5	2.936×10^{-4}	1225	87.8	1.3	Some
33	Tubes	4.5	4.026×10^{-4}	1225	90.0	N.A.	-
34	Tubes	3.0	5.224×10^{-4}	1225	94.4	0.37	Yes
35	Tubes	1.5	1.733×10^{-3}	1225	98.2	0.12	-
36	Tubes	2.2	5.661×10^{-4}	1225	99.8	0.12	-
37	Tubes	3.0	1.297×10^{-4}	380	100	0.54	-
38	Tubes	6.9	6.636×10^{-5}	380	98.7	1.03	-
		4.5					
40	Mesh	1.5	2.579×10^{-5}	84	94.3	0.620	-
41	Mesh	7.1	1.403×10^{-5}	84	100	0.084	-
43	Mesh	3.0	9.48×10^{-6}	84	97.7	1.36	Yes
45	Mesh	6.9	5.685×10^{-5}	84	50	0.29	-
46	Mesh		2.577×10^{-5}	84	91.8		-

Table A-1. OVERALL PERFORMANCE OF ENTRAINMENT SEPARATOR (continued)

Exp. No.	Test Section	Air Velocity m/sec	Liquid to Gas Ratio m^3/m^3	Median Drop Diameter μm	Collection Efficiency %	Pressure Drop cm W.C.	Reentrainment Present in Observation Section
47	Mesh	4.8	4.21×10^{-5}	84	64.8	0.87	-
48	Mesh	6.0	3.532×10^{-5}	84	63.1	1.3	Yes
49	Mesh	5.0	2.448×10^{-5}	84	80.8	0.87	Yes
50	Tubes	6.0	1.317×10^{-4}	380	100	0.87	Some
51	Tubes	5.4	N.A.	380	N.A.	0.87	
52	Tubes	4.8	9.782×10^{-5}	380	100	0.66	Very little
53	Tubes	4.0	1.0127×10^{-4}	380	100	0.55	Some
54	Tubes	7.0	9.374×10^{-5}	380	83.2	1.5	-
55	Tubes	4.2	8.445×10^{-5}	380	93.7	0.5	-
56	Tubes	5.2	8.442×10^{-5}	380	95.1	0.79	Some
58	Tubes	6.8	4.859×10^{-5}	380	100	1.3	-
59	Tubes	4.2	5.739×10^{-5}	380	94.94	0.54	-
60	Tubes	5.4	4.552×10^{-5}	380	98.6	0.91	-
61	Tubes	7.1	2.171×10^{-5}	380	74.6	1.36	Yes
63	Mesh	7.4	8.38×10^{-4}	84	61.5	1.6	Yes
64	Mesh	6.0	8.23×10^{-4}	84	57.6	1.1	-
65	Mesh	7.8	2.34×10^{-5}	84	100	1.9	Some
66	Mesh	6.0	3.442×10^{-5}	84	73.22	1.3	Yes
67	Mesh	4.5	4.616×10^{-5}	84		0.78	
69	Mesh	6.0	8.354×10^{-5}	84	100	1.0	Some

Table A-1. OVERALL PERFORMANCE OF ENTRAINMENT SEPARATOR (continued)

Exp. No.	Test Section	Air Velocity m/sec	Liquid to Gas Ratio m^3/m^3	Median Drop Diameter μm	Collection Efficiency %	Pressure Drop cm W.C.	Reentrainment Present in Observation Section
70	Mesh	4.5	5.383×10^{-5}	380	100	0.54	Slight
71	36" Pall	5.0	6.607×10^{-5}	380	100	8.9	No
73	36" Pall	4.9	2.950×10^{-4}	380	100	9.3	No
74	36" Pall	1.0	4.588×10^{-4}	1,225	100	0.37	No
75	36" Pall	5.0	1.131×10^{-3}	1,225	90.8	4.2	No
76	36" Pall	4.9	1.553×10^{-3}	-	100	9.5	No
77	Baffle	6.9	6.873×10^{-5}	-	80	3.2	Yes
78	Baffle	6.0	4.733×10^{-5}	380	97.7	2.5	Some
79	Baffle	5.0	7.005×10^{-5}	380	100	1.8	Very little
80	Baffle	6.0	5.849×10^{-5}	380	100	2.4	-
81	Baffle	6.8	6.297×10^{-5}	380	77.9	2.9	Yes
82	Baffle	3.0	7.850×10^{-5}	380	100	0.5	Little
83	Baffle	3.0	4.351×10^{-4}	380	100	0.5	Little
84	Baffle	7.0	2.330×10^{-4}	1,225	100	3.0	Some
85	Baffle	6.0	2.393×10^{-4}	1,225	100	2.2	Some
86	Baffle	1.5	5.384×10^{-4}	1,225	100	0.45	Little
88	Baffle	7.0	1.602×10^{-4}	1,225	100	2.9	Little
89	Baffle	6.0	1.718×10^{-4}	1,225	100	2.0	Little
90	Baffle	4.5	2.784×10^{-4}	1,225	100	1.2	Some
91	Baffle	3.0	3.501×10^{-4}	1,225	100	0.45	-

Table A-1. OVERALL PERFORMANCE OF ENTRAINMENT SEPARATOR (continued)

Exp. No.	Test Section	Air Velocity m/sec	Liquid to Gas Ratio m^3/m^3	Median Drop Diameter µm	Collection Efficiency %	Pressure Drop cm W.C.	Reentrainment Present in Observation Section
92	Baffle	2.0	4.281×10^{-4}	1,225	100	0.25	-
93	Baffle	1.0	6.913×10^{-4}	1,225	100	0.33	-
94	Baffle	7.1	8.008×10^{-4}	1,225	100	2.6	Yes
95	12" Pall	5.8	9.672×10^{-4}	-	100	N.A.	Slight
97	12" Pall	2.0	2.038×10^{-3}	-	100	0.54	No
98	12" Pall	1.0	3.233×10^{-3}		100	0.12	No
99	12" Pall	5.9	1.310×10^{-3}		100	7.6	-
100	12" Pall	4.5	1.689×10^{-3}		100	5.0	-
101	1' Pall Rings	2.0	2.48×10^{-3}	-	100	0.45	No
102	"	1.0	3.86×10^{-3}	-	100	0.17	No
103	"	1.0	6.56×10^{-5}	84	100	0.21	No
104	"	6.0	2.28×10^{-5}	84	88.7	6.5	Slight
105	"	3.5	4.33×10^{-5}	84	100	2.2	No
106	"	6.0	5.16×10^{-5}	84	100	6.5	No
107	"	3.5	1.37×10^{-4}	84	100	2.3	No
108	"	6.0	2.76×10^{-5}	84	100	6.6	No
109	"	6.0	1.15×10^{-4}	380	93.7	6.5	Some
110	"	4.5	5.21×10^{-5}	380	100	3.7	No
111	"	6.0	2.88×10^{-4}	1,225	N.A.	6.6	Some
112	"	4.5	3.53×10^{-4}	1,225	100	4.2	No

Table A-1. OVERALL PERFORMANCE OF ENTRAINMENT SEPARATOR (continued)

Exp. No.	Test Section	Air Velocity m/sec	Liquid to Gas Ratio m^3/m^3	Median Drop Diameter μm	Collection Efficiency %	Pressure Drop cm W.C.	Reentrainment Present in Observation Section
113	1' Pall Rings	6.0	2.85×10^{-4}	1,225	N.A.	6.7	Some
114	"	6.0	2.20×10^{-4}	1,225	N.A.	6.6	Some
115	"	6.0	2.07×10^{-4}	1,225	N.A.	6.7	Some
116	"	6.0	2.60×10^{-4}	1,225	N.A.	7.1	
117	"	4.5	3.47×10^{-4}	1,225	100	4.3	
118	"	6.0	2.58×10^{-5}	84	100	6.4	
119	"	3.5	4.12×10^{-5}	84	100	2.60	
120	"	6.0	1.67×10^{-5}	84	100	7.3	
121	"	3.5	1.74×10^{-4}	84	100	2.5	
122	"	6.0	2.75×10^{-5}	84	100	4.5	
123	Mesh	7.2	8.03×10^{-5}	84	88.7	1.9	
124	"	4.5	4.06×10^{-5}	84	100	0.87	
125	"	1.0	4.67×10^{-5}	84	100	0.04	
126	"	3.0	4.55×10^{-5}	84	100	0.29	
127	"	7.0	2.48×10^{-5}	84	87.6	1.9	
128	"	6.0	3.00×10^{-5}	84	79.1	1.4	
130	"	3.5	5.87×10^{-5}	84	100	0.45	
131	"	2.0	8.81×10^{-5}	84	100	0.12	
132	"	3.0	1.920×10^{-4}	1,225	100	0.54	
133	"	7.2	2.794×10^{-4}	1,225	100	1.9	

Table A-1. OVERALL PERFORMANCE OF ENTRAINMENT SEPARATOR (continued)

Exp. No.	Test Section	Air Velocity m/sec	Liquid to Gas Ratio m^3/m^3	Median Drop Diameter μm	Collection Efficiency %	Pressure Drop cm W.C.	Reentrainment Present in Observation Section
134	Mesh	5.0	3.390×10^{-4}	1,225	100	1.5	
135	"	6.6	2.861×10^{-4}	1,225	100	2.5	
136	"	6.8	2.73×10^{-4}	1,225	100	2.5	
137	"	6.8	8.31×10^{-4}	-	100	2.9	
138	"	6.8	8.34×10^{-4}	-	100	2.8	
140	"	2.4	5.62×10^{-5}	380	100	0.27	
141	"	3.2	2.23×10^{-4}	1,225	100	0.62	
142	"	6.0	4.606×10^{-5}	84	100	1.5	
143	"	5.0	5.836×10^{-5}	84	100	0.95	
145	"	7.0	4.96×10^{-5}	84	99	1.6	
146	Tubes	1.2	1.006×10^{-4}	84	99.5	0.04	
147	"	2.4	8.634×10^{-5}	84	99.2	0.21	
148	"	7.0	1.099×10^{-5}	380	99.5	1.5	
149	"	6.4	3.022×10^{-4}	1,225	100	1.20	
150	"	4.5	3.471×10^{-5}	1,225	99.8	0.79	
151	Baffle	6.8	6.807×10^{-5}	380	99.8	2.8	
152	"	1.2	6.627×10^{-5}	84	99.7	0.08	
153	Packed Bed 12"	6.0	4.277×10^{-5}	84	100	5.4	

Table A-2. DROP DIAMETERS OF THE ENTRAINMENT ENTERING AND LEAVING THE TEST SECTION

Exp. No.	Water Feed Rate cm³/sec	Water Pressure atm.(gauge)	Type & No. of nozzles	Inlet		Outlet	
				Median Drop Diameter um	Geometric Standard Deviation	Median Drop Diameter um	Geometric Standard Deviation
1	9.48×10^1	5.44	M6SS(12)	97	1.4	-	-
2	9.48×10^1	5.78	M6SS(12)	94	1.3	-	-
3	1.52×10^2	13.61	M6SS(12)	97	1.3	-	-
4	1.52×10^2	14.29	M6SS(12)	102	1.4	-	-
5	1.52×10^2	14.29	M6SS(12)	94	1.3	N.A.	N.A.
6	1.52×10^2	14.97	M6SS(12)	87	1.3	N.A.	N.A.
8	3.16×10^2	3.40	M26(12)	79	1.3	-	-
9	1.77×10^2	N.A.	M6SS(12)	76	1.3	-	-
11	1.64×10^2	N.A.	M6SS(12)	78	1.3	-	-
12	1.48×10^2	N.A.	M6SS(12)	84	1.3	-	-
13	1.26×10^2	N.A.	M6SS(12)	83	1.3	93	1.3
14	1.33×10^2	N.A.	M6SS(12)	82	1.3	86	1.3
15	1.33×10^2	N.A.	M6SS(12)	78	1.3	70	1.2
17	2.21×10^2	3.33	GG3(6)	1225	1.8	-	-
18	2.21×10^2	1.95	GG3(6)	1225	1.8	-	-
19	4.11×10^2	3.27	GG3(12)	1225	1.8	-	-
20	1.90×10^2	3.27	GG3(6)	1225	1.8	-	-
21	1.90×10^2	3.33	GG3(6)	1225	1.8	91	1.3
22	1.90×10^2	3.33	GG3(6)	1225	1.8	120	1.2
23	1.90×10^2	3.33	GG3(6)	1225	1.8	91	1.3

Table A-2. DROP DIAMETERS OF THE ENTRAINMENT ENTERING AND LEAVING THE TEST SECTION (continued)

Exp. No.	Water Feed Rate cm^3/sec	Water Pressure atm. (gauge)	Type & No. of nozzles	Inlet		Outlet	
				Median Drop Diameter µm	Geometric Standard Deviation	Median Drop Diameter µm	Geometric Standard Deviation
24	1.90x10^2	3.33	GG3(6)	1225	1.8	91	1.3
25	1.90x10^2	3.33	GG3(6)	1225	1.8	-	-
26	1.90x10^2	3.33	GG3(6)	1225	1.8	-	-
27	3.16x10^2	3.33	GG3(9)	1225	1.8	-	-
28	3.16x10^2	3.33	GG3(9)	1225	1.8	96	1.3
29	3.16x10^2	3.33	GG3(9)	1225	1.8	76	1.2
30	3.16x10^2	3.33	GG3(9)	1225	1.8	83	1.3
31	4.11x10^2	3.33	GG3(12)	1225	1.8	115	1.4
32	3.45x10^2	3.40	GG3(12)	1225	1.8	94	1.3
33	4.00x10^2	3.40	GG3(12)	1225	1.8	125	1.4
34	4.01x10^2	3.4	GG3(12)	1225	1.8	109	1.4
35	3.98x10^2	3.4	GG3(12)	1225	1.8	97	1.3
36	4.01x10^2	3.4	GG3(12)	1225	1.8	103	1.3
37	2.15x10^2	3.4	M26(12)	380	1.5	-	-
38	1.94x10^2	3.4	M26(12)	380	1.5	330	1.6
40	6.64x10^1	13.95	M6SS(6)	84	1.3	87.6	1.2
41	5.36x10^1	13.6	M6SS(6)	84	1.3	-	-
43	4.75x10^1	13.6	M6SS(6)	84	1.3	232	1.4
45	1.010x10^2	13.6	M6SS(12)	84	1.3	-	-
46	1.072x10^2	13.6	M6SS(12)	84	1.3	211	1.7

Table A-2. DROP DIAMETERS OF THE ENTRAINMENT ENTERING AND LEAVING THE TEST SECTION (continued)

Exp. No.	Water Feed Rate cm^3/sec	Water Pressure atm.(gauge)	Type & No. of nozzles	Inlet		Outlet	
				Median Drop Diameter μm	Geometric Standard Deviation	Median Drop Diameter μm	Geometric Standard Deviation
47	$1.074\text{x}10^2$	13.6	M6SS(12)	84	1.3	-	-
48	$9.736\text{x}10^1$	13.6	M6SS(12)	84	1.3	1377	2.3
49	$7.264\text{x}10^1$	13.6	M6SS(12)	84	1.3	123	1.4
50	$3.056\text{x}10^2$	3.40	M26(12)	380	1.5	414	1.7
51	$2.833\text{x}10^2$	3.40	M26(12)	380	1.5	317	1.7
52	$2.61\text{x}10^2$	3.40	M26(12)	380	1.5	413	1.8
53	$2.41\text{x}10^2$	3.40	M26(12)	380	1.5	1063	2.3
54	$1.914\text{x}10^2$	3.40	M26(9)	380	1.5	300	1.6
55	$1.714\text{x}10^2$	3.40	M26(9)	380	1.5	300	1.6
56	$1.78\text{x}10^2$	3.40	M26(9)	380	1.5	336	1.6
58	$1.267\text{x}10^2$	3.40	M26(6)	380	1.5	392	1.8
59	$1.161\text{x}10^2$	3.40	M26(6)	380	1.5	87	1.3
60	$1.069\text{x}10^2$	3.40	M26(6)	380	1.5	78	1.2
61	$5.472\text{x}10^1$	3.40	M26(3)	380	1.5	308	1.8
63	$3.79\text{x}10^1$	13.6	M6SS(3)	84	1.3	109	1.5
64	$3.79\text{x}10^1$	13.6	M6SS(3)	84	1.3	264	1.7
65	$1.105\text{x}10^2$	13.6	M6SS(9)	84	1.3	389	1.9
66	$1.105\text{x}10^2$	13.6	M6SS(9)	84	1.3	252	1.8
67	$1.074\text{x}10^2$	13.6	M6SS(9)	84	1.3	-	-
68	$2.595\text{x}10^2$	3.4	M26(12)	380	1.3	109	1.4

Table A-2. DROP DIAMETERS OF THE ENTRAINMENT ENTERING AND LEAVING THE TEST SECTION (continued)

Exp. No.	Water Feed Rate	Water Pressure	Type & No. of nozzles	Inlet		Outlet	
				Median Drop Diameter	Geometric Standard Deviation	Median Drop Diameter	Geometric Standard Deviation
	cm³/sec	atm. (gauge)		µm		µm	
69	2.333×10^2	3.40	M26(12)	380	1.5	115	1.4
70	2.198×10^2	3.40	M26(12)	380	1.5	-	-
71	2.164×10^2	3.40	M26(12)	380	1.5	-	-
73	3.881×10^2	3.40	1/8"GG3(12)	1,225	1.8	-	-
74	3.564×10^2	3.40	1/8"GG3(12)	1,225	1.8	-	-
75	1.079×10^3	3.06	small garden hose (1)	-	-	-	-
76	1.459×10^3	2.04	large garden hose (1)	-	-	-	-
77	1.165×10^2	3.40	M26(12)	380	1.5	1080	2.2
78	1.272×10^2	3.40	M26(9)	380	1.5	798	1.8
79	2.027×10^2	3.40	M26(12)	380	1.5	688	2.1
80	1.763×10^2	3.40	M26(12)	380	1.5	419	1.7
81	1.767×10^2	3.40	M26(12)	380	1.5	634	1.6
82	1.761×10^2	3.40	M26(12)	380	1.5	162	1.4
83	3.644×10^2	3.40	1/8"GG3(12)	1,225	1.8	714	1.6
84	3.594×10^2	3.40	1/8"GG3(12)	1,225	1.8	3025	2.4
85	3.439×10^2	3.40	1/8"GG3(12)	1,225	1.8	1060	1.9
86	3.442×10^2	3.40	1/8"GG3(12)	1,225	1.8	981	1.6
88	2.661×10^2	3.40	1/8"GG3(9)	1,225	1.8	614	1.7
89	2.567×10^2	3.40	1/8"GG3(9)	1,225	1.8	454	1.7
90	3.194×10^2	3.40	1/8"GG3(9)	1,225	1.8	511	1.7

Table A-2. DROP DIAMETERS OF THE ENTRAINMENT ENTERING AND LEAVING THE TEST SECTION (continued)

Exp. No.	Water Feed Rate cm³/sec	Water Pressure atm.(gauge)	Type & No. of nozzles	Inlet		Outlet	
				Median Drop Diameter µm	Geometric Standard Deviation	Median Drop Diameter µm	Geometric Standard Deviation
91	3.206×10^2	3.40	1/8"GG3(9)	1,225	1.8	795	1.8
92	3.192×10^2	3.40	1/8"GG3(9)	1,225	1.8	696	1.5
93	3.15×10^2	3.40	1/8"GG3(9)	1,225	1.8	N.A.	N.A.
94	1.086×10^3	3.12	small garden hose (1)			N.A.	N.A.
95	1.069×10^3	3.20	small garden hose (1)			95	1.3
97	1.077×10^3	3.20	small garden hose (1)			-	-
98	1.078×10^3	3.20	small garden hose (1)			-	-
99	1.454×10^3	2.04	Large garden hose (1)			88	1.3
100	1.453×10^3	2.04	Large garden hose (1)			-	-

Table A-2. DROP DIAMETERS OF THE ENTRAINMENT ENTERING AND LEAVING THE TEST SECTION (continued)

Exp. No.	Water Feed Rate cm³/sec	Water Pressure atm. (gauge)	Type & No. of nozzles	Inlet		Outlet	
				Median Drop Diameter µm	Geometric Standard Deviation	Median Drop Diameter µm	Geometric Standard Deviation
101	$1.453\mathrm{x}10^{3}$	2.041	11-1/2F35	-	-	-	-
102	$1.449\mathrm{x}10^{3}$	2.041	11-1/2F35	-	-	-	-
103	$1.263\mathrm{x}10^{2}$	13.605	M6(12)	84	1.3	-	-
104	$1.137\mathrm{x}10^{2}$	13.605	M6(12)	84	1.3	69	1.3
105	$1.137\mathrm{x}10^{2}$	13.605	M6(12)	-	-	-	-
106	$7.264\mathrm{x}10^{1}$	13.605	M6(6)	84	1.3	-	-
107	$9.159\mathrm{x}10^{1}$	13.605	M6(6)	84	1.3	-	-
108	$3.474\mathrm{x}10^{1}$	13.605	M6(3)	84	1.3	294	1.6
109	$1.327\mathrm{x}10^{2}$	3.401	M26(12)	380	1.5	510	1.8
110	$3.097\mathrm{x}10^{2}$	3.401	M26(12)	380	1.5	-	-
111	$4.453\mathrm{x}10^{2}$	3.401	GG3(12)	12	1.8	298	1.6
112	$4.492\mathrm{x}10^{2}$	3.401	GG3(12)	12	1.8	-	-
113	$4.233\mathrm{x}10^{2}$	3.401	GG3(12)	12	1.8	-	-
114	$3.050\mathrm{x}10^{2}$	3.401	GG3(9)	12	1.8	281	1.5
115	$3.058\mathrm{x}10^{2}$	3.401	GG3(9)	12	1.8	351	1.6
116	$3.567\mathrm{x}10^{2}$	3.40	GG3(12)	12	-	277	1.6
117	$3.878\mathrm{x}10^{2}$	3.40	GG3(12)	12	-	-	-
118	$1.137\mathrm{x}10^{2}$	13.61	M6(12)	84	1.3	-	-
119	$1.137\mathrm{x}10^{2}$	13.61	M6(12)	84	1.3	-	-
120	$7.264\mathrm{x}10^{1}$	13.61	M6(6)	84	1.3	-	-

Table A-2. DROP DIAMETERS OF THE ENTRAINMENT ENTERING AND LEAVING THE TEST SECTION (continued)

Exp. No.	Water Feed Rate cm³/sec	Water Pressure atm. (gauge)	Type & No. of nozzles	Inlet		Outlet	
				Median Drop Diameter µm	Geometric Standard Deviation	Median Drop Diameter µm	Geometric Standard Deviation
121	1.137×10^2	13.61	M6(12)	84	1.3	-	-
122	3.474×10^1	13.61	M6(3)	84	1.3	-	-
123	1.074×10^2	13.61	M6(12)	84	1.3	798	1.9
124	1.074×10^2	13.61	M6(12)	84	1.3	-	-
125	1.074×10^2	13.61	M6(12)	84	1.3	-	-
126	1.074×10^2	13.61	M6(12)	84	1.3	-	-
127	1.074×10^2	13.61	M6(9)	84	1.3	605	1.9
128	1.074×10^2	13.61	M6(9)	84	1.3	152	1.5
130	1.074×10^2	13.61	M6(9)	84	1.3	-	-
131	1.074×10^2	13.61	M6(9)	84	1.3	-	-
132	3.494×10^2	3.40	1/8GG3(12)	1225	1.8	-	-
133	4.536×10^2	3.40	1/8GG3(12)	1225	1.8	-	-
134	4.392×10^2	3.40	1/8GG3(12)	1225	1.8	-	-
135	4.261×10^2	3.40	1/8GG3(12)	1225	1.8	441	1.6
136	4.182×10^2	3.40	GG3(12)	1225	1.8	472	1.6
137	1.067×10^3	3.06	11-1/2F18	-	-	-	-
138	1.069×10^3	3.06	11-1/2F18	-	-	-	-
140	2.565×10^2	3.40	M26(12)	380	1.5	-	-
141	4.185×10^2	3.40	GG3(12)	1225	1.7	-	-
142	1.263×10^2	13.60	M6(12)	84	1.3	-	-

Table A-2. DROP DIAMETERS OF THE ENTRAINMENT ENTERING AND LEAVING THE TEST SECTION (continued)

Exp. No.	Water Feed Rate cm³/sec	Water Pressure atm.(gauge)	Type & No. of nozzles	Inlet		Outlet	
				Median Drop Diameter µm	Geometric Standard Deviation	Median Drop Diameter µm	Geometric Standard Deviation
143	1.263×10^2	13.60	M6(12)	84	1.3	-	-
145	1.390×10^2	13.60	M6(12)	84	1.3	-	-
146	1.273×10^2	13.60	M6(12)	84	1.3	86	1.3
147	1.334×10^2	13.60	M6(12)	84	1.3	87	1.3
148	2.353×10^2	3.40	M26(12)	380	1.5	-	-
149	4.321×10^2	3.40	GG3(12)	1225	1.8	-	-
150	4.214×10^2	3.40	GG3(12)	1225	1.8	-	-
151	2.118×10^2	3.40	M26(12)	380	1.5	-	-
152	1.314×10^2	13.60	M6(12)	84	1.3	-	-
153	1.300×10^2	13.60	M6(12)	84	1.3	-	-

Table A-3. LIQUID MATERIAL BALANCE

Exp. No.	Input cm^3	Before Test Section % of Input	Test Section: Section I % of Input	Section II % of Input	Section III % of Input	Section IV % of Input	After Test Section in air % of Input
1	$6.07\text{x}10^5\alpha$	68.2	17.1	12.9	1.7β	0.04β	0
2	$3.329\text{x}10^5\alpha$	81.3	14.2	0.4	0	0	0
3	$7.61\text{x}10^5\alpha$	57.7	27.0	7.4	5.4β	1.6β	0
4	$5.36\text{x}10^5$	84.4	10.1	2.7	0	0.05β	0
5	$7.91\text{x}10^5$	93.9	5.8	0.6	0	0	N.A.
6	$7.28\text{x}10^5$	91.1	5.2	0.6	0.4	0	2.7α
8	$1.367\text{x}10^6\alpha$	64.9	18.9	8.0	7.3β	0.8β	0
9	$1.337\text{x}10^6$	35.6	64.0α	0.3	0	0	0
12	$5.076\text{x}10^5$	88.1	10.9	12.1	0	0	0
13	N.A.	$3.226\text{x}10^5$	$3.659\text{x}10^4$	$3.94\text{x}10^4$	0	0	N.A.
14	$3.741\text{x}10^5$	85.0	10.9	11.9	0	0	3.2α
15	$4.775\text{x}10^5$	85.7	5.4	5.8	0	0	3.5α
17	$6.63\text{x}10^5$	7.8	28.3	16.5	19.7β	0.2β	0
18	N.A.	$4.42\text{x}10^5$	$5.438\text{x}10^5$	$3.315\text{x}10^3$	$2.805\text{x}10^3\beta$	$3.545\text{x}10^4\beta$	N.A.
19	$1.232\text{x}10^6$	13.9	63.3	0	0	0	0
20	$5.12\text{x}10^5$	18.7	23.9	23.5	25.9β	3.1β	4.9
21	$5.481\text{x}10^5$	21.1	49.7	6.7	2.1	1.9	N.A.
22	$7.618\text{x}10^5$	38.1	60.4	0.4	0	0	1.1
23	$7.391\text{x}10^5$	41.1	61.7	0	0	0	N.A.
24	$5.912\text{x}10^5$	52.0	65.0	0	0	0	N.A.

(See notes on page A-23)

Table A-3. LIQUID MATERIAL BALANCE (continued)

Exp. No.	Input cm³	Before Test Section % of Input	Test Section Section I % of Input	Section II % of Input	Section III % of Input	Section IV % of Input	After Test Section in air % of Input
25	6.822×10^5	44.3	60.3	0	0	0	N.A.
26	5.685×10^5	54.4	56.8	0	0	0	0
27	1.137×10^6	47.3	50.8	0	0	0	0
28	1.137×10^6	35.7	57.4	0.4	0.3β	0	6.2
29	1.137×10^6	32.8	34.1	16.8	9.5β	6.9β	14.9
30	4.738×10^5	10.6	31.5	29.2β	14.8β	19.2β	N.A.
31	1.355×10^6	41.2	27.4	6.6β	11.1β	8.3β	5.3
32	6.917×10^5	7.6	36.1	45β	0	0	11.3
33	1.470×10^6	17.5	62.5	18.6β	0.5	0	0.9
34	1.481×10^6	26.8	63.5	5.5β	0	0.2	4.1
35	2.888×10^6	39.4	47.7	11.3β	0.1	0	1.5
36	1.470×10^6	41.3	28.9	27.5β	0	0.1	2.2
37	7.954×10^5	67.2	26.3	12.3	0	0	0
38	7.915×10^5	47.5	21.0	17.2	0	0	14.3
40	2.285×10^5	66.0	32.0	0	0	0	1.92α
41	1.895×10^5	92.6	9.1	0	0	0	0
43	1.545×10^5	71.0	15.7	12.8	0	0	0.5α
45	3.568×10^5	68.0	16.0	0	0	0	16.0α
46	3.705×10^5	67.9	10.2	19.3β	0	0	2.6α
47	3.754×10^5	64.0	20.6	2.6	0.06	0	12.7α

(see notes on page A-23)

Table A-3. LIQUID MATERIAL BALANCE (continued)

Exp. No.	Input cm^3	Before Test Section % of Input	Test Section				After Test Section in air % of Input
			Section I % of Input	Section II % of Input	Section III % of Input	Section IV % of Input	
48	$3.365x10^{5}$	57.9	17.7	8.9	0	0	15.5α
49	$2.499x10^{5}$	67.2	26.5	1.6	0	0	4.7α
50	$1.126x10^{6}$	59.7	32.7	7.8β	0	0	0
51	$1.007x10^{6}$	N.A.	34.2	12.7	0	0	N.A.
53	$8.567x10^{5}$	69.5	34.4	2.1β	0	0	0
54	$6.727x10^{5}$	34.8	28.7	25.6β	0	0	10.9α
55	$6.072x10^{5}$	60.9	35.4	1.2	0	0	2.5α
56	$6.289x10^{5}$	53.4	39.1	5.2β	0	0	2.3α
57	$6.140x10^{5}$	44.1	35.6	12.6β	0	0	7.7α
58	$4.402x10^{5}$	53.4	30.2	24.3β	0	0	0
59	$4.082x10^{5}$	60.5	35.5	2.0	0	0	2.0α
60	$3.724x10^{5}$	55.8	39.7	3.8β	0	0	0.7α
61	$1.805x10^{5}$	43.0	30.0	12.6β	0	0	14.4α
63	$1.192x10^{5}$	65.2	6.4	15.0β	0	0	13.4α
64	$1.224x10^{5}$	73.1	12.4	3.14	0	0	11.4
65	$3.803x10^{5}$	68.6	6.7	28.3	0	0	0
66	$3.840x10^{5}$	64.0	18.7	7.6β	0	0	9.7α
67	$3.761x10^{5}$	63.1	24.1	0.3	0	0	12.5α
68	$9.165x10^{5}$	60.7	25.6	33.0	0	0	N.A.
69	$8.259x10^{5}$	59.4	26.9	17.0	0	0	0

(see notes on page A-23)

Table A-3. LIQUID MATERIAL BALANCE (continued)

Exp. No.	Input cm ^{3}	Before Test Section % of Input	Test Section				After Test Section in air % of Input
			Section I % of Input	Section II % of Input	Section III % of Input	Section IV % of Input	
70	7.806×10^5	79.2	31.5	1.6	0	0	N.A.
71	7.675×10^5	71.2	41.9	8.5	0.9	0	N.A.
73	1.386×10^6	30.2	46.6	3.4	2.3	0	N.A.
74	1.281×10^6	76.0	40.9	0	0	0	N.A.
75	3.872×10^6	2.3	15.4	67.6	6.8		7.9α
76	5.243×10^6	2.9	25.3	60.1	11.9	0.4	0
77	4.033×10^5	45.4	40.4	3.3	0	0	10.9α
78	4.438×10^5	57.2	38.7	3.1	0	0	1.0α
79	7.182×10^5	67.4	37.9	0.5	0	0	0
80	6.205×10^5	62.2	37.3	3.4	0	0	0
81	6.207×10^5	53.9	35.8	2.0	0.1	0	8.2α
82	6.268×10^5	74.9	25.6	0.9	0	0	0
83	1.305×10^6	33.1	74.2	2.4	0	0	N.A.
84	1.278×10^6	14.6	78.8	16.4	0	0.3	N.A.
85	1.238×10^6	21.3	78.2	9.6	0	0.1	N.A.
86	1.236×10^6	56.3	53.4	1.0	0	0	N.A.
88	9.418×10^5	20.4	80.2	10.3	0	0.1	N.A.
89	9.100×10^5	24.2	78.7	8.1	0.1	0.17	N.A.
90	1.139×10^6	26.4	80.6	4.3	0	0.1	N.A.
91	1.147×10^6	38.8	70.8	2.7	0	0	N.A.

(see notes on page A-23)

Table A-3. LIQUID MATERIAL BALANCE (continued)

Exp. No.	Input cm³	Before Test Section % of Input	Test Section				After Test Section in air % of Input
			Section I % of Input	Section II % of Input	Section III % of Input	Section IV % of Input	
92	1.144×10^6	49.7	60.9	1.8	0	0	N.A.
93	1.132×10^6	59.1	53.5	0.75	0	0	N.A.
94	3.892×10^6	2.3	29.7	35.5	24.7	12.5	N.A.
95	3.835×10^6	2.1	13.3	69.8	15.9	0.6	0
97	3.873×10^6	29.6	72.4	0.3	0	0	0
98	3.880×10^6	44.3	57.2	0.17	0	0	0
99	5.219×10^6	0.9	11.6	67.4	19.3	1.7	N.A.
100	5.448×10^6	2.5	37.8	51.3	4.9	0.4	3.1α

(see notes on page A-23)

Table A-3. LIQUID MATERIAL BALANCE (continued)

Exp. No.	Input cm³	Before Test Section % of Input	Test Section: Section I % of Input	Test Section: Section II % of Input	Test Section: Section III % of Input	Test Section: Section IV % of Input	After Test Section in air % of Input
101	5.224×10^6	36.4	67.5	1.6	0.09	0	0
102	5.216×10^6	50.4	50.2	0.2	0	0	0
103	4.526×10^5	90.3	44.8	0	0	0	0
104	3.954×10^5	76.8	16.3	4.3	0	0	0
105	4.014×10^5	74.7	20.2	0.8	0	0	0
106	2.473×10^5	61.2	14.5	6.7	0	0	0
107	3.214×10^5	34.3	18.1	0	0	0	0
108	1.107×10^5	62.4	11.0	5.5	0	0	0
109	4.635×10^5	69.9	23.7	4.0	0.2	0	2.2
110	1.105×10^6	85.8	28.5	0.3	0	0	0
111	1.589×10^6	27.1	33.3	46.9	0.4	0	N.A.
112	1.607×10^6	33.9	58.0	13.9	0	0	0
113	1.510×10^6	21.1	32.4	52.5	0.2	0	N.A.
114	1.084×10^6	18.4	41.7	50.9	0.4	0	N.A.
115	1.088×10^6	23.5	34.8	57.7	0	0	N.A.
116	1.269×10^6	17.7	35.4	60.0	0.4	0	N.A.
117	1.385×10^6	24.4	62.9	19.9	0	0	0
118	4.046×10^5	74.4	14.0	14.8	0	0	0
119	4.007×10^5	75.9	23.8	0	0	0	0
120	2.470×10^5	72.8	16.1	49.9	0	0	0

(see notes on page A-23)

Table A-3. LIQUID MATERIAL BALANCE (continued)

Exp. No.	Input cm³	Before Test Section % of Input	Test Section				After Test Section in air % of Input
			Section I % of Input	Section II % of Input	Section III % of Input	Section IV % of Input	
121	$4.088\text{x}10^5$	75.1	20.0	0	0	0	0
122	$1.106\text{x}10^5$	63.8	13.7	2.1	0	0	0
123	$3.87\text{x}10^5$	86.5	28.0	1.75	0	0	3.59
124	$3.86\text{x}10^5$	68.1	28.8	0	0	0	0
125	$3.86\text{x}10^5$	91.9	2.6	0	0	0	0
126	$3.84\text{x}10^5$	76.7	19.5	0	0	0	0
127	$3.56\text{x}10^5$	67.4	26.9	1.6	0	0	4.0
128	$3.56\text{x}10^5$	66.1	26.8	0	0	0	6.8
130	$3.78\text{x}10^5$	63.6	21.5	0	0	0	0
131	$3.85\text{x}10^5$	69.4	8.2	0	0	0	0
132	$1.252\text{x}10^6$	69.2	43.6	0	0	0	N.A.
133	$1.631\text{x}10^6$	17.4	57.7	29.6	0.3	0	N.A.
134	$1.574\text{x}10^6$	27.9	74.5	1.1	0	0	N.A.
135	$1.529\text{x}10^6$	17.3	56.0	30.4	0.6	0	N.A.
136	$3.000\text{x}10^6$	16.6	59.3	29.0	0.9	0	0.1
137	$7.627\text{x}10^6$	0.8	22.0	61.3	15.7	0.2	0.2
138	$7.629\text{x}10^6$	0.5	21.8	65.4	13.8	0.6	N.A.
140	$1.842\text{x}10^6$	90.2	17.8	0	0	0	N.A.
141	$3.005\text{x}10^6$	68.2	39.2	0	0	0	N.A.
142	$8.876\text{x}10^5$	58.3	24.7	0.3	0	0	0

(see notes on page A-23)

Table A-3. LIQUID MATERIAL BALANCE (continued)

Exp. No.	Input cm ^{3}	Before Test Section % of Input	Test Section				After Test Section in air % of Input
			Section I % of Input	Section II % of Input	Section III % of Input	Section IV % of Input	
143	9.025×10^5	56.7	26.5	0	0	0	0
145	9.87×10^5	52.9	23.3	0.2	0	0	0.1
146	9.160×10^5	82.2	3.0	0.2	0	0	0
147	9.415×10^5	71.9	8.7	1.3	0	0	0.1
148	1.667×10^6	36.8	29.0	22.3	0	0	0.2
149	3.099×10^6	16.8	46.9	41.4	0	0	N.A.
150	3.006×10^6	30.4	10.5	65.6	0.2	0	N.A.
151	1.473×10^6	61.6	43.9	3.2	0	0	N.A.
152	9.454×10^5	87.9	12.4	0	0	0	N.A.
153	9.365×10^5	63.3	19.3	2.8	0	0	0

α = Obtained by material balance
β = Liquid overflowing from previous section
* = If the liquid input is not available (N.A.) liquid flow is given in cm ^{3}

Table A-4. PRESSURE DROP DATA

Exp. No.	System Pressure mm Hg gauge	Pressure Drop Over Test Section	
		ΔP_{dry} cm W.C.	ΔP_{wet} cm W.C.
1	N.A.	1.7	1.7
2	N.A.	0.41	0.41
3	N.A.	3.0	3.3
4	N.A.	0.41	0.41
5	-24.36	0.08	0.12
6	-26.39	0.12	0.12
8	-25.12	1.5	1.5
9	-24.61	0.74	0.82
11	-23.09	0.29	0.29
12	-23.09	0.12	0.16
13	-23.09	0.08	0.08
14	-24.87	0.12	0.12
15	-26.14	0.04	0
17	-25.12	1.2	1.3
18	-24.80	1.20	1.4
19	-23.60	1.1	1.5
20	-23.50	1.03	2.2
21	-26.80	0.58	1.3
22	-23.0	0.29	0.62
23	-24.4	0.21	0.54
24	-24.3	N.A.	0.21
25	-22.1	0.29	0.45
26	-21.9	0.04	0.21
27	-19.9	0.04	0.29
28	-3.7	0.21	0.54
29	-20.5	0.29	0.8
30	-22.0	1.3	1.6
31	-22.0	1.3	1.8
32	-22.6	1.3	1.3
33	-32.0	N.A.	N.A.

Table A-4. PRESSURE DROP DATA (continued)

Exp. No.	System Pressure mm Hg gauge	Pressure Drop Over Test Section	
		ΔP_{dry} cm W.C.	ΔP_{wet} cm W.C.
34	-22.0	0.37	0.37
35	-22.0	0.41	0.12
36	-23.0	0.12	0.12
37	-23.0	0.29	0.54
38	-25.0	1.0	1.03
39	-25.5	1.1	1.45
40	N.A.	0.45	0.62
41	-23.0	0.08	0.08
42	-21.9	0.04	0.04
43	-20.5	0.99	1.4
45	-23	0.29	0.29
46	-23	1.0	1.7
47	-23.5	0.54	0.87
48	-19	0.78	1.3
49	-18	0.61	0.87
50	N.A.	0.78	0.87
51	-24	0.95	0.87
52	-24	0.66	0.66
53	-24	0.50	0.50
54	-22.8	1.3	0.5
55	-23	0.50	0.50
56	-23	0.79	0.79
58	-20	1.28	1.28
59	-20	0.54	0.54
60	-22	0.83	0.91
61	-21.5	1.3	1.4
63	-19	1.0	1.6
64	-19	0.74	1.1
65	-19	1.1	1.9
66	-19	0.74	1.3

Table A-4. PRESSURE DROP DATA (continued)

Exp. No.	System Pressure mm Hg gauge	Pressure Drop Over Test Section	
		ΔP_{dry} cm W.C.	ΔP_{wet} cm W.C.
67	-20	0.45	0.78
68	-20	1.1	2.0
69	-20	0.78	1.0
70	-21.5	0.45	0.54
71	-20	8.63	8.9
72	-18	0.45	0.45
73	-19	8.6	9.29
74	-19	0.45	0.37
75	-19	9.1	4.2
76	-20	8.7	9.5
77	-19.8	2.8	3.2
78	-22	2.4	2.5
79	-23	1.7	1.8
80	-22.9	2.2	2.4
81	-23	2.7	2.9
82	-23	0.54	0.54
83	-22	0.54	0.54
84	-22	2.7	3.0
85	-26	2.1	2.2
86	-26	0.12	0.45
88	-19	2.7	2.9
89	-20	2.0	2.0
90	-20	1.2	1.2
91	-20	0.540	0.45
92	-20	0.25	0.25
93	-20	0.41	0.330
94	-20	2.7	2.6
95	-20.5	6.1	N.A.
97	-20	0.62	0.54
98	-20	0.21	0.12
99	-17	5.9	7.6
100	-17	3.4	5.0

Table A-4. PRESSURE DROP DATA (continued)

Exp. No.	System Pressure mm Hg gauge	Pressure Drop Over Test Section	
		ΔP_{dry} cm W.C.	ΔP_{wet} cm W.C.
101	-17.5	0.87	0.45
102	-17.5	0.21	0.17
103	-19.0	0.21	0.21
104	-18.0	6.2	6.5
105	-18.0	2.21	2.2
106	-17.0	6.2	6.5
107	-17.0	2.2	2.3
108	-20.0	6.2	6.6
109	-20.5	6.1	6.5
110	-20.0	3.4	3.7
111	-22.0	5.9	6.7
112	-22.0	3.5	4.2
113	-18.0	5.9	6.7
114	-18.0	6.1	6.6
115	-17.0	6.2	6.7
116	-17.0	6.2	7.1
117	-17.0	3.6	4.3
118	-23.0	5.9	6.4
119	-23.0	2.4	2.6
120	-20.0	6.2	7.3
121	-20.0	2.4	2.5
122	-20.0	6.2	6.5
123	-26.0	1.1	1.9
124	-25.0	0.45	0.87
125	-23.0	0.04	0.04
126	-23.0	0.29	0.29
127	-20.0	1.0	1.9
128	-20.0	0.79	1.4
130	-16.0	0.29	0.45
131	-17.0	0.12	0.12

GLOSSARY

COLLECTION EFFICIENCY or OVERALL COLLECTION EFFICIENCY

Collection efficiency or overall collection efficiency is the mass ratio of net liquid collected in the entrainment separator to the liquid present in the inlet entrainment. It can also be expressed as the difference between primary efficiency and reentrainment. We use either fraction or percent, as specified in the text or figure.

PENETRATION

Penetration is the mass ratio of drops in the outlet to that of the inlet of the entrainment separator. Penetration is also equal to "1 - collection efficiency", if in fractional form. We use either fraction or percent, as specified in the text or figure.

PRIMARY COLLECTION

Primary collection is defined as fractional collection of the drops present in the original entrainment by various mechanisms which is reported in terms of mass fraction as an efficiency. Primary efficiency includes only the collection of drops present in the original entrainment. The reentrainment of these collected drops or the subsequent collection of these reentrained drops does not affect the primary collection efficiency.

REENTRAINMENT

Reentrainment is the mass ratio of drops entering the gas from the liquid in the entrainment separator to drops present in the inlet entrainment.

REENTRAINMENT VELOCITY

Reentrainment velocity is the gas velocity at which drops are first observed to become reentrained in the gas. The reentrainment velocity will vary for different kinds of entrainment separators and different operating conditions.

SECONDARY COLLECTION

Secondary collection refers to drops which are absorbed after having been reentrained. The mass ratio of these drops to those present in the inlet entrainment is the secondary collection efficiency.

REFERENCES

Alia, P., L. Cravarola, A. Hassid, and E. Pedrouhi. Liquid Volume Fraction in Adiabatic Two Phase Vertical Upflow-Round Conduit. CISE Report R-105. 1965.

Anderson, J. D., R. E. Bollinger, and D. E. Lamb. Gas Phase Controlled Mass Transfer in Two Phase Annular Horizontal Flow. AIChE Journal. 10:640, 1964.

Baker, O. Simultaneous Flow of Oil and Gas. Oil Gas Journal. 53:185, 1954.

Bell, C. G. and W. Strauss. Effectiveness of Vertical Mist Eliminators in a Cross Flow Scrubber. Journal of the APCA. 23:967-9. November 1973.

Bradie, J. K. and A. N. Dickson. Removal of Entrained Liquid Droplets by Wire Mesh Demisters. Paper 24 in Fluid Mechanics and Measurements in Two-Phase Flow Systems. (A joint symposium of the Inst. of Mech. Engr. and the Yorkshire Branch of the Inst. of Chem. Engr.) 24-25. London. September 1969.

Buerkholz, A. Drop Separation on Wire Fitters. Chemie Ingenieur Tecknik. 42, 21, 1314-1321, 1970.

Calvert, S. Air Pollution. Stern, A. C. (ed.). 3, Academic Press, New York. 1968.

Calvert, S., J. Goldshmid, D. Leith, and D. Mehta. Scrubber Handbook. Prepared for EPA Contract No. CPA-70-95. Vol. I and II, 1972.

Calvert, S. and D. Lundgren. Particle Collection in Closed Packed Arrays. Presented at AIHA. 1970.

Carman, P.C. Fluid Flow Through Granular Beds. Trans. Inst. Chem. Engr. 15:150, 1937.

Castleman, R.A. Bur. Stand. J. Res. Washington. 6:369, 1931.

Carpenter, C. L. and D. F. Othmer. Investigation of Wire Mesh as an Entrainment Separator. AIChE Journal. p. 549, 1955.

Chien, S. F. and W. Ibele. Pressure Drop and Liquid Film Thickness of Two Phase Annular and Annular-Mist Flows. ASME Paper. 62-WA170.

Chilton, H. Elimination of Carryover from Packed Towers With Special Reference to Natural Draught Water Cooling Towers. Trans. ICE. 30, 235.

Collier, J. G. and G. F. Hewitt. Data on Vertical Flow of Air-Water Mixtures in Annular and Dispersed Flow Regions: Part II, Film Thickness and Entrainment data and Analysis of Pressure Drop Measurements. Trans. Inst. Chem. Engr. 39:127, 1961.

Cousins, L. B., W.H. Denton, and G. F. Hewitt. Liquid Mass Transfer in Annular Two Phase Flow. Exeter. 21-23, June 1965.

Cousins, L. B. and G. F. Hewitt. Liquid Phase Mass Transfer in Annular Two Phase Flow-Droplet Deposition and Liquid Entrainment. AERE-R 5657. 1968.

Davis, R. F. Proc. Inst. Mech. Engrs. 149:148, 1940.

Dombrowski, N. and R. P. Frazer. A Photographic Investigation into the Disintegration of Liquid Sheets. Phil. Trans. A924, 247, 101, 1954.

Eckert, J. S. Chem. Engr. Prog. 57, 9, 54, 1961.

Edgerton, H. E., K. J. Germeshansen, and H. E. Grier. Photography J. 76:198, 1936.

Fage, A. and F. C. Johansen. Proc. Roy Soc. (London). 116A:170, 1927.

Fairs, G. L. Calder-Fox Scrubbers and the Factors Influencing Their Performance. Trans. I Chem. E. London. 22, 110.

Foust, A. S., L. A. Wenzel, C. W. Clump, L. Maus, and L. B. Andersen. Principles of Unit Operations. Toppan Company. Tokyo. 1959.

Garner, F. H., S. R. M. Ellis, and J. A. Laay. The Size Distribution and Entrainment of Droplets. Trans. Inst. Chem. Engr. 32:222, 1954.

Gill, L. E., G. F. Hewitt, J. W. Hitchon, and P. M. C. Lacy. Sampling Probe Studies of the Gas Core in Annular Two Phase Flow: 1, The Effect of Length on Phase and Velocity Distribution. Chem. Engr. Sci. 18:525, 1963.

Golovin, M. N., and A. A. Putnam. Ind. Engr. Chem. Fund. 1:264, 1962.

Grimison. Trans. Am. Soc. Mech. Engr. 59:583-94, 1937.

Grimley, S. S. Trans. Inst. Chem. Engr. (London). 23, 228-235, 1948.

Haenlein, A. Forsch. Ing. Wes. 2:139, 1931.

Hall-Taylor, N. S. and R. M. Nedderman. The Coalescence of Disturbance Waves in Annular Two-Phase Flow. Chem. Engr. Sci. 23:551-64, 1963.

Hanratty, T. J. and D. E. Woodmansee. Stability of the Interface for a Horizontal Air-Liquid Flow. Symposium on Two Phase Flow. Exeter. Paper A1, 21-23, June 1965.

Hinze, J. O. Forced Deformation of Viscous Liquid Globules. Appl. Sci. Res. Ai. 263-72, 1948.

Hinze, J. O. Critical Speed and Sizes of Globules. Appl. Sci. Res. A1, 275-88, 1948a.

Houghton, J. G. and W. H. Radford. Trans. Am. Inst. of Ch. E. 35:427, 1939.

Hughmark, G. A. Film Thickness Entrainment, and Pressure Drop in Upward Annular and Dispersed Flow. AIChE Journal. 19, 5, 1062-7, 1973.

Jackson, S. and S. Calvert. AIChE Journal. 12:1075, 1966.

Jashnani, I. L. Coalescence and HTU in Foam Fractionation Columns. Ph.D. Dissertation, U. ov Cincinnati. 1971.

Kitchener, J. A. Foams and Free Liquid Films. in Recent Progress in Surface Science. Academic Press. New York. 1964.

Kotov, N. A. Influence of Spray Entrainment on Gas Scrubber Efficiency. Translated by EPA from Vodosnabzheniye i Sanitaria Technika. 7:31-4, 1972.

Lane, W. R. Shatter of Drops in Streams of Air. Ind. Engr. Chem. 43, 1312, 1951.

Lapple, C. E. and C. B. Shepherd. IEC Ind. 32, 605, 1940.

Leith, D. and W. Licht. The Collection Efficiency of Cyclone Type Particle Collectors - A New Theoretical Approach. Paper presented at San Francisco meeting of AIChE. December 1971.

Leva. M. Chem. Engr. Prog. Symp. Ser. No. 10, 50, 51, 1954.

Lobo, W. E., L. Friend, F. Hashmall, and F. A. Zenz. Trans. AIChE. 41, 693, 1945.

Mercer, T. T. and H. Y. Chow. J. of Coll. and Interface Sci. 27:75-83, 1968.

Miles, J. W. On the Generation of Surface Waves by Shear Flows. J. Fluid Mech. 3, 185, 1957.

Moyers, C. G., Jr. Entrainment Separator Selection and Evaluation. Engr. Res. Report ER-60-1010. Union Carbide. October 1960.

Newitt, D. M., N. Dombrowski, and F. H. Knelman. Liquid Entrainment: 1 The Mechanism of Drop Formation from Gas or Vapor Bubbles. Trans. Inst. Chem. Engr. 32, 244, 1954.

Nukiyama, S. and Y. Tarrasawa. Trans. Soc. of Mech. Engr. (Japan). 4, 5, 6, 1938-1940.

Perry, J. H. Chemical Engineering Handbook. 4th Edition. McGraw-Hill. New York. 1963.

Rayleigh, Lord, Proc. Lond. Math. Soc. 10, 4, 1879.

Rayleigh, Lord, Phil. Mag. 48, 321, 1889.

Roberts, D. C. and D. E. Hartley. A Correlation of Pressure Drop Data for Two Phase Annular Flows in Vertical Channels. Queen Mary College. (London). Nuclear Research Memorandum, No. Q6.

Satsangee, P. D. Master's Thesis. Polytechnic Institute of Brooklyn. 1948.

Scott, D. S. Properties of Cocurrent Gas-Liquid Flow. in Advances in Chemical Engineering. Vol. 4. Academic Press. New York. 1963.

Shearer, C. J. and R. M. Nedderman. Pressure Gradient and Liquid Film Thickness in Cocurrent Upwards Flow of Gas-Liquid Mixtures: Application of Film Cooler Design. Chem. Engr. Sci. 20:671-83, 1965.

Shepherd, C. B. and C. E. Lapple. IEC Chem. 31, 1246, 1940.

Sherwood, T. K. and R. L. Pigford. Adsorption and Extraction. McGraw-Hill. New York. 265, 1952.

Sherwood, T. K., G. H. Shipley, and F. A. L. Holloway. Ind. Engr. Chem. 30, 765, 1938.

Sorokin, Y. L., L. N. Demidova, and N. P. Kuzmin. Principles of Drop Separation from Vapor or Gas Streams. Translated from Khimicheskoyi i Nedtinoye Mashinostroyiniye. No. 8, p. 20, 1968.

Stearman, F. and G. J. Williamson. Spray Elimination in Processes for Air Pollution Control. Nonhebel, 2nd ed., CRC Press. Cleveland. 1972.

Steen, D. A. and G. B. Wallis. The Transition from Annular to Annular-Mist Cocurrent Two-Phase Down Flow. NYO-3114-2, 1964.

Stuhlman, D. Physics, 2, 457, 1932.

Stumpner, R. Die Werme. 59, 463, 1936.

Taheri, M. and S. Calvert. APCA Journal. 18, 240, 1968.

Wallis, G. B. The Onset of Droplet Reentrainment in Annular Gas-Liquid Flow. General Electric Report. No. 62 GL127, 1962.

Weber, C., Z. Angen. Math. Mech. 2, 139, 1931.

Wicks, M. and A. E. Dukler. Entrainment and Pressure Drop in Cocurrent Gas Liquid Flow. AIChE Journal. 6, 463, 1960.

Wicks, M. and A. E. Dukler. In Site Measurements of Drop Size Distribution in Two Phase-Flow: A New Method for Electrically Conducting Liquids. Paper presented at International Heat Transfer Conference, Chicago. 1966.

York, O. H. Performance of Wire Mesh Demisters. Chem. Engr. Prog. Vol. 50, No. 8, 421, 1954.

York, O. H. and E. W. Poppele. CEP. 59, 45, 1963.

Zhivaiking, L. Y. Liquid Film Thickness in Film Type Units. Int. Chem. Engr. 2, 237, 1962.